Copyright

by

Masoumeh Kordi

2013

The Dissertation Committee for Masoumeh Kordi Certifies that this is the approved version of the following dissertation:

Characterization and prediction of reservoir quality in chlorite-coated sandstones: evidence from the Late Cretaceous Lower Tuscaloosa Formation at Cranfield Field, Mississippi, U.S.A.

Committee:

William L. Fisher, Supervisor

Susan D. Hovorka, Co-Supervisor

Earle F. McBride

Ronald J. Steel

Mrinal K. Sen

Characterization and prediction of reservoir quality in chlorite-coated sandstones: evidence from the Late Cretaceous Lower Tuscaloosa Formation at Cranfield Field, Mississippi, U.S.A.

by

Masoumeh Kordi, B.S.; M.S.

Dissertation

Presented to the Faculty of the Graduate School of

The University of Texas at Austin

in Partial Fulfillment

of the Requirements

for the Degree of

Doctor of Philosophy

The University of Texas at Austin

May 2013

Dedication

With Love to my parents (Ebrahim and Esmat), my husband (Hesam),

my daughter (Yasaman) and my son (Yasin).

Acknowledgements

In the name of God, the most gracious, the most merciful, and all the praises and thanks be to God.

Most sincere appreciation goes to my supervisor, Professor William L. Fisher, for his continuous support and guidance during my graduate studies, and also for his valuable suggestions and comments on this dissertation. It is a great advantage to have a supervising professor who always keeps his door open, and who is readily available to help remove obstacles encountered on the academic path.

I would like to extend my appreciation to my co-supervisor, Dr. Susan D. Hovorka, for her guidance, help, and friendship. Without her generous financial support as a research assistant during the first 3 years of my Ph.D. studies, I could not have overcome many obstacles. I would like also to thank her for giving me the opportunity to be part of her research team (CO_2 injection) at the Gulf Coast Carbon Center, to work with friendly people, and to have access to great datasets.

My special thanks go to other members of my committee, Professor Earle F. McBride, Professor Ronald J. Steel, and Professor Mrinal K. Sen, for their contributions and constructive reviews. This dissertation has greatly benefited from their knowledge, experience, and comments.

I am grateful to the Department of Geological Sciences and the Bureau of Economic Geology of the Jackson School of Geosciences, The University of Texas at Austin for providing me facilities and partial financial support to conduct this study. Special thanks go to the faculty, staff, and students for providing a pleasant environment

and learning atmosphere during my Ph.D. program. It is a pleasure to thank my co-workers at the Gulf Coast Carbon Center for their help, sharing their technical expertise and friendship while I was a research assistant working with them. I would like to thank Philip Guerrero for helping as Graduate Program Administrator. Thanks go to Dr. Kitty L. Milliken for the useful scientific discussions that we had, and also for providing me with petrographic equipment. I acknowledge Robert M. Reed for helping with SEM equipment. My special thanks go to Amanda R. Masterson for editing this dissertation.

I would like to express my gratitude to Linda M. Bonnell and Robert H. Lander from Geocosm for their help during my proposal writing. I thank Zetaware for free access to their Genesis software.

This study, a part of the CO_2 injection project for CO_2-EOR and CO_2 monitoring at the Cranfield site, was funded by the National Energy Technology Laboratory and the U.S. Department of Energy and managed by the Southern States Energy Board through the Southeast Regional Carbon Sequestration Partnership (SECARB). Denbury Onshore LLC is the site host and partner of the Cranfield project. All of them are greatly appreciated. I am especially grateful to Essam Sharaf from Denbury Onshore LLC for his technical support.

I am very thankful for grants from the Department of Geological Sciences of The University of Texas at Austin, American Association of Petroleum Geologists (AAPG), GDL Foundation (Structural Diagenesis Research Program), and International Student and Scholar Services of The University of Texas at Austin.

I would like to express my gratitude to all of my friends in the USA for sharing their happiness and sadness with me through these years and for helping me in difficult situations.

Last but not least, I would like to thank my family: Sincere appreciation and warmest thanks are sent to my devoted parents, who I owe them everything that I have in my life. I wish I could show them just how much I love and appreciate them for their love, support, inspiration, prayers, and patience. I also extend my utmost appreciation to my brothers, my sisters, my parents-in-law, my brothers-in-law and my sisters-in-law, who were always with me in spite of the many miles that separated us and who have always supported me in every possible way. Thanks to them all for their love, support, encouragement, prayers, and patience during these years.

I owe my heart-felt and deepest gratitude to my loving husband, Hesam, who has been a constant and unconditional source of support and love in all my endeavors. My achievement would have been impossible without his ample help, encouragement, understanding, and love. I am indebted to him for every step of this journey. I am also very grateful to our darling kids, our daughter Yasaman and our son Yasin, who are great blessings in my life. Their arrival during the years of my graduate studies made my life more enjoyable and exciting, and their love gave me the strength and motivation to finish this dissertation. THANK YOU.

Characterization and prediction of reservoir quality in chlorite-coated sandstones: evidence from the Late Cretaceous Lower Tuscaloosa Formation at Cranfield Field, Mississippi, U.S.A.

Masoumeh Kordi, Ph.D.

The University of Texas at Austin, 2013

Supervisor: William L. Fisher

Co-Supervisor: Susan D. Hovorka

The effectiveness of CO_2 injection in the subsurface for storage and EOR are controlled by reservoir quality variation. This study determines the depositional processes and diagenetic alterations affecting reservoir quality of the Lower Tuscaloosa Formation at Cranfield Field. It also determines the origin, time and processes of the grain-coating chlorite and its impacts on reservoir quality. Moreover, by integrating depositional and diagenetic characteristics and by linking them to sequence stratigraphy, the distribution of reservoir quality, could be predicted within a sequence stratigraphic framework.

The studied sandstones are composed of medium to coarse-grained, moderately sorted litharenite to sublitharenite with composition of $Q_{76.1}F_{0.4}L_{23.5}$. Depositional environment of this formation in the Mississippi Interior Salt Basin is interpreted as incised-valley fluvial fill systems. The cross sections and maps at the field show trend of the sandy intervals within channels with a NW-SE paleocurrent direction.

During burial of the sandstones, different digenetic alterations including compaction, dissolution, replacement and cementation by chlorite, quartz, carbonate,

kaolinite, titanium oxides, pyrite and iron-oxide modified the porosity and permeability. Among these, formation of chlorite coats plays the most important role in reservoir quality. The well-formed, thick and continuous chlorite coatings in the coarser grain sandstones inhibited formation of quartz overgrowth, resulted in high porosity and permeability after deep burial; whereas the finer grain sandstones with the poorly-formed, thin and discontinuous chlorite coatings have been cemented by quartz. The optimum amount of chlorite to prevent formation of quartz overgrowths is 6% of rock volume.

The chlorite coats are composed of two layers including the inner chlorite layer formed by transformation of the Fe-rich clay precursors (odinite) through mixed-layer clays (serpentine-chlorite) during early eodiagenesis and the outer layer formed by direct precipitation from pore waters through dissolution of ferromagnesian rock fragments during late eodiagenesis to early mesodiagenesis.

In the context of the reservoir quality prediction within sequence stratigraphic framework, the late LST and early TST are suitable for deposition of chlorite precursor clays, which by progressive burial during diagenesis could be transformed to chlorite, and thus results in preserving original porosity and permeability in deep burial.

Table of Contents

List of Tables xiii

List of Figures xiv

Chapter 1: Introduction 1

1.1-Introduction and research objectives 1

1.2-Carbon dioxide storage and enhanced oil recovery 5

1.3-Study area, The Cranfield Field as CO_2 storage and CO_2 -EOR site 7

1.4-Geologic setting 13

1.4.1-Stratigraphic Setting-The Tuscaloosa Group 13

1.4.1.1-The Lower Tuscaloosa Formation 14

1.4.1.2-The Middle Tuscaloosa Formation 15

1.4.1.3-The Upper Tuscaloosa Formation 16

1.4.2-Tectonic and structural settings 19

1.4.2.1-The Mississippi Interior Salt Basin 19

1.4.2.2-Paleotopographic features 20

1.4.2.3-The shelf margin trend 20

1.4.3-Sediment provenance 22

Chapter 2: Depositional Characteristics Affecting Reservoir Quality 23

2.1-Introduction 23

2.2-Data set 24

2.3-Sedimentary facies and facies associations based on core descriptions 25

2.4-Lithostratigraphic correlation using well-logs 31

2.5-Sequence stratigraphic well-log correlation 36

2.6-Sand-shale analysis and net-sand thickness measurment 42

2.7-Mapping sandy intervals using well logs and seismic data 44

2.8-Hydrocarbon production analysis 54

2.9-Discussion 56

2.9.1-Sequence stratigraphic interpretation of the Tuscaloosa Group in the Gulf of Mexico and Gulf Coastal Plain 56
2.9.2-Depositional environment of the Lower Tuscaloosa Formation in the Mississippi Interior Salt Basin 62
2.9.3-Reservoir architecture at Cranfield Field....68
2.10-Conclusions 69
Chapter 3: Diagenetic Characteristics Affecting Reservoir Quality....71
3.1-Introduction 71
3.2-Samples and analytical methods....73
3.3-Sandstones architecture 76
3.4-Conglomerate....77
3.5-Detrital composition and classification of sandstones....77
3.5.1-Framework grains 78
3.5.1.1-Quartz 79
3.5.1.2-Feldspars....79
3.5.1.3-Rock fragments....79
3.5.1.4-Accessory minerals....81
3.5.2-Matrix 81
3.6-Restored framework grains composition....85
3.7-Pore type and distribution....87
3.8- Textural characteristics....92
3.9-Burial-Thermal history 94
3.10- Diagenetic alterations affecting reservoir quality....97
3.10.1-Compaction....97
3.10.1.1-Relative importance of compaction and cementation to original porosity reduction....102
3.10.2- Authigenic mineral cementation and replacement 104
3.10.2.1-Chlorite....105
3.10.2.2-Quartz 112
3.10.2.3-Titanium oxide....115

3.10.2.4-Carbonates 119
3.10.2.5-Kaolinite 122
3.10.2.6-Pyrite and iron oxide-Minor authigenic minerals.....123
3.10.3-Dissolution and porosity enhancement.....125
3.11-Disscusions 128
3.11.1-Diagenetic evolution and reservoir quality of the Lower Tuscaloosa Formation.....128
3.11.1.1-Eodiagenesis 128
3.11.1.2-Mesodiagenesis.....131
3.11.2-Origin, time and process of chlorite coating.....135
3.11.2.1-General remarks-origin and controlling factors of chlorite coating.....135
3.11.2.2-Origin, time and process of chlorite coating in the Lower Tuscaloosa Formation 137
3.11.3-Interplay between chlorite coating and quartz cementation and their effects on reservoir quality 144
3.12-Conclusions 148
Chapter 4: Reservoir Quality Controls and Prediction in the Chlorite-coated Sandstones.....150
4.1-Controls on reservoir quality of chlorite-coated sandstones 150
4.1.1-Depositional environment control 150
4.1.2-Textural control 151
4.1.3- Provenance control 152
4.1.4- Diagenetic control.....152
4.2-Linking diagenesis to sequence stratigraphy for chlorite coating prediction 155
Appendices.....157
References.....165
Vita.....193

List of Tables

Table 1.1-General stratigraphy of Albian to Santonian deposits showing relationship and variable subsurface lithostratigraphic nomenclature of the Tuscaloosa-Woodbine Formations from eastern Texas to southern Alabama. The studied area (southwestern Mississippi) has been highlighted in yellow (modified from Mancini et al., 2008). ...17

Table 2.1-Summary of the principal lithologies and facies interpretation for the 13 main facies and 2 facies associations that comprise the Massive Sand Member of the Lower Tuscaloosa Formation, Cranfield Field. 30

Table 3.1-Stratigraphic data used in burial-thermal history reconstructions of Wells CFU#31F2 and CFU#31F3. 95

Table 3.2-Bottom-hole temperatures and corrected formation temperatures using time-since-circulation for burial-thermal history reconstructions of Wells CFU#31F2 and CFU#31F3. 95

Table 3.3-Chemical composition of the outer layer of the chlorite coat. 110

Table 3.4-Chemical composition of the inner layer of the chlorite coat. 110

Table 3.5-Chemical composition of the ferroan dolomite/ankerite cement. 120

List of Figures

Figure 1.1-Schematic of a CO_2 sequestration and CO_2-EOR system 7

Figure 1.2-Location of the Cranfield Field in the Gulf coast of the United States (Modified from Google map); The CO_2 is transported from the natural geologic sources at Jackson Dome, central Mississippi (~160 km away) to the Cranfield site via Denbury Onshore LLC (DRI) pipelines. 10

Figure 1.3-Cranfield Field base-map illustrates location of historic and new wells that have been used in this study with the last five number of their API. Wells that have core and sidewall cores are shown by small red rectangle. Locations of roads, faults, oil rim and gas cap are from SECARB phase II final report (2011). Pink rectangle denotes the Detailed Area Study (DAS) and the representative photo (from Hovorka et al., 2013) shows the injector well (CFU#31F1) and two observation wells (CFU#31F2, 69m and CFU#31F3, 111m far from the injector well) that are marked by arrows. 11

Figure 1.4-Sketch of observation well completion design in the Well Ella G. Lees#7, correlating with resistivity and sp logs showing injection, confining and monitoring intervals (Diagram modified from Meckel et al., 2013, photos courtesy of Meckel, 2011). 12

Figure 1.5-Stratigraphic section for Cranfield site developed from literature and adjusted to site-specific conditions. Depths are representative of top intervals in Well CFU#29-12. The SP log in more detail shows the Tuscaloosa Group, its different formations, members and local unit names at the Cranfield Field. 18

Figure 1.6-Location of the Mississippi Interior Salt Basin and other basins and paleotopographic features during deposition of Tuscaloosa Formation in the northern Gulf Coastal Plain (modified from Pilger, 1981; Mancini et al., 2001). 21

Figure 1.7-Location of the Early Cretaceous shelf edge and updip, middip and downdip trends, location of two main source areas of the Tuscaloosa Formation (the Appalachian, and Ouachita Mountains), depocenter of the Tuscaloosa and Woodbine Formations, and the Gulf of Mexico's connection to Western Interior Seaway of North America. Gray areas denote present-day Tuscaloosa and Woodbine outcrops (modified from Mancini et al., 1996; Dubiel and Pitman, 2004; Mancini and Puckett, 2005). 22

Figure 2.1-Core photographs of the well CFU#29-12 showing D and E units (Massive Sand Member) of the Lower Tuscaloosa Formation that is reservoir interval at the Cranfield Field and their related facies associations. Contact of the Lower Tuscaloosa Formation and the underlying Dantzler Formation is an erosional channel that is marked by presence of the calcareous nodules at top of the Dantzler Formation. 28

Figure 2.2-Sedimentary graphic logs through the cored reservoir intervals in wells CFU#31F3 and CFU#31F2. 29

Figure 2.3-Cross section (AA') comprising the whole Tuscaloosa Group at the northeastern part of the field, showing correlation of Lower, Middle and Upper Tuscaloosa Formations as well as the sequence stratigraphic framework that includes different system tracts and surfaces by GR, SP and resistivity logs. The Cranfield Field map shows the position of the cross section. 33

Figure 2.4-(a) Dip transect cross section (BB') correlating the Lower Tuscaloosa Formation and its members over a distance of about 6.5 km (4 miles). (b) Correlation of the Lower Tuscaloosa Formation and its members in strike orientation (CC') over a distance of about 6.5 km (4 miles). The Cranfield Field map shows the position of the cross sections. 34

Figure 2.5-(a) Structure contour map of the top of the Lower Tuscaloosa Formation. (b) Structure contour map of the base of the Lower Tuscaloosa Formation. Locations of oil rim, gas cap and main faults that are plotted on the maps are from SECARB phase II final report, 2011 35

Figure 2.6-Sequence stratigraphic framework of the Tuscaloosa Group, including different system tracts and surfaces correlated with SP, GR and resistivity logs of wells in the DAS area (CO_2 injection and two monitoring wells at the east of the field). 40

Figure 2.7-The core photo, sedimentary graphic log correlated with X-ray fluorescence (XRF) elemental concentrations for major and trace elements, and high GR curves (GR log and GR core scan) showing the condensed section within Middle Tuscaloosa Formation in well CUF#31F2 from depth 3104.3 to 3106 m (10184.71 – 10190.29 ft). This interval is composed of homogeneous, silt-bearing clay-rich mudstone with high amount of pyrite and organic matter. Presence of highly burrowed interval above the section (depth 3104 m) is associated with slow rates of sediment accumulation and higher activity of the burrowing organisms (sedimentary graphic log and XRF from Lu et al., 2011). 41

Figure 2.8-Two histograms showing average of minimum (a), and average of maximum (b), of the SP values in the 93 studied wells, which were considered for rescaling the SP logs in normalization.....43

Figure 2.9-The normalized SP log in the Lower Tuscaloosa Formation interval showing the shale base line (0% deflection, 12 mV) and, parallel to it, the clean sand line (100% deflection, -134 mV) on the curve as well as the 50% (-61 mV) cut-off line for calculating the thickness of the net sand (yellow shaded) within the Massive Sand Member (gross), correlated with GR and resistivity logs.....44

Figure 2.10-An interpreted seismic cross-line extracted from the seismic volume at reservoir level. There are two relatively strong peak separated by a strong trough corresponding to the Tuscaloosa sand units. Black line is smoothed approximation of the top of reservoir interval (E and D Units) (courtesy of Meckel, 2011). 45

Figure 2.11-A 30 Hz amplitude stratal slice, Units E and D, Lower Tuscaloosa Formation generated by Zeng, (2009). 46

Figure 2.12-Summarized workflow for generating spectrally blued decomposed 40 Hz stratal volume. Blueing pushes higher limit of the seismic spectrum and allows decomposing of higher frequencies. 48

Figure 2.13-(a) An inline from the original seismic cube, and (b) from the blued seismic cube. Spectral blueing enhances the seismic resolution. Black arrows point to example areas where more details are revealed in blued data (b), in contrast to original data (a). 49

Figure 2.14-40 Hz stratal slice extracted close to top reservoir (E and D Sand Units) shows more details of the incised valleys system and sand body distribution. A meandering feature is revealed by red color and is outlined by the thick black dashed lines. Outline of the Cranfield filed can be estimated by the oil rim and gas cap from SECARB phase II final report (2011). 50

Figure 2.15-The Wells with sand units thicker than 60 ft are overlaid on the 40 Hz stratal slice corresponding to top reservoir. Most of the wells are located inside the meandering feature on seismic. Wells are labeled with sand thickness...……52

Figure 2.16-Net-sand map of the Massive Sand Member, generated from well data and constrained by seismic. The map shows the extension and geometry of the sandy intervals that are the reservoir in the Cranfield Field. 53

Figure 2.17-Histograms showing the minimum, maximum and mean of the yearly production rate for oil (a), and for gas (b), in the 57 wells at Cranfield Field. 54

Figure 2.18-Bubble maps showing the average yearly oil (a) and gas (b) production. The radius of each circle varies in size depending on the yearly production rate's magnitude. The areas with higher rate of hydrocarbon production match with the higher sand thickness in these areas. Locations of oil rim and gas cap that are plotted on the maps are from SECARB phase II final report, 2011. 55

Figure 2.19-Schematic plan view of depositional system of the Lower Tuscaloosa Formation from coastal plain to deep basin of the Gulf of Mexico..60

Figure 2.20-Schematic diagram of the Tuscaloosa Group and its related depositional environments within sequence stratigraphic framework in the Gulf of Mexico and Gulf Coastal Plain. 61

Figure 2.21-Schematic representations of the evolution of incised valleys system of the Lower Tuscaloosa Formation during sea level rise, including their sedimentary facies and stratigraphic boundaries: (a) valley incisions during subaerial erosion; (b) aggradational fluvial deposits (Massive Sand Member) during initial relative sea level rise that grade basin-ward to shelf delta and shelf-edge delta systems; (c) aggradational estuarine system (Stringer Sand Member), at the initiation of back-filling; (d) passive infilling of the estuary, with developed central-basin mud and estuary-mouth complexes; (e) marine transgression and deposition of marine mud (Middle Tuscaloosa Formation) (modified from Allen and Posamentier, 1993). 67

Figure 3.1-Three different diagenetic regimes defined by Morad et al., (2000) including: eodiagenesis (burial depth < 2 km and temperature < 70ºC); (2) mesodiagenesis (burial depth ≥ 2 km and temperature ≥ 70ºC); and (3) telodiagenesis, which occurs after uplift and/or tectonic inversion. 72

Figure 3.2-Sedimentary logs of wells CFU#31F2 and CFU#31F3 prepared for this study including depth and position of the 57 point counted samples.75

Figure 3.3-Present day framework grains composition of the Lower Tuscaloosa reservoir sandstones, based on the classification of Folk (1980).....78

Figure 3.4-Photomicrographs showing framework grains including (a) quartz grains as dominant framework grain, (b) Microcline grain, (c) partially dissolved and totally kaolinitized feldspars, (d) microquartz grains, (e) metamorphic rock fragment, (f) sedimentary rock fragment. 83

Figure 3.5-Photomicrographs showing (a) partially altered rock fragments, (b) remnant of altered rock fragments as meshwork of chlorite and Ti oxide, (c) muscovite grain, (d) heavy minerals, (e) pore filling matrix, (f) deformation of metamorphic rock fragment and formation of pseudomatrix. 84

Figure 3.6-Restored framework composition of the Lower Tuscaloosa reservoir sandstones is classified as litharenite, based on the classification of Folk (1980), with mean modal composition of $Qr_{58.7}Fr_{2.8}Lr_{38.5}$. 87

Figure 3.8-Cross-plot of porosimeter porosity versus thin section porosity. Upper line and arrow show range of variation between visual porosity and porosimeter porosity. 89

Figure 3.7-Photomicrographs showing different types of pores, (a) intergranular and oversized pores, (b) moldic pore delineated by chlorite coating, (c) intragranular pores within microquartz grain, (d) microporosity within kaolinite; and SEM images showing (e) microporosity within chlorite crystals, (f) microporosity within kaolinite crystals. 90

Figure 3.9-Frequency plots of different types of pores in the 57 studied Lower Tuscaloosa sandstones. 91

Figure 3.10-Frequency plot of distribution of the mean grain size in the 57 studied thin sections. 93
Figure 3.11-Frequency plot of distribution of the sorting in the 57 studied thin sections.....93
Figure 3.12-Combined plots of burial and thermal histories in Well CFU#31F2. 96
Figure 3.13-Combined plots of burial and thermal histories in Well CFU#31F3. 96
Figure 3.14-Photomicrographs showing evidences of compaction as (a) broken chlorite rim due to fracturing of a grain and formation of quartz outgrowth, (b) bent mica, (c) bent metamorphic rock fragment, (d) pressure dissolution; and SEM images showing (e) fractured quartz grain, (f) higher magnification with micro-quartz precipitated in the fracture, indicating formation of the fracture during diagenesis before quartz cementation.....100
Figure 3.15-Cross-plot of IGV versus chlorite coat revealed that sandstones with more chlorite coat cement have undergone less mechanical compaction and thus display overall higher IGV, whereas sandstones with less chlorite coat cements were subjected to a considerable compaction and reduction of pore space during burial and thus lower IGV. 101
Figure 3.16-Cross-plot of IGV versus thin section porosity confirmed that samples with higher chlorite coat content and thus higher porosity were less compacted than samples with lower amounts of chlorite coats and thus lower porosity.....101

Figure 3.17-Graph of intergranular volume vs. cement of Houseknecht (1987), showing relative importance of compaction and cementation to porosity reduction. Although both cementation and compaction were important in reducing the original porosity, compaction was slightly more important than cementation in determining ultimate porosity103

Figure 3.18-Pie charts that show relative average amounts of authigenic minerals as (a) cement and (b) replacive phases. 104

Figure 3.19-Frequency of authigenic chlorite in the 57 studied samples. 107

Figure 3.20-Photomicrographs showing (a) pore-lining chlorite, (b) absence of chlorite coats between grain contact, (c) chloritized mica with TiO_2 remnant, (d) chlorite replacing rock fragments; and SEM images showing (e) pore filling chlorite, (f) euhedral platy crystals, displaying face-to-edge crystal habits.....108

Figure 3.21-SEM images showing (a) two superimposed layers of chlorite coats, (b) higher magnification of the previous image, (c) two superimposed layers of chlorite coats on another grain, (d) higher magnification of the previous image and high magnification BSE images showing (e) chlorite coats precipitated perpendicular to the grain surface, (f) X-ray map of distribution of iron element. 109

Figure 3.22-EDS analysis shows that the chlorites are ferroan chlorite / chamosite with variations in their compositions; (a) higher amount of Fe and Mg in the outer layer chlorite coat, (b) lower amount of Fe and Mg in the inner layer chlorite coat. 111

Figure 3.23-Cross-plot of chlorite versus mean grain size shows that the medium to coarse grained sandstones have higher amount of chlorite compared with the fine to very fine grained sandstones.....111
Figure 3.24-Frequency of quartz cement in the 57 studied sandstones. 113
Figure 3.25-Photomicrographs showing (a) quartz cements with thin dustline, (b) quartz overgrowths completely occlude intergranular porosity and form interlocking quartz crystals; and SEM images showing, (c) euhedral quartz overgrowths (d), quartz overgrowths engulfing, and thus postdating, chlorite crystals, (e) quartz outgrowths, (f) euhedral quartz overgrowths engulfing chlorite crystals……...114
Figure 3.26-Photomicrographs showing (a) TiO_2 as remnant of altered ferromagnesian grains, (b) TiO_2 as remnant of altered infiltrated Fe-rich clays (odinite), and BSE images showing (c) TiO_2 rim as remnant of altered grain, (d) well-formed titaniferous crystal (anatase), (e) finely disseminated titaniferous crystals, (f) X-ray map of distribution of different elements (legend shown at the bottom of image) of the previous image.....116
Figure 3.27-EDS analysis showed that composition of opaque aggregates is TiO_2……117
Figure 3.28-Frequency of total TiO_2 in the 57 studied samples.....117

Figure 3.29-BSE image and X-ray maps of distribution of different elements, including (b) Si, (c) O, (d) Al, (e) Ti, (f) Fe, (g) Mg, (h) C, and (i) all of the previous elements in one image showing which element is responsible for the variation. High concentration of titanium in the remnant of altered ferromagnesian grains is representative of the TiO_2. 118

Figure 3.30-Frequency of the authigenic carbonates in the 57 studied sandstones… 120

Figure 3.31-EDS analysis revealed that the carbonate cements are mostly ferroan dolomite/ankerite. 120

Figure 3.32-Photomicrographs showing (a) poikilotopic pore filling ankerite cement completely filling the intergranular pores, (b) ankerite cement filling the secondary pores, (c) BSE image of ankerite pore filling cement, and SEM images showing (d) ankerite engulfing chlorite crystals, (e) euhedral crystal faces of ankerite, (f) close-up view of the previous image. 121

Figure 3.33-Photomicrographs showing (a) pore filling kaolinite, (b) kaolinitized mica displaying accordion-like textures, expand into adjacent intergranular pores, and SEM images showing (c) pore-filling kaolinite with some booklet habit, (d) dickitized kaolinite, (e) photomicrograph of pyrite framboidal aggregates, (f) SEM image of pyrite framboids on the grains surface that are covered by chlorite 124

Figure 3.34-Cross-plots of core porosity versus permeability (a) in Well CFU#31F2, and (b) in Well CFU#31F3. 127

Figure 3.35-Combined burial and diagenetic history diagram showing diagenetic evolution of the Lower Tuscaloosa Formation. 134
Figure 3.36-Cross-plot of chlorite coats versus intragranular plus moldic porosities indicating that chlorites could have originated by dissolution of the rock fragments.....142
Figure 3.37-Schematic model for the two stages of the chlorite coats formation through progressive burial depth. 143
Figure 3.38-Cross-plot of grain size versus original rock fragment abundance does not show any relationship between them. 147
Figure 3.39-Cross-plot of quartz overgrowths abundance versus chlorite coat abundance showing that if the chlorite coat is less than 6%, it could not prevent formation of quartz overgrowths. This graph also shows that the quartz overgrowth volume correlates negatively with variation in chlorite coat volume. 147
Figure 4.1-Reservoir quality interpretation within the studied reservoir interval in Well CFU#31F3 by a combination of core description, core porosity and permeability measurements and petrographic studies.....154

Chapter 1: Introduction

1.1-Introduction and research objectives

Carbon dioxide (CO_2) capture and storage (CCS) in subsurface geologic formations has recently emerged as a feasible alternative for reducing greenhouse gas emission and mitigating global warming (IPCC report, 2005, 2011). Depleted hydrocarbon fields are considered as one of the options for storage of CO_2 (Burruss, 2004; NETL, 2012). The injected CO_2 into reservoir, previously considered depleted, could increase the pressure and result in mobilization of reservoir's remaining oil and thus recovery production, known as CO_2 enhanced oil recovery (CO_2-EOR) (Holloway, 2007; NETL, 2010).

Cranfield Field, located in Adams and Franklin Counties, southwestern Mississippi, USA depleted for 42 years (1966-2008), was targeted for large scale CO_2 injection in 2008, for CO_2-EOR and also for a research program to study different aspects of CO_2 storage. The reservoir and CO_2 injection interval in Cranfield Field is composed of the Late Cretaceous siliciclastic deposits of the Lower Tuscaloosa Formation, situated approximately 3 km (10,000 ft) below the surface.

The Lower Tuscaloosa Formation has been a major hydrocarbon producer in the USA since the1940's and it is thought to have significant remaining potential in both onshore (Gulf Coastal Plain) and deep offshore (Gulf of Mexico) (Mississippi Geological Society, 1957; Hansley, 1996; Meylan, 1997; Dubiel, 2002; Mancini, 2003; Pitman, 2007; McMoRan Exploration Co., 2011; Horn, 2011). The Lower Tuscaloosa Formation is well-known interval in the US Gulf Coastal trend, as generally in this formation growth of grain coating chlorite during diagenesis inhibits quartz cementation, and thus results in high porosity and permeability in deep burial (e.g. Thomson, 1979; Hamlin and Cameron, 1987; Klicman et al., 1988; Genuise and McBride 1990; Paxton et al., 1990; Pittman et al., 1992; Cameron et al., 1992; Ryan and Reynolds, 1996, 1997; Ajdukiewicz and

Lander; 2010; Kordi et al., 2010). Authigenic grain coating chlorite in sandstones, like the Lower Tuscaloosa Formation, attracts the attention of researchers, because of its impacts on reservoir quality and productivity.

The Lower Tuscaloosa Formation at the Cranfield Field produced hydrocarbon for 22 years from 1944 until depletion in 1966 (Mississippi Geological Society, 1957). The CO_2 injection to the reservoir interval was started in June 2008 by Denbury Onshore LLC for the CO_2-EOR (SECARB phase II). Denbury Onshore LLC collaborated with Southeastern Regional Carbon Sequestration Partnership (SECARB) conducted a research program to accomplish goals of the U.S. Department of Energy (DOE) with regard to research on CO_2 storage. Southern States Energy Board manages SECARB and the Gulf Coast Carbon Center (GCCC) of the Bureau of Economic Geology, The University of Texas at Austin conducted the research at Cranfield site on behalf of SECARB. The monitoring plan (SECARB phase III) started in 2009 by injection of CO_2 in down-dip of the reservoir (brine leg) for CO_2 monitoring and studying different aspects of CO_2 storage in deep-brine aquifers.

The efficiency and effectiveness of CO_2 injection in subsurface geological formations for both CO_2 storage and hydrocarbon production in EOR are controlled by reservoir properties that affect reservoir quality, most importantly, porosity and permeability. The injected CO_2 can migrate and distribute through preferential flow pathways that are generated by reservoir quality variation and heterogeneity. Therefore, ascertaining and predicting these heterogeneities within reservoirs are strategic for understanding the reservoir performance. Characterization of reservoir quality is needed throughout the entire "life cycle" of a reservoir from exploration, to field development, through reservoir management and recovery plans for optimum production (e.g., Sneider, 1990; Bloch, 1991; Kupecz, et al., 1997).

Reservoir quality variation and heterogeneity in sandstones are controlled by two main factors: (1) initial or depositional processes that result in lithologic variation control

the vertical and lateral distribution of facies, geometry of sandstone bodies (lens-shaped, tabular, etc.), distribution of mudstone and other low-permeability baffles, sedimentary structures (cross-bedding, burrowing, etc.), primary sedimentary composition, texture (grain size, sorting, etc.) and porosity-permeability network (Milliken, 2001; Ajdukiewicz and Lander; 2010; Morad et al., 2010); and (2) modification of sediments by diagenetic alterations during burial, including physical, chemical and biological alterations. The initial heterogeneities can later act as preferred paths for further overprint by diagenesis during the burial, that can reduce, increase, and/or preserve the original porosity and permeability (McBride, 1984; Worden and Morad 2000; Worden and Burley, 2003; Taylor et al., 2010; Ajdukiewicz and Lander; 2010). Therefore, the results from the interplay of depositional and diagenetic attributes would ultimately determine the reservoir quality.

The main objectives of this study are: (1) to determine the factors controlling reservoir quality, and to establish criteria to aid in finding sandstones with the best reservoir quality in the Lower Tuscaloosa Formation at Cranfield Field, and (2) to use the Lower Tuscaloosa Formation at Cranfield Field as an analog for understanding the chlorite grain-coating origin and processes that can result in good reservoir quality in deeply buried sandstones.

In this dissertation, the fundamental approach to determine the controlling factors and distribution of reservoir quality at the Cranfield Field is identification and quantification of both primary depositional processes and subsequent diagenetic alterations and also linking them. For this purpose, a study was made to determine: (1) the lithofacies and/or facies association based on the cores description; (2) the sequence stratigraphic framework of the Tuscaloosa Group by using well logs combined with core data; (3) depositional environment of the Lower Tuscaloosa Formation; (4) the thickness variations and distribution of sandy intervals at the Cranfield Field by cross-sections, net-sand and seismic maps; (5) the sediments composition and texture as well as type and

amount of porosity, by use of modal analysis; (6) burial and thermal history of the sediments; (7) types, volumes, and distribution of diagenetic alterations and also diagenetic evolution of the Lower Tuscaloosa sandstones throughout their burial history by involving petrographic and geochemical data; (8) origin, process and time of chlorite coating as an important diagenetic factor affecting reservoir quality in deep buried sandstones; (9) integrating depositional characteristics and chlorite coating; and (10) linking sequence stratigraphy and chlorite coating.

This dissertation is structured in four main chapters. Chapter 1 is an overview of CO_2 injection project, the history of the Cranfield site as study area, and geologic setting that is composed of stratigraphic, tectonic and structural settings.

Chapters 2 and 3 investigate factors affecting reservoir quality of the Cranfield Field at different scale of observations. Reservoir quality variation at the Cranfield Field exists at multiple scales from macro to micro, vertical and lateral variations along and across the field. This study is approximately divided into two separate but related scales of investigation, including macroscopic and microscopic scales. The macroscopic scale that is composed of field scale (km-scale) and facies/subfacies scale (m-scale) is studied in chapter 2. The macroscopic scale heterogeneity shows by mapping of substantial lateral and vertical variations in stratigraphic architecture and by determining the amount and distribution of facies/subfacies and sandy intervals within the field. In this chapter, effects of depositional characteristics on reservoir quality are linked to a basin-wide depositional environment and sequence stratigraphic context.

The microscopic scale that is pore/thin-section scale (μm-scale) is studied in chapter 3. The microscopic scale heterogeneity is aimed at determining the mechanical and chemical processes associated with diagenesis and their impacts on reservoir quality. In this chapter, origin and processes of chlorite coating and its effects on reservoir quality in deeply buried sandstones is investigated, as an emphasizing part of the research objectives.

Chapter 4 of the dissertation links between depositional characteristics and the chlorite coating. In this chapter the processes of formation of grain-coating chlorite within contexts of depositional facies and sequence stratigraphy is presented, providing a powerful tool to predict the distribution of chlorite and their impact on reservoir quality within deeply buried sandstone successions.

Therefore, this study integrated sequence stratigraphy, facies, depositional environment, diagenesis, thermal and burial histories, well logs and core data, and seismic attributes to understand the factors affecting reservoir quality of the Lower Tuscaloosa Formation that has significant implications for predicting reservoir quality in other part of the basin. By determining controls on the degree of reservoir quality at the Cranfield Field, a more accurate determination of distribution of flow pathways can be gained. Moreover, understanding of processes controlling the distribution of gain-coating chlorite lends to chlorite prediction modeling that is required for forecasting deep reservoir quality in exploration and development plans.

1.2-CARBON DIOXIDE STORAGE AND ENHANCED OIL RECOVERY

Carbon dioxide (CO_2) sequestration (capture, transport and underground storage) is an emerging technology that has been proposed as one of the efficient techniques for reducing greenhouse gas intensity (IPCC report, 2005, 2011). Anthropogenic emissions of CO_2 released from the large emitters of CO_2, especially stationary industrial sources such as fossil fuel power plants, could be reduced by capture and long-term storage of CO_2 into subsurface geologic formations before it is released into the atmosphere (Fig.1.1).

Depleted hydrocarbon fields are considered as one of the options for long-term storage of CO_2 (Burruss, 2004; NETL, 2012). Nowadays there is a growing interest in recovering remaining oil by injecting CO_2 into depleted reservoir, before the reservoir becomes CO_2 storage (IPCC report, 2005, 2011; NETL, 2012). The enhanced oil

recovery can be done through both displacement and re-pressurization by the injected CO_2 (Lake, 1989). Miscibility of the CO_2 and the reservoir's remaining oil, increases volume and decreases viscosity of the oil, the two important oil recovery factors (Lake, 1989; Marini, 2007). These mechanisms that enable a portion of the remaining oil to be mobilized and produced are known as CO_2 enhanced oil recovery (CO_2-EOR). The CO_2-EOR process provides a significant incentive for bringing depleted fields under CO_2 flood. Currently, in most USA oilfields, about 33% of the original oil in place is recoverable through primary and secondary methods, increasing to 50% to 60% with CO_2-EOR (Lake 1989; Denbury Resources Inc annual report, 2009).

During successful CO_2-EOR operations, oil, brine, and CO_2 will rise or be pumped to the surface though the production wells (Fig.1.1). Oil will be extracted from the mixed fluid (hydrocarbon, water, CO_2) in the separation facilities at the surface, and CO_2 will be re-injected to the subsurface (Fig.1.1). However, not all of the CO_2 that was injected can be returned to the surface. The injected CO_2 as free phase or dissolved phase moves into spaces in the reservoir which it cannot be recovered. It has been estimated that in the CO_2-EOR operation, about 1/2 to 1/3 volume of the injected CO_2 remains in the reservoir (Holloway, 2007; NETL, 2010). Therefore, injection of the captured CO_2 for EOR also results in sequestration of the CO_2.

Eventually, when the hydrocarbon will no longer be extracted from the reservoir at the end stage of EOR, the reservoir can be filled to capacity for long-term storage of CO_2 (Holloway, 2007).

Figure (1.1) shows a schematic diagram of a CO_2 sequestration and CO_2-EOR system.

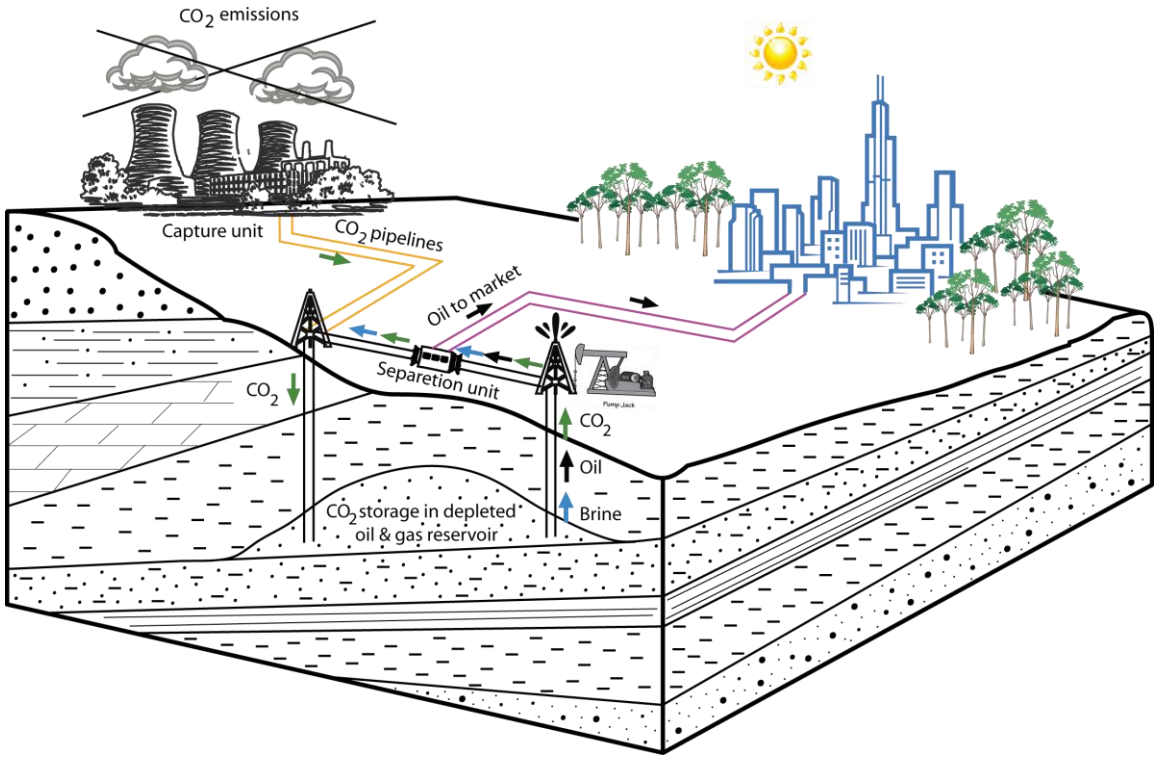

Figure 1.1-Schematic of a CO_2 sequestration and CO_2-EOR system

1.3-STUDY AREA, THE CRANFIELD FIELD AS CO_2 STORAGE AND CO_2-EOR SITE

The Cranfield Field is located approximately 20 km (12 mi) east of the city of Natchez, in Adams and Franklin Counties, southwestern Mississippi (Fig.1.2). This field was discovered in 1943, in a low-relief four-way closure anticline, 6.4 km (4 mi) in diameter created by a deep underlying salt diapirism (Mississippi Geological Society, 1957; Mississippi Oil and Gas Board, 1966).

The reservoir is siliciclastic sediments of the Late Cretaceous Lower Tuscaloosa Formation, situated approximately 2900 m (9,550 ft) subsurface at the crest and 3100 (10,300 ft) subsurface at the eastern flank of the anticline. At the Tuscaloosa interval, dip of the formation ranges from 1° to 3°, with a structural closure of ~ 76 m (250 ft). The reservoir is 14–24 m (45–80 ft) thick, with average core porosity of 25%, and average permeability of 50 md (Mississippi Oil and Gas Board, 1966). The regional top seal for

the reservoir is the Late Cretaceous Middle Tuscaloosa mudstone formation, with average thickness of 60 m (200 ft), however the fine-grained sediments at the top of the Lower Tuscaloosa Formation also act as local confining zone (Lu et al., 2011). The original hydrocarbon accumulation was described as a typical gas cap with underlying oil and water zones (Mississippi Geological Society, 1957; Fig. 1.3).

There are two faults at the Cranfield Field, related to the growth of the underlying salt dome, both NW-SE oriented (Fig. 1.3). One of the faults is at the northeastern flank of the anticline with the southeast compartment being the downthrown and maximum fault throw of ~24 m (80 ft), and the other is southwest of the anticline with the same downthrown compartment northeast of the fault (Mississippi Geological Society, 1957; Nicot et al., 2010, 2012;).

Oil production from the Cranfield Field began in the oil ring in 1944. The productive area of about 31.36 km^2 (3136.31 hectares) was defined by 93 producing wells and 5 dry holes in the field (Mississippi Oil and Gas Board, 1966) (Fig.1.3). Because of declining the reservoir pressure, pressure maintenance program was established in 1947 by reinjection of produced gas to the gas cap to support pressure in the oil rim (Hines, 1950a; Mississippi Oil and Gas Board, 1966). Water was injected for the enhanced oil recovery in 1958-1959 on the western side of the field, however it was considered unsuccessful. Ultimately, the gas cap was produced at the end of the production history and the field was abandoned in 1966 (Mississippi Oil and Gas Board, 1966). Production from the shallower Wilcox Formation, at depth of 1200 m (4000 ft) subsurface in some of the wells continued and it continues today in some wells.

By pressure re-equilibration due to strong aquifer drive during the 42 years abandonment, the reservoir was recovered to original pre-production pressure by 2008, which was the time of CO_2-EOR (Meckel et al., 2008; Lu et al., 2011). The CO_2 with mole fraction of ~98% CO_2 and 2% methane is transported from the natural geologic sources at Jackson Dome, near Jackson, central Mississippi (~160 km away) to the

Cranfield Field via pipeline (Fig. 1.2). In June 2008, CO_2 was injected in the hydrocarbon-dominated media (phase II). The CO_2-EOR was started in the northwest side of the field and moved systematically clockwise around the oil ring. The northern and eastern part of the Cranfield Field is an active CO_2-EOR site by the time of this dissertation (early 2013).

To assess the injection into down-dip saline aquifers below the oil ring (Phase III) three closely-spaced wells were drilled in 2009 on the eastern side of the field (The Detailed Area of Study/DAS) into the brine leg (Fig.1.3). Well CFU#F1 was prepared for CO_2 injection and Well CFU#31F2 and Well CFU#31F3 were drilled as observation wells about 69 m (227 ft) and 111 m (367 ft), respectively, from the injection well, to the east (Fig.1.3). This provided a unique opportunity to track and monitor the injected CO_2 as it moves through the reservoir. Other new injector wells, as well as a few offsets for damaged producer wells were drilled at the northern and eastern part of the field (Fig.1.3). These provided opportunities to collect modern log suites, sidewall cores, and several full cores. Additional collected data including pre-injection 3-D seismic survey, repeat time-lapse surface seismic data (4D), borehole seismic data (cross-well and vertical seismic profiling), pressure and temperature monitoring data, production data, and tracer data created a favorable data-dense experimental setting for measuring reservoir response to the large volumes of CO_2 injection. Measurement and monitoring of the subsurface CO_2 plume, was accomplished in both injection zone (Lower Tuscaloosa Formation) and above-zone (AZMI) in the monitoring interval ~120 m above the injection interval (regionally continues sandy zone in the Upper Tuscaloosa Formation) using a diverse suite of technologies (Fig.1.4). The monitoring data showed significant non-uniformity of fluid flow and demonstrated that the CO_2 travels through at multiple breakthroughs and different flow paths developed over time and injection rate (Meckel et al., 2008; Lu et al., 2012). The initial CO_2 breakthrough to the CFU#31F2 observation well occurred in the lower unit of the Lower Tuscaloosa Formation (unit E), 9 days after

initiation of injection and in the upper unit (unit D) of the CFU#31F3 observation well, 13 days after CO_2 injection. This showed heterogeneity at the Cranfield Field and showed that the reservoir quality variation in the field has profound effects on fluid flow pattern and pathway migration.

By the time of this dissertation (early 2013), the mass of stored CO_2 was around 4 million metric tons (Hovorka et al., 2013). However, the commercial CO_2 injection at the Cranfield Field may continue for decades.

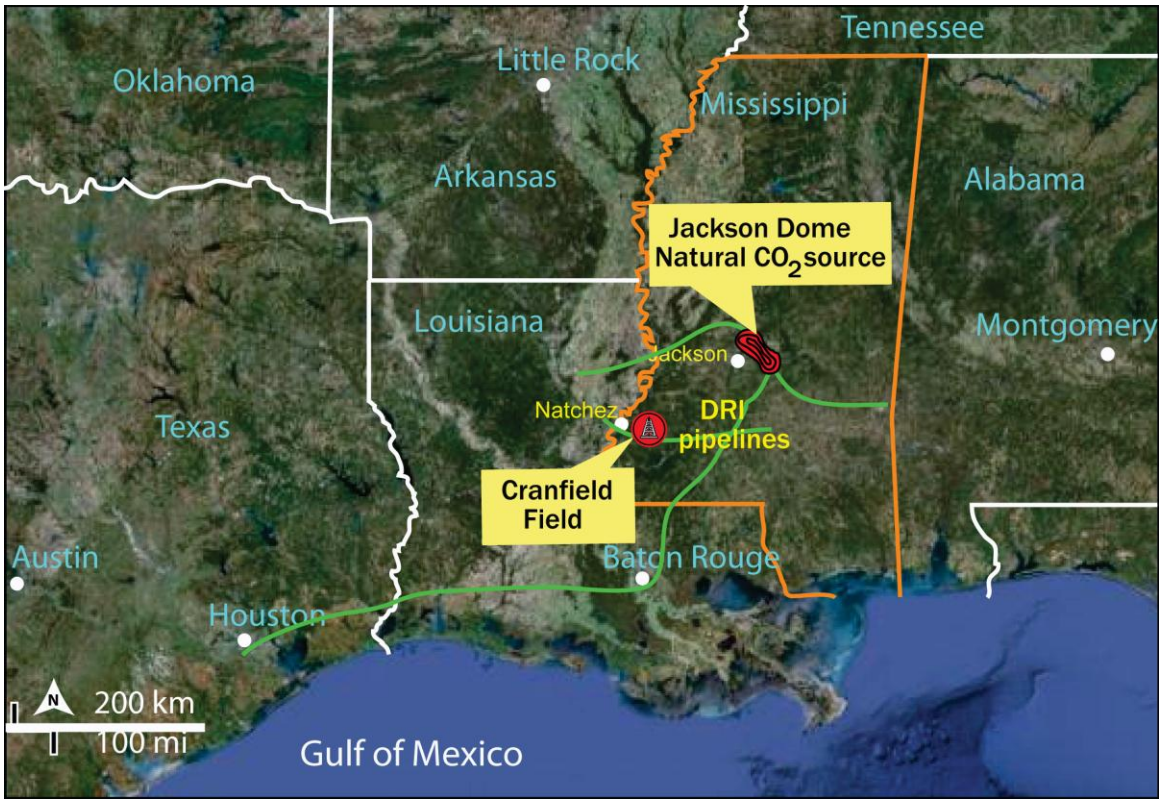

Figure 1.2-Location of the Cranfield Field in the Gulf coast of the United States (Modified from Google map); The CO_2 is transported from the natural geologic sources at Jackson Dome, central Mississippi (~160 km away) to the Cranfield site via Denbury Onshore LLC (DRI) pipelines.

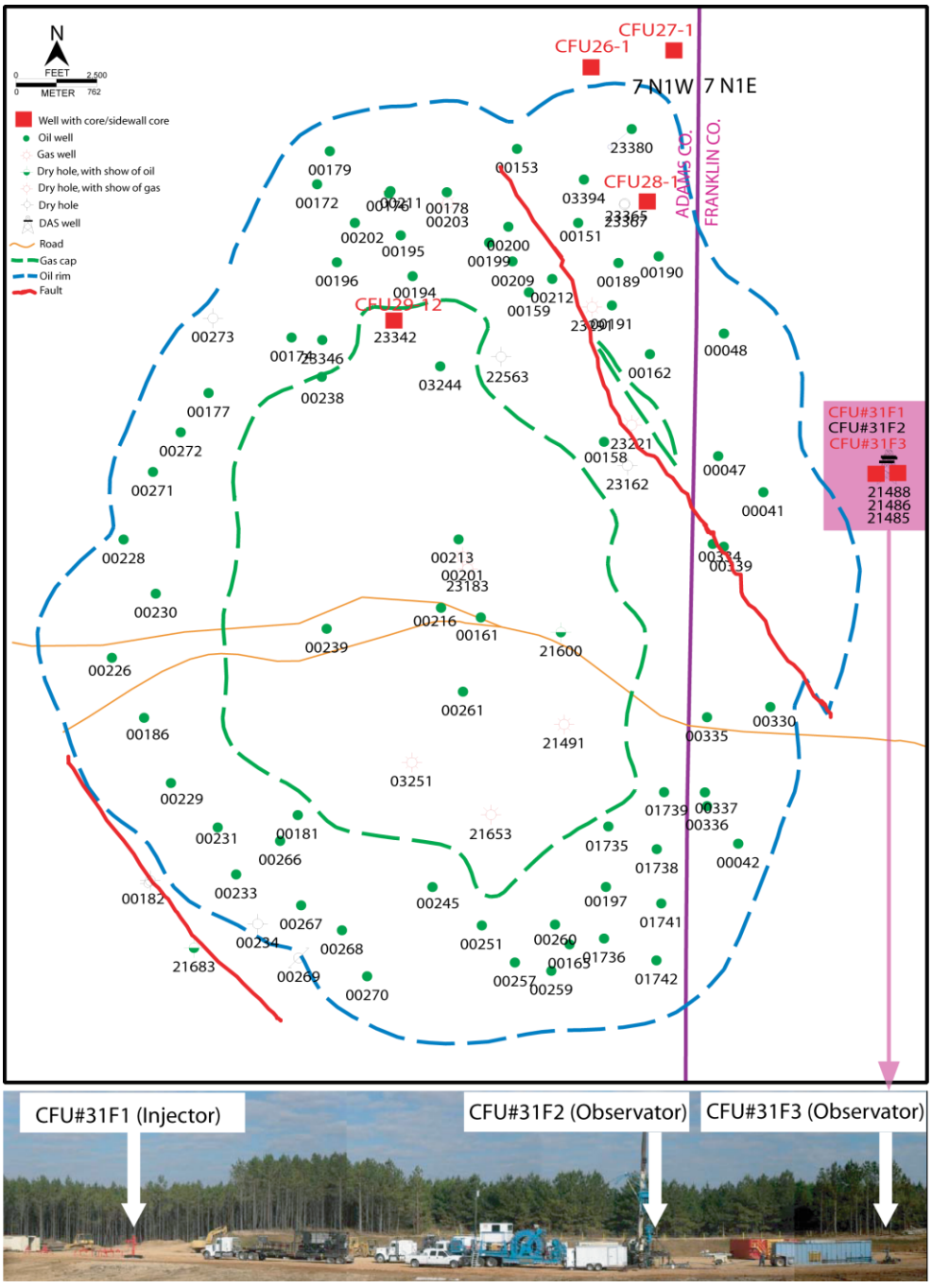

Figure 1.3-Cranfield Field base-map illustrates location of historic and new wells that have been used in this study with the last five number of their API. Wells that have core and sidewall cores are shown by small red rectangle. Locations of roads, faults, oil rim and gas cap are from SECARB phase II final report (2011). Pink rectangle denotes the Detailed Area Study (DAS) and the representative photo (from Hovorka et al., 2013) shows the injector well (CFU#31F1) and two observation wells (CFU#31F2, 69m and CFU#31F3, 111m far from the injector well) that are marked by arrows.

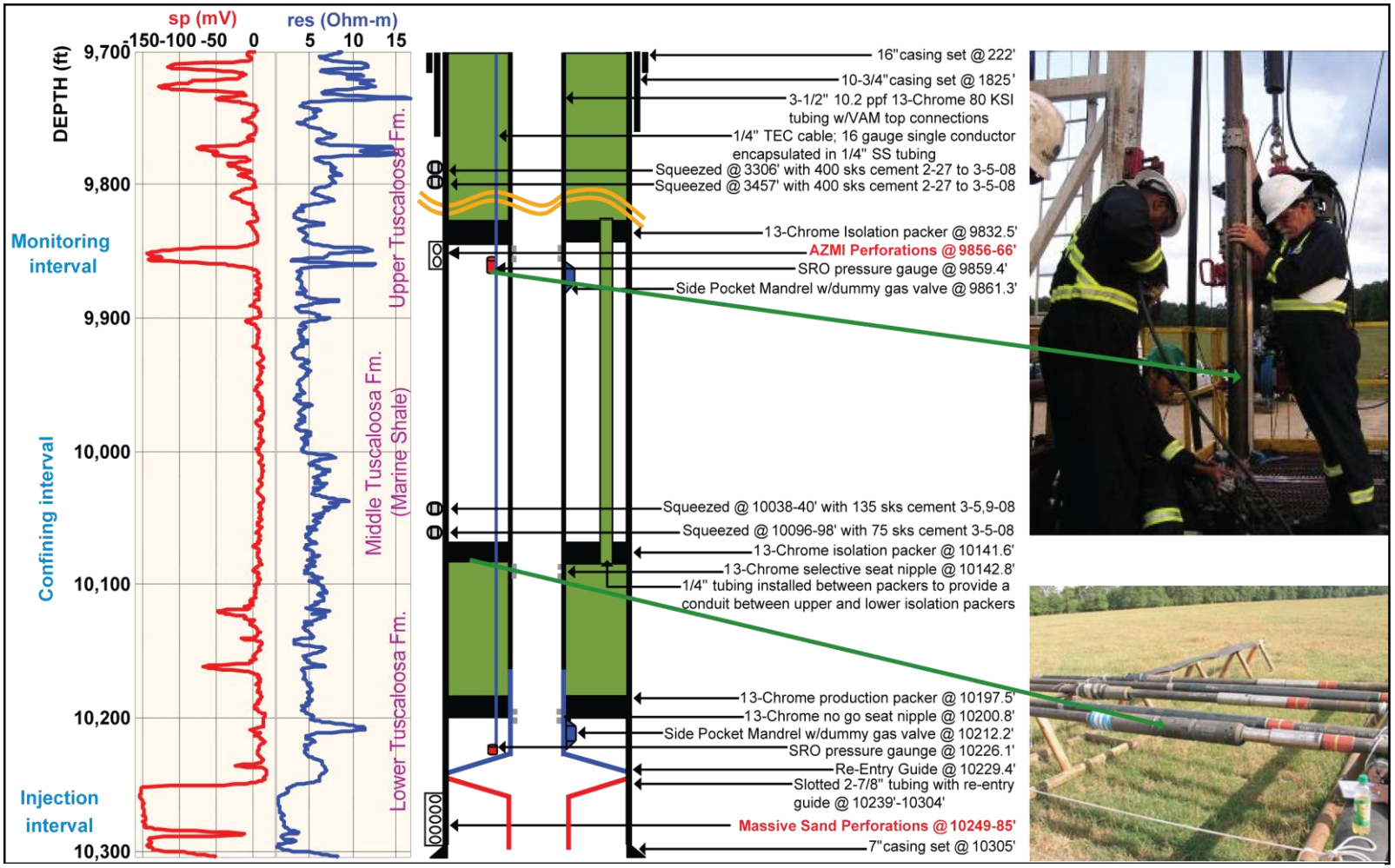

Figure 1.4-Sketch of observation well completion design in the Well Ella G. Lees#7, correlating with resistivity and sp logs showing injection, confining and monitoring intervals (Diagram modified from Meckel et al., 2013, photos courtesy of Meckel, 2011).

1.4-GEOLOGIC SETTING

A key to determine the reservoir quality of the Upper Cretaceous Lower Tuscaloosa Formation at the Cranfield Field is an understanding of the regional-scale stratigraphic, structural and Tectonic relationships in which the sediments accumulated. In this part, based on the literature review, I describe the stratigraphic and structural and tectonic settings in regional scale that are associated with the Cranfield Tuscaloosa reservoir.

1.4.1-Stratigraphic Setting-The Tuscaloosa Group

The term "Tuscaloosa" was used for the first time by Smith and Johnson (1887), based on exposures near the city, county, and river of that name in the western Alabama that occur between the Paleozoic sediments and the Upper Cretaceous Eutaw Formation. The Tuscaloosa Group is distributed over a large geographic area in the subsurface, mainly in Mississippi, Louisiana and Alabama and is time equivalent to the Woodbine Group in Texas (Cameron et al., 1992; Mancini and Puckett, 2005). Table 1.1 shows the lithostratigraphic equivalents of the Tuscaloosa and Woodbine Groups at the subsurface of these states.

The Tuscaloosa Group in the subsurface of Mississippi is divided into three formations including, the Lower Tuscaloosa, the Middle Tuscaloosa or Marine Shale and the Upper Tuscaloosa Formations (e.g. Mississippi Geological Society, 1957; Spooner, 1964; Wiygul and Young, 1987, Mancini, 2008; Table 1.1, Fig.1.5). The contact between the Tuscaloosa Group and the underlying Lower Cretaceous Dantzler Formation (undifferentiated Washita-Fredericksburg Groups) is considered to be unconformable (Mid-Cretaceous regional unconformity) in the Mississippi Interior Salt Basin (Mississippi Geological Society, 1957; Spooner, 1964; Wiygul and Young, 1987; Salvador, 1991; Mancini and Puckett, 2005; Fig.1.5). The upper contact of the Tuscaloosa Group in the northern Gulf of Mexico has been considered as another

unconformity with the overlaying Upper Cretaceous Eutaw Formation of the Eagle Ford Group (Mancini et al., 1995; Liu, 2005; Mancini and Puckett, 2005).

1.4.1.1-The Lower Tuscaloosa Formation

The Lower Tuscaloosa Formation, which is the topic of this study, is the most important formation of the Tuscaloosa Group with respect to oil and gas production and many examples of large reservoirs. It was first discovered in southwest Mississippi at the Cranfield and Brookhaven fields in 1943 and then at Mallalieu and Baxterville fields in 1944 (Hersch, 1987; Hansley, 1996). However, it is thought that the region still has enormous potential for hydrocarbon exploration and development (Meylan, 1997; Dubiel, 2002; Mancini, 2003; Pitman, 2007; McMoRan Exploration Co., 2011).

The Lower Tuscaloosa Formation is composed of intervals of sandstone, siltstone, mudstone and shale deposited during Middle to Late Cenomanian stage (Childs et al., 1988; Mancini and Puckett, 2005). Depositional environment of the Lower Tuscaloosa Formation were described as fluvial to deltaic to nearshore shallow-marine environments (e.g., Devery, 1980; Stancliffe and Adams, 1986; Wiygul and Young, 1987; Klicman et al., 1988; Minter et al., 1992; Petty, 1997; Mancini et al., 1999). The onshore part of the Lower Tuscaloosa, in the north, was deposited in fluvial to fluvial-deltaic environments (Minter et al., 1992; Mancini et al., 1999). Southward, in the more distal part, as the system approached the shelf-edge it increasingly transformed to the shelf and shelf-edge deltas (Petty, 1997; Mancini et al., 1999).

The Lower Tuscaloosa Formation in Mississippi is divided into two informal members: (1) the Massive Sand at the base, which predominantly consists of conglomerate and sandstones with subordinate amounts of mudstones, and (2) the Stringer Sand at the top, which usually contains alternating interbeds of sandstones, siltstones, mudstone and shale (Wiygul and Young, 1987; Mancini et al., 1987, 1999, Minter et al., 1992; Fig.1.5; Table 1.1). The Stringer Sand Member is named Pilot or

Moye sand in Alabama (Payton, 1984; Klicman et al., 1988; Minter et al., 1992; Mancini et al., 1999). Where the Massive Sand Member is not present, the Stringer sand represents the entire Lower Tuscaloosa Formation.

In the Cranfield Field the sandstone and conglomerate zones of the Lower Tuscaloosa Formation are separated by fine-grained sediments, locally known as the "A" through "E" units from top to bottom (Hovorka et al., 2009; Fig.1.5). The two lower units (E and D), which are equivalent with the Massive Sand Member, are the main oil-pay zones produced in the field, the target for CO_2 injection and focus of this study (Fig.1.5). The overlying "A" through "C" units are equivalent with the Stringer Sand and they were not produced for oil, but were produced for gas at the field (Hovorka et al., 2009; Fig.1.5).

1.4.1.2-The Middle Tuscaloosa Formation

The Middle Tuscaloosa or Marine shale Formation in Mississippi is composed of calcareous and organic-rich mudstone with minor very fine-grained sandstone (Smith and Mancini, 1983; Mancini et al., 1987; Lu et al., 2011; Fig.1.5). Based on macro- and microfossils assemblages, the Middle Tuscaloosa Formation was deposited on a shallow open-marine shelf during Late Cenomanian to Middle Turonian stages (Smith and Mancini, 1983; Mancini et al., 1987; Childs, 1988; Mancini and Puckett, 2005; Table 1.1). The base and top contacts of the Middle Tuscaloosa Formation with the Lower and Upper Tuscaloosa Formations are transitional in the Mississippi Interior Salt Basin (Spooner, 1964; Wiygul and Young, 1987). This formation is a useful stratigraphic interval for regional correlation in the area. The Middle Tuscaloosa Formation is the main source rock and also the most important top seal for the Lower Tuscaloosa reservoirs (Evans, 1987; Hersch, 1987; Sassen, 1990; Dubiel et al., 2003). In the Cranfield Field this formation is the regional confining zone for the Lower Tuscaloosa reservoir (Lu et al., 2011).

1.4.1.3-The Upper Tuscaloosa Formation

The Upper Tuscaloosa Formation is mainly comprised of interbedded sandstone, siltstone mudstone and shale (Fig.1.5). A continuous sandy interval is present within Upper Tuscaloosa Formation at the Cranfield Field (AZMI) that acted as CO_2 monitoring interval in the field (Fig.1.4). Age of the formation has been considered to be Middle Turonian to Late Turonian stage (Childs et al., 1988; Mancini and Puckett, 2005; Table 1.1). This formation was deposited in fluvial-deltaic and marine-shelf complex environments (Mancini et al., 1987; Mancini and Puckett, 2005). The Upper Tuscaloosa Formation gradationally overlies the Middle Tuscaloosa Formation; however its contact with the overlying Eutaw Formation of the Eagle Ford Group has been considered as an unconformity in the Mississippi Interior Salt Basin (Salvador, 1991; Mancini and Puckett, 2005; Mancini et al., 2008). The hiatus between the Tuscaloosa Group and the Eagle Ford Group has been considered from Late Turonian to Middle Coniacian (Salvador 1991; Mancini and Puckett; 2005; Fig.1.5). The representative unconformity is recognized in outcrop throughout the eastern and western Gulf Coastal Plain (Pessango 1990).

<table>
<tr><th colspan="11">Generalized Tuscaloosa-Woodbine Subsurface Lithostratigraphic Equivalents</th></tr>
<tr><th>System</th><th>Series</th><th>Stage</th><th>Eastern Texas</th><th colspan="3">Southern Louisiana</th><th colspan="3">Southwestern Mississippi</th><th colspan="2">Southern Alabama</th></tr>
<tr><td rowspan="9">Cretaceous</td><td rowspan="7">Upper Cretaceous</td><td>Santonian</td><td rowspan="3">Eagle Ford Group</td><td rowspan="5">Tuscaloosa Group</td><td rowspan="3">Upper Tuscaloosa Fm.</td><td>Eagle Ford</td><td colspan="3">Eutaw Formation</td><td colspan="2">Eutaw Formation</td></tr>
<tr><td>Coniacian</td><td rowspan="3">Tuscaloosa Group</td><td rowspan="2">Upper Tuscaloosa Formation</td><td rowspan="2">Tuscaloosa Group</td><td>Upper Tuscaloosa Formation</td></tr>
<tr><td>Turonian</td><td rowspan="2">Top Basal Tuscaloosa</td><td rowspan="2">Middle Tuscaloosa Formation (Marine Shale)</td><td rowspan="2">Middle Tuscaloosa Formation (Marine Shale)</td></tr>
<tr><td rowspan="3">Cenomanian</td><td rowspan="3">Woodbine Group</td><td rowspan="2">Lower Tuscaloosa Fm.</td><td>19600 sandstone 20300 sandstone</td><td rowspan="2">Lower Tuscaloosa Formation</td><td>Stringer Sand Member</td><td rowspan="2">Lower Tuscaloosa Formation</td><td>Pilot Sand Member</td></tr>
<tr><td>Massive Sand Member</td><td>Massive Sand Member</td><td>Massive Sand Member</td></tr>
<tr><td rowspan="2">Lower K</td><td colspan="2" rowspan="2">Lower K</td><td rowspan="2">Washita-Fredericksburg undifferentiated Group</td><td colspan="2" rowspan="2">Dantzler Formation</td><td rowspan="2">Washita-Fredericksburg undifferentiated Group</td><td colspan="2" rowspan="2">Dantzler Formation</td></tr>
<tr><td>Lower Cretaceous</td><td>Albian</td></tr>
<tr><td></td><td></td><td></td><td></td><td></td><td></td><td></td><td colspan="2">Andrew Formation</td><td></td><td colspan="2">Andrew Formation</td></tr>
</table>

Table 1.1-General stratigraphy of Albian to Santonian deposits showing relationship and variable subsurface lithostratigraphic nomenclature of the Tuscaloosa-Woodbine Formations from eastern Texas to southern Alabama. The studied area (southwestern Mississippi) has been highlighted in yellow (modified from Mancini et al., 2008).

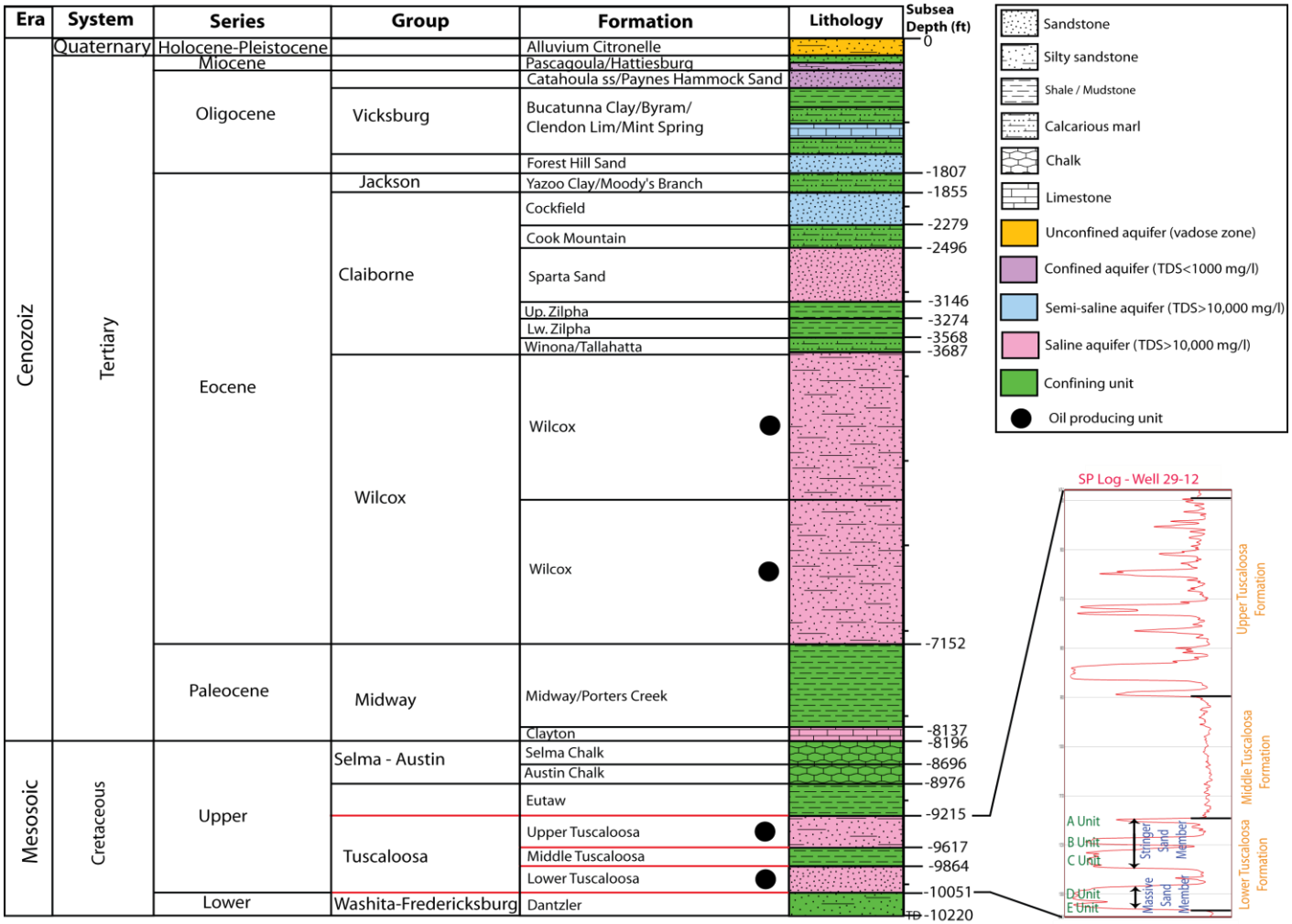

Figure 1.5-Stratigraphic section for Cranfield site developed from literature and adjusted to site-specific conditions. Depths are representative of top intervals in Well CFU#29-12. The SP log in more detail shows the Tuscaloosa Group, its different formations, members and local unit names at the Cranfield Field.

1.4.2-Tectonic and structural settings

During Cretaceous time in the northern Gulf Coastal Plain, three major tectonic and structural features influenced the stratigraphy and sediment distribution of the Tuscaloosa Group. These are the Mississippi Interior Salt Basin, the paleotopographic features, and the shelf margin trend.

1.4.2.1-The Mississippi Interior Salt Basin

The Mississippi Interior Salt Basin is a transform-type passive continental margin characterized by extensional rifting and strike-slip faulting (Pilger, 1981; Miller, 1982; Winkler and Buffler, 1988; Mancini et al., 2001). The structural and stratigraphic framework of the basin has been highly influenced by tectonic history associated with the opening of the Gulf of Mexico due to breakup of the Pangaea, during the late Triassic to Early Jurassic (Pilger, 1981; Miller, 1982; Sawyer et al., 1991; Mancini et al., 1999; Harry and Londono, 2004; Galloway, 2008). As a conclusion of the rifting, low and high crustal blocks generated in the region, that formed salt basins and the uplifts, respectively (Sawyer et al., 1991; Mancini et al., 1999; Fig. 1.6). During this time, the Mississippi Interior Salt Basin, which is the largest in a series of continental margin sag basins (according to the classification of Kingston et al., 1983) in the northern Gulf region, developed along the southern edge of the Ouachita Orogen (Buffler, 1991; Mancini et al., 1999). The basin was actively subsiding depocenter throughout the Upper Cretaceous time providing accommodation space and hosting the Tuscaloosa Group siliciclastic sediments (Mancini et al., 1999).

The basin geometrically extended from present-day east Texas to Louisiana, to Mississippi, to southwestern Alabama and to offshore Florida (Mancini et al., 1999). The Cranfield Filed lies on the northwestern flank of the Mississippi Interior Salt Basin, which is the most productive sedimentary basin for oil and natural gas in the southeastern Gulf of Mexico region and also it has the first rank as the most important provinces in the

North America as ranked by the USGS (Klett et al., 1997; Ahlbrandt, 1999; Mancini et al., 1999, 2001).

1.4.2.2-Paleotopographic features

Paleotopographic features remained before deposition of the Tuscaloosa Group, same as horst and graben systems associated with basement rift, structures related to Jurassic Louann salt movements. Local structures due to igneous activities also had significant influence on deposition pattern of the Tuscaloosa Group (Salvador, 1991; Mancini et al., 2008). The most important heights situated east to west of the Gulf Coastal Plain during the deposition of Tuscaloosa were the Baldwin high, Wiggins arch, Jackson dome, the Monroe uplift, the Lasalle arch, the Sabine uplift and the Liano uplift (Jackson and Laubach, 1991; Fig. 1.6).

1.4.2.3-The shelf margin trend

During the Early Cretaceous, the continental shelf margin developed due to a combination of a change in the slope of the basement by differential subsidence along the crustal hinge zone and Jurassic sediment depositional patterns (Dobson, 1990; Sawyer et al., 1991; Galloway, 2008). Situation of the Early Cretaceous shelf margin strongly affected the depositional patterns and situation of the sedimentary environments during deposition of the Tuscaloosa Group.

The hydrocarbon production from the Tuscaloosa and Woodbine (its equivalent in Texas) Formations is divided generally into three strike-trending regions of the Early Cretaceous shelf margin trend (Fig. 1.7): The updip (shallower than 10,000 ft) which is mostly oil-producing, the middip (10,000 – 16,000 ft depth) which is oil and gas-condensate producing and the downdip (deeper than 16,000 ft) which is gas-producing trend (Harrison, 1980; Hearne and Lock, 1985; Garrison and Chancellor, 1991; Cameron et al., 1992). The updip and the middip trends are located to the north of the shelf edge trend and include fluvial point bar, floodplain, and nearshore marine depositional

environments, whereas the downdip, at the shelf margin and south of the shelf margin are mostly marine facies and delta front deposits (Harrison, 1980; Garrison and Chancellor, 1991).

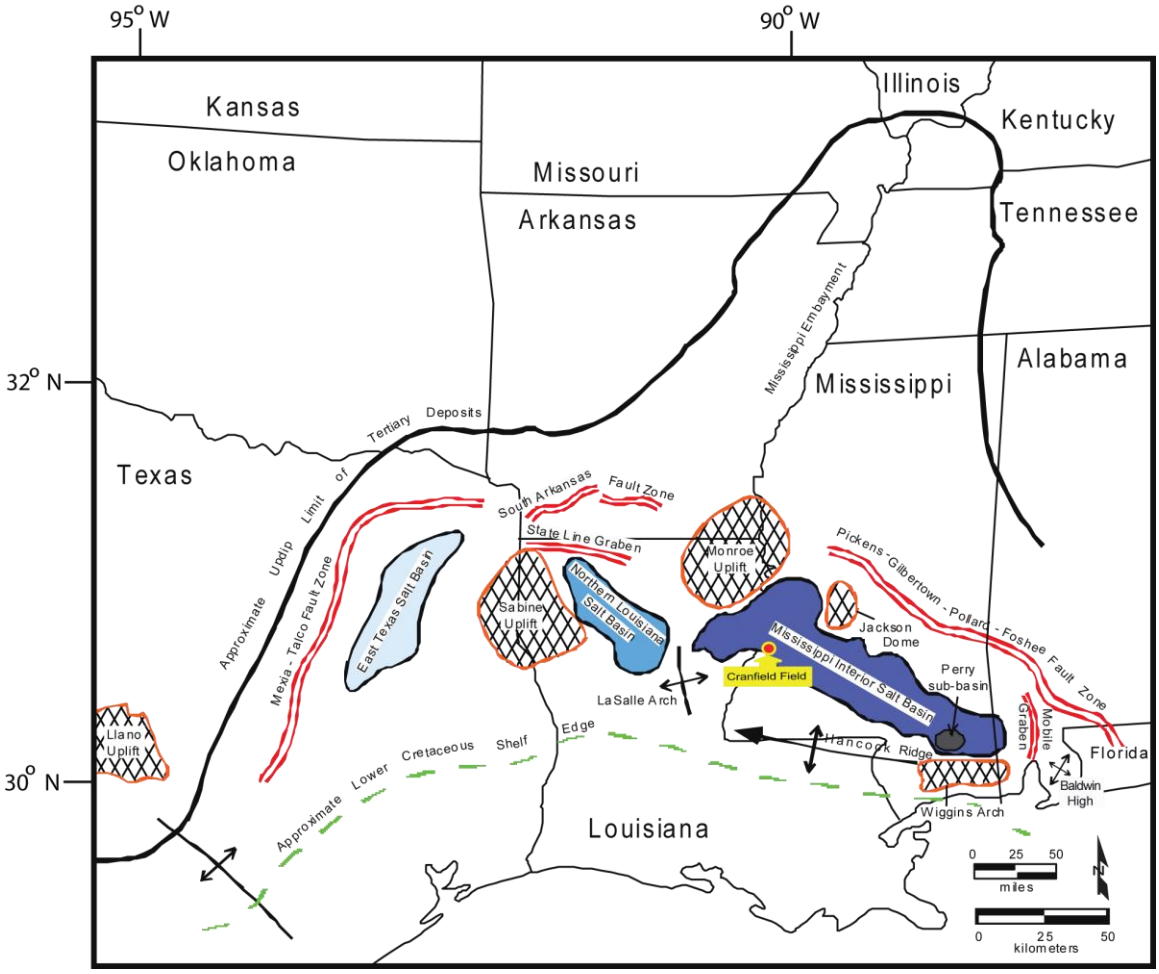

Figure 1.6-Location of the Mississippi Interior Salt Basin and other basins and paleotopographic features during deposition of Tuscaloosa Formation in the northern Gulf Coastal Plain (modified from Pilger, 1981; Mancini et al., 2001).

1.4.3-Sediment provenance

In most of the literature, the provenance of the Tuscaloosa Formation has been considered to be from Laramide orogeny, southern Appalachian and Ouachita Orogenic belts, the southern Arkansas volcanic belt north of the trend and the continental interior (e.g. Salvador, 1991; Corcoran et al., 1993; Sayers and Uddin, 2010; Fig. 1.7). The regional isopach map studies by Woolf and Wood (2011) showed that the majority of sediment feeder valleys were trending from the east and north of the region (ancient Appalachian Mountains) during deposition of the Massive Sand Member. However, the northwestern source from the Ouachita belt has been considered for the Stringer Sand Member (Woolf and Wood, 2011).

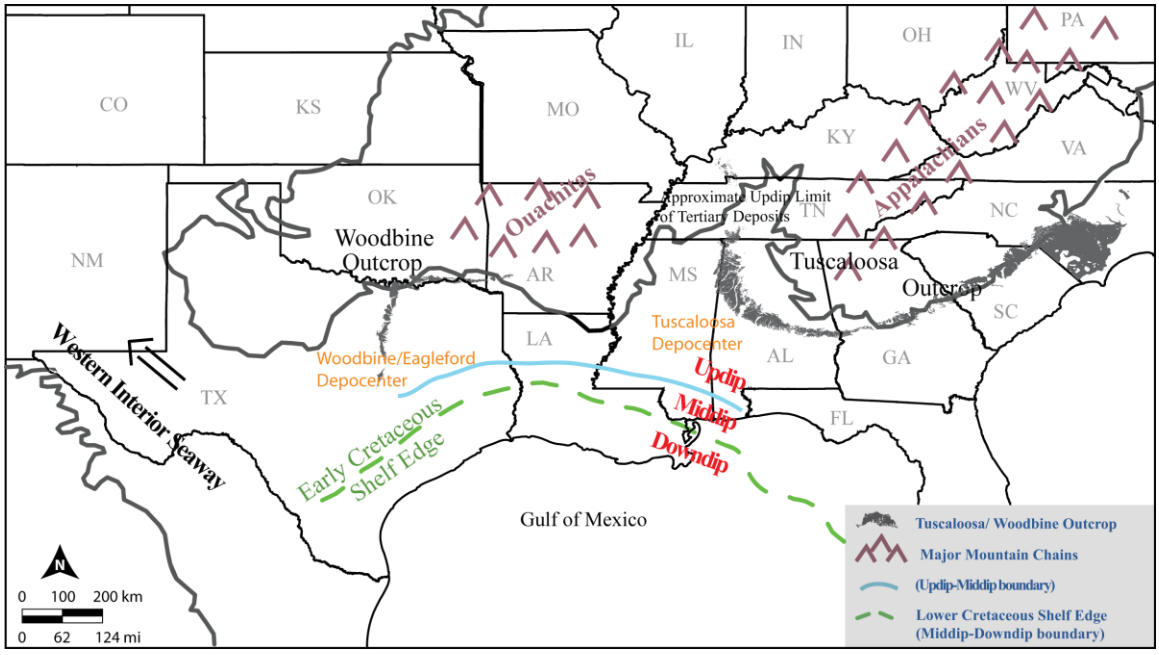

Figure 1.7-Location of the Early Cretaceous shelf edge and updip, middip and downdip trends, location of two main source areas of the Tuscaloosa Formation (the Appalachian, and Ouachita Mountains), depocenter of the Tuscaloosa and Woodbine Formations, and the Gulf of Mexico's connection to Western Interior Seaway of North America. Gray areas denote present-day Tuscaloosa and Woodbine outcrops (modified from Mancini et al., 1996; Dubiel and Pitman, 2004; Mancini and Puckett, 2005).

Chapter 2: Depositional Characteristics Affecting Reservoir Quality

2.1-INTRODUCTION

In the reservoirs, the fluid (hydrocarbon, injected CO_2, etc.) can distribute and transfer through preferential flow pathways that are generated by reservoir quality variation and heterogeneities. For ascertaining reservoir quality and understanding reservoir performance, determining initial or depositional processes that result in lithologic variation during sedimentary deposition is essential. In this chapter, I investigated the depositional system and process that influenced on lithofacies distribution and developed the depositional related heterogeneity in Cranfield Field.

In the previous studies, due to the complex architecture of the sandy intervals and sand thickness variations smaller than the well spacing at the Cranfield site and also due to low resolution of the 3-D seismic data, the reservoir architectures and heterogeneities within the reservoir through the field was not clearly determined. Here in this chapter of the dissertation, I determined the depositional facies and facies associations of the Tuscaloosa reservoir on the basis of log motif and core description. The core descriptions provided direct lithofacies calibration of the log motif and form the basis for depositional facies and sedimentary environment interpretation. I used the log correlation technique to determine the vertical and lateral distribution of the Lower Tuscaloosa Formation and its lithostratigraphic units as well as sequence architecture including system tracts and their boundaries at the field. Net-sand isochore maps and seismic map were provided to find out the sandstone trends and geometry of the sand body reservoirs at the field. I also characterized the production behavior of the Tuscaloosa reservoir by constructing bubble maps for historic oil and gas production.

In the discussions section of this chapter, based on literature and also evidences that have been confirmed by Cranfield Field data, I interpreted the sequence stratigraphy of the Tuscaloosa Group and determined the depositional environment of the Lower Tuscaloosa Formation in the regional context of the basin. This will help us to understand

the reservoir architecture at the field in a local scale, which has been discussed in a separate section.

2.2-DATA SET

a) Wireline logs

Based on depth of penetration to the base of Lower Tuscaloosa Formation and log availability, logs from 93 wells at the Cranfield field were selected for this study. List of the wells that have been used in this study have been reported in Appendix (I). The Spontaneous Potential (SP), shallow and deep resistivity (R_s and R_d) and Gamma Ray (GR) logs, when available, were used for correlation and net-sand mapping purposes. The SP logs are available for all wells; however resistivity logs for 45 wells and GR logs just for 12 wells exist. The logs were combination of the old (1943 - 1966) paper logs and the new (2008 and later) digitized logs. The new wells have more complete modern log suites. However, all of the old paper logs were digitized for the Gulf Coast Carbon Center (GCCC) projects.

b) Cores

Four conventional whole cores (wells CFU#29-12, CFU#28-1, CFU#31F2 and CFU#31F3) as well as sidewall cores in wells CFU#26-1 and CFU#27-1 were collected from the reservoir interval (the Massive Sand Member) during field development after 2008. Core from the seal interval, 14 m (46 ft) from lower portion of the Middle Tuscaloosa Formation for well CFU#31F2, was also collected. All of the cored intervals were calibrated with log data.

c) 3D seismic data

A pre-injection 3D seismic data was acquired over the entire field by Denbury Onshore LLC, in 2007. The main objective of the survey was to get more detailed subsurface geological information. It also provided a baseline for further time lapse study and monitoring of the injected CO_2 and other fluids movements.

d) Cumulative production data

Oil and gas cumulative production data prior to EOR was digitized from historic records by BEG for 57 wells. The cumulative production data show the total amount of water, oil and gas that each well has produced from discovery up to depletion (1943-1966).

2.3-SEDIMENTARY FACIES AND FACIES ASSOCIATIONS BASED ON CORE DESCRIPTIONS

To study the different facies and facies associations, lithologies, fabrics, sedimentary structures and bedding thicknesses, as well as the depositional environment of the Lower Tuscaloosa Formation at the Cranfield Field, I describe the four available whole cores (wells CFU#29-12, CFU#28-1, CFU#31F2 and CFU#31F3) and draw their sedimentary graphic logs. Figure (2.1) shows core photographs of the well CFU#29-12. Figure (2.2) summarizes the sedimentary graphic logs through the cored reservoir intervals in wells CFU#31F3 and CFU#31F2. The sedimentary graphic logs of the Well CFU#29-12 and Well CFU#28-1 are reported in Appendix (II).

The cored intervals are from Massive Sand Member of the Lower Tuscaloosa Formation (named as E and D Units at the Cranfield Field), which are the main oil-pay zone in the field and the target for CO_2 injection (Fig1.5). The lower boundary of the reservoir interval (base of the Lower Tuscaloosa Formation) is an erosional channelized contact with the underlying fossiliferous marine mudstone and carbonate deposits of the undifferentiated Washita-Fredricksburg Groups (Dantzler Formation). Below this contact, which has been recovered at the well CFU#29-12, the Dantzler Formation is composed of bivalve-rich carbonate and dark gray bioturbated mudstone and it has been marked by presence of calcareous nodules at top of the interval (Fig 2.1). The contact between the Lower Tuscaloosa Formation and the undifferentiated Washita-Fredricksburg Groups has been described in publications as a subaerial unconformity

throughout the Gulf Coastal Plain (Mississippi Geological Society, 1957; Spooner, 1964; Wiygul and Young, 1987; Salvador, 1991; Mancini and Puckett, 2005).

In the studied cores the entire reservoir intervals are composed of two fining-upward units (E and D Units), separated by 1 to 2 m of mudstone (Figs 1.5, 2.1 and 2.2). In both fining-upward units, the sediments are predominantly composed of vertically amalgamated, erosionally based, fining-upward cycles from conglomerate to sandstone to mudstone. Thicknesses of the cycles varies from 30 cm to 5 m, separated by mudstone deposits with thickens of 10 cm to 2 m. The multiple erosional and depositional episodes (cut and fill) are characteristics of lateral channel accretions. Overall from bottom to top of the interval, the fining-upward cycles become thicker and the sandstones become finer compared with the previous one, indicating upward-decreasing energy of the system, through time.

Each fining-upward unit starts with conglomerates ranging from matrix-supported conglomerate with coarse sandstone matrix, to grain-supported conglomerate with chert and sandstone clasts. The clasts are white- light gray lithic clasts and pale red chert pebble, and moderately to well rounded, up to 3 cm in diameter. The dark-gray shale rip-up clasts (up to 5 cm in diameter) are observed in the basal conglomerate. Some parts of the conglomerates are noticeably cemented; however some parts are not fully lithified. Poorly developed cross bedding, approximately 30º can be observed in the conglomerates.

The conglomerates are generally overlain by light to medium gray to faint green, moderately sorted, very coarse to medium-grained sandstones with scattered lithic and mud rip-up clasts, to more homogeneous, fine-grained sandstones to siltstone. The sandstones mostly exhibit low-angle cross-lamination, horizontal lamination, and flaser bedding. Coal/lignite debris is present parallel to the sandstone laminations. Mud rip-up clasts are mostly observed in the coarser grain sandstones. Top of the some fining-upward cycles are overlain by 10-30 cm dark gray to black mudstone deposits.

Sediments of the lower unit (E) are composed of more homogeneous conglomerate and very coarse grained sandstone with abundant large, chert pebbles and less shale breaks, while the upper unit (D) has finer grain size sandstones with scattered lithic clasts and basal pebble lags, more mud drapes and cross-beddings, indicating decreasing energy through the time.

Uppermost part of the reservoir interval (top of Unit D) in most of the cores was capped by red-brown, mottled, burrowed mudstones with 2 to 4 m thickness (Figs 1.5, 2.1 and 2.2). The mottled texture and the observed root casts in this part are indicator of soil-forming processes (paleosol) in a terrestrial environment and overbank/interfluves deposits.

Overall, a total of 13 facies and 2 facies associations including valley-fill/channel-fill/ point bar and overbank/interfluves deposits were distinguished in the studied cores. Table (2.1) shows the facies, facies associations and their lithology in the reservoir interval.

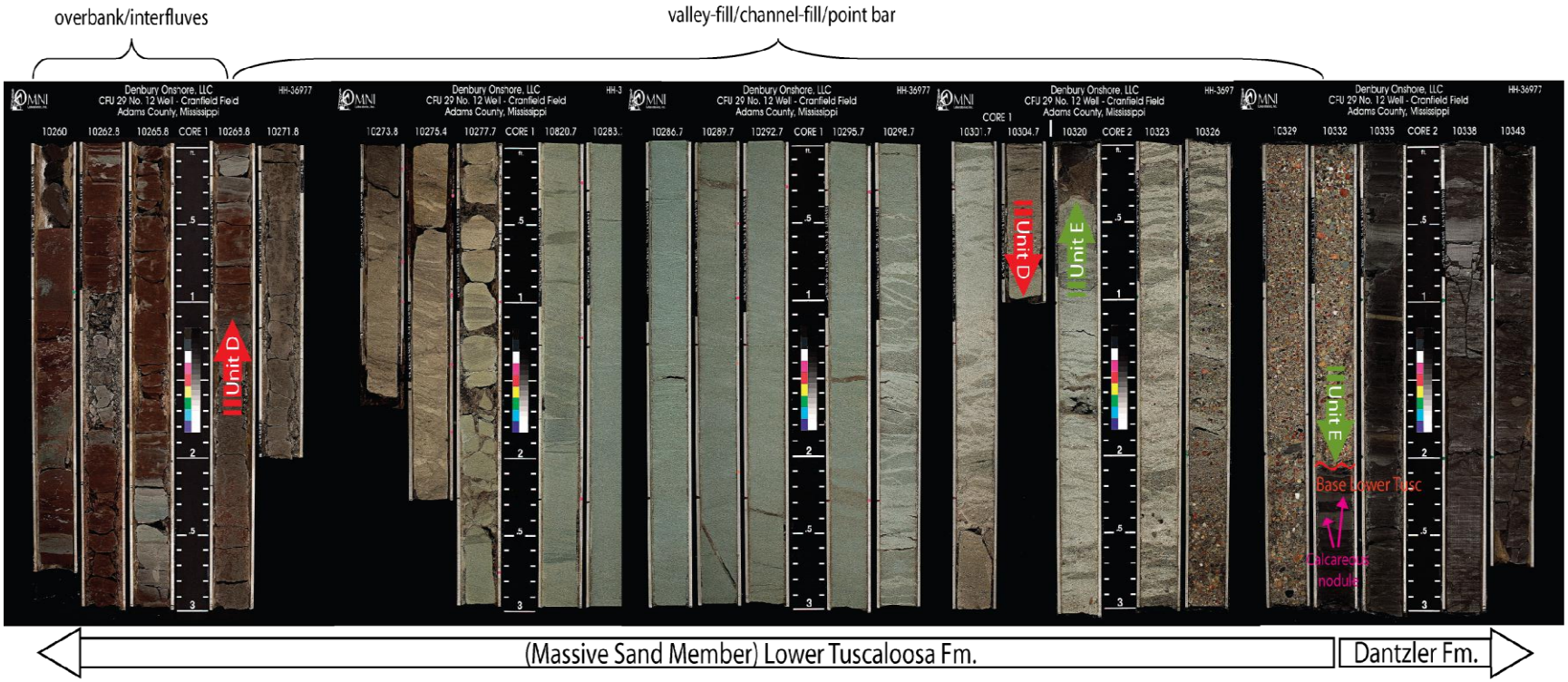

Figure 2.1-Core photographs of the well CFU#29-12 showing D and E units (Massive Sand Member) of the Lower Tuscaloosa Formation that is reservoir interval at the Cranfield Field and their related facies associations. Contact of the Lower Tuscaloosa Formation and the underlying Dantzler Formation is an erosional channel that is marked by presence of the calcareous nodules at top of the Dantzler Formation.

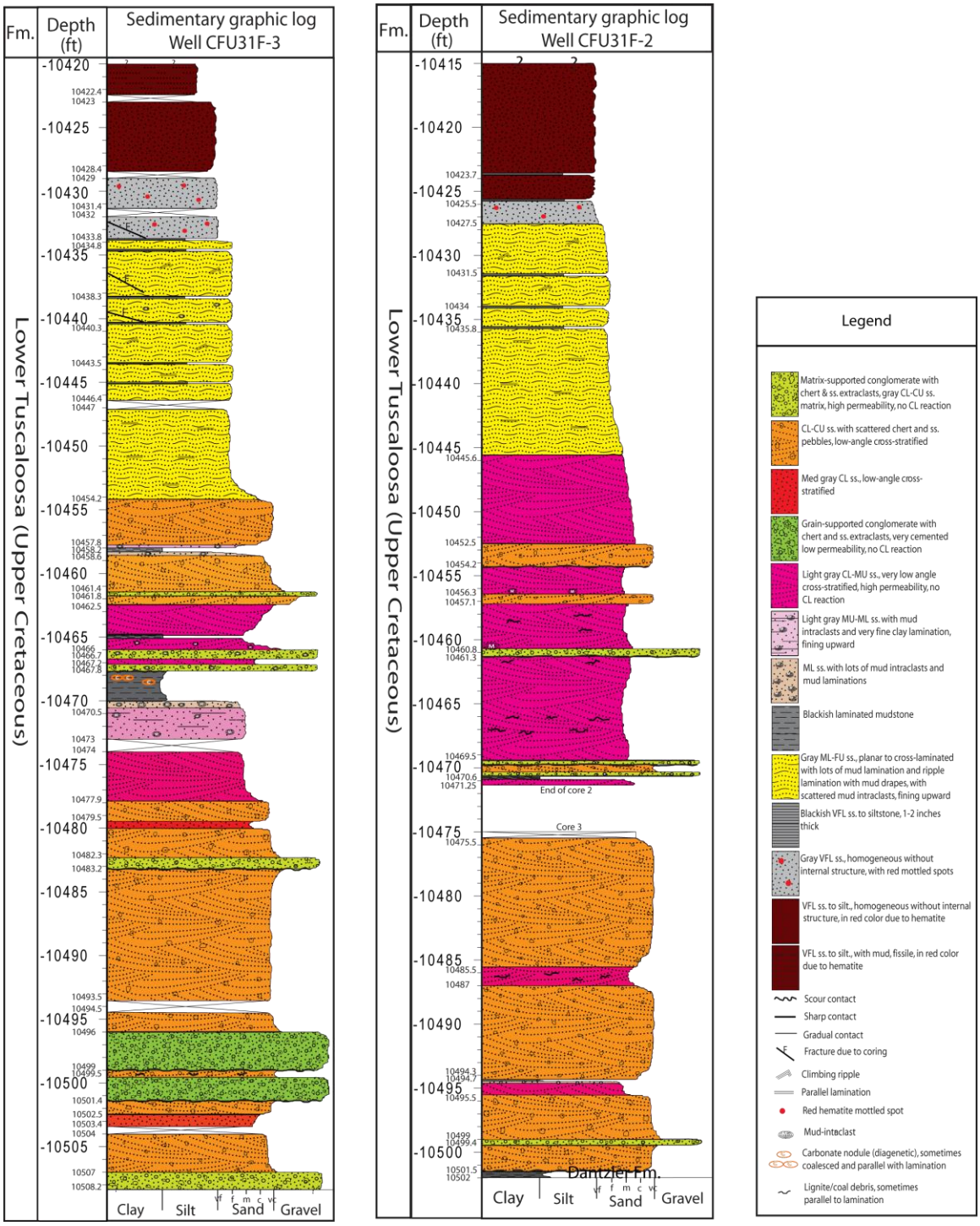

Figure 2.2-Sedimentary graphic logs through the cored reservoir intervals in wells CFU#31F3 and CFU#31F2.

Facies	Facies association	Lithology
1A	Valley-fill / channel-fill / point bar	Grain supported conglomerate
1B		Matrix supported conglomerate
1C		CL-CU ss. with scattered chert and ss. pebbles
1D		Med gray CL ss.
1E		CL-MU ss., low angle cross-stratified
1F		MU-ML ss. with mud intraclast
1G		ML ss. with mud intraclast and mud lamination
1H		ML-FU ss. with ripple lamination
1I		Grey VFL ss., homogeneous
1J		Blackish VFL ss. to siltstone
1K		Blackish laminated mudstone
2A	Overbank / interfluves	VFL ss., red color due to hematite
2B		Red VFL ss. with mud, fissile

Table 2.1-Summary of the principal lithologies and facies interpretation for the 13 main facies and 2 facies associations that comprise the Massive Sand Member of the Lower Tuscaloosa Formation, Cranfield Field.

2.4-LITHOSTRATIGRAPHIC CORRELATION USING WELL-LOGS

In order to determine geometry of the Tuscaloosa Group, the Lower Tuscaloosa Formation and its lithostratigraphic units, particularly the Massive Sand Member (reservoir), and distribution of the related depositional facies at the Cranfield Field, log sets from the 93 wells were calibrated with cores where available and correlated through the field. The logs selection was based on the log availability and depth of penetration to the base of Lower Tuscaloosa Formation. For the lithostratigraphic correlation, cross sections that followed strike and dip transects were constructed using the log sets especially SP, resistivity and GR logs, considering their signature and motif (Figs. 2.3, 2.4a and b). The SP log was available in all wells and it was the most effective tool for identifying dominant lithologies – sand and shale.

In the stratigraphic correlation, the first recognizable formation of the Tuscaloosa Group was the Middle Tuscaloosa Formation (Marine Shale) with a constant high SP and high resistivity zone (Fig. 2.3), readily correlative on all wells. Therefore this formation acted as a key interval and stratigraphic marker in correlation throughout the field.

The Lower Tuscaloosa Formation, positioned below the Middle Tuscaloosa Formation, was determined by a distinguishing lower SP, GR and resistivity log responses (Figs. 2.3, 2.4a and b). The contact of the Lower and Middle Tuscaloosa Formations was marked by a sharp increase in GR and resistivity responses from Lower Tuscaloosa Formation to the Middle Tuscaloosa Formation. Base of the Lower Tuscaloosa Formation was picked at the base of the first recognized sandy interval at the bottom of formation with significant low SP, GR and resistivity readings which corresponds to the basal unconformity. This surface was easily recognizable and correlative across the field.

Due to discontinuous extension of the sandy units (A to E Units) within Lower Tuscaloosa Formation, correlation of all sandy units was not possible; however, top and base of the Lower Tuscaloosa Formation were determined in all of the studied wells. The

Massive Sand Member (E and D Units) at the base of the Lower Tuscaloosa Formation was distinguished in some of the wells (88 wells), characterized by blocky and/or funnel shaped motifs of the SP and GR logs (Figs. 2.4a and b), that are common in channel-fill/valley-fill and point bars. The log correlation showed that the Massive Sand Member has discontinuous distribution through the field. Well log patterns at top of the Lower Tuscaloosa Formation (Stringer Sand Member) showed spiky motifs, with thin shale and sand intervals indicating more heterolithic deposits. The log responses at the Stringer Sand Member (C to A Units) show that the sand intervals became thinner upward.

The Upper Tuscaloosa Formation above the Middle Tuscaloosa Formation (key interval) was recognized by the lower GR and resistivity readings compare to the Middle Tuscaloosa Formation (Fig. 2.3). Basal boundary of the Upper Tuscaloosa Formation was distinguished by a sharp decrease in the Sp, GR and resistivity responses from the Middle Tuscaloosa Formation to the Upper Tuscaloosa Formation. Top boundary of the Upper Tuscaloosa Formation was recognizable by lowering the GR and resistivity responses with ending of the sandstone strata at the top.

The stratigraphic log correlations illustrate vertical and lateral extension of the Tuscaloosa Formations and their lithostratigraphic units. Representative cross sections are shown in Figures 2.3, 2.4a and b. The cross section in Figure 2.3 comprises the whole Tuscaloosa Group in northern and eastern part of the field that has available logs for whole Tuscaloosa Group interval. The Figures 2.4a and b show dip and strike transects for the Lower Tuscaloosa Formation over a distance of about 6.5 km (4 miles) in both directions. All of the cross sections were hung from the Maximum Flooding Surface (MFS), which is relatively a synchronous horizon in the sequence stratigraphic framework (Mancini et al., 1995, 1999). I will discuss the MFS within sequence stratigraphic framework, in the next part of this chapter. Figures 2.5a and b show structure maps on top and base of the Lower Tuscaloosa Formation, based on the collected tops data in the log correlations.

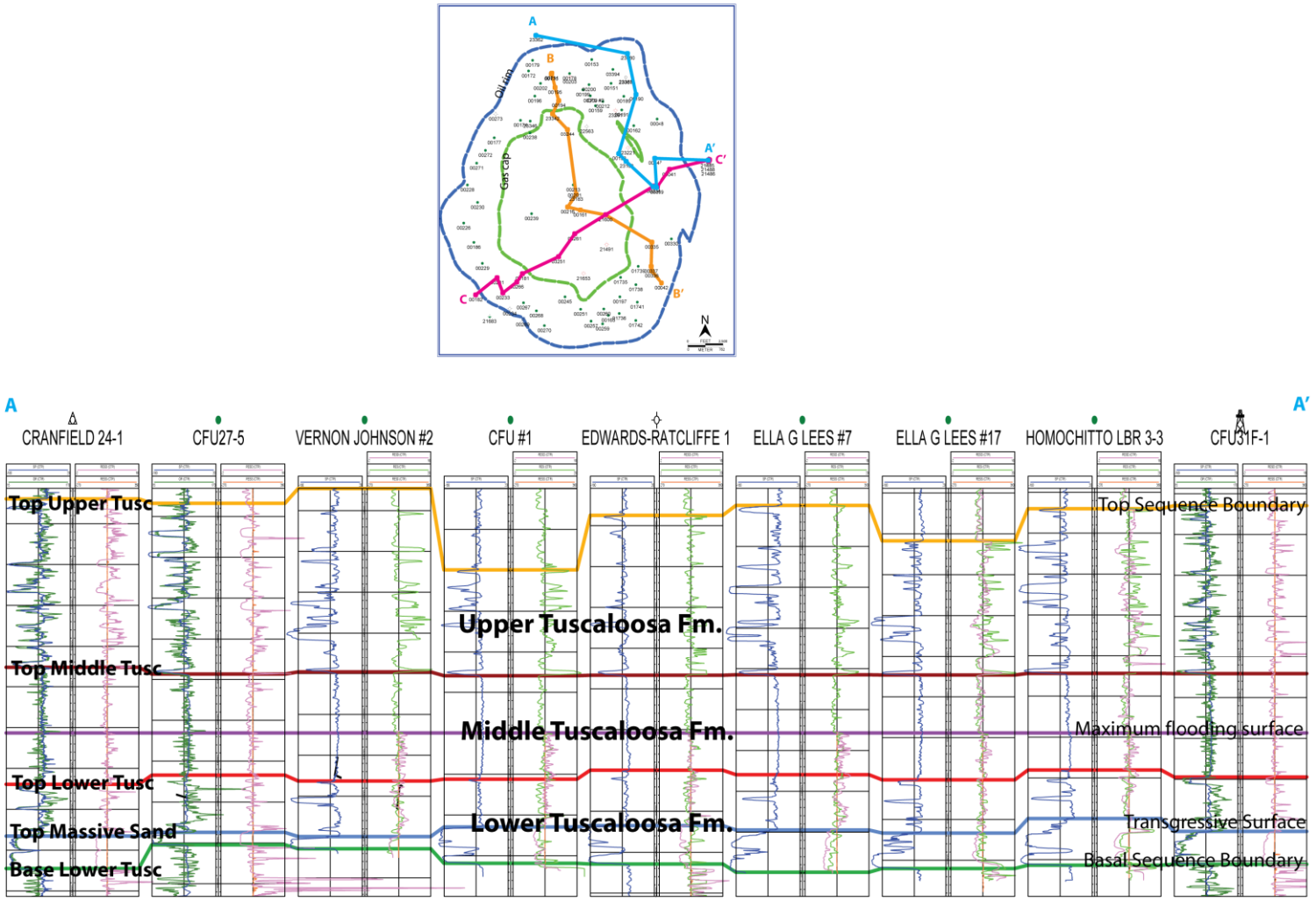

Figure 2.3-Cross section (AA') comprising the whole Tuscaloosa Group at the northeastern part of the field, showing correlation of Lower, Middle and Upper Tuscaloosa Formations as well as the sequence stratigraphic framework that includes different system tracts and surfaces by GR, SP and resistivity logs. The Cranfield Field map shows the position of the cross section.

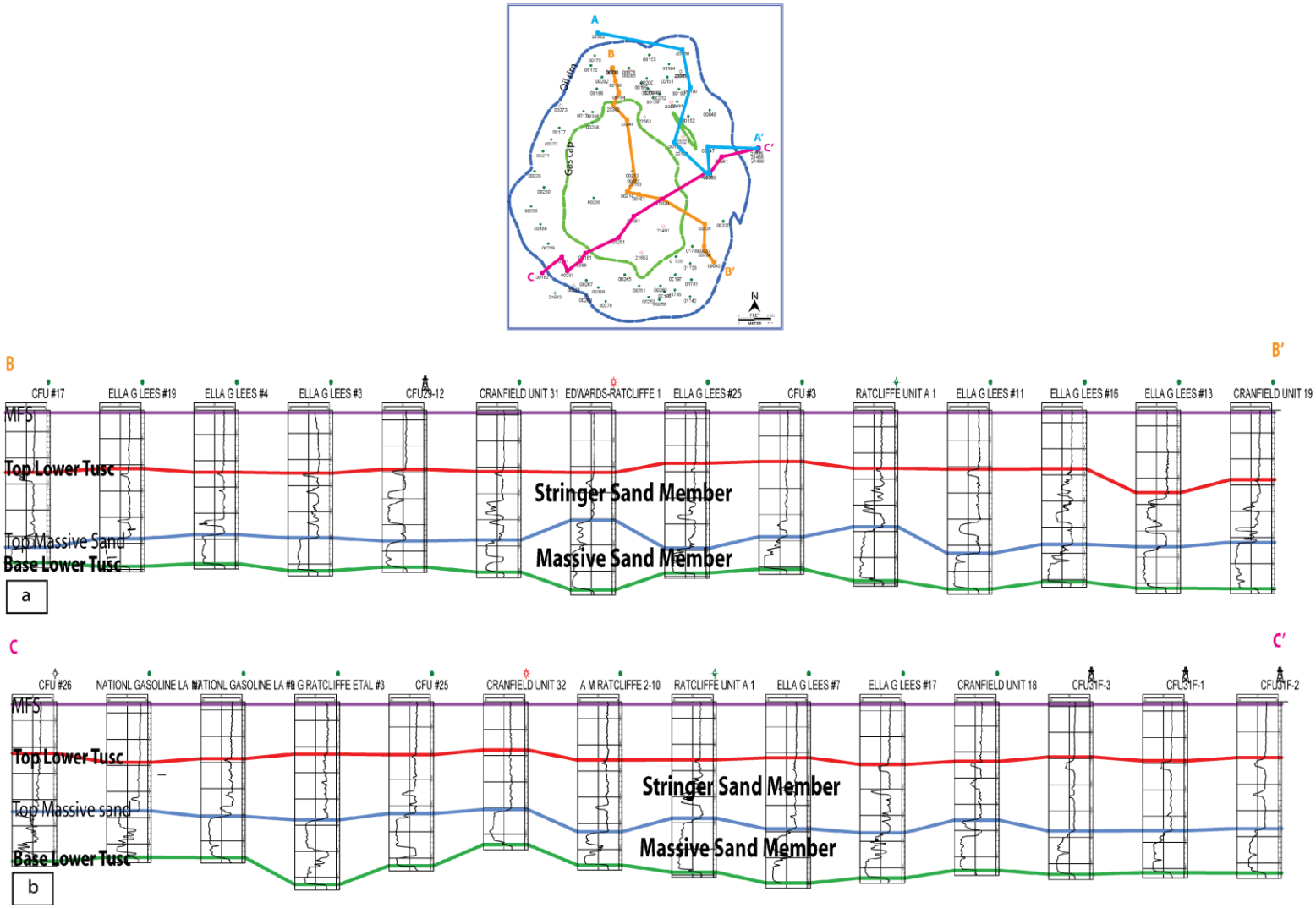

Figure 2.4-(a) Dip transect cross section (BB') correlating the Lower Tuscaloosa Formation and its members over a distance of about 6.5 km (4 miles). (b) Correlation of the Lower Tuscaloosa Formation and its members in strike orientation (CC') over a distance of about 6.5 km (4 miles). The Cranfield Field map shows the position of the cross sections.

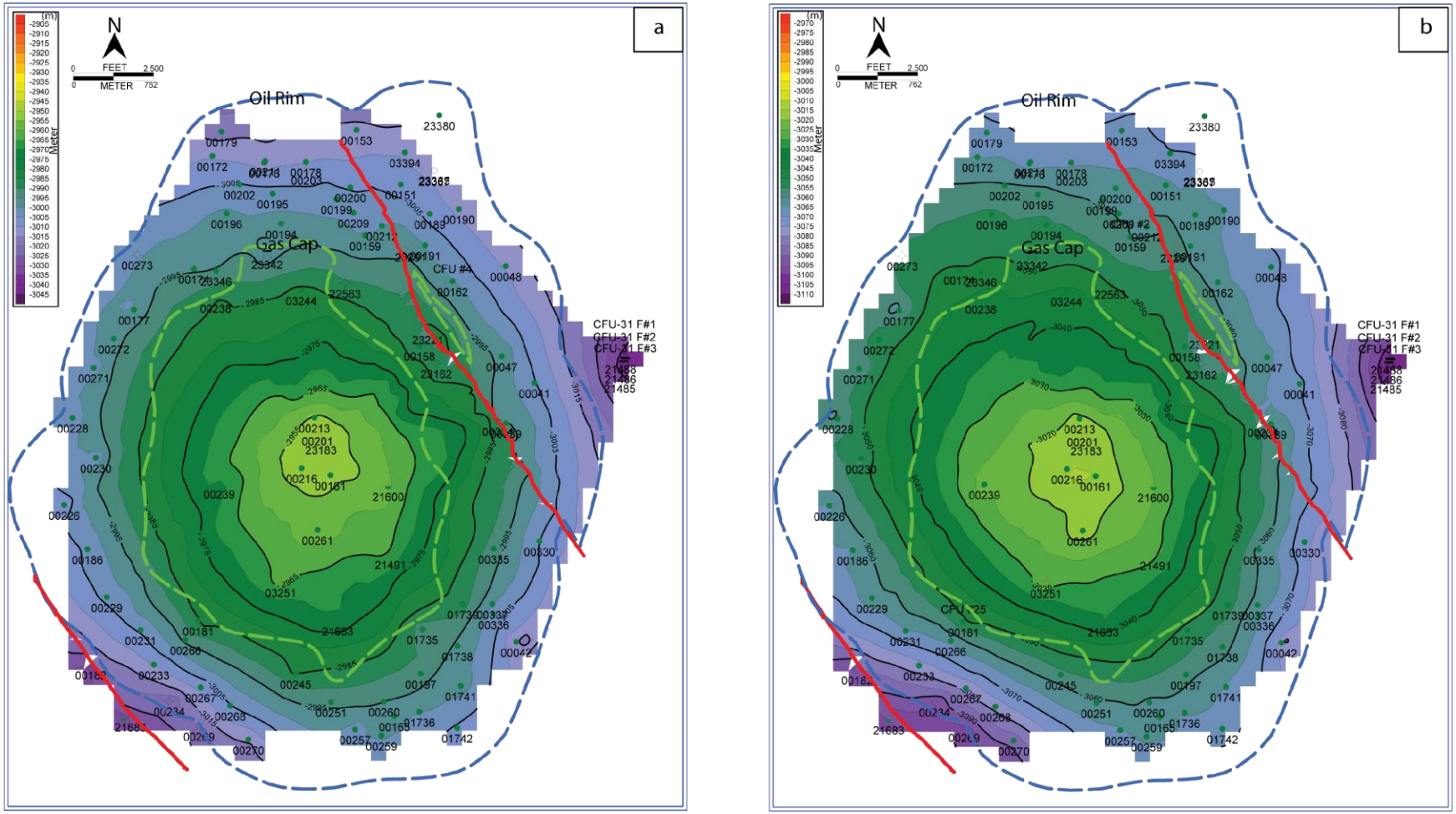

Figure 2.5-(a) Structure contour map of the top of the Lower Tuscaloosa Formation. (b) Structure contour map of the base of the Lower Tuscaloosa Formation. Locations of oil rim, gas cap and main faults that are plotted on the maps are from SECARB phase II final report, 2011.

2.5-SEQUENCE STRATIGRAPHIC WELL-LOG CORRELATION

In order to construct the sequence stratigraphic framework of the Tuscaloosa Group across the field, correlations of the well logs were done by considering log facies stacking patterns. The log sets for the whole Tuscaloosa Group are available in 30 wells, mostly located at the northern and eastern Cranfield Field. The sequence architecture, including system tracts and their boundaries was established based upon a network of dip and strike oriented cross sections using available well logs, preferably SP, resistivity and GR (Fig 2.3). Figure 2.6 illustrates sequence stratigraphic framework of the Tuscaloosa Group, including different system tracts and surfaces correlated with logs of wells in the DAS area (CO_2 injection and two monitoring wells at the east of the field). The sequence stratigraphic interpretation techniques that were applied in this study are based on fundamentals discussed in Van Wagoner et al., (1990), Vail and Wornardt, (1991) and Mitchum et al., (1991a, b and 1993).

The system tracts and surfaces within sequence stratigraphic framework of the Tuscaloosa Group were recognized as below:

- **Basal sequence boundary (Base of the Lower Tuscaloosa Formation)**

The basal sequence boundary (SB) represents an abrupt change from open marine deposits of the predominantly carbonate and mudstone succession below (undifferentiated Washita-Fredricksburg Groups/Dantzler Formation) to the predominantly continental/non marine siliciclastic succession above (Lower Tuscaloosa Formation). This sequence boundary is widely recognized and easily correlates across the entire Gulf Coastal Plain (Mississippi Geological Society, 1957; Spooner, 1964; Wiygul and Young, 1987; Salvador, 1991; Mancini and Puckett, 2005; Galloway, 2008).

From well log readings at the Cranfield Field, the base of the Lower Tuscaloosa Formation corresponds to the basal sequence boundary and is recognized by an abrupt change in the SP and GR responses. It is picked at the base of the first major sandstone at the lower boundary of the Tuscaloosa Group.

- **Lowstand systems tract**

The Lowstand Systems Tracts (LST) of the studied sequence was described as the aggradational to retrogradational stacking of parasequences. They are characterized by stacked sharp-based blocky, blocky serrated or fining-upward motif of SP and GR logs. The LST consist of channel fills/valley fills and point bar deposits of the Massive Sand Member of the Lower Tuscaloosa Formation. The channel fills/valley fills are interpreted to have aggraded during the late LST, through an interval of stable to slow relative base-level rise. The average thickness of the LST is 24 m (79 ft); locally they reach 49 m (162 ft) and show lateral variations.

- **Transgressive systems tract**

The Transgressive Systems Tract (TST) is recognized by retrogradational stacking of parasequences and fining-upward SP and GR log-facies successions of the Stringer Sand Member (above the Massive Sand Member). The TST was deposited during the relative sea level-rise, when the rate of creation of accommodation space was greater than the sediment supply. The overall increase in GR or change to more positive SP log (bell-shape) from top of the Massive Sand towards the Middle Tuscaloosa marine Formation indicates a deepening/fining-upward trend of marine transgression.

The TST terminated in a high GR, high SP, and low resistivity picks within Middle Tuscaloosa Formation, which was interpreted as the Maximum Flooding Surface (MFS). Therefore, the successions in the TST are composed of back-stepping deltaic/estuarine deposits of the Stringer Sand Member overlain by the lower portion of the Middle Tuscaloosa Formation, capped by the MFS. The average thickness of the TST is 70 m (230 ft).

- **Maximum flooding surface**

From log readings, the maximum flooding surface within Middle Tuscaloosa Formation was identified by a shift from higher to lower GR, from more to less positive SP log and from lower to higher resistivity responses. The MFS represents a change from

retrogradational parasequence stacking patterns in the TST (Stringer Sand Member and lower part of the Middle Tuscaloosa Formation) to aggradational and progradational parasequence stacking patterns in the HST (upper part of the Middle Tuscaloosa Formation and the Upper Tuscaloosa Formation) (Fig.2.6).

The seal study and core description of the Middle Tuscaloosa Formation in well CUF#31F2 at the Cranfield Field by Lu et al., (2011) in the GCCC team has reported a 1.5 m thick interval from depth 3104.3 to 3106 m (10184.71 – 10190.29 ft) composed of homogeneous, silt-bearing clay-rich mudstone within Middle Tuscaloosa Formation (Fig. 2.7). I could correlate this zone as a high GR, high SP, low density, high neutron and low resistivity picks in logs of most of the wells (Fig. 2.3). I interpreted this interval as a condensed section. The condensation which was associated with slow rates of sediment accumulation during the maximum transgression resulted in, (1) accumulation of pyrite and organic matter within condensed section (reported in X-ray fluorescence (XRF) elemental concentrations for major and trace elements by Lu et al., 2011), and (2) formation of burrowed interval at top of the condensed section (depth 3104 m; reported in core description by Lu et al., 2011), due to higher activity of the burrowing organisms during this time. Figure 2.7 shows position of the condensed section on the core photo, a sedimentary graphic log correlated with XRF elemental concentrations for major and trace elements, and a GR log and GR core scan in the Middle Tuscaloosa Formation at well CFU#31F2.

- **Highstand systems tract**

Overall decreases in gamma ray or change to more negative SP log (funnel-shape) from the MFS within Middle Tuscaloosa Formation toward top of the Upper Tuscaloosa Formation (a regional subaerial unconformity), represent a regression during the Highstand System Tract (HST). The progradational sequences can be distinguished from either progradational stacking of parasequence cycles, or from the large-scale coarsening/cleaning upward. The HST is capped by another sequence boundary that is

located at top of the Upper Tuscaloosa Formation. The early highstand parasequences represent deposition of mudstone in prodelta or open marine environments (upper portion of the Middle Tuscaloosa Formation), while the late highstand parasequences signify deposition of more sandy intervals in fluvial and delta-front of a prograding delta (Upper Tuscaloosa Formation). The average thickness of HST is 159 m (522 ft).

- **Top sequence boundary (Top of the Upper Tuscaloosa Formation)**

The boundary between the Upper Tuscaloosa and the Eutaw Formations is a regional subaerial unconformity that represents the top sequence boundary (Mancini et al., 1995; Liu, 2005; Mancini and Puckett, 2005). This SB was identified as an abrupt change in the SP and GR log responses at the top of the progradational stacking of HST parasequences cycles.

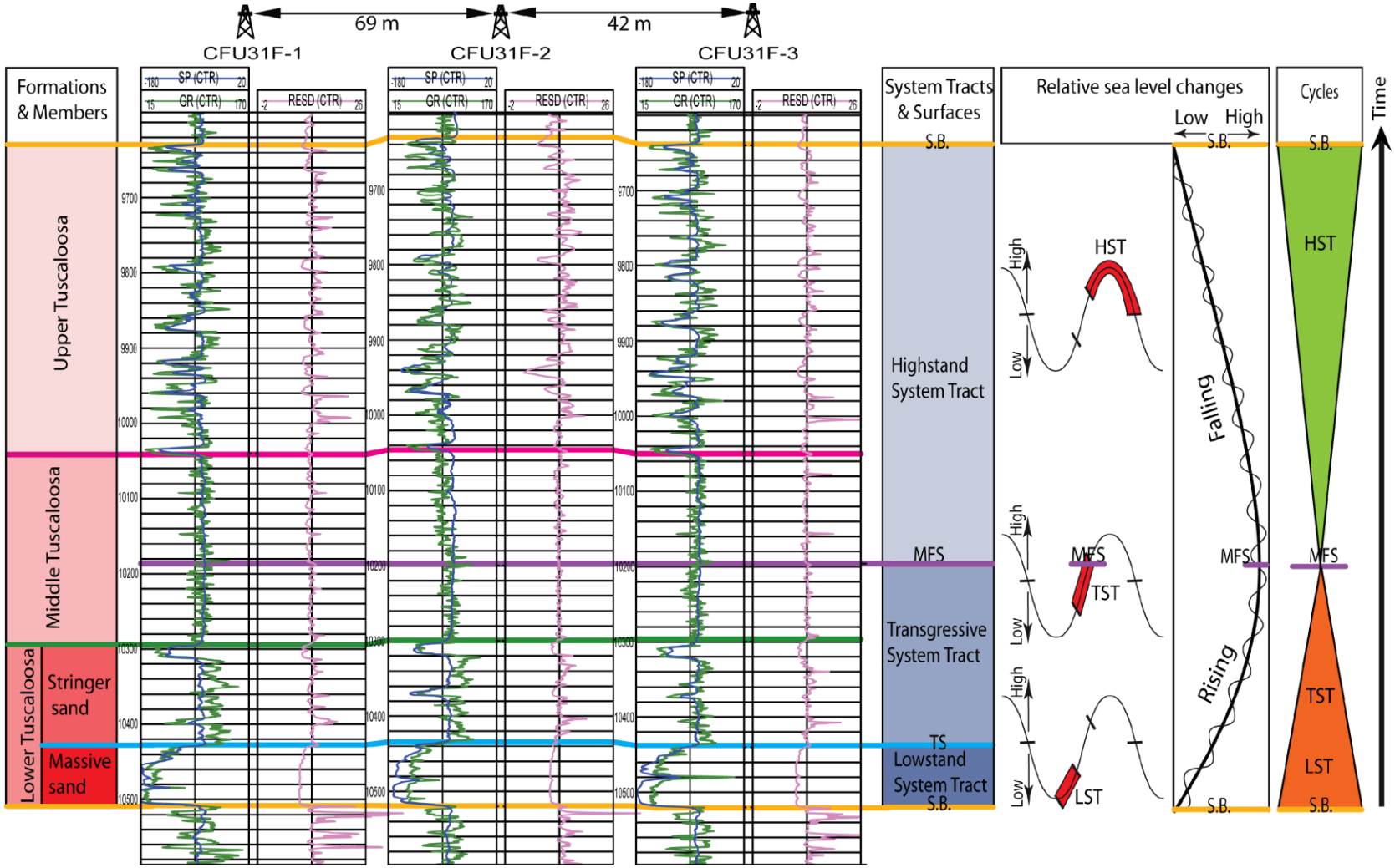

Figure 2.6-Sequence stratigraphic framework of the Tuscaloosa Group, including different system tracts and surfaces correlated with SP, GR and resistivity logs of wells in the DAS area (CO_2 injection and two monitoring wells at the east of the field).

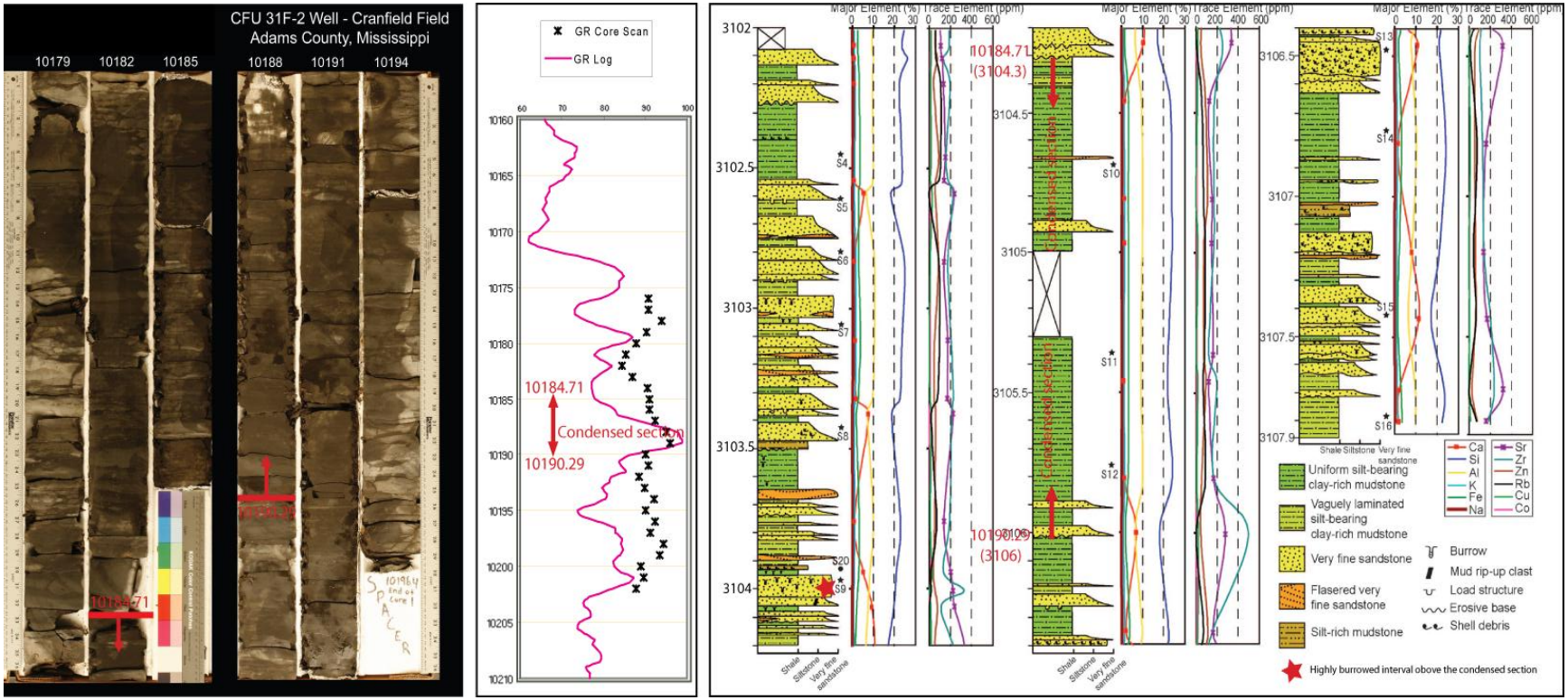

Figure 2.7-The core photo, sedimentary graphic log correlated with X-ray fluorescence (XRF) elemental concentrations for major and trace elements, and high GR curves (GR log and GR core scan) showing the condensed section within Middle Tuscaloosa Formation in well CUF#31F2 from depth 3104.3 to 3106 m (10184.71 – 10190.29 ft). This interval is composed of homogeneous, silt-bearing clay-rich mudstone with high amount of pyrite and organic matter. Presence of highly burrowed interval above the section (depth 3104 m) is associated with slow rates of sediment accumulation and higher activity of the burrowing organisms (sedimentary graphic log and XRF from Lu et al., 2011).

2.6-SAND-SHALE ANALYSIS AND NET-SAND THICKNESS MEASURMENT

After determining distribution of the different formations and their lithostratigraphic units, it is important to find out the extension and geometry of the sandy intervals that are the reservoir and flow pathways in the Cranfield Field. For this purpose, first step is to measure the thickness of sandy intervals within the Massive Sand Member by using the SP logs. This section explains the method used to measure the sand thickness and next section (section 2.7) gives explanations on mapping the reservoir sands based on results from this section and the seismic analysis. To measure the reservoir sand thickness, I analyzed logs from 93 wells, considering depth of penetration to the base of the Massive Sand member.

The process of the calculation of net and gross thickness started by normalization of the SP logs, because the SP logs were not in the same scale. To have a common minimum and maximum value over the studied interval in all wells, the SP logs were normalized by rescaling the curves, using the "Petra" software. The normalization method, which is called the scale range (High-Low) adjustment method, is used when the database includes the old, less sensitive logs with newer, more sensitive logs, same as in the Cranfield site database (Aguirre et al., 2001; Petra software help). For the normalization, the average of minimums and the average of maximums of SP values (-134.283 mV and 11.939 mV, respectively) were statistically considered as minimum and maximum value for the normalized SP logs. Figure 2.8 illustrating two histograms that show average of minimum and average of maximum of the SP values in the 93 studied wells, which were considered for rescaling the SP logs.

After normalization, a SP cut-off was set to calculate the thickness of sandy intervals (net) within the total thickness of the Massive Sand Member (gross). For this purpose, a 50% (-61 mV) cut-off line was created between the shale base line (0% deflection, 12 mV) and the clean sand line (100% deflection, -134 mV) on the normalized SP curve (Fig. 2.9). Calibration of the SP logs with the four described cores showed that

this cut-off is a realistic cut-off for extracting the sandy intervals. After that, net thickness values of the sandy intervals, recognized by this 50% cut-off line, were computed within the Massive Sand Member on the normalized SP curves.

As it will be described in the next section, these measured thicknesses will be used to generate net-sand map for the reservoir guided by seismic data.

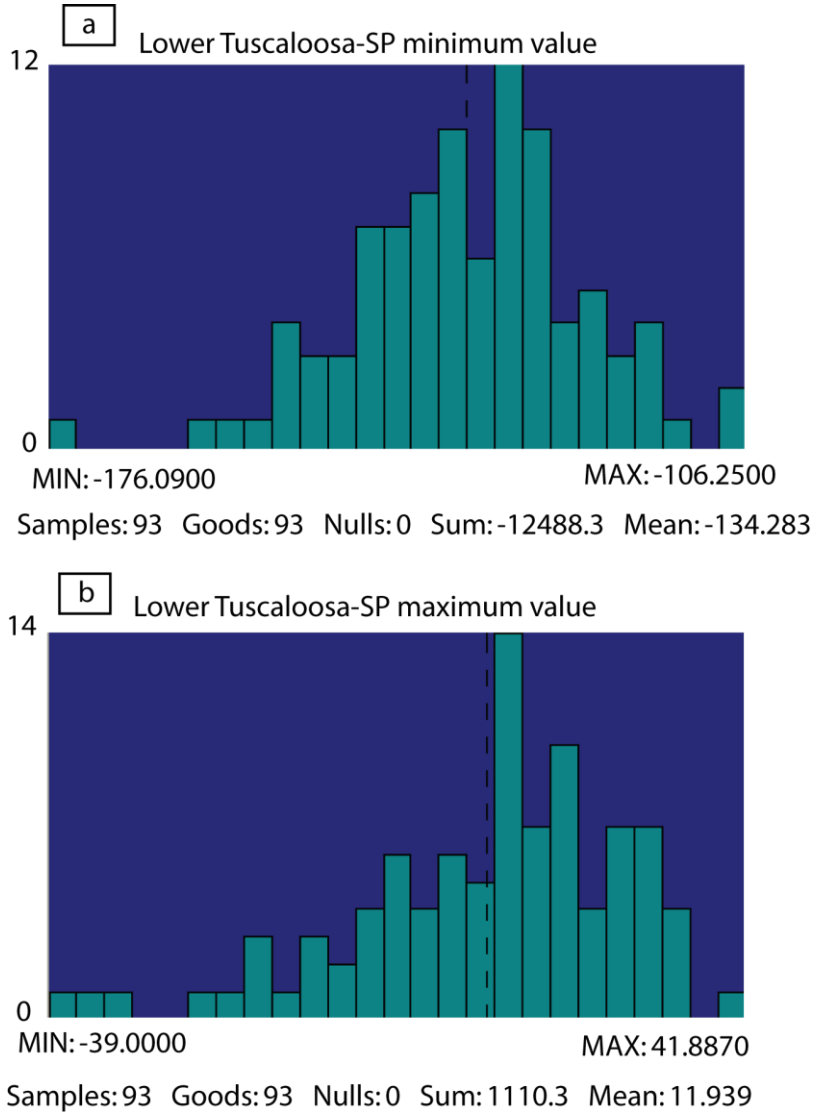

Figure 2.8-Two histograms showing average of minimum (a), and average of maximum (b), of the SP values in the 93 studied wells, which were considered for rescaling the SP logs in normalization.

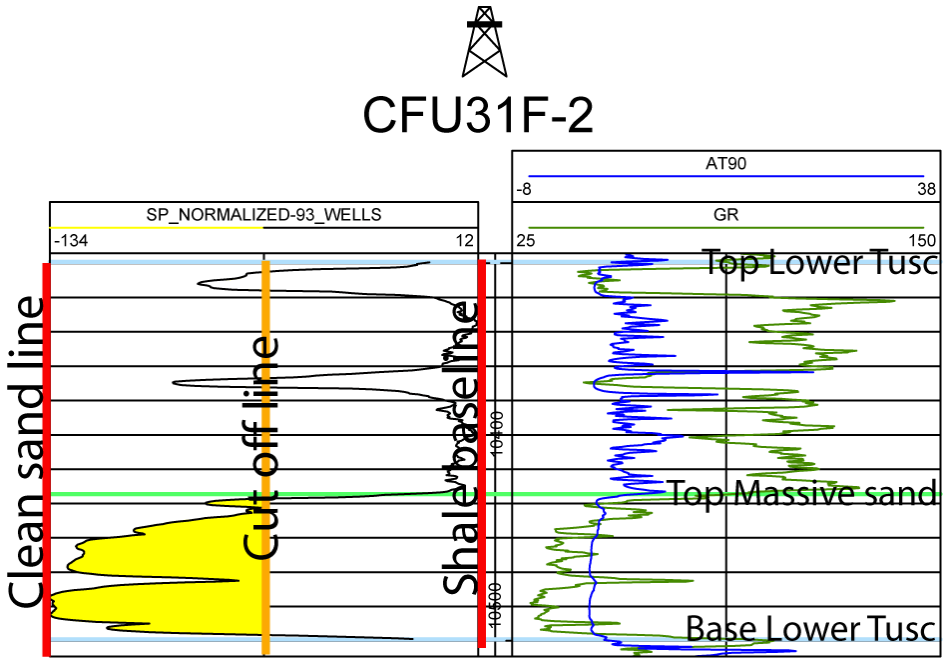

Figure 2.9-The normalized SP log in the Lower Tuscaloosa Formation interval showing the shale base line (0% deflection, 12 mV) and, parallel to it, the clean sand line (100% deflection, -134 mV) on the curve as well as the 50% (-61 mV) cut-off line for calculating the thickness of the net sand (yellow shaded) within the Massive Sand Member (gross), correlated with GR and resistivity logs.

2.7-MAPPING SANDY INTERVALS USING WELL LOGS AND SEISMIC DATA

Stratigraphic interpretation of the seismic data is a valuable technique for determining subsurface stratigraphic facies (Brown and Fisher, 1977, 1980). This section integrates wells and seismic data to map the reservoir sands. Figure 2.10 shows an interpreted seismic inline extracted from the seismic volume. The quality of seismic data in general is acceptable; however resolution of the data in the deeper part is not enough to clearly separate the Tuscaloosa Sand units. Although routine seismic interpretation improved the subsurface structural maps, it did not result in a clear understanding of the sands distribution at the reservoir level, due to poor seismic resolution and weak acoustic impedance contrast between reservoir units.

Despite this limitation, several attempts have been made to use the seismic data for mapping sand bodies through different seismic interpretation techniques. For example, figure 2.11 shows a stratal slice generated from spectrally decomposed seismic data by Zeng (2009); some channel features are suggested using this technique.

As the seismic data are the only available data that gives relatively uniform sampling of the subsurface, they are used to extract more information from the internal architecture of the reservoir through a more sophisticated workflow in this study. Results from this work revealed more details of the sand distribution patterns and is used to constrain the reservoir sands thickness mapping.

are from SECARB phase II final report (2011)

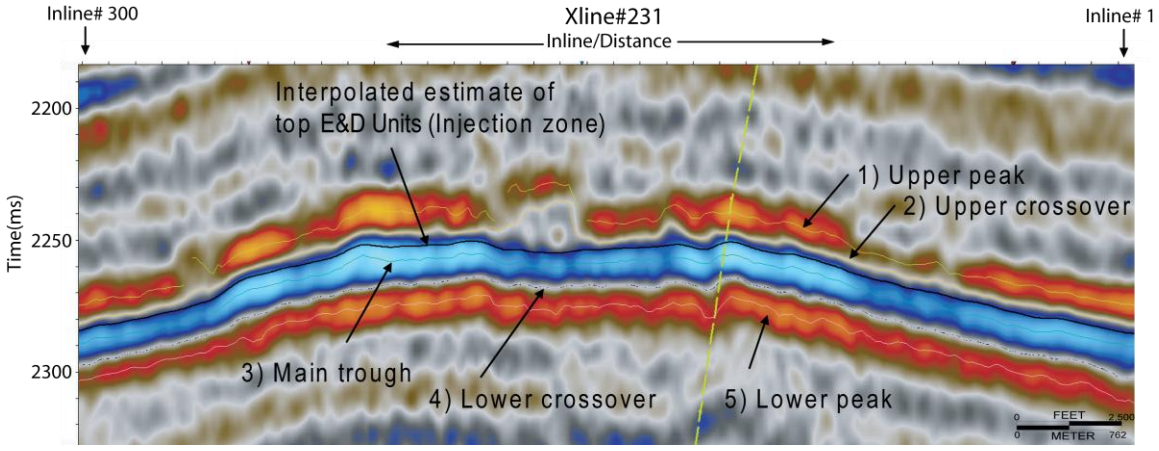

Figure 2.10-An interpreted seismic cross-line extracted from the seismic volume at reservoir level. There are two relatively strong peak separated by a strong trough corresponding to the Tuscaloosa sand units. Black line is smoothed approximation of the top of reservoir interval (E and D Units) (courtesy of Meckel, 2011).

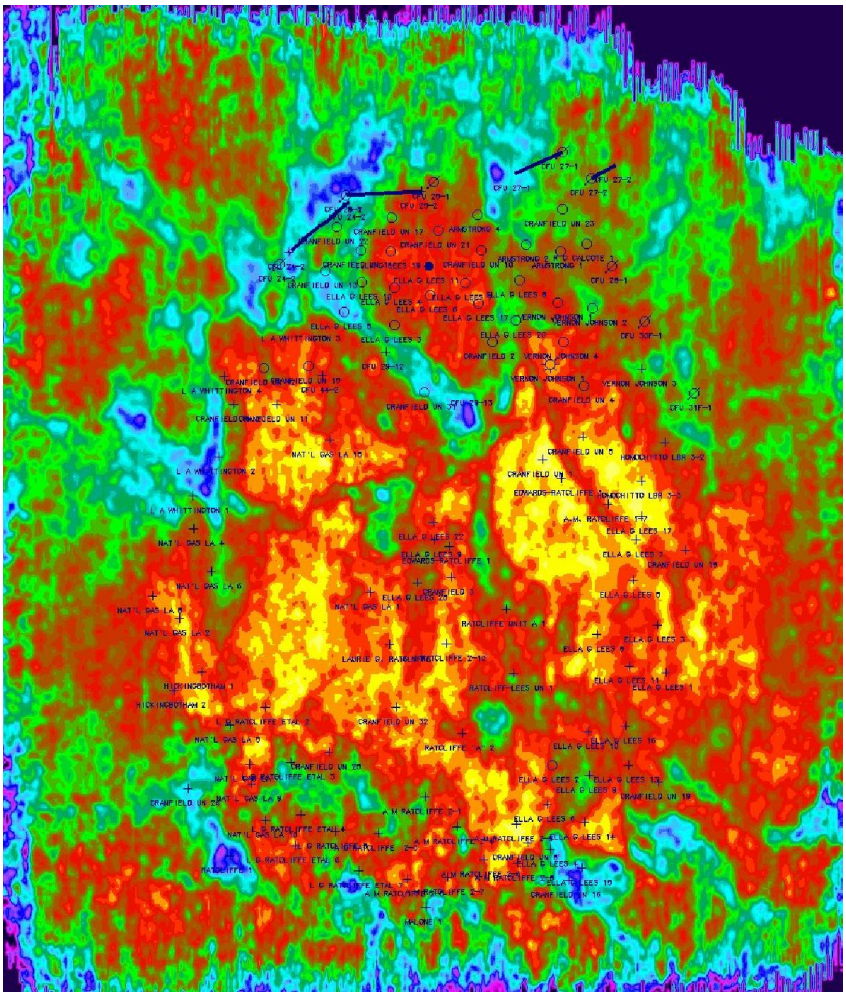

Figure 2.11-A 30 Hz amplitude stratal slice, Units E and D, Lower Tuscaloosa Formation generated by Zeng, (2009).

2.7.1-Seismic Workflow for Enhancing Resolution

To overcome seismic resolution issues, an efficient workflow including several modern seismic interpretation analyses is utilized in this study. These techniques are not part of the routine structural and stratigraphic seismic interpretation. Figure 2.12 summarizes the workflow for this study. Here a very brief explanation of the utilized workflow is given, but the detailed explanation of each technique is beyond the aim of this dissertation and can be obtained in the cited references.

First step of the workflow was to perform "Spectral Blueing" technique (Blache-Fraser and Neep, 2004) on the input seismic data. The spectral blueing enhances seismic

data resolution using well log data. Spectral blueing basically shapes the seismic data spectrum to the spectrum of the well-derived reflectivity. Therefore it can compensate higher frequency lost within seismic frequency bandwidth. The method is used in industry quite frequently as a powerful tool to improve seismic data resolution (Kazemeini et al., 2010).

In this study, first the sonic and density logs from well CFU#44-2 were used to generate a reflectivity log and then the mean seismic spectrum was matched to the reflectivity log spectrum. By doing so, high frequencies are boosted to a level controlled by the reflectivity log and seismic resolution is improved. Figures 2.13a and b compare the seismic resolution before and after blueing for Inline (184) from the seismic volume. As shown, the data after blueing have resolved more of the thin sand features compared with the original seismic.

In the next step, the spectrally blued seismic volume is decomposed into different volumes with different frequencies using the "Spectral Decomposition" technique (Sinha et al., 2005). By decomposing seismic data into its constituent frequencies, amplitude interferences from different frequencies are minimized which helps in getting more detailed information from subtle stratigraphic features. Spectral blueing allows higher frequency in decomposition stage (i.e. 40 Hz).

Stratigraphic features are initially deposited over the paleo-depositional surfaces and later are displaced due to structural deformation stages. The deformation of the paleo-depositional surfaces obscures stratigraphic features. In order to reveal these features, structural effects need to be removed from the seismic data. Flattening horizons and proportional slicing proposed by Zeng et al., (1998a, b) are two methods of removing structural effects from seismic data. However, these two methods are only valid in the vicinity of a horizon and could not handle faults and unconformities properly (Dorn, 2013). A better way of removing structures from seismic data are "Stratal Domain Transformation" where entire seismic data are transformed to stratal domain in such a

way that each slice through the stratal volume represents a paleo-depositional surface corresponding to a geologic time.

Stratal Domain Transformation is used in this study to map sand bodies in the Lower Tuscaloosa Formation. Decomposed seismic volumes generated in the previous step were transformed to stratal domain using picked horizons. Stratal slices from a higher frequency volume are appropriate for showing the stratigraphic features (sand distribution pattern) as they provide a map across the paleo-depositional surfaces with higher resolution and less amplitude interference.

Figures 2.14 shows a stratal slice through the 40 Hz decomposed blued seismic volume near the top of the reservoir (E and D Units). As shown more detail of the channel system and sand body distribution is revealed by using the decomposed blued seismic volume through stratal domain transformation. In the discussion part of this chapter, the seismic map is integrated with net-sand map, core description, log response correlations and production rate maps to interpret the depositional environment of the Lower Tuscaloosa Formation.

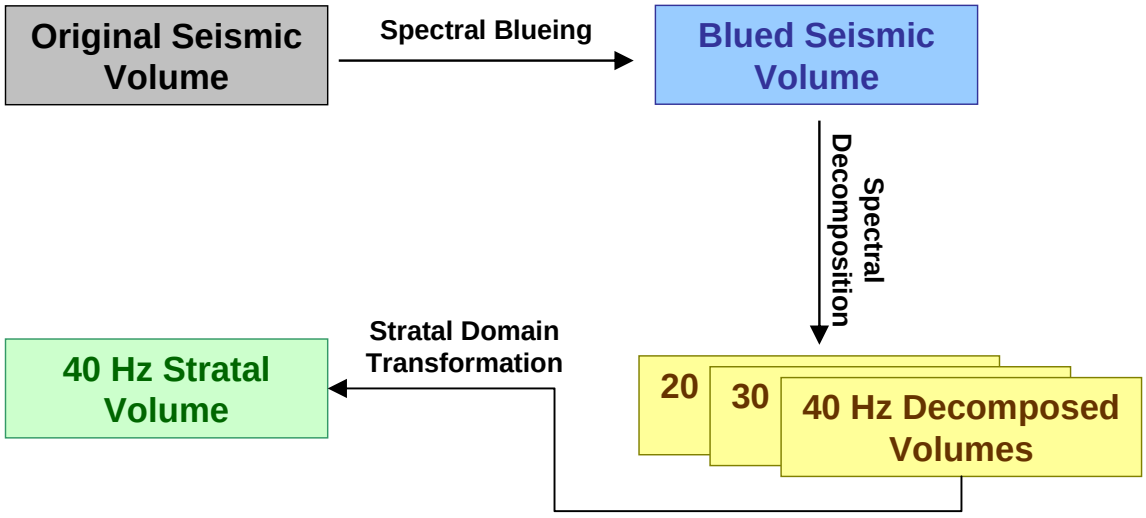

Figure 2.12-Summarized workflow for generating spectrally blued decomposed 40 Hz stratal volume. Blueing pushes higher limit of the seismic spectrum and allows decomposing of higher frequencies.

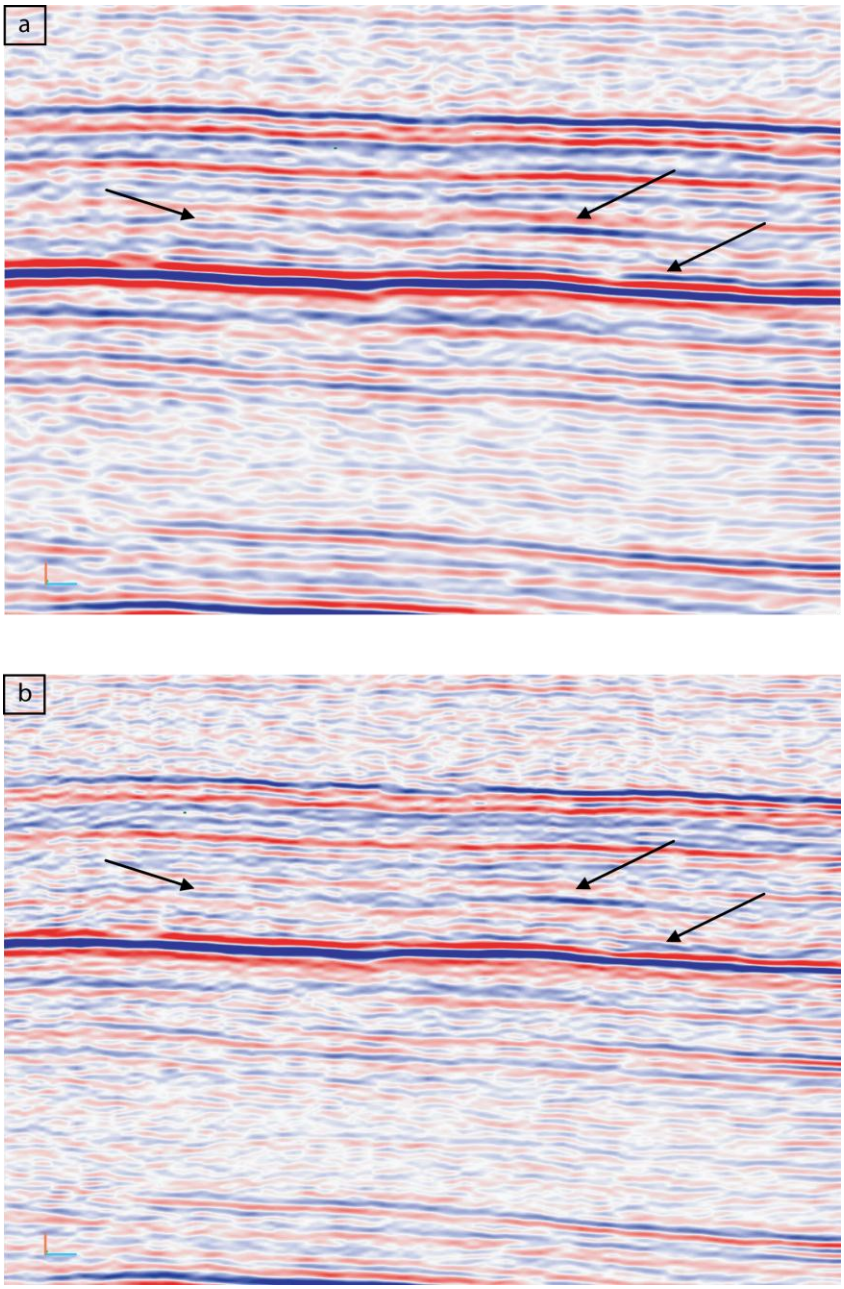

Figure 2.13-(a) An inline from the original seismic cube, and (b) from the blued seismic cube. Spectral blueing enhances the seismic resolution. Black arrows point to example areas where more details are revealed in blued data (b), in contrast to original data (a).

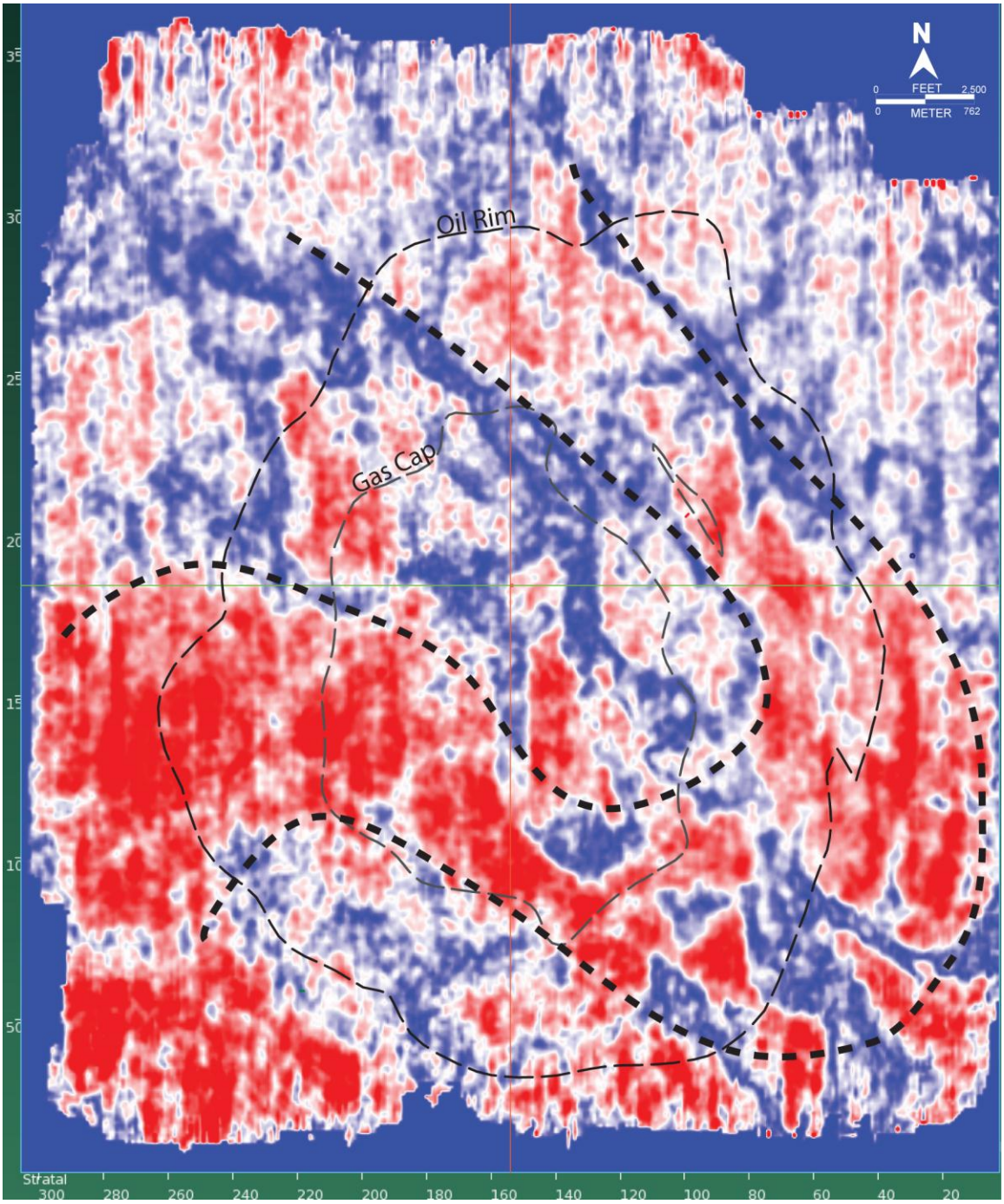

Figure 2.14-40 Hz stratal slice extracted close to top reservoir (E and D Sand Units) shows more details of the incised valleys system and sand body distribution. A meandering feature is revealed by red color and is outlined by the thick black dashed lines. Outline of the Cranfield filed can be estimated by the oil rim and gas cap from SECARB phase II final report (2011).

2.7.2- Reservoir Sand Mapping

In order to map reservoir sand distribution properly, the well-measured sand thicknesses are integrated with seismic data. In general, seismic data have fine sampling in lateral direction and therefore are able to show the patterns of sand distribution and other stratigraphic features laterally. However the vertical sampling of the seismic data is relatively coarse and seismic maps are valid only where vertical resolution allows detecting the sands. On the other hand, well data which provide very good vertical resolution are usually sparse with no control between wells. By combining seismic and well data we are benefiting from higher vertical resolution and better control on the sand distribution patterns between wells.

For this purpose, in Figure 2.15 wells with sand units thicker than 60 ft (estimated seismic resolution) are overlaid on the 40 Hz stratal slice corresponding to top reservoir shown in Figure 2.14. As it can be seen, the wells follow the sinuous feature on seismic. Therefore it can be inferred that the meandering feature is the main pattern of the sand distribution for the reservoir.

In next step, the well-measured thickness from wells with thicker sands are contoured and constrained with seismic pattern. Figure 2.16 shows the reservoir net-sand thickness map, generated from well data.

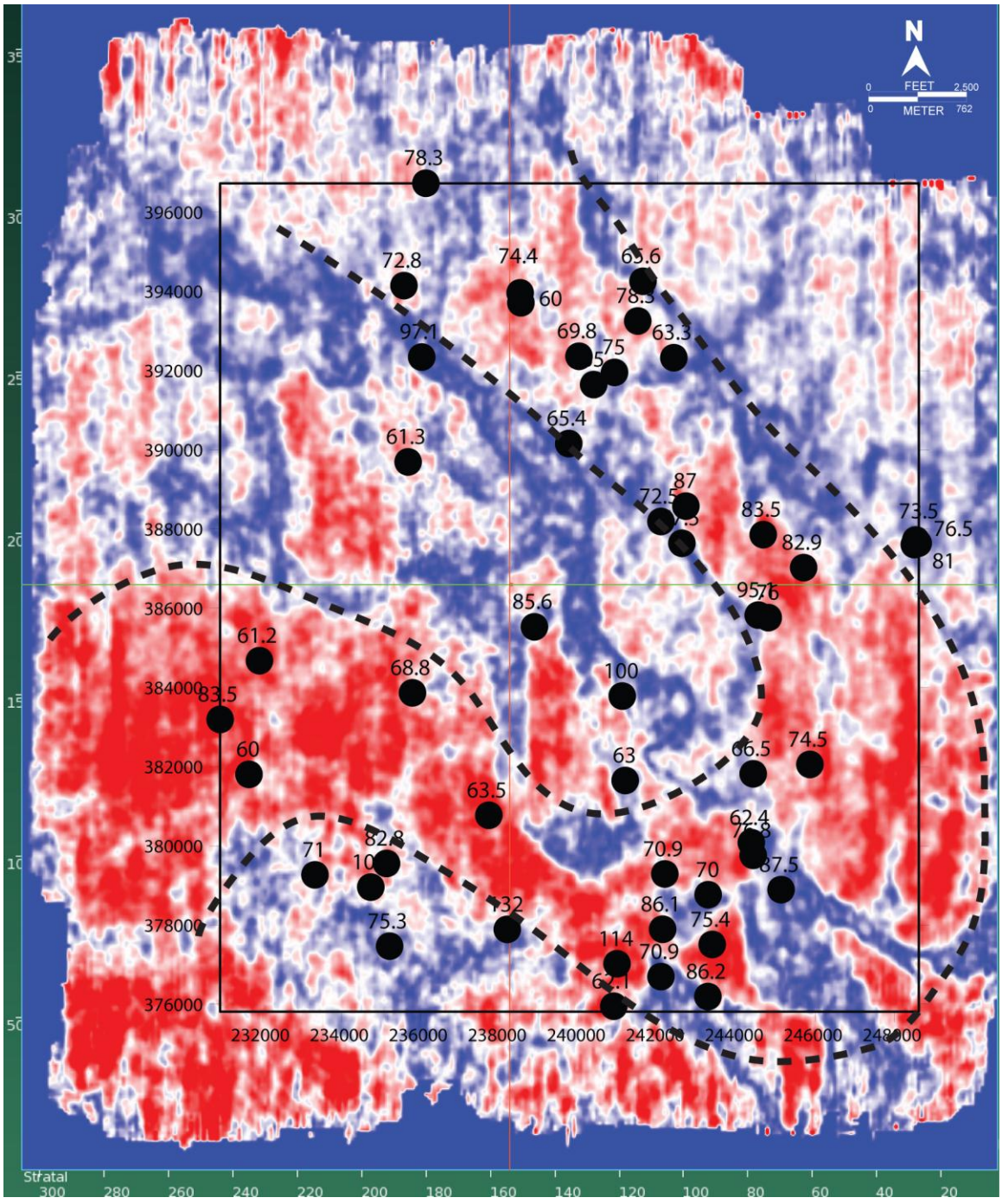

Figure 2.15-The Wells with sand units thicker than 60 ft are overlaid on the 40 Hz stratal slice corresponding to top reservoir. Most of the wells are located inside the meandering feature on seismic. Wells are labeled with sand thickness.

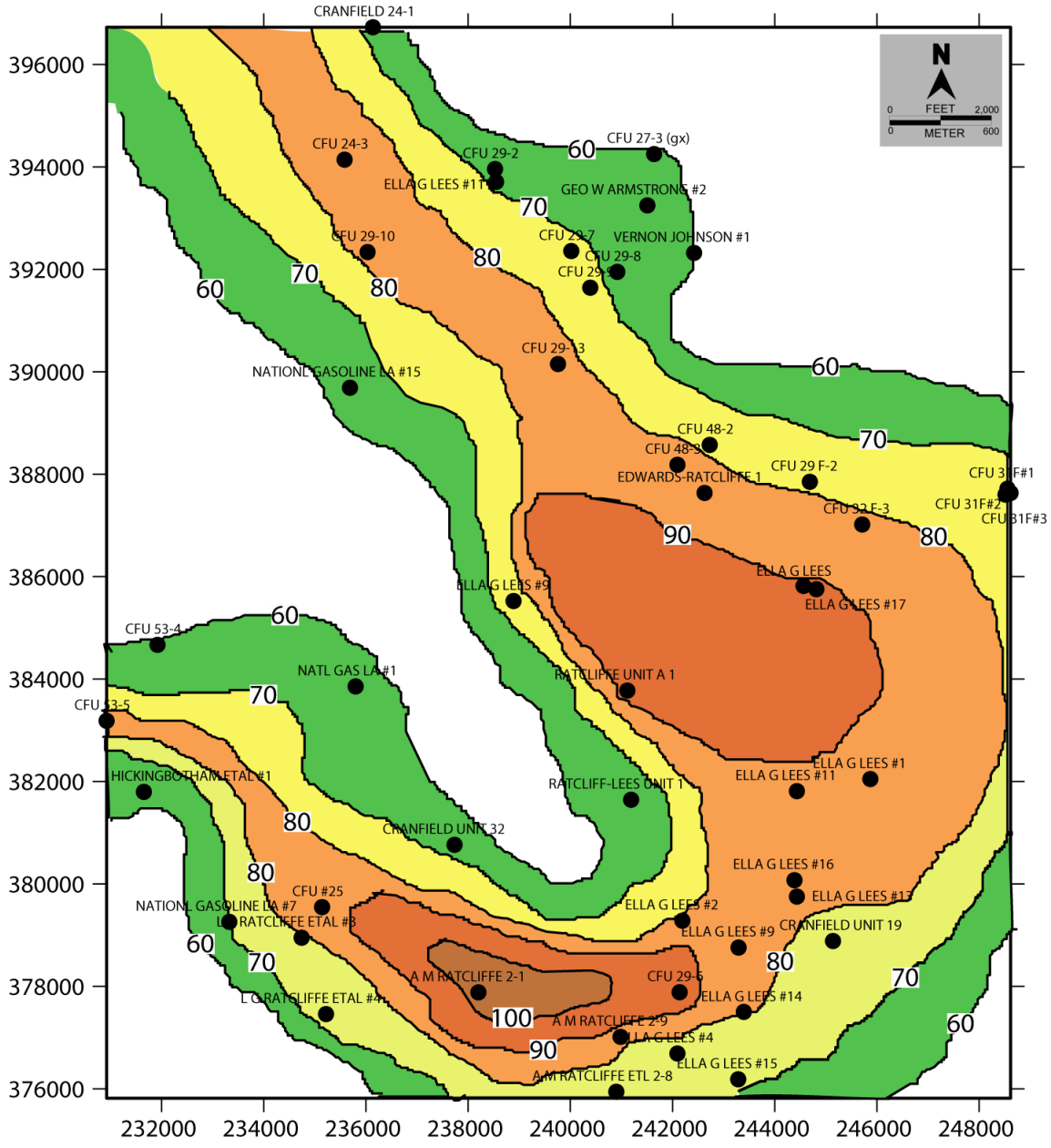

Figure 2.16-Net-sand map of the Massive Sand Member, generated from well data and constrained by seismic. The map shows the extension and geometry of the sandy intervals that are the reservoir in the Cranfield Field.

2.8-HYDROCARBON PRODUCTION ANALYSIS

The cumulative production from field discovery to depletion (1943–1966) is available for 57 producer wells in Cranfield Field. To characterize and analyze the production behavior of the Tuscaloosa reservoir at Cranfield Field, the production rate of each well on a yearly basis was calculated by omitting years when there was no production or significantly less production due to workovers or other reasons. The two histograms in Figures 2.17a and b show the minimum, maximum and mean of the yearly production rate for the 57 available wells. The average yearly gas and oil production rates were mapped as bubble maps for each well (Figs 2.18a and b). The radius of each circle varies in size depending on the yearly production rate's magnitude.

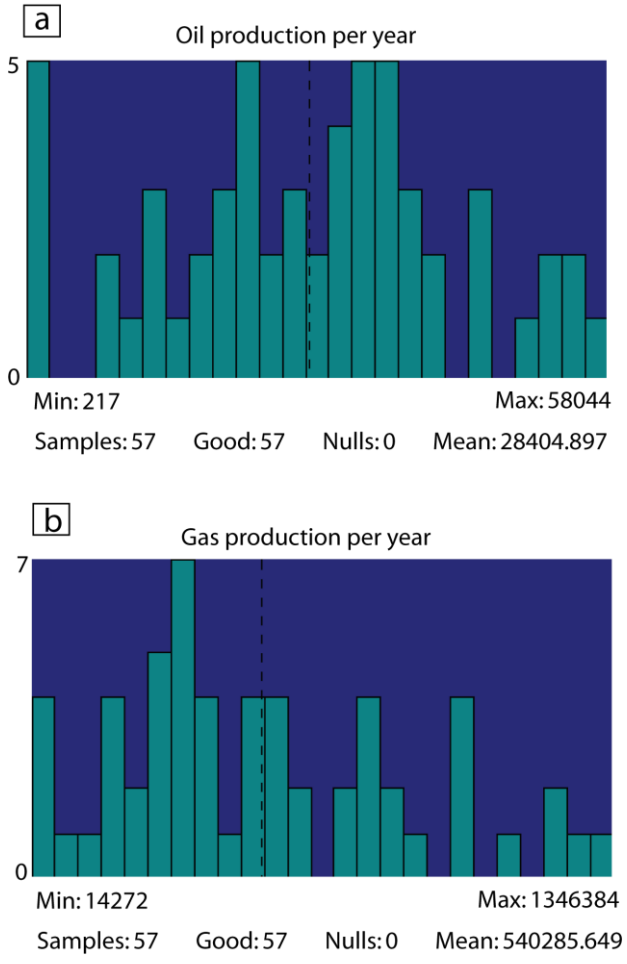

Figure 2.17-Histograms showing the minimum, maximum and mean of the yearly production rate for oil (a), and for gas (b), in the 57 wells at Cranfield Field.

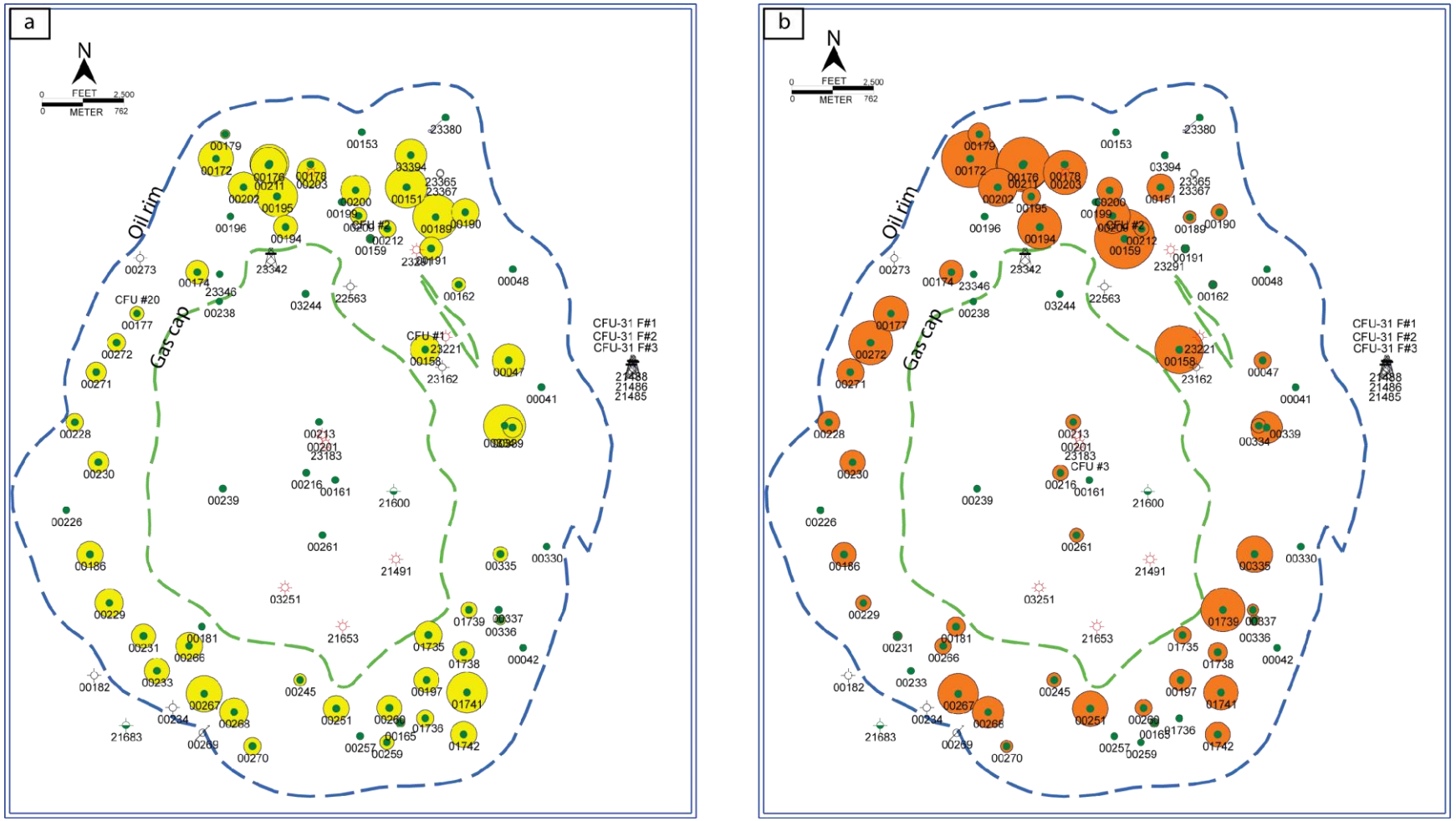

Figure 2.18-Bubble maps showing the average yearly oil (a) and gas (b) production. The radius of each circle varies in size depending on the yearly production rate's magnitude. The areas with higher rate of hydrocarbon production match with the higher sand thickness in these areas. Locations of oil rim and gas cap that are plotted on the maps are from SECARB phase II final report, 2011.

2.9-DISCUSSION

In this section based on literature and evidences from Cranfield Field, I will assess the sequence stratigraphy of the Tuscaloosa Group and the depositional environment of the Lower Tuscaloosa Formation in the basin-wide context. Determining the sequence stratigraphy and depositional environment on a regional scale will improve our understanding of the Tuscaloosa reservoir architecture on a local scale. The results from the Cranfield Field data have been interpreted and discussed in a separate section to reveal the sand-body distribution and reservoir architecture at the field, which are the flow-pathways for the CO_2 and hydrocarbon.

2.9.1-Sequence stratigraphic interpretation of the Tuscaloosa Group in the Gulf of Mexico and Gulf Coastal Plain

During the Early Cretaceous in the Gulf of Mexico, the shelf margin developed due to a combination of a change in the slope of the basement by differential subsidence along the crustal hinge zone and Jurassic sediment depositional patterns (Sawyer et al., 1991; Galloway, 2008). Development of a series of fringing carbonate reefs at the shelf margin (Edwards reef trend) separated the shelf from deep-water slope and basin (Horn, 2011). At the eastern reef trend, where the Tuscaloosa successions were deposited (east of Louisiana), the reefs were better developed and were vertically stacked, creating greater topographic relief at the shelf margin and steeper slope gradient, compared to the western trend, where the Woodbine successions were deposited (Horn, 2011).

During the Mid-Cretaceous, prior to deposition of the Lower Tuscaloosa Formation, at the onshore of Gulf Coastal Plain, basin-wide subaerial erosions developed regional unconformities (Mississippi Geological Society, 1957; Salvador, 1991; Mancini et al., 2008; Horn, 2011). The unconformities have been considered as unconformities with some headward eroding canyons that formed by cut-and-fill actions (excavation type, based on calcification of Bornhauser, 1966) or as drowning unconformities,

(defined by Schlager and Camber, 1986) in the onshore Gulf of Mexico basin (Fisher, personal communication, 2013).

At the same time in the offshore, fluvial systems delivered sediment to the shelf, creating lowstand prograding shelf deltas and shelf edge deltas, bypassing the sediments to the slope and basin as slope fans and basin floor fans (Funkhouser, 1981; Berg, 1982; Dubiel and Pitman, 2004; Barrel, 1997; Bunge, 2011; Woolf and Wood, 2011; Horn, 2011) (Fig. 2.19 and Fig. 2.20). The delta systems on the shelf were prograding and once they reached the shelf edge, significant sediments were stalled on the reef trend and eventually massive turbidite fan complex were deposited on the steep slope in the fore-reef trough as well as on the basin floor (Berg, 1982) (Fig. 2.19 and Fig. 2.20). Seismic studies of the deep-water Gulf of Mexico showed that the lower part of the deep Tuscaloosa was fed by shelf edge deltas down the steep Lower Cretaceous carbonate slope and basin floor (Berg, 1982; Dubiel, 2002; Bunge, 2011). Recent drillings in farther offshore and stratigraphically deeper intervals in the Gulf of Mexico, has discovered the present of the Tuscaloosa age turbidite deposits in the distal part of the basin (Dubiel, 2002; Zarra, 2006; Meyer, 2007; Rains, 2007; Wornardt, 2010; McMoRan Exploration Co., 2011). However, the regional extent of turbidite deposits of the deepwater facies is not well known (Woolf and Wood, 2011).

Within the sequence stratigraphic framework, at the onshore Gulf coastal region, the subaerial unconformity at the base of the Lower Tuscaloosa Formation represents the basal sequence boundary. Basinward, its correlative conformity has been situated within shelf edge deltas and turbidite piles (Fisher, personal communication, 2013). This sequence boundary at Cranfield Field is picked at base of the first conglomerate interval of the Massive Sand Member through erosional channelized contact with the underlying dark gray marine mudstone and carbonate deposits of the undifferentiated Washita-Fredericksburg Group (Dantzler Formation) in cores, with an abrupt decrease in the SP and GR responses in logs (Figs. 2.1, 2.2).

By initial rise of sea level/base level in the late Lowstand System Tract, during the late Middle-Cenomanian to Late-Cenomanian, the Massive Sand Member was aggradationally deposited in nearshore and onshore, filling the developed incised valleys that were formed during subaerial erosion. As shown by cores and logs from Cranfield Field, the fining-upward cycles with basal gravels, reactivation surfaces and cross bedding founded in cores as well as blocky and funnel shaped responses in GR and SP logs of this member are characteristics of channel fill or point bar deposits within incised valleys (Figs. 2.1, 2.1, 2.6).

Overall by this interpretation, the Lowstand System Tract is composed of the Massive Sand Member, which is equivalent to the lowstand shelf edge deltas and turbidite piles at the shelf margin and deepwater basin. By more rapid rise of relative sea level in the early Transgressive System Tract, during the Late Cenomanian, the shelf deltas and shelf edge deltas retrograded and developed a backstepping deltas system. This resulted in deposition of a deltaic-estuarine interval of the Stringer Sand Member over the Massive Sand Member. The Transgressive Surface/ravinement surface was developed at the top of the aggradational interval of the Massive Sand Member, followed by the retrogradational interval of the Stringer Sand Member. Depositional environment of the Stringer Sand Member is reported as marginal marine and mainly transgressive deltaic systems, representing transgression of the sea over the fluvial system at the coastal plain (e.g. Spooner, 1964; Devery, 1980; Chasteen, 1983; Stancliffe and Adams, 1986; Wiygul and Young, 1987; Klicman et al., 1988; Minter et al., 1992; Petty, 1997; Mancini et al., 1999). Well log patterns of the Stringer Sand Member in Cranfield Field show retrogradational stacking of parasequences and fining-upward log-facies successions, indicating a deepening/fining-upward trend of transgression.

By gradual rising of relative sea level and marine transgression during the Late Cenomanian to Early Turonian, the continental and transitional deposits of the Lower Tuscaloosa Formation (Massive Sand and Stringer Sand Members) were overlain by

marine deposits of the Middle Tuscaloosa Formation. The Middle Tuscaloosa Formation represents a major flooding event in the Gulf Coastal Plain, extending to the foothills of the paleo-Appalachian and Ouachita Mountains and transgressing northwest into the Western Interior Seaway (Wu, 1990; Salvador, 1991; Sohl et al., 1991; Blakey, 2011). The Early Turonian was the time of maximum transgression and formation of the Maximum Flooding Surface within the Middle Tuscaloosa Formation, which separates the Transgressive System Tract from the Highstand System Tract. Therefore, the Transgressive System Tract includes the Stringer Sand Member and lower portion of the Middle Tuscaloosa Formation that is capped by a Maximum Flooding Surface (Fig. 2.6). As evidenced from log responses of Cranfield Field, the Maximum Flooding Surface is marked by a high GR, high SP, low density, high neutron and low resistivity picks. This surface corresponds to a homogeneous, silt-bearing, clay-rich mudstone condensed section in the core of the Middle Tuscaloosa Formation at Cranfield Field (Fig. 2.7).

By falling of relative sea-level during the Middle Turonian to Late Turonian, the shoreline migrated basinward, resulting in deposition of fluvial-deltaic deposits of the Upper Tuscaloosa Formation (Mancini et al., 1987; Mancini and Puckett, 2005). Deposition of the predominantly transitional to continental sediments represents regression of the sea over the Gulf Coastal Plain. The progradational event associated with high siliciclastic sediments influx into the basin resulted in formation of a Highstand System Tract that includes the upper portion of the Middle Tuscaloosa and Upper Tuscaloosa Formations (Fig. 2.6).

The Highstand System Tract was followed by a major relative sea level fall and another major subaerial exposure in the northeastern Gulf of Mexico (Salvador, 1991; Mancini et al., 1995; Mancini et al. 1999; Liu, 2005; Mancini and Puckett, 2005). Therefore the entire sequence is capped by another sequence boundary positioned between the Upper Tuscaloosa and the Eutaw Formations (Salvador, 1991; Mancini and Puckett, 2005). The hiatus representative of this sequence boundary has been considered

to be from Late Turonian to Mid Coniacian age (Spooner, 1964; Salvador, 1991; Mancini and Puckett, 2005). Figure 2.19 shows a plan view of the depositional system of the Lower Tuscaloosa Formation from coastal plain to deep basin of the Gulf of Mexico. Figure 2.20 shows a schematic diagram of the Tuscaloosa Group and its related depositional environments within the sequence stratigraphic framework.

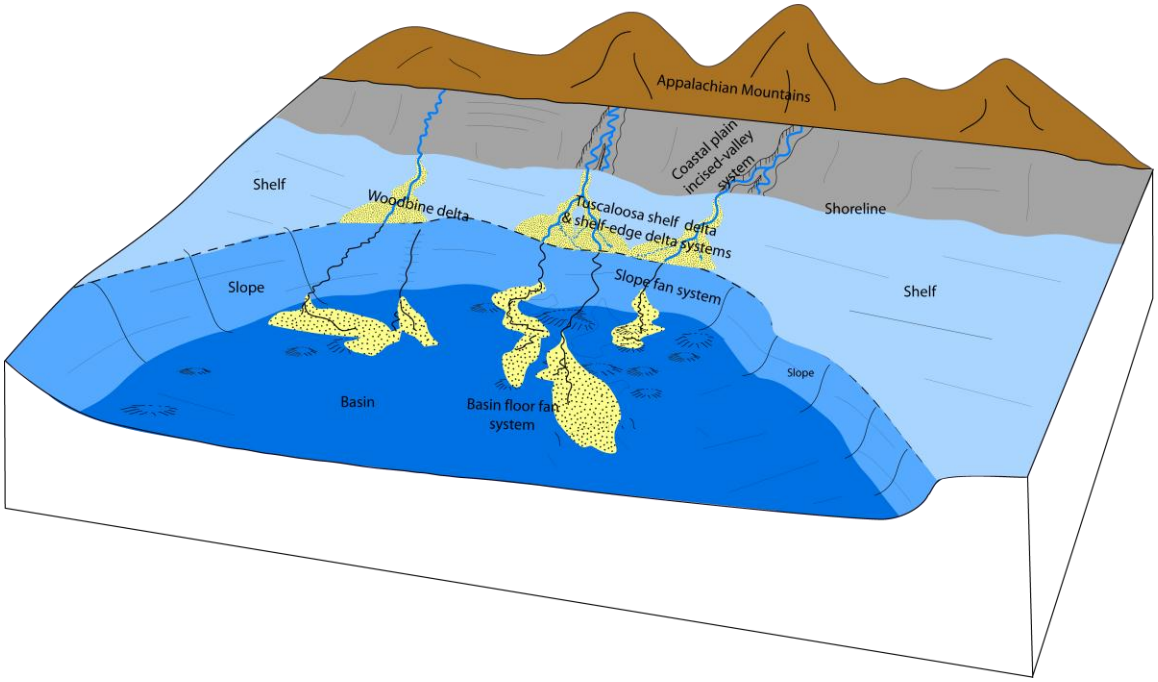

Figure 2.19-Schematic plan view of depositional system of the Lower Tuscaloosa Formation from coastal plain to deep basin of the Gulf of Mexico.

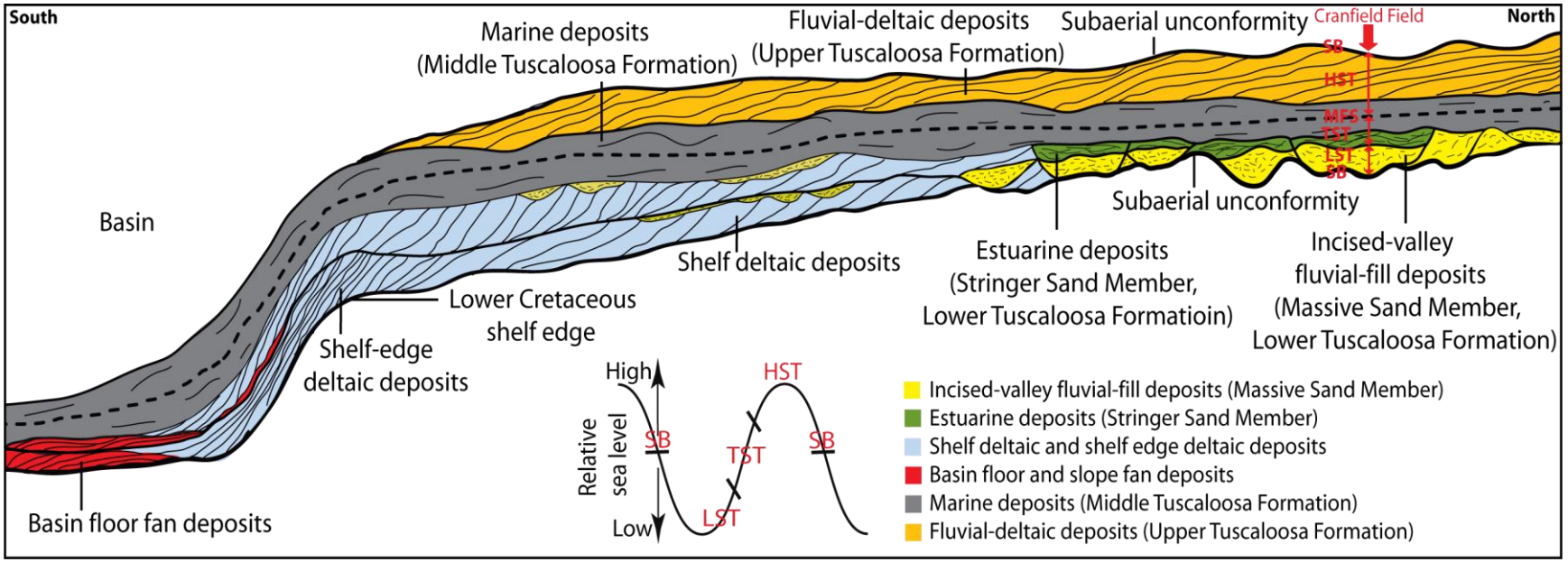

Figure 2.20-Schematic diagram of the Tuscaloosa Group and its related depositional environments within sequence stratigraphic framework in the Gulf of Mexico and Gulf Coastal Plain.

2.9.2-Depositional environment of the Lower Tuscaloosa Formation in the Mississippi Interior Salt Basin

As discussed in the sequence stratigraphy section, during the Mid-Cretaceous prior to deposition of the Lower Tuscaloosa Formation, subaerial exposure and incisions were developed in the onshore and nearshore Gulf coastal region, representing a basal sequence boundary. By rising relative sea level during late Lowstand System Tract and early Transgressive System Tract, the fluvial interval of the Massive Sand Member and deltaic successions of the Stringer Sand Member were deposited at this part of the basin. Presence of a sequence boundary that is covered by fluvial deposits is one of the most important criteria for recognition of incised valleys fills. Therefore in this section I will discuss the possibility of incised valley system as the depositional environment of the Lower Tuscaloosa Formation in the Mississippi Interior Salt Basin.

In the literature, several definitions and criteria for recognition of incised valleys have been suggested (e.g. Van Wagoner et al., 1990; Zaitlin et al., 1994; Van Wagoner, 1995a; Posamentier, 2001; Fielding and Gibling, 2005; Gibling, 2006). However, Maynard et al., (2010) reappraised the definition and recognition criteria for incised valleys. Maynard et al., (2010) revised the definition of the incised valleys as *"any fluvial incision that is bounded below by a sequence boundary". "Incised valleys form in response to a relative fall in sea level and, unlike distributary channels, are not in facies relationship with the surrounding sediments into which they are incised*". The main criteria for recognition of incised valleys from other types of multi-story sandstone deposits are determined by Maynard et al., (2010) as presence of elongate, channel-shaped incisions that can be correlated over a long distance; and presence of a sequence boundary at the base of incision that can be correlated regionally on the sequence boundary/interfluve flooding surface.

The valley systems can be filled during transgression with different depositional systems ranging from fluvial to estuary to open marine. However in most instances,

incised valleys initially contain continuous fluvial deposits at their base (Dalrymple et al., 1994; Zaitlin et al., 1994; Posamentier, 2001). On the shelf, the incised valleys of sequence boundaries correlate laterally with interfluves, and the exposure surface may be characterized by palaeosols or rooted horizons, formed on the margins of incised valleys (Van Wagoner et al., 1990; Leckie and Singh, 1991). Figure 2.21 shows the evolution of incised valley system during sea level rise.

Presence of the sequence boundary at the base of the Lower Tuscaloosa Formation is important for at least two reasons that are critical criteria for recognition of this formation as incised valley fill.

1. It is regionally recognized and easily correlates across the northern Gulf coastal region (Mississippi Geological Society, 1957; Spooner, 1964; Wiygul and Young, 1987; Salvador, 1991; Mancini and Puckett, 2005). In the log correlations of Cranfield Field this surface was easily recognized by an abrupt decrease in the SP, GR and resistivity log responses and was correlated across the field (Figs. 2.3; 2.4). The erosional channelized contact at the base of the Lower Tuscaloosa was observed in two cores.

2. It represents a dramatic change in depositional environments that their sediments are not in facies relationship with each other. As shown from cores of Cranfield Field, the sequence boundary represents a sudden jump from the marine deposits of the predominantly carbonate and mudstone section below (Washita-Fredericksburg Group/ Dantzler Formation) to the predominantly continental/non-marine clastic section above (Lower Tuscaloosa Formation). Therefore, there is no genetic linkage between the fluvial (incised-valley fill) and the underling open marine systems.

Subsequent to the sequence boundary, initial rise of base-level during the late Middle-Cenomanian resulted in partial filling of the incised valleys by fluvial system and deposition of the aggradational interval of the Massive Sand Member (Cranfield reservoir) (Fig. 2.21). The core description of Cranfield Field showed the presence of fining-upward cycles with basal pebble lags, reactivation surfaces and cross beddings,

coal/lignite debris and lack of marine trace fossils in the Massive Sand Member. The GR and SP logs responses also show blocky and funnel shaped motifs in this member. These are interpreted to represent multi-story channel fill and point-bar deposits within incised valley (incised-valley fluvial fill system). As discussed in the core description, the two units (E and D Units) in the Massive Sand Member represent upward-decreasing energy of the system through time. This could be result of increasing accommodation space due to relative base level/sea level rise. Presence of red-brown, mottled, burrowed mudstone interval at the top of the upper unit (Unit D) of the Massive Sand Member in the cores is interpreted to represent interfluves deposits. The mottled texture and the observed root casts in this part are indicators of soil-forming processes (paleosol) in a terrestrial environment.

As discussed in the sequence stratigraphy section, after deposition of the Massive Sand Member, more rapid rise in the base-level and marine transgression during the late Cenomanian resulted in deposition of the Stringer Sand Member in a marginal marine complex to transgressive deltaic/estuarine environments (e.g. Dickas, 1962; Hamilton and Cameron 1987; Klicman et al., 1988) (Fig. 2.21). In some studies, presence of glauconite and intense bioturbation in the sandstones and presence of oyster fossils in the shale intervals of the Stringer Sand Member have been reported (e.g. Drennen, 1953; Chasteen, 1983). These indicate influence of the marine/brackish water on the incised valleys system during deposition of the Stringer Sand Member.Well log patterns of the Stringer Sand Member in Cranfield Field showed fining-upward log-facies successions with smaller shale and sand intervals, indicating more heterolithic deposits. The sand intervals became thinner with more clay upward, indicating rising of the relative sea-level. Since there is not any available core from the Stringer Sand Member at the Cranfield Field, the facies interpretations is just based on observation from logs and other fields.

By this explanation, the incised valleys fill composed of fluvial and transgressive deltaic/estuarine deposits of the Lower Tuscaloosa Formation. However relative sea level

rise continued in the Gulf Coastal Plain, resulted a major flooding events and deposition of the Middle Tuscaloosa Formation in marine environment (Fig. 2.21). Drennen (1953) noted the marine influence in the Tuscaloosa outcrops, situated in a belt across northern Mississippi to central Alabama, Georgia, South Carolina, and North Carolina.

Overall, the incised valley system interpretation of the Lower Tuscaloosa deposits is supported by several lines of evidence: (1) the basal erosion surfaces are a sequence boundary that can be correlated in regional scale across the Gulf Coastal Plain; (2) base of the incised valleys represents a dramatic change in depositional environments that their sediments are not in facies relationship with each other; (3) valley fill begins to accumulate during the subsequent base-level rise and contains deposits of the late Lowstand System Tract followed by early Transgressive System Tract; (4) the valley fills contain stacked fluvial deposits followed by transgressive deltaic deposits and covered by marine deposits; (5) the fluvial deposits at the basal part of the valley have a complex nature and exhibit decreasing-upward energy of the system, reflecting increasing accommodation space during base-level rise; (6) facies associations of valley fill deposits reflect a significant basin-ward shift in facies with respect to the underlying units.

Zaitlin et al., (1994) classified the incised valleys into two types, (1) piedmont incised-valley systems that have their headwaters in a hinterland, and that cross a "fall line" where there is a significant reduction in gradient, and (2) coastal-plain incised-valley systems that do not cross a "fall line" and that are confined to low gradient coastal plains. The piedmont incised-valley systems are usually associated with rapid sea level fall, while the coastal-plain incised valley systems are not necessarily related to sea level changes, and mainly are associated with erosion due to tectonic uplift of an inland area, or to an increase in fluvial discharge caused by climatic change (Schumm et al., 1987; Blum, 1992; Dalrymple et al., 1994; Schumm and Ethridge, 1994; Posamentier 2001; Martin et al., 2011). Based on the Zaitlin's (1994) classification, the incised valleys of the

Lower Tuscaloosa Formations are coastal-plain incised-valley systems (Fig. 2.19 and Fig. 2.20).

Maynard et al., (2010) reported that incision size alone cannot be used as a criterion for valley recognition. In the literature, incised valleys have been typically documented in width from tens of meters to tens of kilometers, and in depth from tens to hundreds of meters in different geological records (e.g., Van Wagoner et al. 1990; Dalrymple et al. 1994; Zaitlin et al. 1994; Morton et al. 1996; Anderson et al. 2004; Rodriguez et al. 2005; Gibling, 2006). Incised valleys can be simple, containing only a single channel fill, or complex, with several channel fills (Schumm and Ethridge, 1994; Maynard et al., 2010). Valley patterns range from straight to sinuous to anastomosis with multiple patterns (Schumm and Ethridge, 1994). Previous studies of exposed incised valleys revealed that valley width generally increases downstream due to increases in discharge and sediment flux (Tuttle et al. 1966; Feldman et al. 2005; Martin et al., 2011).

The regional isopach map of the basal-most parasequence of the Lower Tuscaloosa Formation in the Gulf Coastal Plain provided by Woolf and Wood (2011) showed presence of four major valley axes at the onshore Gulf coastal region that originated from the eastern ancestral Appalachia highlands and the central paleo-Mississippi embayment, and continued toward the deltaic complexes in central and south Mississippi and Alabama. Width of the channel axes ranged from 30 to 80 km (18 to 49 mi) in their fluvial/northern reaches, widening in the deltaic south reaches to over 200 km (124 mi). These show the tendency for the Tuscaloosa incised valleys to widen downstream and also emphasize the size of incision to the shelf edges. However, the provided net-sand maps and seismic map of Cranfield Field show the position of incised valleys on a local scale.

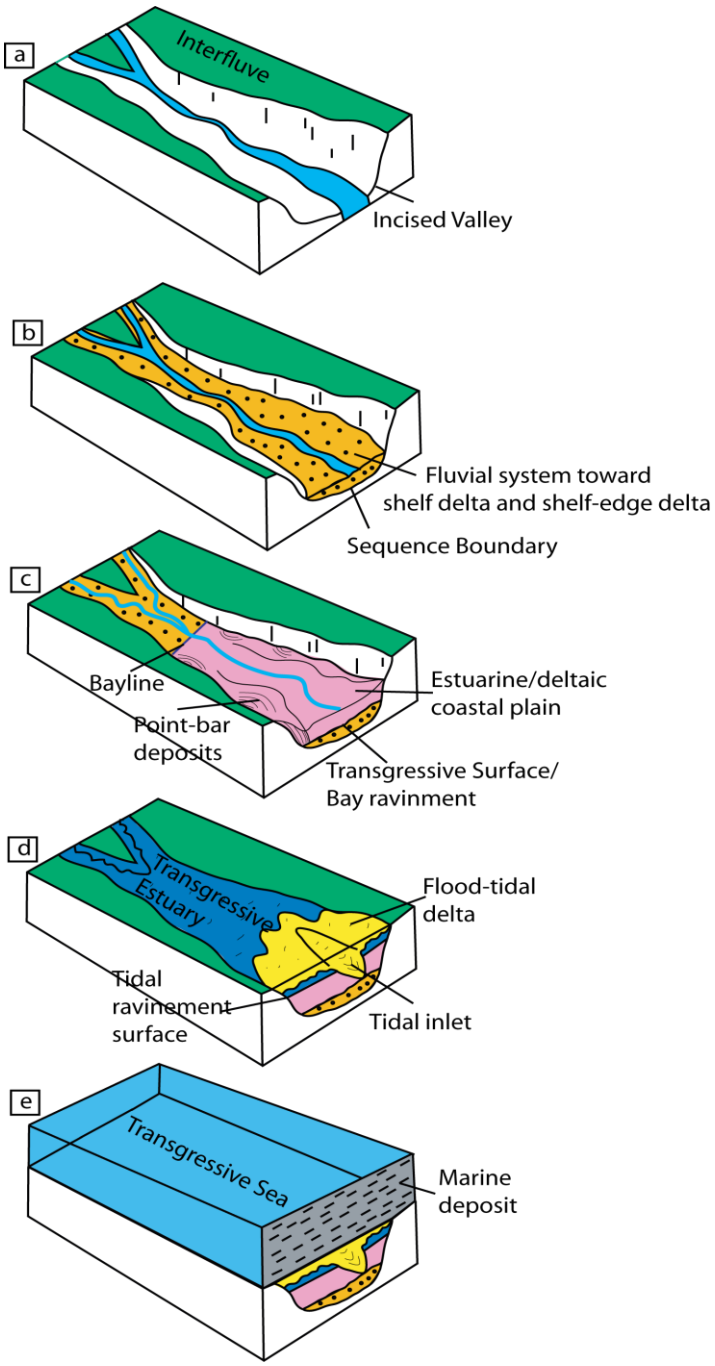

Figure 2.21-Schematic representations of the evolution of incised valleys system of the Lower Tuscaloosa Formation during sea level rise, including their sedimentary facies and stratigraphic boundaries: (a) valley incisions during subaerial erosion; (b) aggradational fluvial deposits (Massive Sand Member) during initial relative sea level rise that grade basin-ward to shelf delta and shelf-edge delta systems; (c) aggradational estuarine system (Stringer Sand Member), at the initiation of back-filling; (d) passive infilling of the estuary, with developed central-basin mud and estuary-mouth complexes; (e) marine transgression and deposition of marine mud (Middle Tuscaloosa Formation) (modified from Allen and Posamentier, 1993).

2.9.3-Reservoir architecture at Cranfield Field

The core descriptions at Cranfield Field showed that the reservoir interval (Massive Sand Member) is composed of amalgamated fining-upward units (E and D Units) with multiple erosional and depositional episodes (cut and fill), that are interpreted as valley-fill/channel-fill and point-bar deposits (Fig. 2.2). However, the cored intervals are limited to just four wells and two of them (Wells CFU-31F#2 and CFU-31F#3) are just 42m apart. In the field-wide scale, the log correlations and strike and dip transect cross-sections demonstrated that the sandy units (E and D Units) are not extended through the entire field and the facies change laterally and vertically over short distances (Figs. 24a and b). The discontinuous distribution and lenticular geometry of the Massive Sand Member ant its sandy units in the field indicate lateral accretion and avulsion of the channels and/or present of multi-story channel complexes. This generated lots of complexity and depositional heterogeneities in the reservoir of Cranfield Field.

The provided seismic map (Fig. 2.14) and net-sand map of the Massive Sand Member (Fig.2.16) show spatial extension and geometry of the sand-bodies, which are flow-pathways at the field. The sand-bodies show sinuous pattern (meandering) with a NW-SE trend. This trend is representative of paleocurrent direction toward the delta/estuary/shoreline at the south (Gulf of Mexico). The area with high sand accumulations in the seismic map and net-sand map of the Massive Sand Member are in agreement with higher rate of hydrocarbon production in the bubble maps of yearly production rate (Fig. 2.18). However, due to sparseness and uneven distribution of the well location, they can not be fully matched.

In the basin-wide context, the channel complexes at the Cranfield Field are part of coastal-plain incised-valley systems (Fig. 2.19). The incised-valleys are filled by fluvial deposits of the Massive Sand Member, overlaid by deltaic/estuarine deposits of the Stringer Sand Member (Figs. 2.20 and 2.21). The fill of the incised valleys occurred during late Lowstand System Tract to early Highstand System Tract (Figs 2.6 and 2.20).

The relative sea level/ base level rise during this time could result in highly avulsion of the incised-valley fluvial-fill systems.

Despite the presence of vertical and lateral lithostratigraphic variations at the field, the structure maps on the top and base of the Lower Tuscaloosa Formation show little changes (Figs. 2.5a and b). This suggests apparent structural stability in the Gulf Coastal region during deposition of the Lower Tuscaloosa Formation. Therefore most of the heterogeneities presented at the Cranfield reservoir were created by depositional facies changes during depositional of the Lower Tuscaloosa Formation.

2.10-CONCLUSIONS

In this chapter, I assessed the depositional systems and sequence stratigraphy of the Lower Tuscaloosa Formation that influenced lithofacies distribution and developed the depositional related heterogeneity and reservoir quality variation at Cranfield Field.

The core descriptions at Cranfield Field showed that the Massive Sand Member (reservoir interval) is composed of valley-fill/channel-fill and point-bar deposits. However the log correlations and the cross sections showed the discontinuous distribution and lenticular geometry of the Massive Sand Member ant its sandy units in the field, indicating lateral accretion and avulsion of the channels and/or present of multi-story channel complexes. Seismic map and net-sand map of the Massive Sand Member showed that the sand-bodies have a NW-SE trend and meandering pattern, representing paleocurrent direction toward the delta/estuary/shoreline at the south

Depositional environment of the Lower Tuscaloosa Formation in the Mississippi Interior Salt Basin has been interpreted as a network of coastal-plain incised valleys. This interpretation is supported by several lines of evidence, including presence of a sequence boundary at the base of the Tuscaloosa Group; subsequence to the sequence boundary a base-level rise followed by regional marine transgression that resulted in valley fill deposition; absence of a transitional facies between the valleys fill deposits and the

underlying strata; facies associations of valley fill deposits reflect a significant basinward shift in facies with respect to the underlying units; presence of multi-story channel fill/point bars at the base of valley fills followed by brackish/marine water influences and estuarine to deltaic deposits. Basinward the coastal-plain incised valleys correlate to the shelf deltas and shelf-edge deltas, bypassing the sediments to the slope and basin as slope fans and basin floor fans.

The fill of incised valleys in the Mississippi Interior Salt Basin is interpreted to be subdivided into lowstand channel-fill/point bars (E and D Units, Massive Sand Member of the Lower Tuscaloosa Formation), followed by transgressive deltaic/estuarine/marginal marine deposits (C to A Units, Stringer Sand Member of the Lower Tuscaloosa Formation). The incised valley fills were followed by a regional marine transgression and formation of the marine shale of the Middle Tuscaloosa Formation. Extent of the maximum flooding surface has been evidenced by formation of the condensed section within the Middle Tuscaloosa Formation. The maximum flooding surface, followed by sea-level fall and shoreline migration basinward, resulted in deposition of marine-shelf and fluvial-deltaic deposits of the Upper Tuscaloosa Formation during the highstand system tract. The highstand system tract was followed by a major relative sea level fall and formation of the top sequence boundary at the top of the Upper Tuscaloosa Formation.

As a consequence, the interpretation of the Lower Tuscaloosa Formation depositional environment within a sequence stratigraphic framework may lead to a better understanding of the geometry and reservoir characteristics of similar sandstone bodies in other hydrocarbon-prospective basins.

Chapter 3: Diagenetic Characteristics Affecting Reservoir Quality

3.1-INTRODUCTION

Diagenetic alterations in siliciclastic successions, which are controlled by a variety of chemical, physical, and biochemical interactions, have a substantial impact on modifying primary porosity and permeability, and consequently, on reservoir quality (e.g. Curtis, 1977; Giles and Marshall, 1986; Wright, 1993; Bloch et al., 2002; Worden and Burley, 2003; Mackenzie, 2005; Taylor et al., 2010, Morad et al., 2010, 2012). One of the goals of this chapter is to identify and quantify the principal diagenetic events affecting reservoir quality and to reconstruct the diagenetic evolution of the Lower Tuscaloosa reservoir sandstones through the progressive burial. For this purpose, the petrographic and geochemical data on the Lower Tuscaloosa sandstones have been analyzed to evaluate the effects of postdepositional alterations (e.g. compaction, cementation, replacement and dissolution) linked to the depositional sediment composition and texture, on the reservoir's petrophysical properties.

Understanding the diagenetic alterations and evolution of the reservoir sandstones through the burial history is crucial, as diagenesis can result in both positive and negative deviations from a simple trend of declining porosity and permeability with increasing depth. The Lower Tuscaloosa reservoir sandstone at Cranfield Field, with high porosity (~25%) in the deep subsurface (more than 3 km) is an ideal example. Extensive studies showed that usually in the Lower Tuscaloosa Formation, growth of grain coating chlorite during diagenesis inhibits quartz cementation and thus results in preservation of original porosity in deep burial (e.g. Thomson, 1979; Hamlin and Cameron, 1987; Klicman et al., 1988; Genuise and McBride 1990; Paxton et al., 1990; Pittman et al., 1992; Cameron et al., 1992; Ryan and Reynolds, 1996, 1997; Kordi et al., 2010).

As another goal of this chapter, I used the Tuscaloosa Formation as an analog for understanding the origin, time and processes of formation of chlorite coats that can result in good reservoir quality in deeply buried sandstones. Moreover, I studied the amount of

interaction between degree of chlorite coating occurrence and quartz cementation and the extent of the inhibition process. These topics are not well described in the literature. This can help us in understanding the factors controlling the degree of reservoir quality variation in the chlorite-bearing sandstones.

The diagenetic processes and evolution of the Lower Tuscaloosa sandstones were studied within three different diagenetic regimes defined by Morad et al., (2000) including: (1) eodiagenesis, or early diagenesis with burial depth <2 km and temperature <70ºC, in which pore water chemistry is controlled by depositional and surface waters; (2) mesodiagenesis, or burial diagenesis with burial depth ≥2 km and temperature ≥70ºC, which is mediated by evolved formation waters; and (3) telodiagenesis, which occurs after uplift and/or tectonic inversion, and thus creates exposure of previously buried sedimentary sequences (Fig. 3.1).

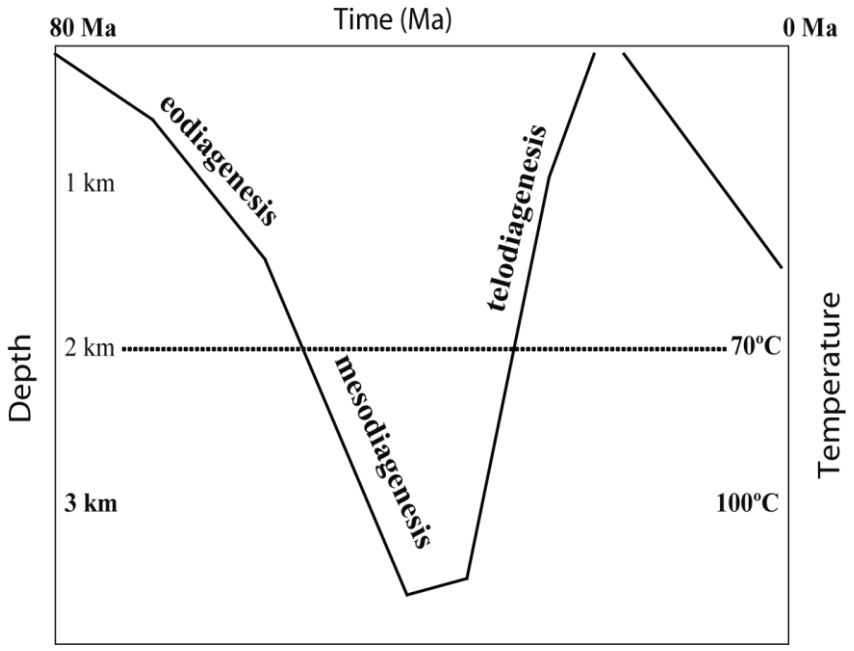

Figure 3.1-Three different diagenetic regimes defined by Morad et al., (2000) including: eodiagenesis (burial depth < 2 km and temperature < 70ºC); (2) mesodiagenesis (burial depth ≥ 2 km and temperature ≥ 70ºC); and (3) telodiagenesis, which occurs after uplift and/or tectonic inversion.

3.2-SAMPLES AND ANALYTICAL METHODS

Four whole cores from the reservoir interval, that is the Massive Sand Member (E and D Units) of the Lower Tuscaloosa Formation, were sampled and analyzed in Wells CFU#28-1, CFU#29-12, CFU#31F2 and CFU#31F3 at Cranfield Field. Twenty-four core plugs from Well CFU#28-1, 65 from Well CFU#29-12, 52 from Well CFU#31F2, and 47 from Well CFU#31F3 were measured for core porosity and permeability by Denbury Onshore LLC.

One hundred thirty-one samples representing various facies, texture, composition and reservoir properties in different depths were collected from the four cores for petrographic studies. Detailed optical microscopy of the samples has been performed in both transmitted light (plane and polarized) and in bright-field reflected light on the 131 thin sections that were prepared after impregnation with blue epoxy resin under vacuum. The quantitative amount and types of detrital framework grains, authigenic components, and pore types were obtained by counting 350 points per thin section in the 58 representative samples from wells CFU#31F2 and CFU#31F3. Figure 3.2 shows the depth and position of the point counted samples in the sedimentary logs of the two wells.

Mean grain size was determined by measuring the longest axis of 100 randomly selected grains per thin section on each of the 58 point counted samples. The standard deviation and grain-size distribution of these measurements were used to estimate the sorting. Modal analysis determined detrital and authigenic mineralogy and porosity and investigated any possible controls on the diagenetic events by depositional systems and textural properties of the sandstone.

Scanning electron microscopy (SEM) was performed using the FEI Nova™ NanoSEM 430, which has high resolution imaging quality, at the Bureau of Economic Geology, The University of Texas at Austin. A total of 18 bulk samples were coated with a thin layer of gold-platinum and examined by scanning electron imaging to investigate crystal and textural habits, as well as the paragenetic relationship between diagenetic

components. Among the thin sections, 27 thin sections were coated with carbon and examined using the SEM by backscattered electron (BSE) high-magnification imaging. The SEM was equipped with an energy-dispersive X-ray spectroscope detector (EDS). The EDS was used for qualitative analysis of elemental composition of the different authigenic minerals. X-ray mapping or compositional imaging from the EDS was used to examine the two-dimensional distribution of elements on the specimen surfaces.

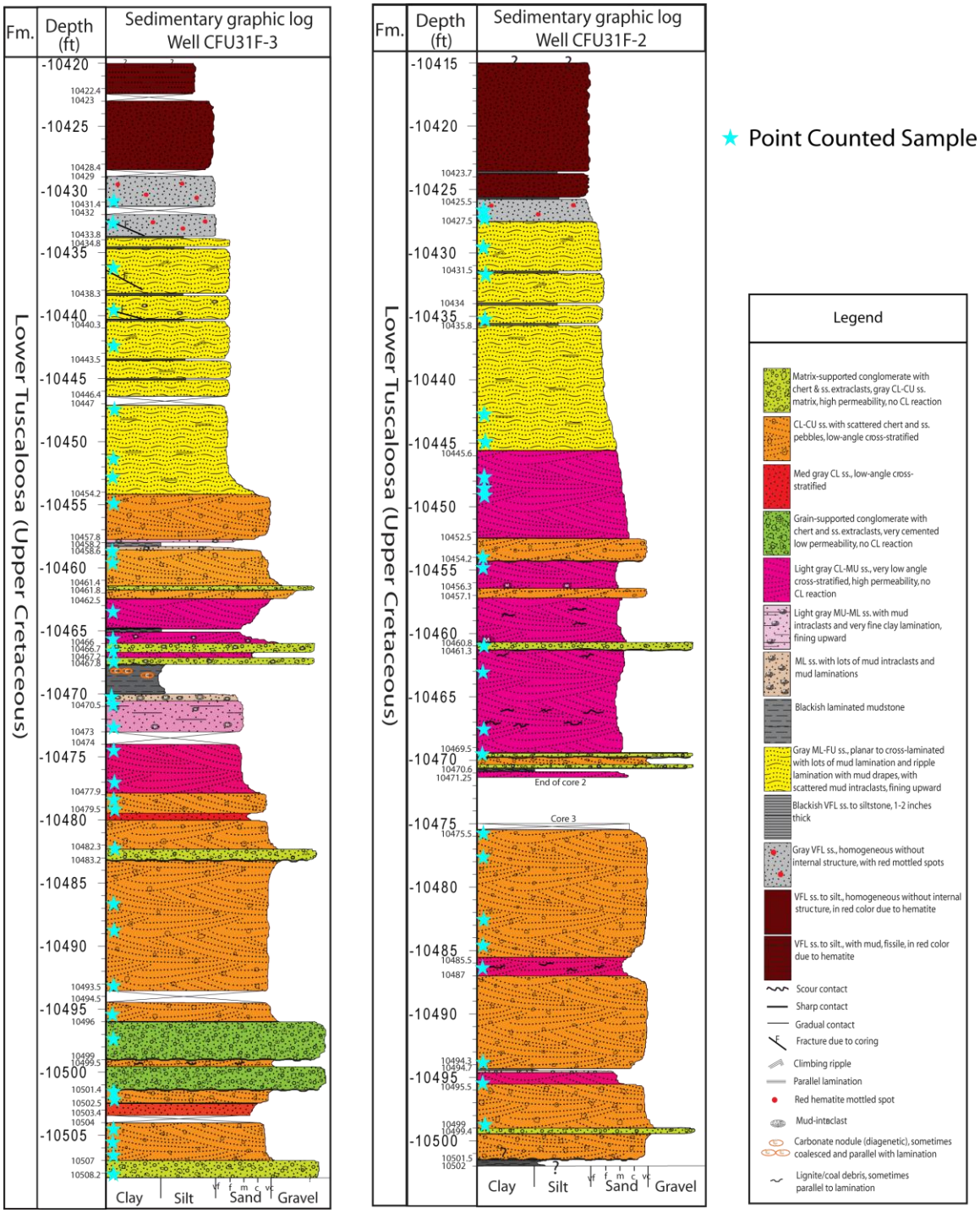

Figure 3.2-Sedimentary logs of wells CFU#31F2 and CFU#31F3 prepared for this study including depth and position of the 57 point counted samples.

3.3-SANDSTONES ARCHITECTURE

The four architectural components of sandstones, including framework grains (F), matrix (M), cement (C), and porosity (P), were distinguished and quantified in the Massive Sand Member of the Lower Tuscaloosa Formation. The overall average sandstone architecture for the Lower Tuscaloosa reservoir sandstones is $F_{57.3}M_{1.7}C_{10.9}P_{19.3}$ (Appendix III).

Framework grains are mainly composed of quartz with an average of 76.1% of framework grains, and a variety of rock fragments with an average of 23.5% of framework grains. Feldspar grains can hardly be seen in the thin sections (average of 0.4% of framework grains). Minor amounts of other grains, including heavy minerals and micas (average of 0.7% of framework grains), are also present in the sandstones.

Matrix commonly is present as detrital pore-filling muds (average 1.4% of rock volume) and less commonly as mechanically infiltrated muds around the grains (average 0.3% of rock volume).

The most important authigenic minerals as cement phase in the Lower Tuscaloosa reservoir sandstones are chlorite pore-lining (chlorite coat) (ranging from 1.8% to 11.4% with average of 6.8%), quartz (ranging from 0% to12.3% with average of 2.2%) and carbonate (ranging from 0% to 11.6% with average of 1.6%). Minor amounts of titanium oxide (average of 0.2%), kaolinite (average 0.1%), pyrite and iron oxide (average 0.1%) cements are also present in the sandstones.

Various types of porosity including intergranular (av. 15%), intragranular (av. 2.4%), moldic (av. 1.2%), oversized (av. 0.6%), and micropores are observed in the Lower Tuscaloosa reservoir sandstones. Framework grains, matrix and porosities will be explained in more detail in sections 3.5 and 3.7. In the diagenetic alterations section, different types of cements will be described quantitatively.

3.4-CONGLOMERATE

Conglomerates (containing more than 80% angular to subangular gravel coarser than 2 mm; Folk, 1980) are present at the base of the fining-upward units in the channel fill intervals of the Massive Sand Member (Fig. 3.2). They range in thickness from 5 cm to 90 cm and average 15 cm. Conglomerates are polymodal, ranging from matrix-supported conglomerate with coarse sandstone matrix to grain-supported conglomerate with chert and sandstone clasts. The clasts are white to light gray lithic clasts, quartzite and pale red chert pebbles, and moderately to well rounded, up to 3 cm in diameter. The dark-gray mud rip-up clasts (up to 5 cm in diameter) are also observed in the basal conglomerate. Some parts of the conglomerates are noticeably cemented by carbonates, but some parts are not fully lithified.

3.5-DETRITAL COMPOSITION AND CLASSIFICATION OF SANDSTONES

Framework composition of the Lower Tuscaloosa reservoir sandstones is classified as sublitharenite to litharenite by present day mean modal composition of $Q_{76.1}F_{0.4}L_{23.5}$ (Folk, 1980) (Fig. 3.3; Appendix III). Diagenesis overprinted the original detrital composition through dissolution and/or replacement of framework grains (mostly feldspars and rock fragments). The restored composition of the sandstones will be discussed in section 3.6.

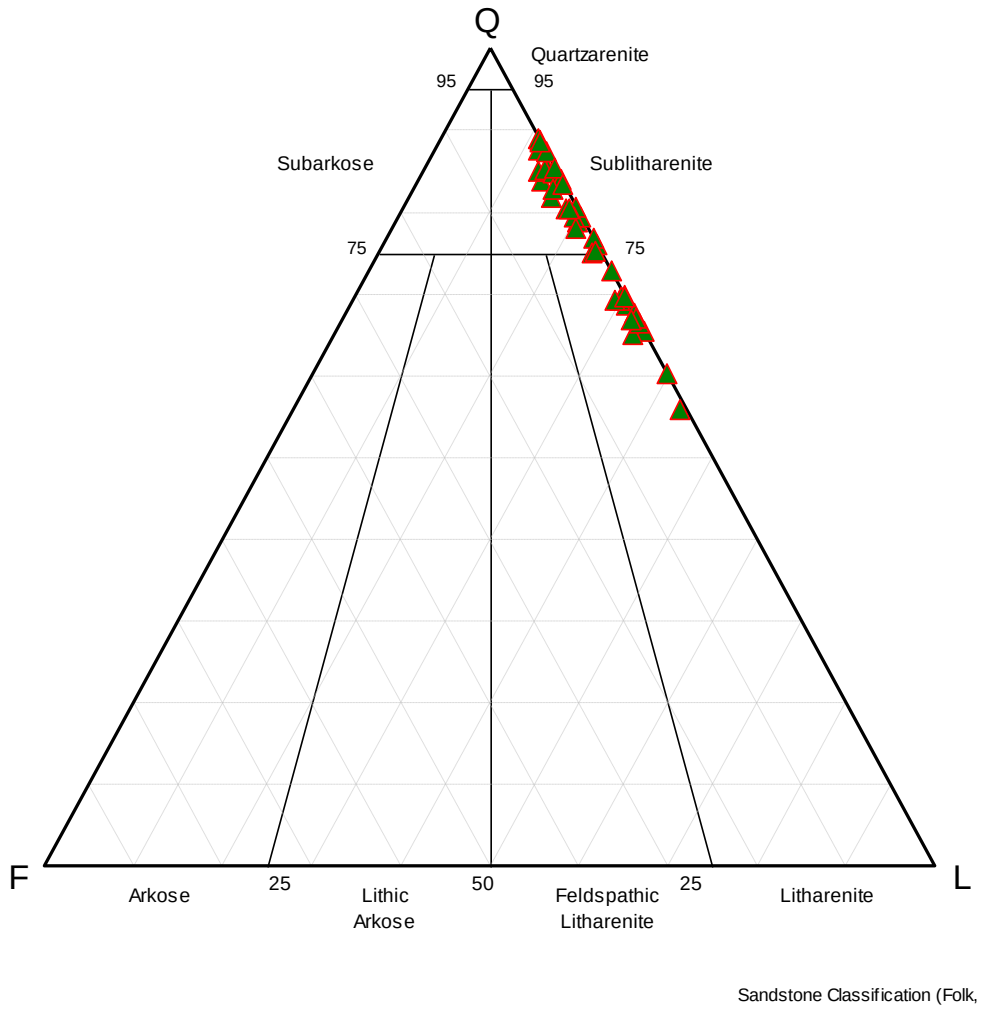

Figure 3.3-Present day framework grains composition of the Lower Tuscaloosa reservoir sandstones, based on the classification of Folk (1980).

3.5.1-Framework grains

Point counting category and their related values in modal analysis, including percent value of framework grains, in the 57 studied thin sections are reported in Appendix (III).

3.5.1.1-Quartz

Quartz grains are the major detrital component of framework constituents in all studied samples, ranging from 51.7% to 89.1% (average 76.1%) of framework grains. Among the total quartz grains, approximately 82.7% of quartz grains are monocrystalline, 6.5% polycrystalline with less than five subcrystals, and 10.8% polycrystalline with more than five subcrystals. Monocrystalline quartz grains have straight or slightly undulose extinction (Fig. 3.4a). Some of the monocrystalline grains have minor amount of inclusions (tourmaline and rutile minerals) and vacuoles. Polycrystalline quartz grains have polygonal crystal boundaries or crenulated crystal boundaries.

3.5.1.2-Feldspars

The amount of feldspars including potassium feldspar (orthoclase and microcline) and plagioclase in most of the sandstones is small, with average of 0.4% of framework grains (Fig. 3.4b). Presently, feldspar grains are mostly observed in the fine to very fine grained sandstones at top of the reservoir interval. Most of the observed feldspars are partly dissolved, kaolinitized or sericitized (Fig. 3.4c). Textural evidence, such as partly dissolved and replaced feldspars, moldic pores, kaolinite patches with well-defined relic outlines and similar in size to the original detrital feldspar grains indicate that original feldspar content was greater at the time of deposition.

3.5.1.3-Rock fragments

The distinguishable rock fragments in the studied samples range from 10.9% to 48.3% and average 23.5% of the framework grain fraction. Different type of rock fragments including metamorphic, igneous and sedimentary are present in the samples. Microquartz grains with average of 11.9% and foliated metamorphic rock fragments with average of 7.7% are the most abundant lithic components. The microquartz grains are microcrystalline or cryptocrystalline chert grains and microfibrous chalcedony rock fragments (Fig. 3.4d). Some of the grains include circular or ovoid ghosts of former

silicified carbonate particles and intragranular pores due to dissolution of dolomite crystals and fine carbonate fragments and thus were considered as chert (sedimentary rock fragment). The microquartz grains that do not have such evidence could be either silicified volcanic or metamorphic rock fragments (extrabasinal) or reworked from silcrete layers (intrabasinal).

The metamorphic rock fragments are mostly metamorphosed chert, phyllite, schist and slate (Fig. 3.4e). Quartz grains composed of high amount of biotite or muscovite flakes between subcrystals were considered as metamorphic rock fragments. The metamorphic rock fragments usually show an elongation of grain fabric and deformation that are effects of mechanical compaction.

Sedimentary rock fragments, averaging 3.8%, are mostly composed of siltstone/claystone grains (average of 1.3%) and rip-up mudstone clasts (average of 2.5%; Fig. 3.4f). The rip-up mudstone clasts are intraclasts that are locally derived; so they are considered as rock fragments in the present day sandstone composition and classification, but they have not been considered in the restored sandstone composition. The rip-up mudstone clasts are more common at the base of channel fills and are indicative of a high energy environment with great erosion potential (Fig. 3.2). Many of the rip-up mudstone clasts and other ductile rock fragments (like claystone sedimentary and metamorphic rock fragments) are squeezed between more rigid grains during the mechanical compaction, forming pseudomatrix. However, they have been considered as rock fragments in the point counting and present day sandstone classification.

In the thin sections, abundant altered rock fragments are present as dark green and black grains or partially to totally opaque aggregates (Figs. 3.5a and b). In some cases, unoriented, white feldspar crystals can be seen within altered grains. It is common for these altered grains to be partially dissolved or broken up. Numerous studies reported that the chlorite present in the Lower Tuscaloosa sandstones derived from alteration of volcanic rock fragments (e.g. Thomson, 1979; Hearne and Lock, 1985; Hamlin and

Cameron, 1987; Klicman et al., 1988; Genuise and McBride 1990; Paxton et al., 1990; Pittman et al., 1992; Cameron et al., 1992; Ryan and Reynolds, 1996, 1997). Considering the provenance of the Lower Tuscaloosa Formation (for sediment provenance, see Chapter 1, section1.4.3), it is highly likely that most of the altered rock fragments seen in the thin sections originally were volcanic rock fragments. Presence of abundant altered volcanic rock fragments indicates that original volcanic rock fragments content was high at the time of deposition. As I will explain in the diagenesis section, the SEM, EDS and X-ray mapping on polished thin sections showed that the opaque remnants are titanium oxide (TiO_2) in composition (Fig. 3.5b). This shows that the original compositions of volcanic rock fragments were mafic and ultramafic, which can contain a high amount of TiO_2 (up to 10%) in composition (Whitney and McClelland 1983; Newman, 1987; Brigatti et al., 1991; Deer et al. 1992).

3.5.1.4-Accessory minerals

Micas (muscovite and biotite), heavy minerals and organic matter (lignite/coal) make up an average of 0.7% of the framework grains (Figs. 3.5c and d). Micas, as major type of micaceous minerals, can be mostly observed in fine to very fine grained sandstones and siltstone at the top of the fining-upward cycles of the reservoir interval (Figs. 3.5c and 3.2). In some instance, muscovite appears to be dissolved or replaced by kaolinite. Biotites also have been partially to completely replaced by Ti oxide or chlorite. Bent or broken micas were observed as a result of mechanical compaction. Zircon and tourmaline are the most common heavy minerals in the studied samples (Fig. 3.5d). Organic matter as lignite/coal is observed as a minor component in a few samples.

3.5.2-Matrix

In the studied sandstones, detrital matrix averages 1.7% of total rock volume. Although matrix commonly constitutes less than 1%, it can reach up to 13.3% in some samples. Matrix is present as both detrital pore-filling muds (average 1.4%; Fig. 3.5e)

and as mechanically infiltrated muds around the grains (average 0.3%). Pseudomatrix, which formed by deformation of ductile grains (Fig 3.5f), is not considered as matrix.

Petrographic studies show a general fining-upward and consequently increase of matrix in the sandstones from the bottom to top of the channel fill cycles (Fig. 3.2). Sandstones of the basal E Unit have lower amount of matrix with average of 0.5%, compared with the upper D Unit with an average of 2.8%, indicating the decreasing energy of the system from the lower unit to the upper unit (for depositional environment, see Chapter 2, section 2.9.2). The infiltrated muds are made up of a few micrometers of irregular, iron-oxide-stained clays. These features, in addition to the fact that they can be found at grain contacts, contain clay particles oriented parallel to grain surfaces or around the margin of pores and concentrate in finer-grained laminae, are characteristics of the mechanically infiltrated muds (Wilson, 1992; Moraes and DeRos, 1992).

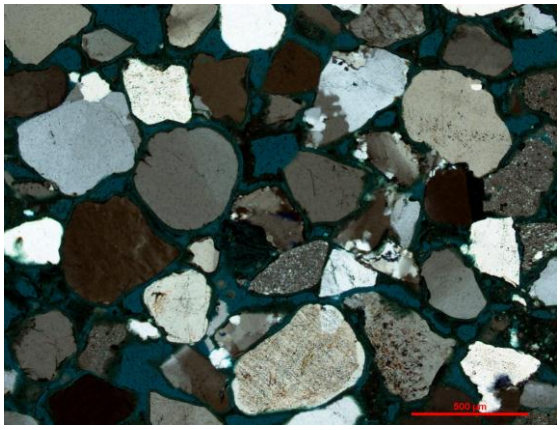

a

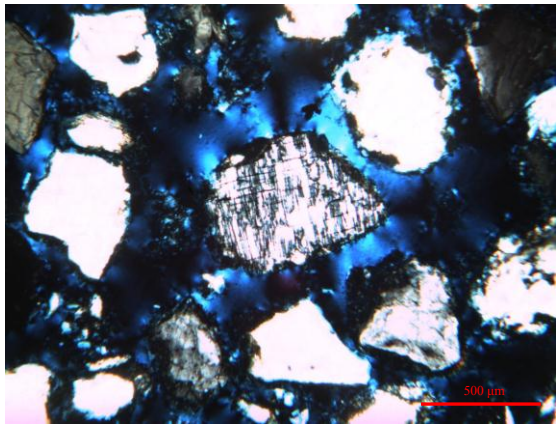

b

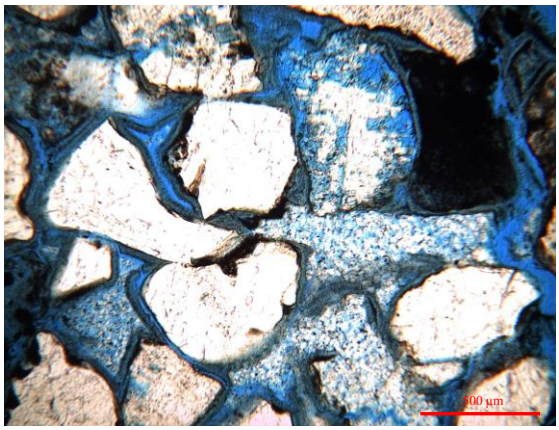

c

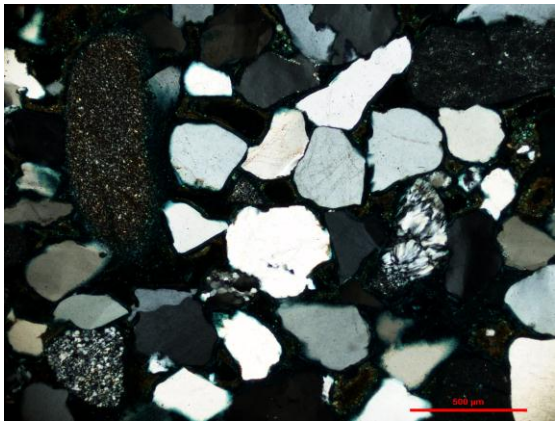

d

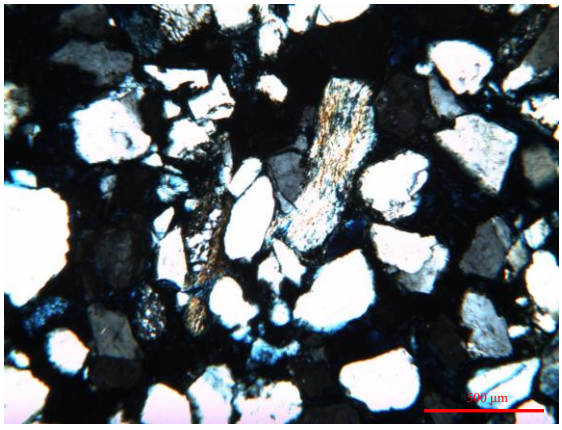

e

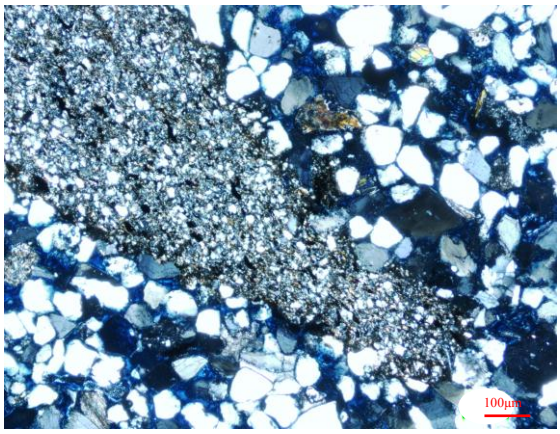

f

Figure 3.4-Photomicrographs showing framework grains including (a) quartz grains as dominant framework grain, (b) Microcline grain, (c) partially dissolved and totally kaolinitized feldspars, (d) microquartz grains, (e) metamorphic rock fragment, (f) sedimentary rock fragment.

a

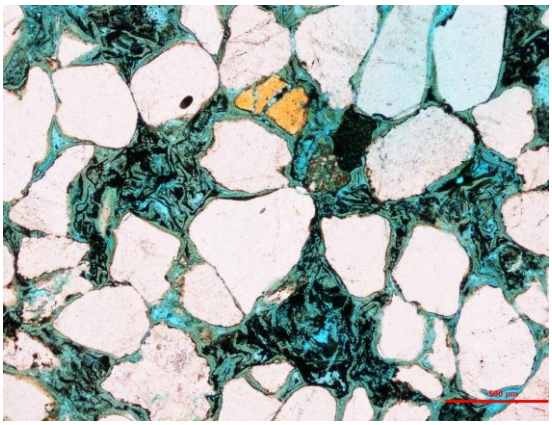

b

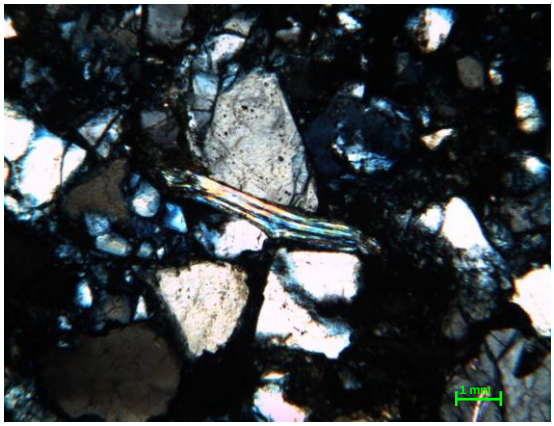

c

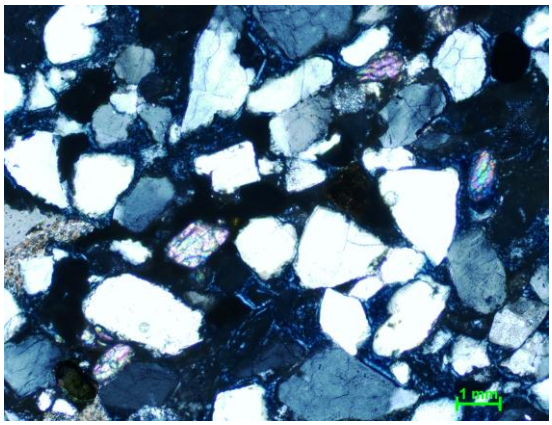

d

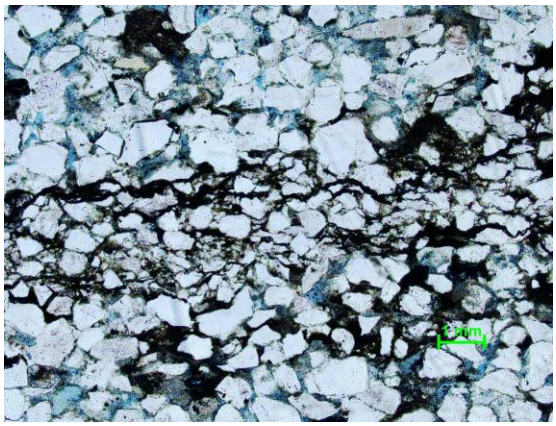

e

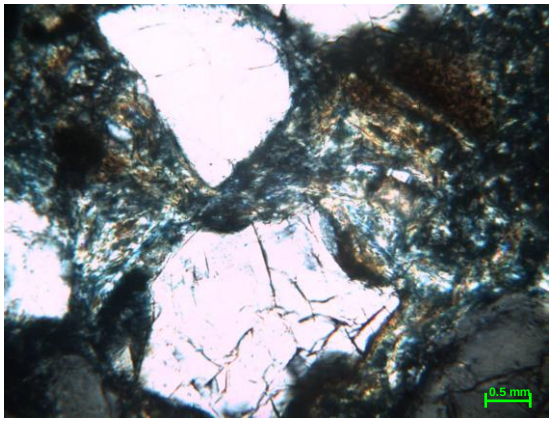

f

Figure 3.5-Photomicrographs showing (a) partially altered rock fragments, (b) remnant of altered rock fragments as meshwork of chlorite and Ti oxide, (c) muscovite grain, (d) heavy minerals, (e) pore filling matrix, (f) deformation of metamorphic rock fragment and formation of pseudomatrix.

3.6-RESTORED FRAMEWORK GRAINS COMPOSITION

Detrital composition of sandstones may be significantly altered by dissolution or replacement of the framework grains (mostly feldspars and rock fragments) during diagenesis (Pettijohn et al., 1987). The original content of feldspars and rock fragments in the Lower Tuscaloosa sandstone reservoirs were restored through detailed petrographic and modal analysis.

The original content of feldspars was calculated as:

$$FO= F + IP + RK + RA/3+ OP/3 + MP/3 + mP/4$$

Where:

FO= original feldspar content

F= current feldspar content (k-feldspar and plagioclase)

IP= intragranular pores within feldspars

RK= replacive kaolinite

RA= replacive ankerite

OP = oversized pores

MP = moldic pores

mP= micropores

The original content of rock fragments was calculated as:

$$RFO= RF + IP + RC + RT + RA/3+ OP/3 + MP/3 + mP/2$$

Where:

RO= original rock fragments content

RF= current extrabasinal rock fragment content

IP= intragranular pores within rock fragments

RC= replacive chlorite

RT= replacive Ti oxide

RA= replacive ankerite

OP = oversized pores

MP = moldic pores

mP= micropores

One-third of the oversized pores were interpreted to be primary porosity and one-third of the moldic porosities were considered to be related to dissolution of other grains than extrabasinal rock fragments and feldspars (intabasinal mudstone clasts, rip-up clasts, heavy minerals, etc.). One-third of the replacive ankerite was thought to be replaced other grains than rock fragments and feldspars. One-fourth of the microporosities were considered to be associated with the kaolinite that replaced feldspars (not kaolinite cement) and two fourth (one half) of the microporosities were estimated to be related to chlorite and also Ti oxide that replaced rock fragments (not chlorite and Ti oxide cements).

The reconstruction of the restored framework composition of the Lower Tuscaloosa sandstones revealed that they were mostly litharenite with a mean modal composition of $Qr_{58.7}Fr_{2.8}Lr_{38.5}$ (Fig. 3.6; Appendix III). During diagenesis they altered to the present day framework composition, which is sublitharenite to litharenite by mean modal composition of $Q_{76.1}F_{0.4}L_{23.5}$ (Fig. 3.3). The restored composition of the sandstones shows that they were more feldspar-rich and especially more lithic-rich during deposition, considering that the mud intraclast and rip-up clasts that were intrabasinal clasts and added to the sandstone composition during sedimentation were not taken into account in the original sandstone composition. By adding the intrabasinal clasts to the restored composition, it is revealed that an average of 18.8% of original rock fragments content was lost during diagenesis. Most of this amount may be related to the original volcanic rock fragments content.

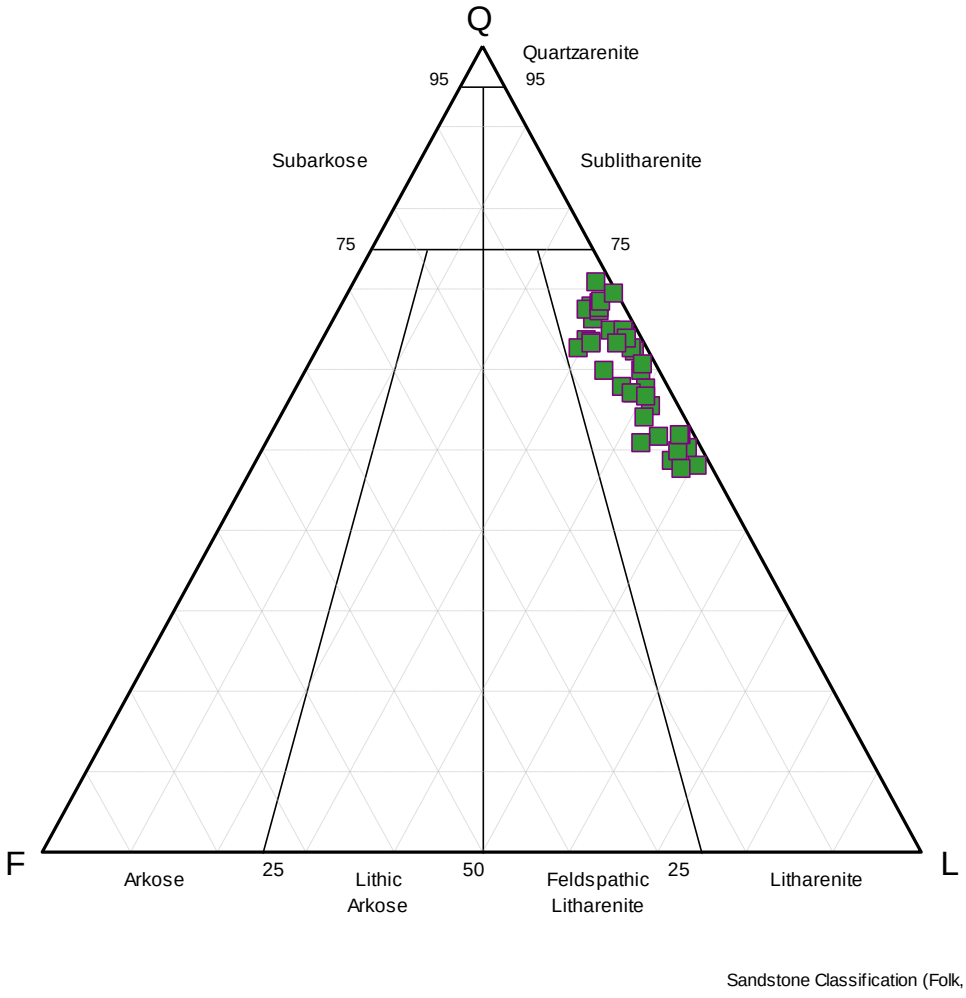

Figure 3.6-Restored framework composition of the Lower Tuscaloosa reservoir sandstones is classified as litharenite, based on the classification of Folk (1980), with mean modal composition of $Qr_{58.7}Fr_{2.8}Lr_{38.5}$.

3.7-PORE TYPE AND DISTRIBUTION

Various types of pores were observed in the Lower Tuscaloosa reservoir sandstones, including intergranular, intragranular, moldic, oversized, which are visual or macropores, as well as micropores. Different types of macropores can be distinguished and point counted under the microscope as optical (thin section) porosity. Total point count (thin section) porosity of the studied samples averages 19.3%, although it varies

widely between 5.8 and 30.9%. Micropores (with pore sizes less than 30 μm) can just be seen at high optical magnification, but their volume can be calculated by a method that I will explain in this section.

Intergranular porosity ranges from 4.9% to 24.9%, with an average of 15% in the Tuscaloosa sandstone reservoir. On average, the intergranular porosity constitutes up to 77.7% of the total visual porosity. Intragranular pores (average of 2.4%), include all pores within partially dissolved framework grains, mostly rock fragments, micas and chert grains (Fig. 3.7c). Fracture porosity, which is a type of secondary porosity, could also generate intragranular pore, however in studied samples, it rarely can be seen and its portion is negligible. Complete dissolution of the detrital grains produced moldic and oversized pores (Figs. 3.7a and b). The moldic pores (average of 1.2%) in the sandstone were usually delineated by characteristic outlines of their completely dissolved precursor or by presence of some relict enclosing material, most importantly chlorite coats (Fig. 3.7a). The oversized pores (average of 0.6%), are larger than normal intergranular pores and are comparable with the average grain size or neighboring grain size (Fig. 3.7a).. In the studied sandstones, usually dissolution of large mud intraclasts, matrix, or pseudomatrix generated oversized pores.

For classification of the visual porosities in this study, all intergranular pores were considered to be primary. Oversized pores are a combination of both secondary pores (dissolved grain) and primary (intergranular pores that surrounded dissolved grain); and thus one-third of the oversized pores are assumed to be primary and two-thirds secondary. Therefore, primary visual porosity is the sum of intergranular porosity, one-thirds of the oversized pores. Secondary macroporosity is the sum of intragranular porosity, moldic porosity, two-thirds of the oversized pores.

The high amount of microporosity is also present in the Lower Tuscaloosa sandstone reservoir. The micropores are visible at high optical magnification or in the scanning electron microscopy (SEM) (Figs. 3.7d, e and f). They are mostly distributed

among clay platelets (mostly chlorite and kaolinite; Figs. 3.7d, e and f) and within oxides (Ti and Fe oxides) and matrix as well as in some secondary pores, that originated by partial dissolution of rock fragments and cherts. Petrophysical tests run on the same sandstone in 17 core samples indicate air porosities ranging from 5.9% to 31%, with averages of 23%. Because the petrophysical porosimeter measurements include both macro and micro porosities, the differences in porosity values between petrophysical and optical measurements provide an estimate of the volume of microporosity in the studied Tuscaloosa sandstones (Fig. 3.8):

Microporosity (microφ) = φ porosimeter - φ thin section

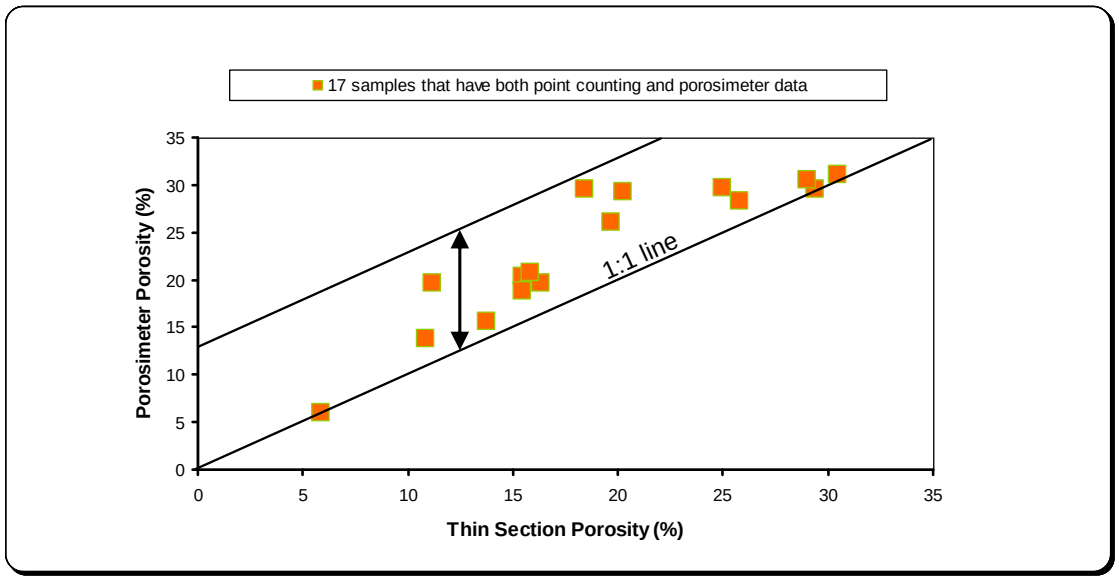

Figure 3.8-Cross-plot of porosimeter porosity versus thin section porosity. Upper line and arrow show range of variation between visual porosity and porosimeter porosity.

Total microporosity of the studied samples averages 5.5% of the rock volume. This could be associated with high amounts of authigenic clays (mostly chlorite, kaolinite), oxides (mostly Ti oxide and Fe oxide) and mudstone and claystone intraclasts.

Figure (3.9) shows frequency plots of different types of pores in the Lower Tuscaloosa sandstones.

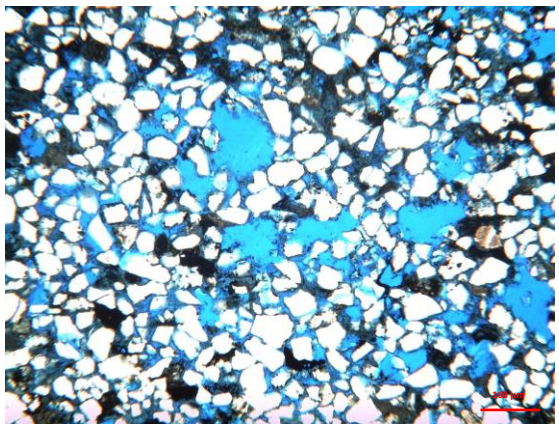

a

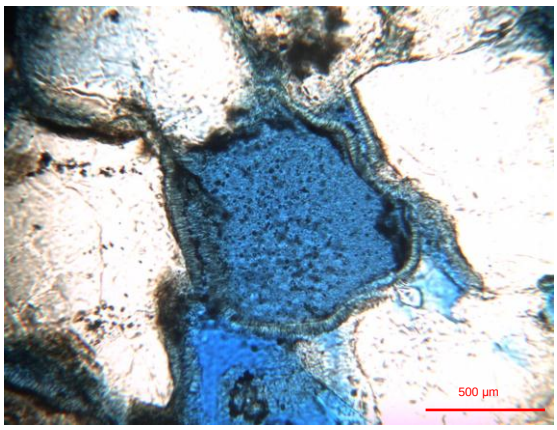

b

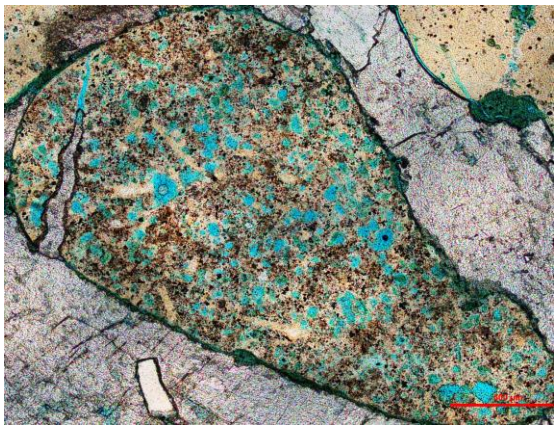

c

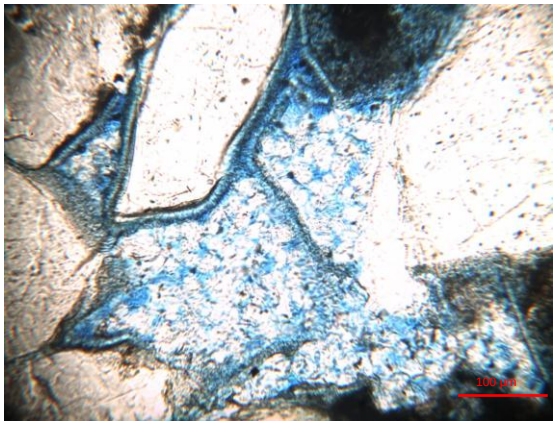

d

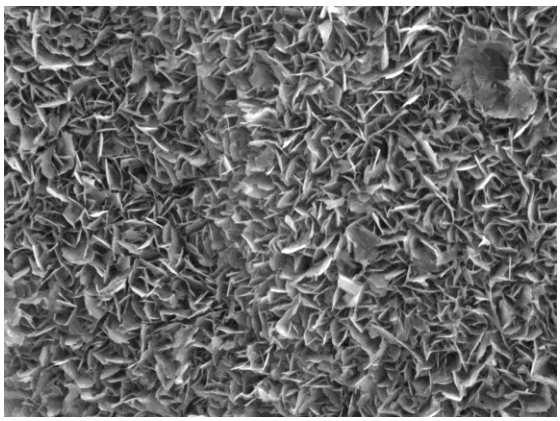

e

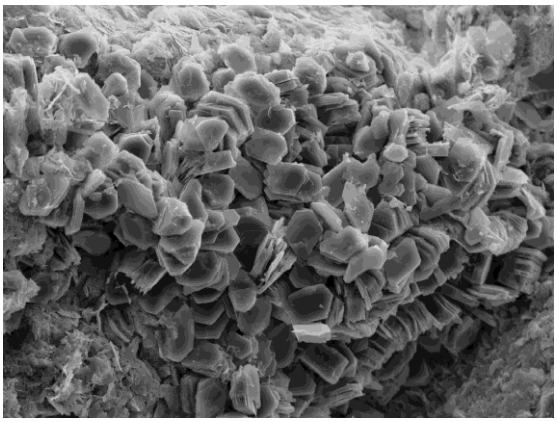

f

Figure 3.7-Photomicrographs showing different types of pores, (a) intergranular and oversized pores, (b) moldic pore delineated by chlorite coating, (c) intragranular pores within microquartz grain, (d) microporosity within kaolinite; and SEM images showing (e) microporosity within chlorite crystals, (f) microporosity within kaolinite crystals.

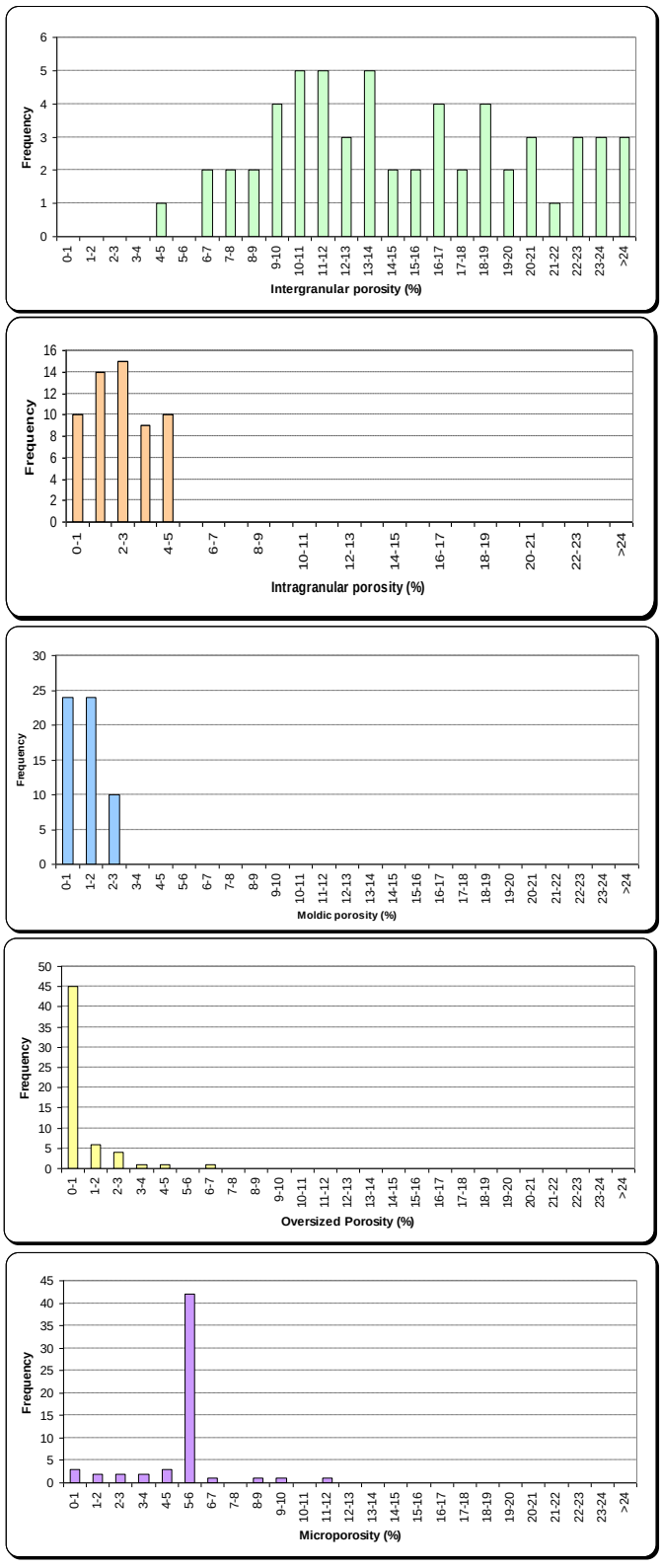

Figure 3.9-Frequency plots of different types of pores in the 57 studied Lower Tuscaloosa sandstones.

3.8- TEXTURAL CHARACTERISTICS

Textural analyses were performed on the 58 studied samples from the cores of the Lower Tuscaloosa sandstone reservoir in order to evaluate and quantify the influence of mean grain size and sorting on the amount and distribution of porosity and reservoir quality. Textural characterization of the samples was performed by measuring the apparent long axis of 100 randomly selected quartz grains on each thin section, following these steps:

i. Taking photomicrographs for each thin section. Depending on the approximate average grain size, the total photomicrographs in each thin section should include at least 100 grains. Traverses were made perpendicular to bedding and laminations, in order to record variations in grain size.

ii. Using the "JMicroVision 1.2.7" program, the drawing tool was calibrated with the scale of each photo; mostly the objective 5 or 10 was used.

iii. Drawing a line along the longest axis of the grains, using the 1D measurement tool in the program. This procedure should be repeated for all of the 100 grains in each sample.

iv. Exporting the line length values for all 100 grains in each sample.

Grain size data were then used to calculate statistical textural parameters including mean grain size and sorting (Appendix IV). Mean grain sizes of analyzed sandstones vary from very fine to very coarse; however, the most distribution is within medium (0.25-0.5mm) to coarse (0.5-1mm) grain size. Figure (3.10) shows the frequency distribution of the mean grain size in the studied thin sections.

Quantitative measurement of the sorting standard deviation was calculated by Trask's sorting coefficient, determined by $(P_{25}/P_{75})^{1/2}$ where P_{25} is the grain size at the 25^{th} percentile of the cumulative distribution and P_{75} is the grain size at the 75^{th} percentile of the cumulative distribution (Trask 1932; Folk 1974). The studied samples are mostly

moderately sorted. Figure (3.11) shows the frequency distribution of the sorting in the studied thin sections. The grain size and sorting values for the studied thin sections are reported in Appendix IV.

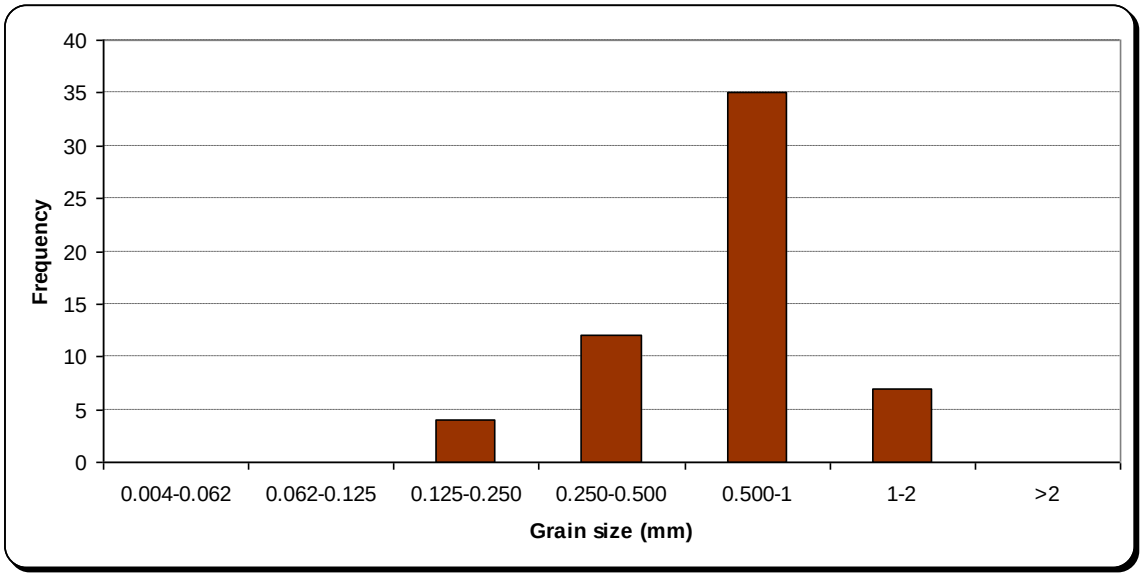

Figure 3.10-Frequency plot of distribution of the mean grain size in the 57 studied thin sections.

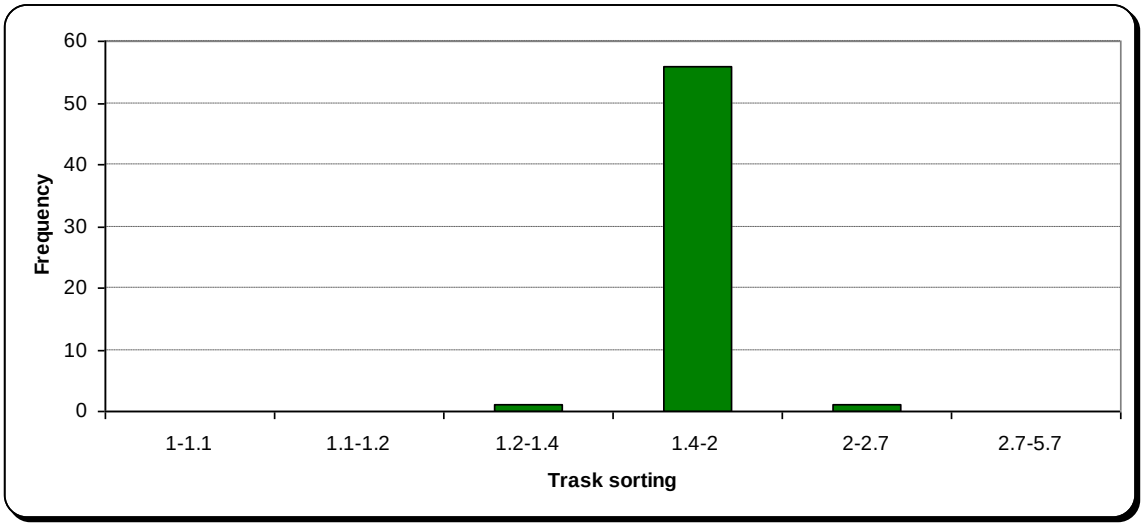

Figure 3.11-Frequency plot of distribution of the sorting in the 57 studied thin sections.

3.9-BURIAL-THERMAL HISTORY

Reconstruction of the burial and thermal histories is very important for understanding and interpreting the diagenetic history and reservoir quality evolution of the sandstones through time. Maximum burial depth and maximum temperature are the most important parameters that can be achieved from burial and thermal histories. For these reasons, burial and thermal histories of the Lower Tuscaloosa Sandstones were reconstructed using a one-dimensional (1-D) basin modeling program (Genesis^{TM} 5.21) developed by ZetaWare). Figures 3.12 and 3.13 show the combined plots of burial and thermal histories in Wells CFU#31F2 and CFU#31F3.

Basin modeling input data were obtained from wireline logs (bottom-hole temperature, time-since-circulation, Kelly bushing elevation, thickness of the penetrated formations and gross lithology), and stratigraphic data (age of formations, gross lithology, timing and magnitude of erosional events, and timing of hiatus) obtained from the literature (AAPG-Correlation of stratigraphic units in North America, 1988; Mancini and Puckett, 2005). The stratigraphic data used in burial-thermal histories reconstruction are reported in Table (3.1). In most cases, the true formation temperature is higher than the measured bottom-hole temperature during the logging, because of the cooling effects of drilling fluid circulation (Johnson and Nuccio, 1986). Therefore, the bottom-hole temperatures were corrected using the time-since-circulation method developed by ZetaWare (Table 3.2; Waples et al., 2004).

Well CFU#31F2			
Stratigraphic Unit/Event	**Base (Sub Sea) (ft)**	**Age (my)**	**Lithology**
Quaternary-Late Tertiary	1807	38	40ss30sh30silt
Cook Mountain	2584	43	80sh20ss-sh
Sparta	3146	45	80ss20sh
Zilpha	3568	47	80sh20silt
Tallahatta	3805	52	80silt20ss
Hiatus		53	
Wilcox	7416	60	60sh20ss20silt
Midway	8350	66	60sh20silt20ss-sh
Hiatus		68	
Selma Chalk	8842	78	90chal10sh
Hiatus		79	
Austin Chalk	9132	88	90chal10sh
Hiatus		89	
Eutaw/Upper Tuscaloosa	9715	92	25sh25ss25silt25sh-ss
Marine Shale/Middle Tuscaloosa	9856	94	90sh10silt
Lower Tuscaloosa	10182	95	80ss10cong10sh

Well CFU#31F3			
Stratigraphic Unit/Event	**Base (Sub Sea) (ft)**	**Age (my)**	**Lithology**
Quaternary-Late Tertiary	1807	38	40ss30sh30silt
Cook Mountain	2588	43	80sh20ss-sh
Sparta	3146	45	80ss20sh
Zilpha	3568	47	80sh20silt
Tallahatta	3809	52	80silt20ss
Hiatus		53	
Wilcox	7409	60	60sh20ss20silt
Midway	8380	66	60sh20silt20ss-sh
Hiatus		68	
Selma Chalk	8848	78	90chal10sh
Hiatus		79	
Austin Chalk	9140	88	90chal10sh
Hiatus		89	
Eutaw/Upper Tuscaloosa	9718	92	25sh25ss25silt25sh-ss
Marine Shale/Middle Tuscaloosa	9860	94	90sh10silt
Lower Tuscaloosa	10187	95	80ss10cong10sh

Table 3.1-Stratigraphic data used in burial-thermal history reconstructions of Wells CFU#31F2 and CFU#31F3.

Well name	Circulation Time (hours)	Depth TVD (ft)	Bottom-hole Temperature (ºF)	Corrected Formation Temperature (ºF)
CFU#31F3	10.33	1043 6	221	254.86
CFU#31F2	10.75	10456	215	248.38

Table 3.2-Bottom-hole temperatures and corrected formation temperatures using time-since-circulation for burial-thermal history reconstructions of Wells CFU#31F2 and CFU#31F3.

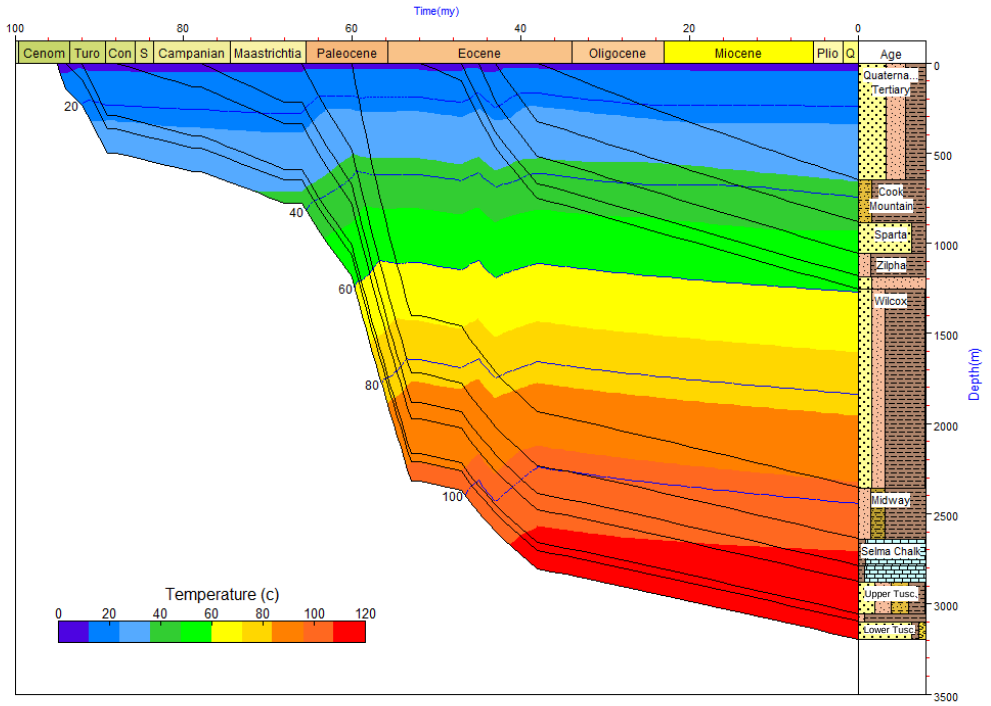

Figure 3.12-Combined plots of burial and thermal histories in Well CFU#31F2.

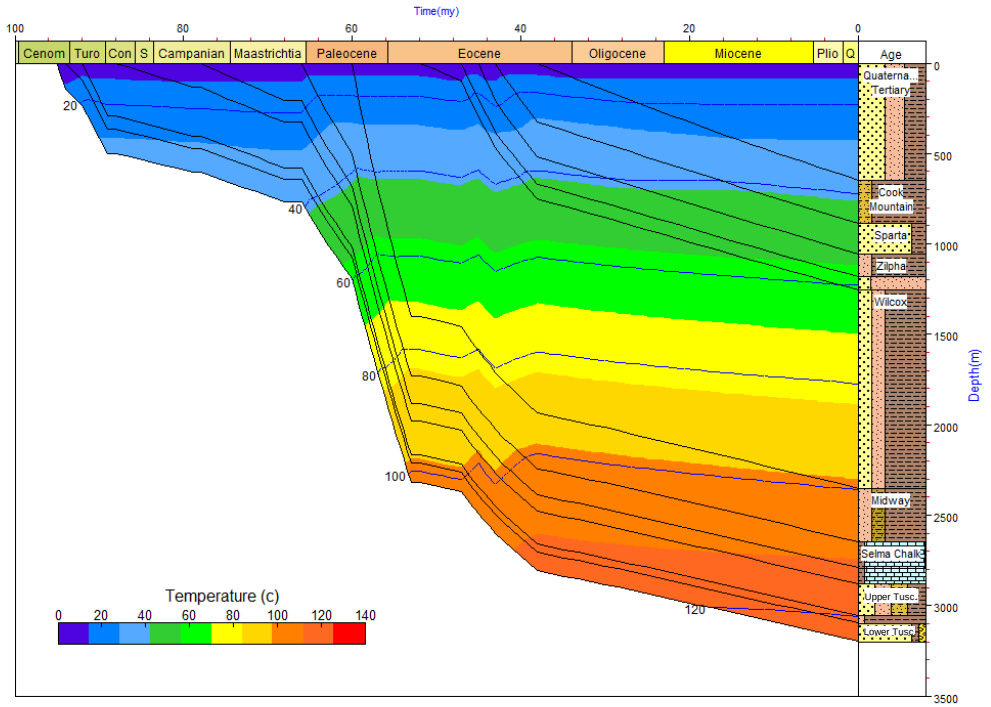

Figure 3.13-Combined plots of burial and thermal histories in Well CFU#31F3.

3.10- DIAGENETIC ALTERATIONS AFFECTING RESERVOIR QUALITY

During burial of the Lower Tuscaloosa sandstones, different diagenetic alterations including compaction, cementation, replacement and dissolution modified the original porosity and permeability. The major objective of the following discussion is to identify and quantify the diagenetic events affecting the reservoir quality.

3.10.1-Compaction

Pittman and Larese (1991) divided compaction into physical and chemical processes. The physical processes or mechanical compaction is an irreversible process that decreases the pore volume and increases the density as a function of increasing effective stress (lithostatic pressure minus pore fluid pressure) through the burial (Croize et al., 2009). Chemical compaction is the bulk volume reduction caused by the dissolution of framework grains at points of contact (Fűchtbauer, 1967; Houseknecht, 1987). It occurs in the form of intergranular pressure dissolution and stylolites. Mechanical compaction, which is controlled by the composition, size, sorting, shape, and mechanical properties of the grains and lithology as wells as by burial history, includes (1) grain rearrangement, (2) ductile deformation, and (3) brittle failure of grains (Paxton et al., 1990, 2002; Pittman and Larese, 1991; Lundegard, 1992; Ehrenberg, 1995; Lander and Walderhaug, 1999; Makowitz and Milliken, 2003; Taylor et al., 2010).

The effects of mechanical compaction on the Lower Tuscaloosa reservoir sandstones are observed as broken and contorted chlorite rims (Fig. 3.14a), bent and deformed ductile grains (argillaceous rock fragments and rip-up clasts, low-grade metamorphic rock fragments and micas; Fig. 3.14b and c), formation of pseudomatrix by soft grain deformation between the rigid grains (Fig. 3.5f) and rarely as fractured brittle grains (quartz and chert; Fig. 3.14a, e and f). Burley et al., (1985) reported that mechanical compaction usually occurs in shallow to intermediate burial (0-2.5 km). Figures (2.14e and f) show SEM images of precipitated micro-quartz in a fracture of

quartz grain, indicating formation of the fracture during diagenesis before quartz cementation.

In the Lower Tuscaloosa sandstones, due to presence of ductile grains (micas, argillaceous rock fragments, mud intraclasts and rip-up clasts) and dissolved/altered volcanic rock fragments, mechanical compaction is more penetrative and the ductile deformation has more effect on reduction of pore volume than brittle deformation. In general, loss of porosity by compaction was by grain rearrangement and ductile grain deformation.

The chemical compaction, that is more important during deeper burial (Giles, 1997), was evidenced by presence of concavo-convex and sutured contacts (pressure dissolution) (Fig. 3.14d). Although the chemical compaction is not very abundant in the studied samples, it is more common in the fine to very fine grained sandstones at the top of the reservoir units (Fig. 3.2). The finer grained sandstones at the top of the reservoir interval contain thin or discontinuous chlorite coatings compared to the coarser grain sandstone at the base. This suggests a relationship between anti-compaction and chlorite coatings, most probably due to inhibition of pressure dissolution by chlorite coatings in coarser-grained sandstones with the thick, well-formed chlorite coats.

Intergranular volume (IGV), which is the sum of intergranular primary porosity, intergranular cement and detrital matrix, has been widely used as a means of evaluating the importance of, and as an indirect measurement of compaction. It is determined by point counting of petrographic thin sections and is reported as a percentage of the rock volume. The IGV is a key parameter for assessing effect of the compaction on porosity reduction during burial by assuming a depositional porosity based on analogs (e.g. Paxton et al., 1990, 2002; Ehrenberg, 1995; Lander and Walderhaug, 1999; Taylor et al., 2004). The initial depositional porosity ranges from about 40% of sediment volume for well-sorted sand-size sediments to much higher values (around 80 %?) for sediments containing abundant clay size particles (Pryor, 1973; Houseknecht, 1987; Atkins and

McBride, 1992; Ehrenberg, 1995). During the initial process of compaction, by stable packing configuration in grain rearrangement, which is commonly achieved by 1.5 to 2.5 km burial depth, the IGV can be reduced to a hypothetical minimum value of ~26% (Houseknecht, 1987; McBride et al., 1991; Paxton et al., 1990, 2002; Ajdukiewicz et al., 1991; Szabo and Paxton, 1991; Ehrenberg, 1995; Lander and Walderhaug, 1999; Taylor et al., 2004; McBride, 2012). Any further reduction of IGV requires the function of other compaction mechanisms such as ductile deformation, brittle deformation and/or pressure dissolution (Dunn 1993; Onasch 1994; Paxton et al. 2002; Makowitz and Milliken 2003; Makowitz 2004; Taylor et al., 2004; McBride, 2012).

In the reservoir sandstones of Cranfield Field, the modal analysis revealed that the IGV was reduced to an average value of 27.2%. This showed that the compaction was an important porosity-reducing agent in the Tuscaloosa reservoir sandstones (Appendix III). A plot of IGV versus chlorite coats (Fig. 3.15) revealed that sandstones with more chlorite coat cements have undergone less mechanical compaction and thus display overall higher IGV, whereas sandstones with less chlorite coat cements were subjected to a considerable compaction and reduction of pore space during burial and thus lower IGV. This could also be related to relationships between thick well-formed chlorite coats in the coarser grain sandstones that act as anti-compaction by inhibition of pressure dissolution.

A comparison of thin section porosity versus IGV (Fig. 3.16) confirms that samples with higher chlorite coat content and thus higher porosity were less compacted than samples with lower amounts of chlorite coat and thus lower porosity.

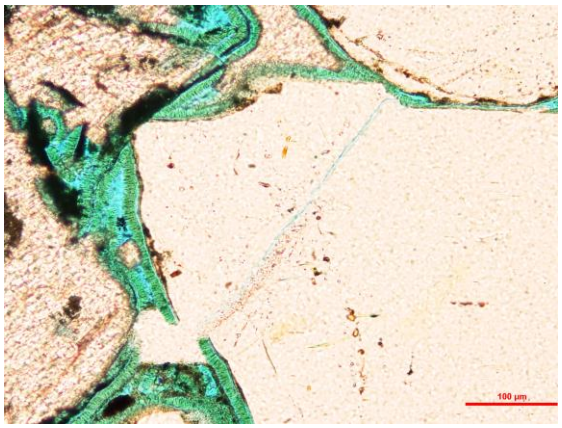

a

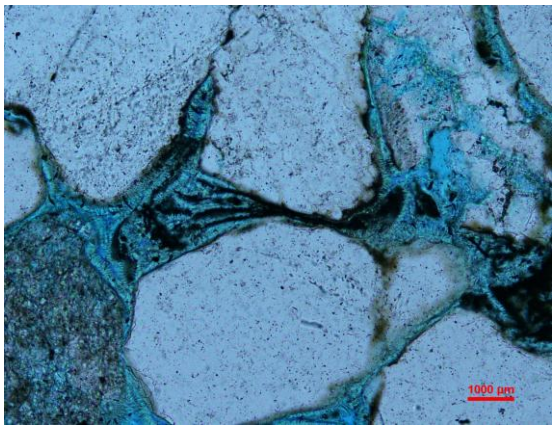

b

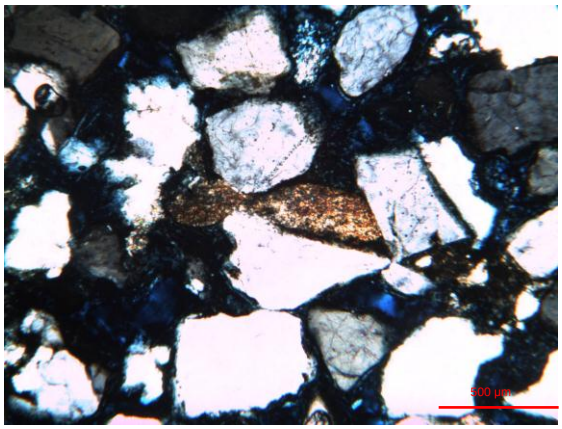

c

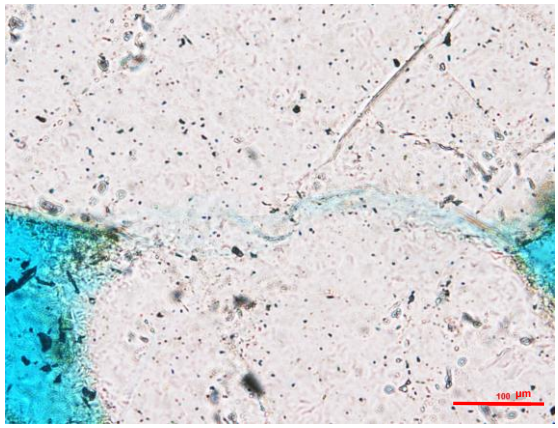

d

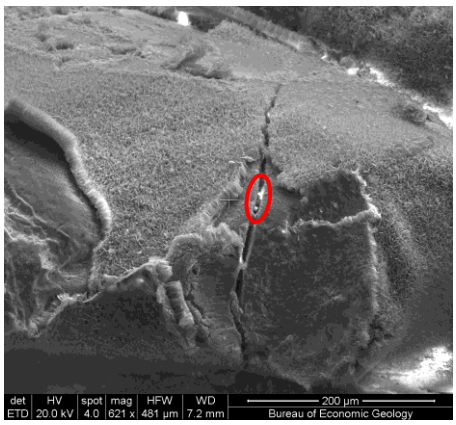

e

f

Figure 3.14-Photomicrographs showing evidences of compaction as (a) broken chlorite rim due to fracturing of a grain and formation of quartz outgrowth, (b) bent mica, (c) bent metamorphic rock fragment, (d) pressure dissolution; and SEM images showing (e) fractured quartz grain, (f) higher magnification with micro-quartz precipitated in the fracture, indicating formation of the fracture during diagenesis before quartz cementation.

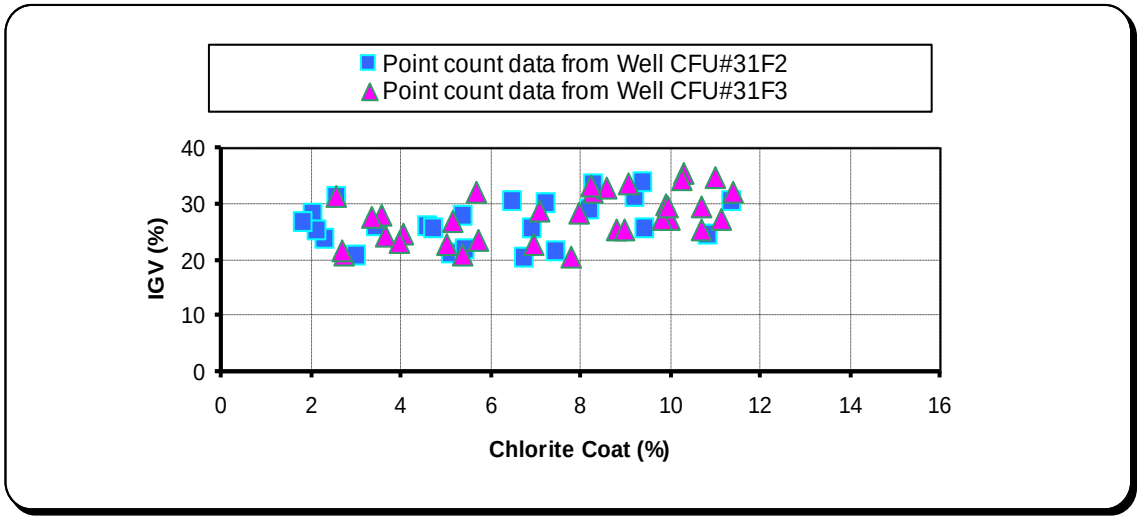

Figure 3.15-Cross-plot of IGV versus chlorite coat revealed that sandstones with more chlorite coat cement have undergone less mechanical compaction and thus display overall higher IGV, whereas sandstones with less chlorite coat cements were subjected to a considerable compaction and reduction of pore space during burial and thus lower IGV.

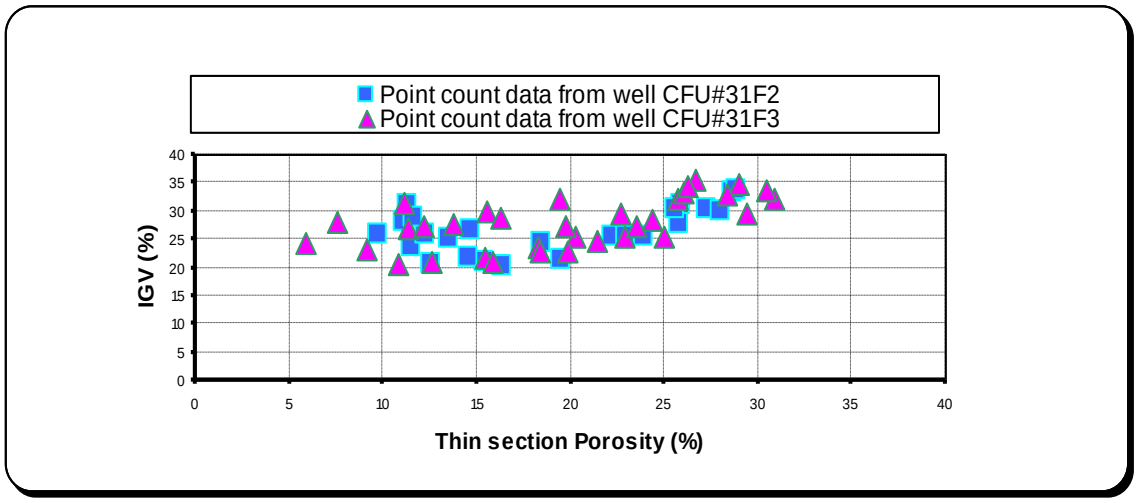

Figure 3.16-Cross-plot of IGV versus thin section porosity confirmed that samples with higher chlorite coat content and thus higher porosity were less compacted than samples with lower amounts of chlorite coats and thus lower porosity.

3.10.1.1-Relative importance of compaction and cementation to original porosity reduction

In this section I calculated and compared the amount of porosity that has been lost by the two most important diagenetic processes, compaction and cementation. The porosity loss by compaction (COPL), porosity loss by cementation (CEPL) and the index of compaction (I_{comp}), which is the ratio of compactional porosity loss to total porosity loss, were calculated from the point count data following established conventions (Ehrenberg, 1995; Lundegard, 1992; Paxton et al., 2002):

$$COPL = P_i - [(100 - P_i) * IGV / (100 - IGV)]$$

$$CEPL = (P_i - COPL) * C / IGV$$

$$I_{comp} = COPL / (COPL + CEPL)$$

Where C is volume of cement and P_i is assumed initial porosity of 40% (Ehrenberg, 1995; Lundegard, 1992). As Ehrenberg (1995) and Lundegard (1992) reported, if compaction index (I_{comp}) values are greater than 0.5, compaction is the predominant contributor to porosity loss compared to cementation, and vice versa.

Considering the initial porosity of 40% for the lower Tuscaloosa sandstones, the porosity loss by compaction ranges from 7.2% to 24.7% and averages 17.3%. The values of porosity loss by compaction vary from 4.7% to 17.6% with an average of 9%. The I_{comp} value in most of the samples is greater than 0.5. These indicate that compaction was more important than cementation in reducing the porosity of the sandstone through burial. Point counting categories and their related values in compaction analysis in the 57 studied thin sections are reported in Appendix (III).

The relative importance of compaction and cementation to porosity reduction also was determined by using the graph of intergranular volume versus cement of Houseknecht (1987). Results of applying this technique to the data from the Lower Tuscaloosa sandstones (Fig. 3.17) indicate that although both cementation and

compaction were important in reducing the original porosity, compaction was slightly more important than cementation in determining ultimate porosity.

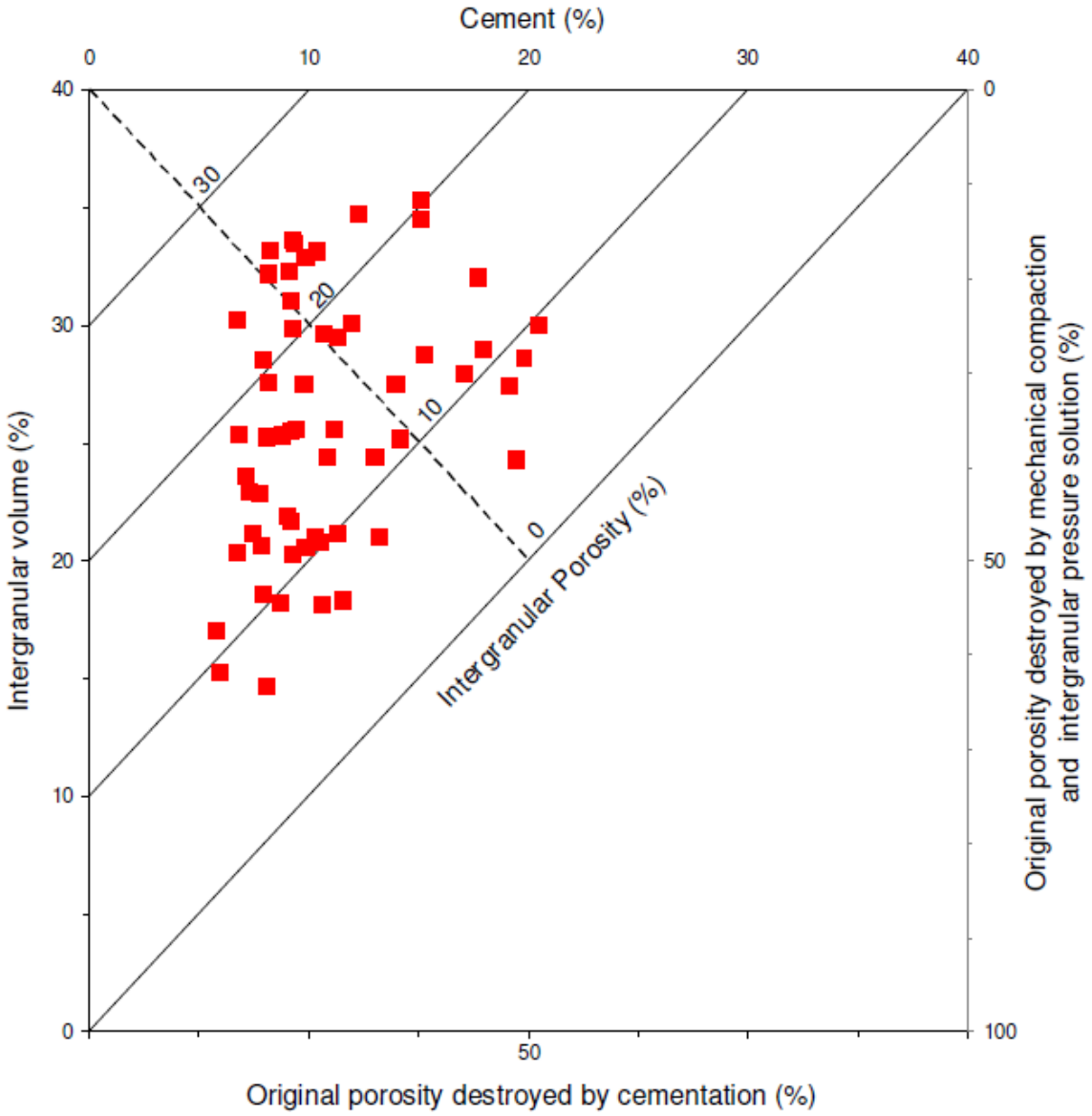

Figure 3.17-Graph of intergranular volume vs. cement of Houseknecht (1987), showing relative importance of compaction and cementation to porosity reduction. Although both cementation and compaction were important in reducing the original porosity, compaction was slightly more important than cementation in determining ultimate porosity.

3.10.2- Authigenic mineral cementation and replacement

Modal analysis revealed that the most important authigenic minerals that affected reservoir quality of the Lower Tuscaloosa sandstones are chlorite and quartz and to a lesser degree of importance, carbonate, kaolinite, titanium oxides, pyrite and iron oxide. Figures 3.18a and b are the pie charts that show relative average amounts of authigenic minerals as both cement and replacive phases. In this section the authigenic minerals are discussed in descending order of their importance on reservoir quality of the Tuscaloosa reservoir sandstones. Point counting category and their related values in modal analysis including percent value of authigenic minerals in the 57 studied thin sections are reported in Appendix (III).

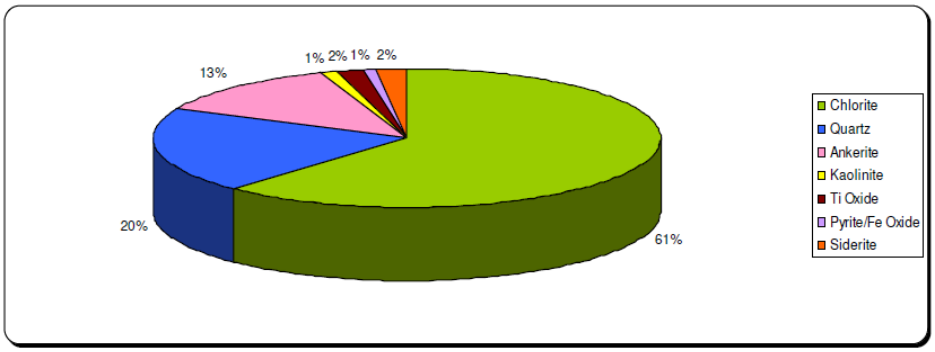

a

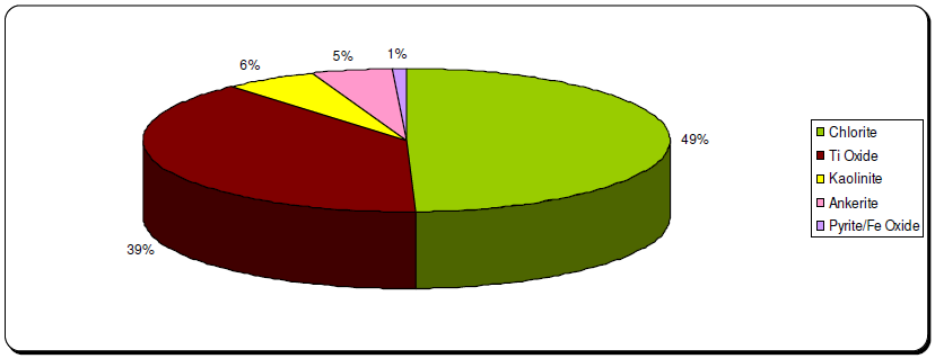

b

Figure 3.18-Pie charts that show relative average amounts of authigenic minerals as (a) cement and (b) replacive phases.

3.10.2.1-Chlorite

Petrographic study of the Tuscaloosa reservoir in Cranfield Field shows that the chlorite is a common authigenic mineral ranging from 7.3% to 17.3% and average of 11.8% of the total rock volume. Figure 3.19 shows the frequency of the authigenic chlorite in the studied samples. The authigenic chlorite occurs as grain coating (pore-lining cement), pore-filling and grain replacing masses.

The chlorite coats (as cement), which are the most abundant form of the chlorite with an average of 6.8%, occur as olive-green, well-formed, 5-10μm-thick rims partially to completely covering detrital grains under the microscope (Figs.3.20a, b and c). The pore-lining chlorite is not visible between detrital grain contacts (Fig. 3.20b). By total dissolution of some detrital grains (moldic pore), only the chlorite coats that covered the grains are remains which outline the original dissolved grain boundaries (Fig. 3.7a). SEM observations showed that chlorite coats consist of small euhedral platy crystals, displaying face-to-edge crystal habits (Fig. 3.20f).

The pore-filling chlorite appears as assemblages that consist of small chlorite plates with parallel orientation and denser packing that partially to completely fill the intergranular pores (Fig. 3.20e). In samples where pore-filling chlorite is abundant, detrital grains float in the matrix-like clay. Chlorite replacing is noted in thin sections replacing biotite grains (Fig. 3.20c); volcanic and metamorphic rock fragments as well as infiltrated Fe-rich clays comprising a chlorite plate meshwork of high microporosity (Fig. 3.20d). In the thin sections, some of the chlorites were observed as coexisting with opaque aggregates of altered or dissolved precursor grains remnants, with a meshwork or lace-like structure (Fig. 3.20d). The SEM, EDS and X-ray mapping on polished thin sections showed that these remnants are titanium oxides (TiO_2) (see authigenic Ti oxide section). Paragenetic analysis has shown that the chlorite crystals are engulfed by both late carbonate cements and quartz overgrowths, and thus pre-dated them (see authigenic carbonate and quartz sections).

The detailed SEM observations revealed development of two superimposed layers of chlorite coats (Figs. 3.21a, b, c and d) including (1) an inner coating composed of fine (<1 μm), poorly crystallized chlorites, oriented oblique or tangential to the detrital grain surface; (2) an outer coating containing coarse (5-10 μm) crystallized chlorites with subhedral to euhedral, pseudo-hexagonal crystal shape displaying face-to-edge crystal habits, oriented perpendicular to the grain surfaces. The underlying fine crystalline chlorites could only be seen at the interface between the two chlorite layers where the overlying coarse crystalline chlorites have broken away.

Energy-dispersive X-ray spectroscope (EDS) analysis showed that the type of chlorite is ferroan chlorite / chamosite (general formula $(Fe_5Al)(AlSi_3)O_{10}(OH)_8$; Figs. 3.21e, 3.22a and b; Tables 3.3 and 3.4) with a mean Fe/ (Fe + Mg) ratio of 0.8 in their chemical composition. However, the two chlorite coating layers showed variations in their compositions by having higher amounts of Fe (av. 30%) and Mg (av. 6%) in the outer layer compared to content of Fe (av. 14%) and Mg (av. 2%) in the inner layer (Figs. 3.22 a and b; Tables 3.3 and 3.4). Figures 3.21e and 3.21f show high magnification and two-dimensional distribution of iron for chlorite coats in BSE images.

As observed in the thin sections, the medium to very coarse grained sandstones, which are located at the lower portion of the fining-upward units at the reservoir interval (Fig. 3.2), have chlorite with larger crystal size and thicker coats compared with fine to very fine grained sandstones at the top of the units. A plot of chlorite versus mean grain size shows this relationship (Fig. 3.23). In the samples with thin, discontinuous or no chlorite coats, intense quartz overgrowths are visible, while samples with well-formed, thick and continuous chlorite coat, quartz overgrowths are absent. As discussed in the compaction section, samples with well-developed chlorite coatings in the coarser grained sandstones show evidence of less compaction compared with the finer grained sandstones. Therefore, chlorite coating thickness and grain coverage play an important role in the reservoir quality of the Tuscaloosa sandstones. Origin, timing and processes of

formation of the chlorite as well as their effect on reservoir quality will be discussed later in the discussion section.

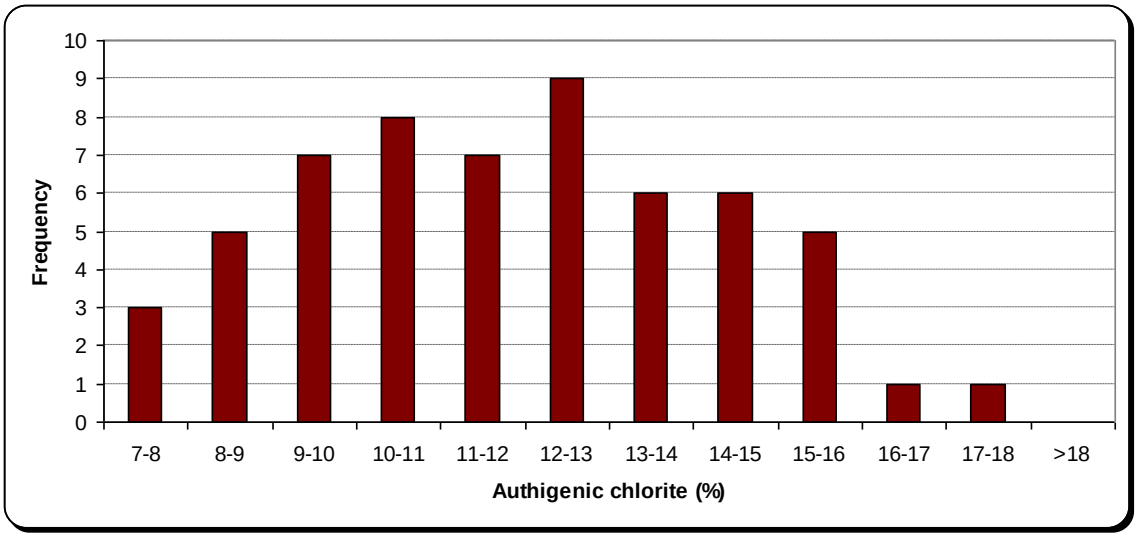

Figure 3.19-Frequency of authigenic chlorite in the 57 studied samples.

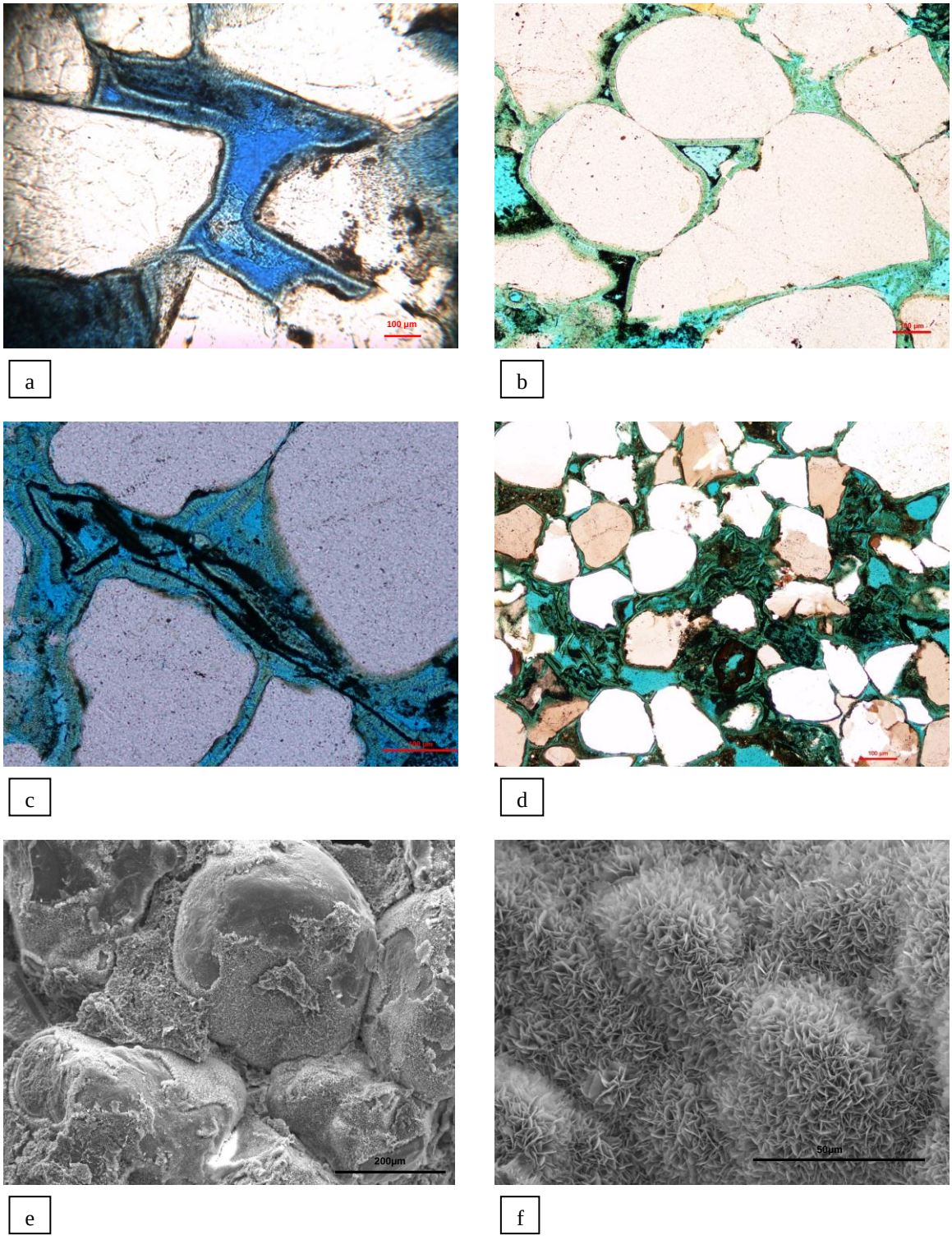

Figure 3.20-Photomicrographs showing (a) pore-lining chlorite, (b) absence of chlorite coats between grain contact, (c) chloritized mica with TiO_2 remnant, (d) chlorite replacing rock fragments; and SEM images showing (e) pore filling chlorite, (f) euhedral platy crystals, displaying face-to-edge crystal habits.

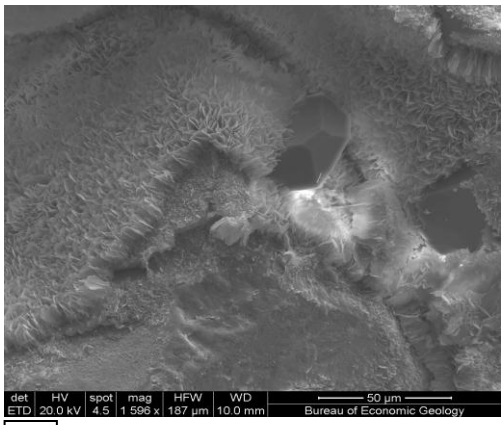

a

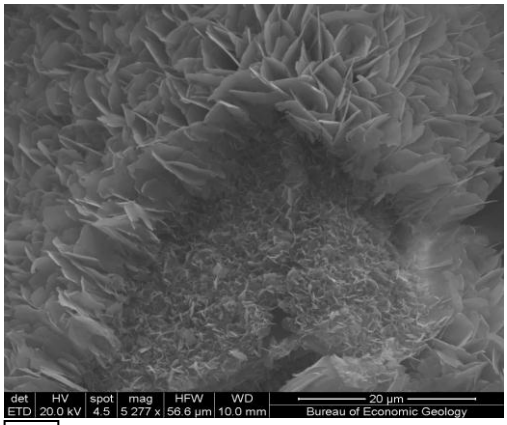

b

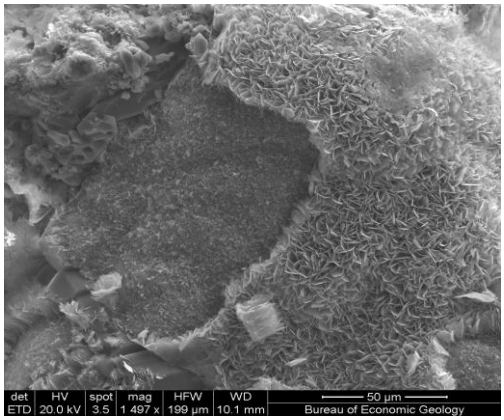

c

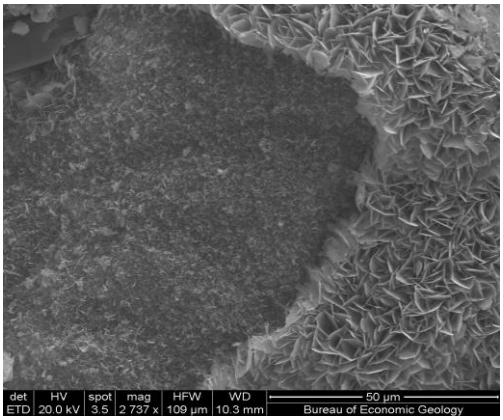

d

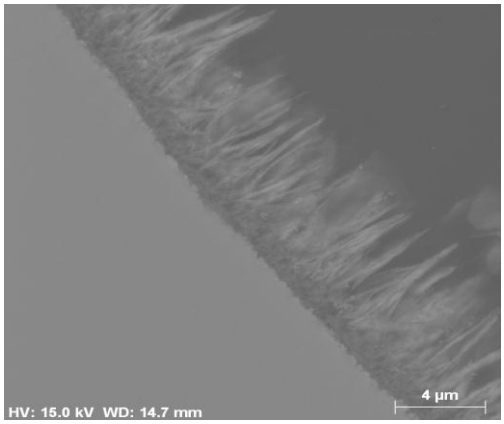

e

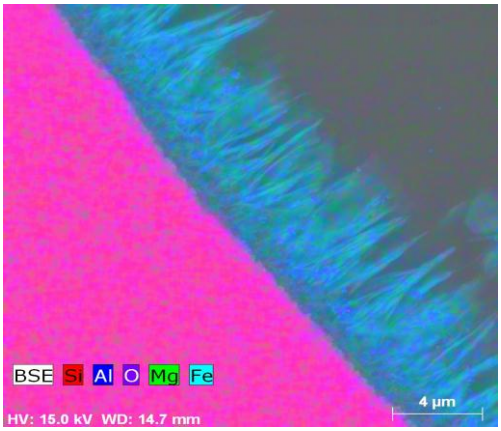

f

Figure 3.21-SEM images showing (a) two superimposed layers of chlorite coats, (b) higher magnification of the previous image, (c) two superimposed layers of chlorite coats on another grain, (d) higher magnification of the previous image and high magnification BSE images showing (e) chlorite coats precipitated perpendicular to the grain surface, (f) X-ray map of distribution of iron element.

Element	series	[wt.%]	[norm. wt.%]	[norm. at.%]	Error in wt.%
Oxygen	K-series	36.40	43.20	62.74	4.79
Iron	K-series	22.45	26.63	11.08	0.66
Silicon	K-series	9.81	11.64	9.63	0.46
Aluminum	K-series	10.45	12.40	10.68	0.54
Magnesium	K-series	5.17	6.13	5.87	0.33
	Sum:	84.27842	100.00	100.00	

Table 3.3-Chemical composition of the outer layer of the chlorite coat.

Element	series	[wt.%]	[norm. wt.%]	[norm. at.%]	Error in wt.%
Oxygen	K-series	26.43	49.10	64.36	3.57
Iron	K-series	3.80	7.04	2.64	0.16
Silicon	K-series	21.20	39.39	29.41	0.94
Aluminum	K-series	1.72	3.20	2.49	0.12
Magnesium	K-series	0.68	1.27	1.10	0.07
	Sum:	53.83	100.00	100.00	

Table 3.4-Chemical composition of the inner layer of the chlorite coat.

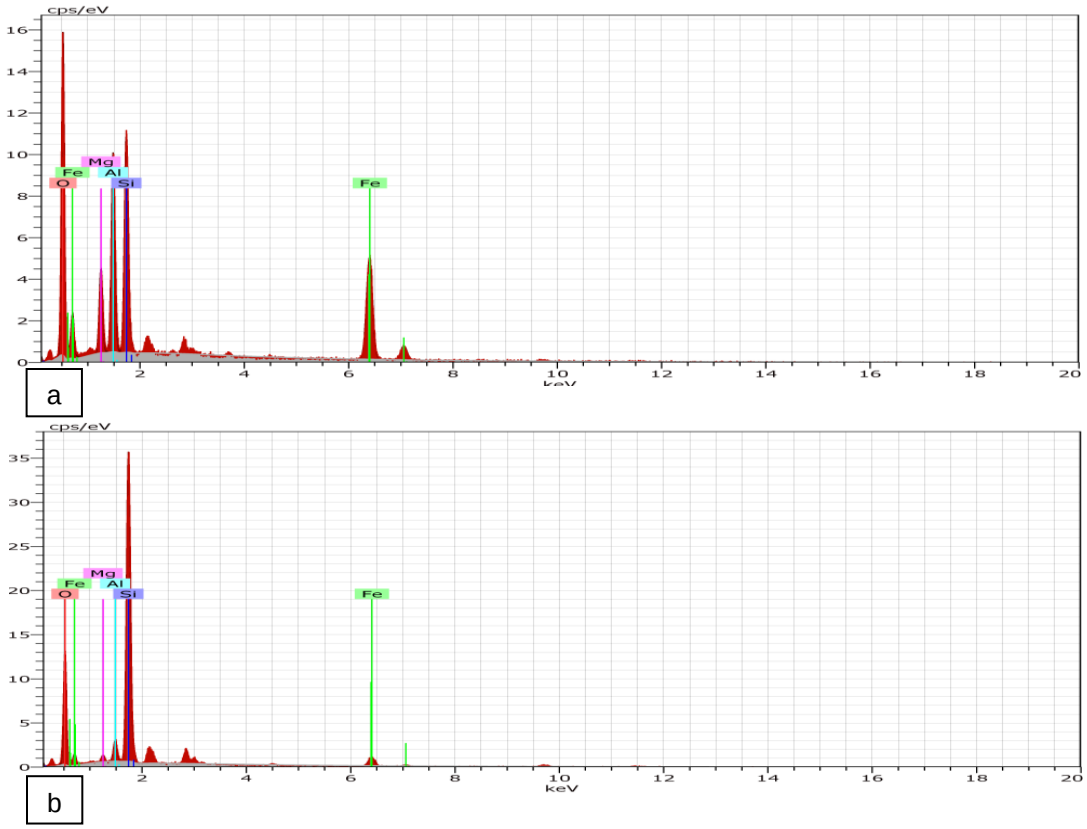

Figure 3.22-EDS analysis shows that the chlorites are ferroan chlorite / chamosite with variations in their compositions; (a) higher amount of Fe and Mg in the outer layer chlorite coat, (b) lower amount of Fe and Mg in the inner layer chlorite coat.

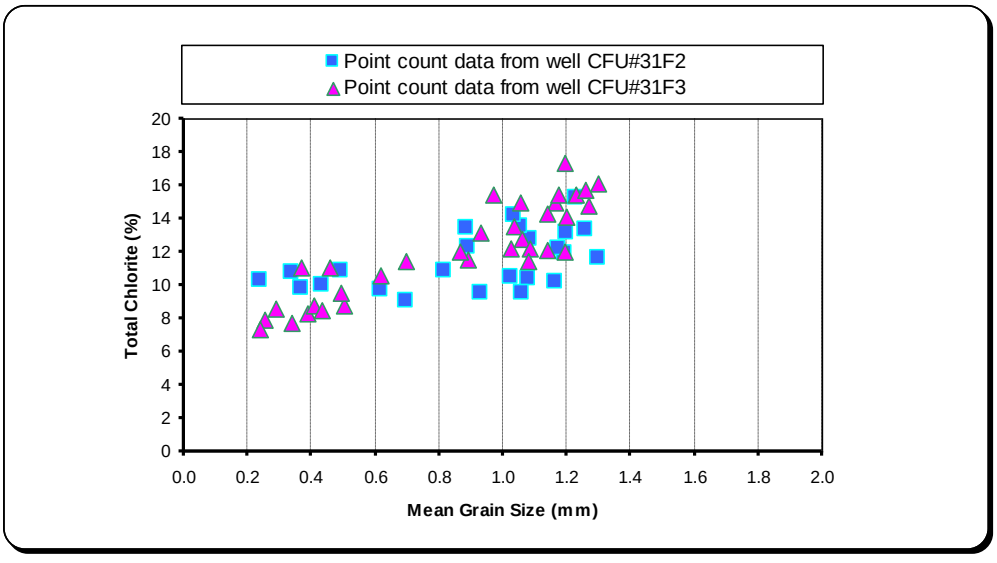

Figure 3.23-Cross-plot of chlorite versus mean grain size shows that the medium to coarse grained sandstones have higher amount of chlorite compared with the fine to very fine grained sandstones.

3.10.2.2-Quartz

Quartz cement in the Cranfield reservoir sandstones occurred commonly as syntaxial overgrowths, ranging from 0% to 12.3% with an average of 2.2% of total rock volume. Figure 3.24 shows the frequency of the quartz cement in the studied sandstones. The quartz cements as overgrowths, which have the same crystallographic orientations and optical continuity as the detrital quartz grains, are usually delineated from the detrital quartz grains by thin dustline (most probably chlorite or infiltrated clays or Fe oxide) (Fig. 3.25a). However in some samples the boundaries between quartz cement and detrital quartz grain were not clear (Fig. 3.25b). The quartz cement also rarely took place as outgrowths, which are quartz crystals locally projected into the pore space rather than rims around the quartz grains (McBride, 1989) (Figs 3.25c and e). This situation occurs when the chlorite coating is absent or broken. SEM studies showed that the euhedral quartz overgrowths engulf, and thus postdate, chlorite crystals, but are engulfed by, and thus pre-date, ankerite cements (Figs. 3.25d and f).

The quartz overgrowths are more common in the top of the reservoir units, where it is composed of fine to very fine grained sandstone (Fig. 3.2), with thin and discontinuous chlorite coatings. In some samples from this part of the reservoir, quartz overgrowths completely occlude intergranular porosity and form interlocking quartz crystals (Fig. 3.25b). In the lower parts of reservoir units with medium to very coarse grained sandstones, thick and continuous chlorite grain coatings prevented formation of quartz as overgrowths. In this part, just in a few samples, minor amounts of quartz cement occurred as outgrowths in the area of discontinuous chlorite coatings. Therefore, as discussed in the chlorite cement section above, the chlorite coatings appear to be an important factor in inhibiting the growth of quartz cements at Cranfield Field. Presence of thin and discontinuous chlorite coatings in the upper part of the reservoir could not inhibit formation of quartz overgrowths and thus in this part of the reservoir, quartz locally

occurred as important porosity destructive cement. Interactions between chlorite coating and quartz cementation will be quantitatively analyzed in the discussion section.

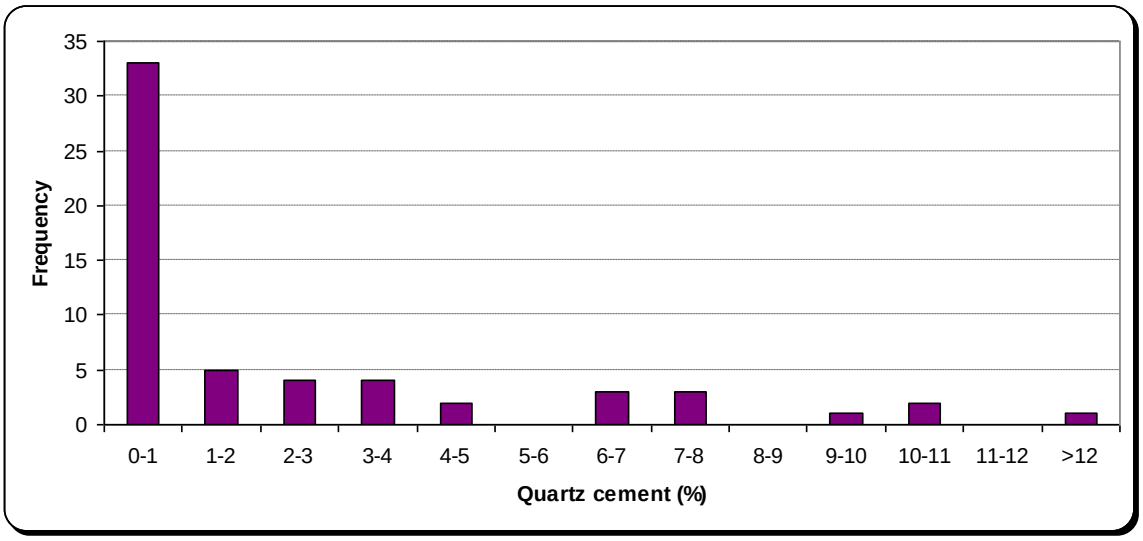

Figure 3.24-Frequency of quartz cement in the 57 studied sandstones.

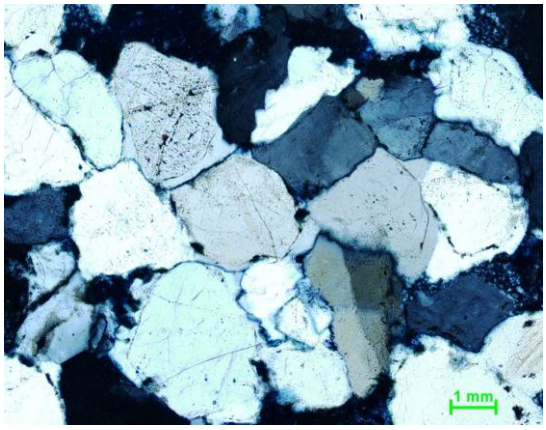

a

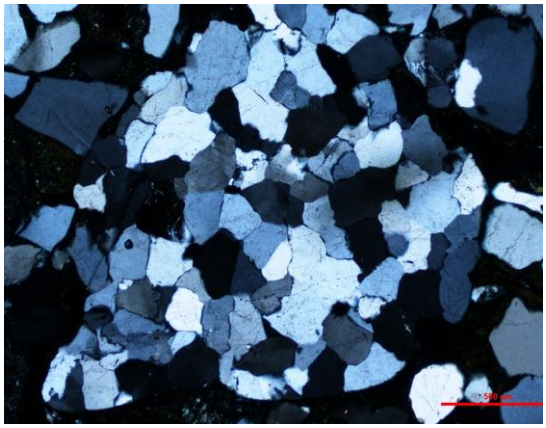

b

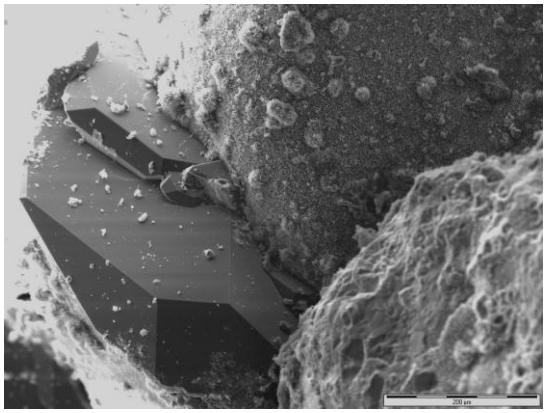

c

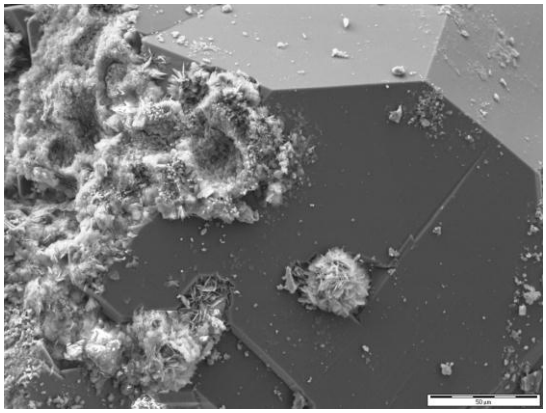

d

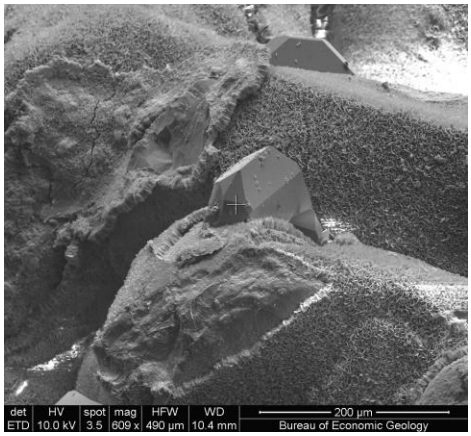

e

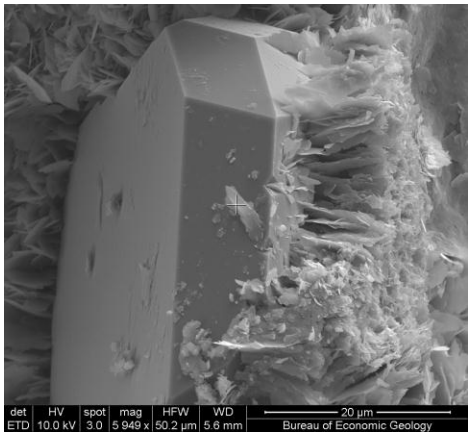

f

Figure 3.25-Photomicrographs showing (a) quartz cements with thin dustline, (b) quartz overgrowths completely occlude intergranular porosity and form interlocking quartz crystals; and SEM images showing, (c) euhedral quartz overgrowths (d), quartz overgrowths engulfing, and thus postdating, chlorite crystals, (e) quartz outgrowths, (f) euhedral quartz overgrowths engulfing chlorite crystals.

3.10.2.3-Titanium oxide

Titanium oxide (TiO_2) mostly occurs as trace mineral in sedimentary rocks, but in the Lower Tuscaloosa Formation sandstone, the total TiO_2 content is abnormally high; ranging from 0.4% to 8.3% and averaging 4.2% of the rock volume. The TiO_2 in the studied samples were observed as opaque aggregates composed of cryptocrystalline or poorly crystalline masses and discrete, euhedral crystals (Figs. 3.5a and b; 3.20d; 3.26a to d). The TiO_2 in the Lower Tuscaloosa sandstones commonly occurred as replacement (av. 4%), replacing ferromagnesian grains, mostly in volcanic and metamorphic rock fragments Figs. 3.5a and b, biotite (Fig. 3.20c), as well as infiltrated Fe-rich clays (odinite) (Fig. 3.26b). The TiO_2 also rarely occurred as cement with an average of 0.2% of the rock volume. SEM, EDS and X-ray mapping on polished thin sections detected presence of finely disseminated TiO_2 and of well-formed titaniferous crystals (Figs. 3.26c, d, e and f; Fig. 3.27). Morad and Aldahan, (1986) noted that these textures indicate authigenic origin of the TiO_2 and the three polymorphs of TiO_2 (rutile, brookite and anatase) can all form authigenically with a variety of crystal structures. Figure (3.29a to i), shows the X-ray maps for distribution of different elements, representing high concentration of titanium. Figure 3.28 shows the frequency of total TiO_2 in the studied samples.

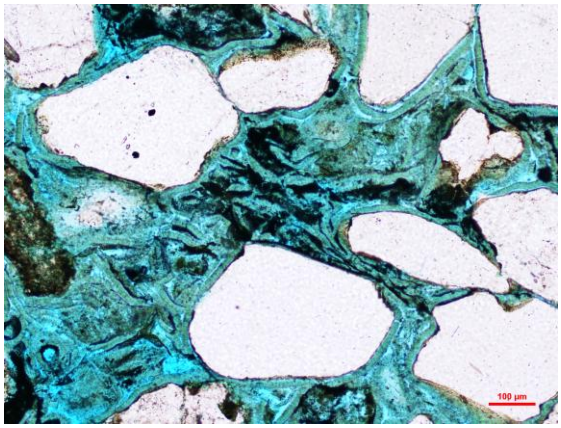

a

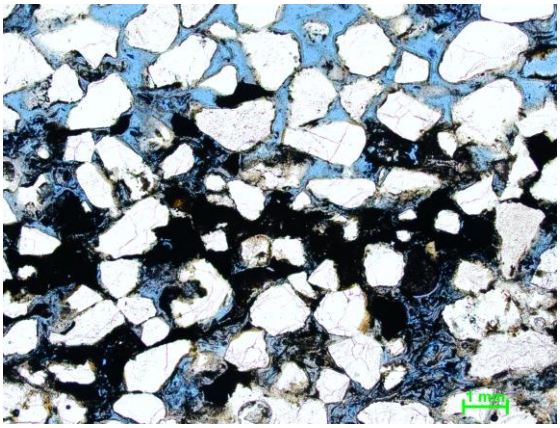

b

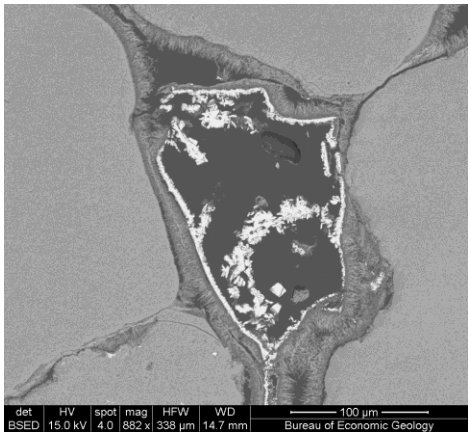

c

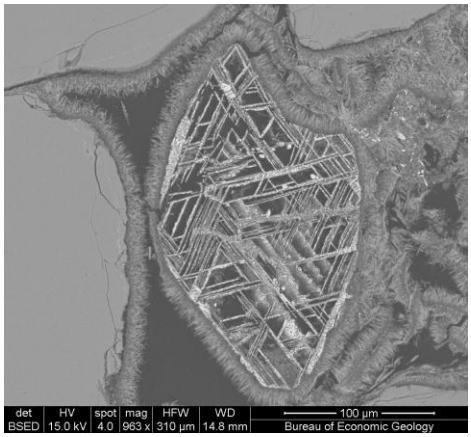

d

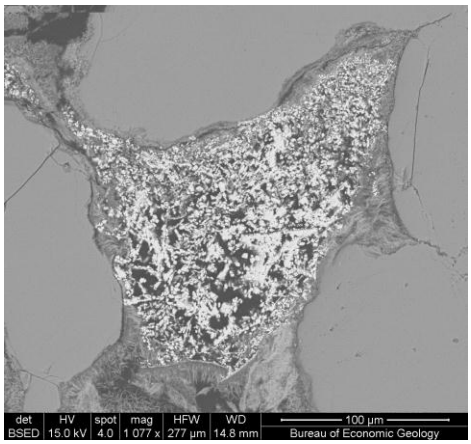

e

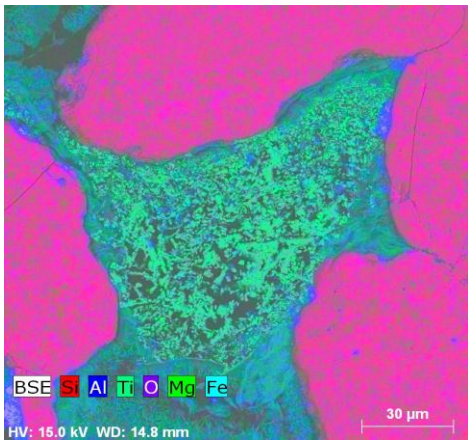

f

Figure 3.26-Photomicrographs showing (a) TiO_2 as remnant of altered ferromagnesian grains, (b) TiO_2 as remnant of altered infiltrated Fe-rich clays (odinite), and BSE images showing (c) TiO_2 rim as remnant of altered grain, (d) well-formed titaniferous crystal (anatase), (e) finely disseminated titaniferous crystals, (f) X-ray map of distribution of different elements (legend shown at the bottom of image) of the previous image.

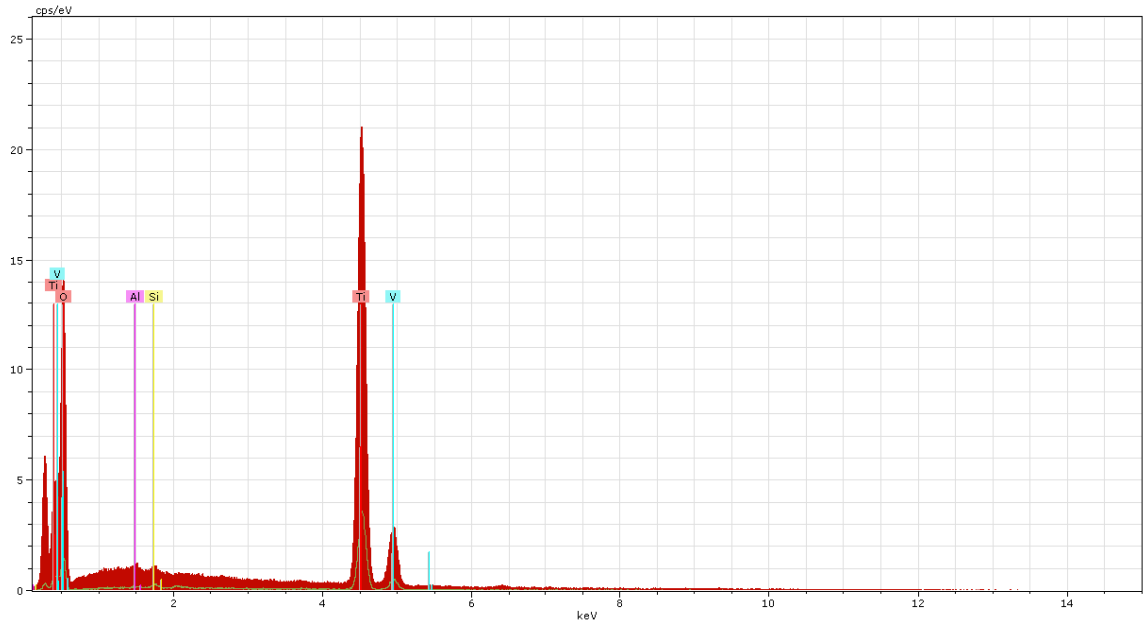

Figure 3.27-EDS analysis showed that composition of opaque aggregates is TiO_2.

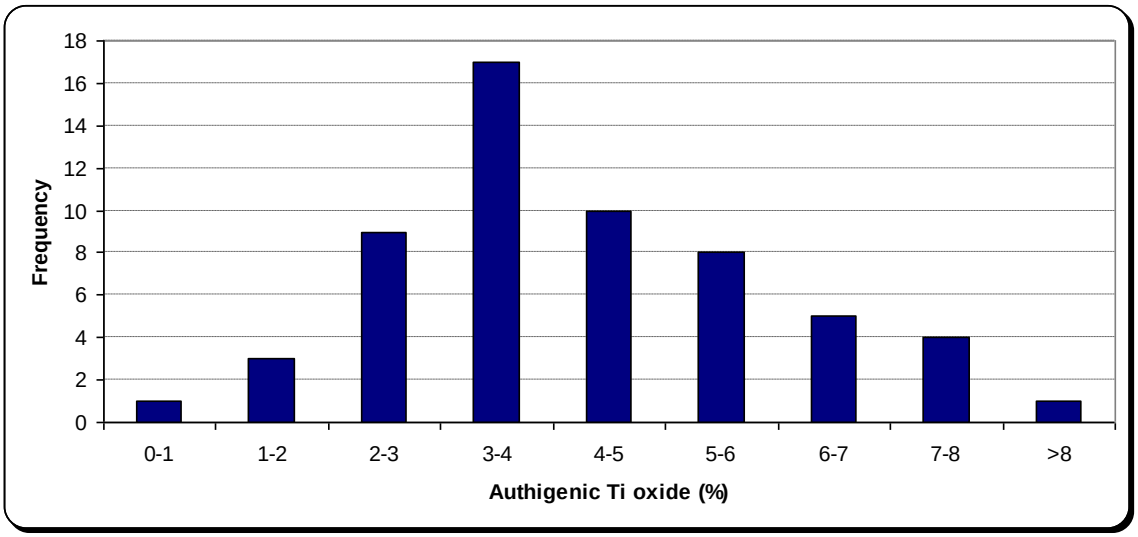

Figure 3.28-Frequency of total TiO_2 in the 57 studied samples.

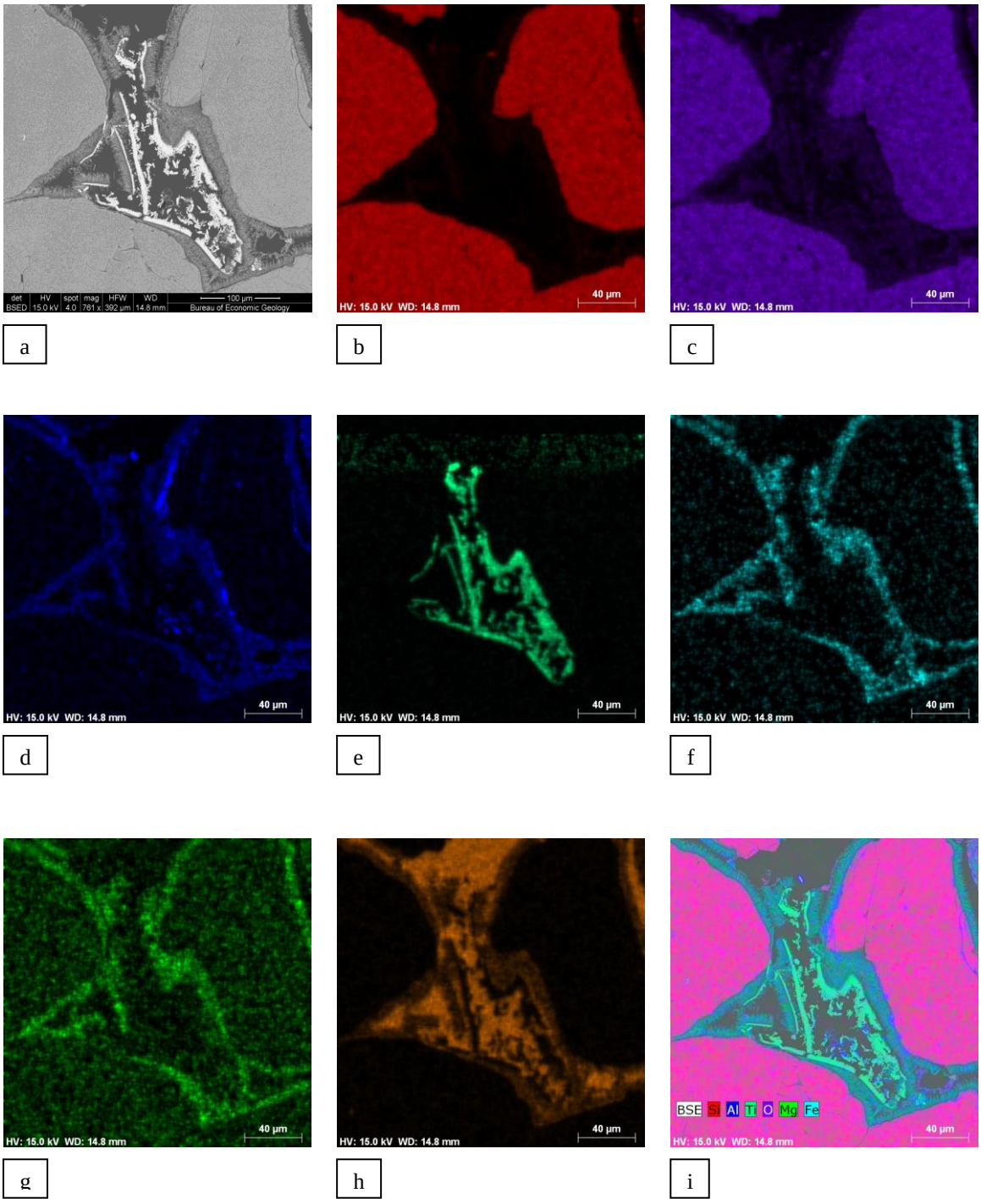

Figure 3.29-BSE image and X-ray maps of distribution of different elements, including (b) Si, (c) O, (d) Al, (e) Ti, (f) Fe, (g) Mg, (h) C, and (i) all of the previous elements in one image showing which element is responsible for the variation. High concentration of titanium in the remnant of altered ferromagnesian grains is representative of the TiO_2.

3.10.2.4-Carbonates

Range of the authigenic carbonates in the Lower Tuscaloosa Formation of Cranfield Field highly varies from 0% to 19.3% with average of 2.1% of the total volume of rock. Figure (3.30) shows the frequency of the authigenic carbonates in the sandstones. The EDS analysis revealed that the carbonate cements are mostly ferroan dolomite/ankerite (Fe and Mg rich carbonate, general formula $Ca(Fe^{2+},Mg,Mn)(CO_3)_2$) (Fig. 3.31; Table 3.5) with an average of 1.9% and rarely siderite (Fe rich carbonate, general formula $FeCO_3$) with an average of 0.2% of the rock volume. Authigenic ankerites occur as both pore-filling cement and replacing phases. The pore filling cements are patches of ankerite that partially to completely fill the intergranular pores (Figs. 3.32a, b and c). Authigenic ankerite also partially to totally replaced the framework grains (mostly rock fragments), matrix or filled the secondary pores in the detrital grains (3.32b.). The ankerite cement forms as poikilotopic and sparry textural habits, exhibiting undulose extinction. The poikilotopic ankerite cements consist of a large single crystal including several grains (Fig 3.32a.). Sparry ankerite cements composed crystals having a range size of 10-15 μm. The SEM observations showed that the ankerite cements occur as subhedral to euhedral crystal faces, which engulfed and thus post-dated both authigenic chlorite and quartz overgrowths (Figs 3.32d, e and f).

As observed from cores of Cranfield Field, the ankerite cemented zones precipitated mostly in the basal conglomerate and very coarse to coarse grained sandstones of the reservoir interval as streaks and sphericules (nodules), however only parts of the nodular cemented zones can be seen within the conventional core. Effect of ankerite cemented zone on reservoir quality of the Tuscaloosa sandstones will be discussed in the discussion part, section 3.11.1.2.

Element	series	[wt.%]	[norm. wt.%]	[norm. at.%]	Error in wt.%
Oxygen	K-series	27.38	36.02	55.78	6.67
Iron	K-series	19.57	25.74	11.42	1.07
Calcium	K-series	22.28	29.30	18.11	0.88
Carbon	K-series	4.06	5.34	11.02	2.16
Magnesium	K-series	2.74	3.60	3.67	0.27
	Sum:	76.03	100.00	100.00	

Table 3.5-Chemical composition of the ferroan dolomite/ankerite cement.

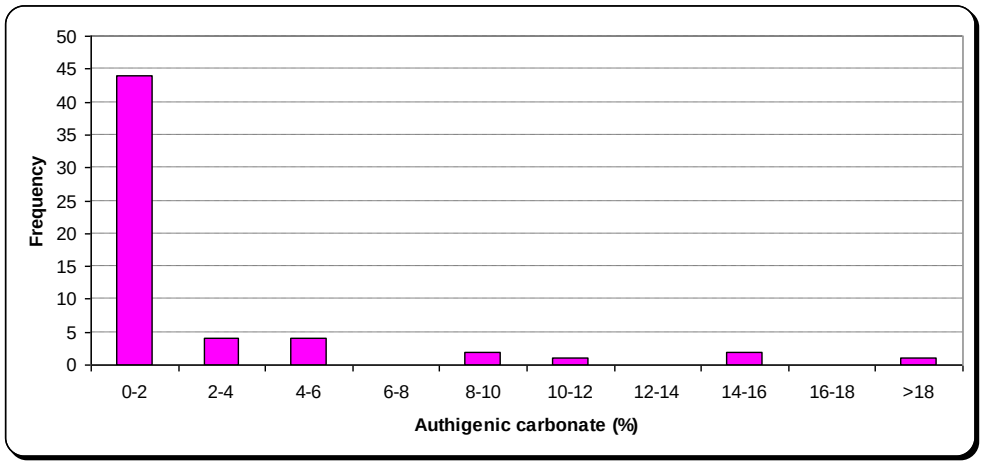

Figure 3.30-Frequency of the authigenic carbonates in the 57 studied sandstones.

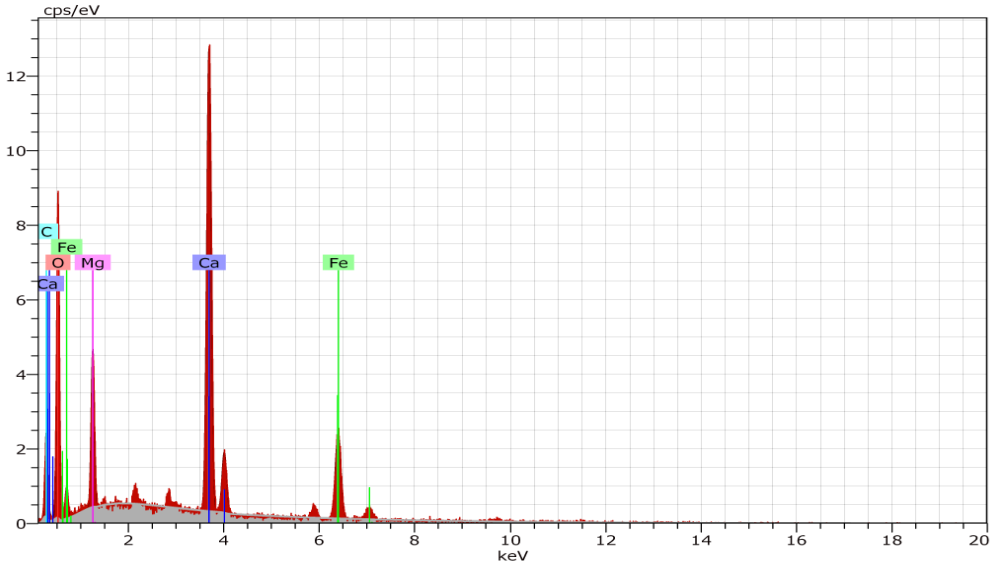

Figure 3.31-EDS analysis revealed that the carbonate cements are mostly ferroan dolomite/ankerite.

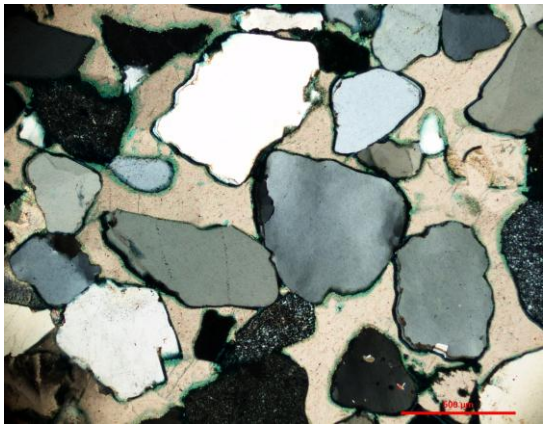

a

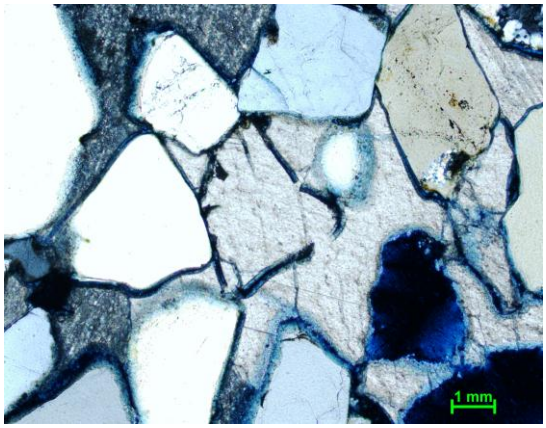

b

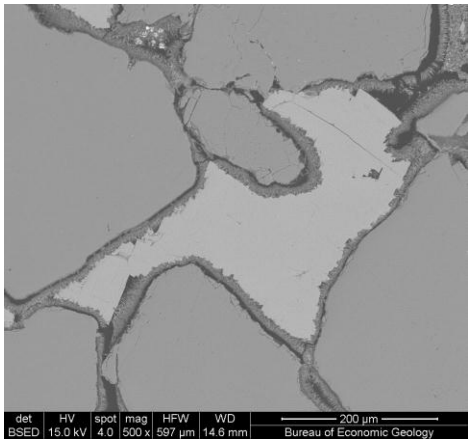

c

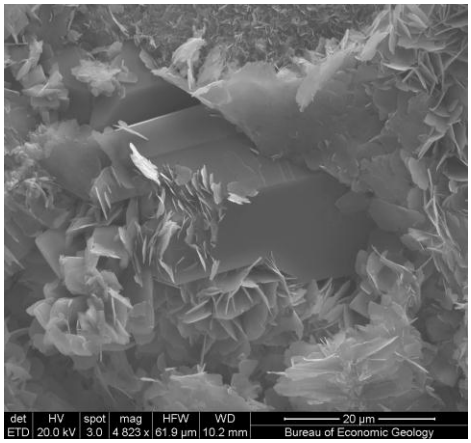

d

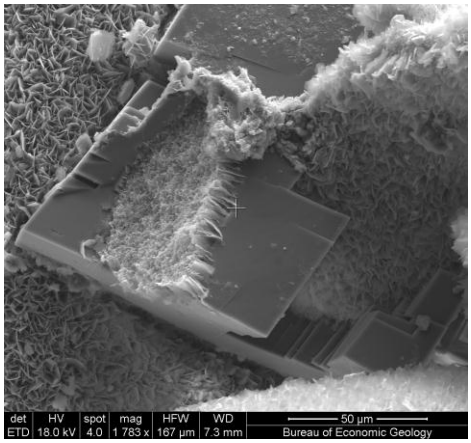

e

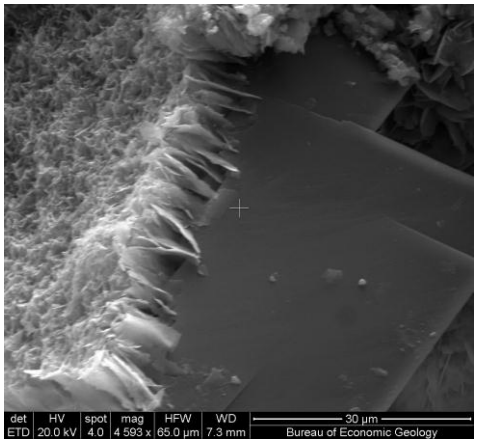

f

Figure 3.32-Photomicrographs showing (a) poikilotopic pore filling ankerite cement completely filling the intergranular pores, (b) ankerite cement filling the secondary pores, (c) BSE image of ankerite pore filling cement, and SEM images showing (d) ankerite engulfing chlorite crystals, (e) euhedral crystal faces of ankerite, (f) close-up view of the previous image.

3.10.2.5-Kaolinite

In the Cranfield Field reservoir, authigenic kaolinite occurred in minor amounts, ranging from 0% to 3.9% and averaging of 0.7 % of total rock volume. Kaolinite was observed under the microscope as grain-replacing and pore-filling aggregates with abundant intercrystalline microporosity (Figs. 3.33a and c; Figs. 3.7d and f). SEM observations showed that the kaolinite crystals form as thin (<1 μm thick), pseudo-hexagonal platelets, with etched surfaces (Fig. 3.33c). In some cases they exhibit a vermicular and/or booklet texture (Fig. 3.33c). Partial to complete kaolinitization of mica, rock fragments, feldspars, mud intraclasts and pseudomatrix are noted in the samples. Accordion-like textures of mica flakes, which expand into adjacent intergranular pores, display kaolinitized micas with pseudomorphic replacement along cleavage planes. Partially kaolinitized mica may contain thin, thread-like remnants of the micas (Fig. 3.33b). Kaolinitized mud intraclasts occur as relatively large, irregular, scattered patches of kaolinite. Some exhibit remnants of detrital mud or silt-size quartz grains. Sometimes kaolinite patches, which are squeezed and deformed between the rigid grains, fill nearby intergranular pores, which indicate kaolinitized pseudomatrix. Completely kaolinitized feldspars occur as patches of kaolinite with well-defined relic outlines, similar in size to the original detrital feldspar grains, and partially kaolinitized feldspars exhibit detrital feldspar remnants. Paragenetic analysis indicated that the kaolinites are engulfed by, and thus pre-date quartz overgrowths and ankerite cements.

In the SEM, some of the kaolinite crystals showed evidence of dickitization (Fig. 3.33d). Dickite, which is a high temperature polymorph of kaolinite, forms by conversion of thin crystals of kaolinite into thicker (up to 6 μm thick), euhedral, and blocky crystals with smooth surfaces. Kaolinite frequently transform into well-ordered kaolinite and then to dickite as thicker crystals due to dissolution-precipitation in the deeper burial and elevated temperature during mesodiagenesis (Morad et al., 1994; Beaufort et al., 1998; Ketzer et al., 2003a; Al-Ramadan et al., 2005; El-Ghali et al., 2006a). Transformation of

kaolinite to dickite indicates neomorphic change to a better-ordered and more stable crystal structure that occurs at temperatures above 80º C (Ehrenberg et al., 1993; McAulay et al., 1994; Lanson et al., 2002).

In the reservoir interval of Cranfield Field, kaolinite is more abundant in the fine to very fine grained sandstones at top of the reservoir interval units compared to the coarser grain sandstone at the base (Fig. 3.2), most probably due to higher amounts of precursor component such as mica, feldspars, mud intraclasts, pseudomatrix for formation of kaolinite in the finer grained sandstones.

3.10.2.6-Pyrite and iron oxide-Minor authigenic minerals

Pyrite and iron oxide are present only in trace amounts (average 0.2% of rock volume) in the samples. Pyrite forms as small patches composed of abundant euhedral microcrystals or as framboidal aggregates (Figs 3.33e and f). Pyrite fills intergranular pores or occurs within pseudomatrix and matrix. The SEM observations showed present of pyrite framboids on the grain surface that are all covered by chlorite (Fig. 3.33f). This indicates that framboids occurred before chlorite formation, during eodiagenesis. Folk (2005) noted that precipitation by nannobacteria in the reducing environment is responsible for the formation of the framboids.

Iron oxide in the form of dark reddish-brown crypto- to microcrystalline cement occurs as scattered patches of pore-filling cement. The matrix in the fine to very fined-grained sandstones is generally pigmented by iron oxides and has a reddish-brown color under the optical microscope. Precipitation of Fe-oxide commonly occurs by dissolution of iron-bearing minerals in the oxic geochemical zone.

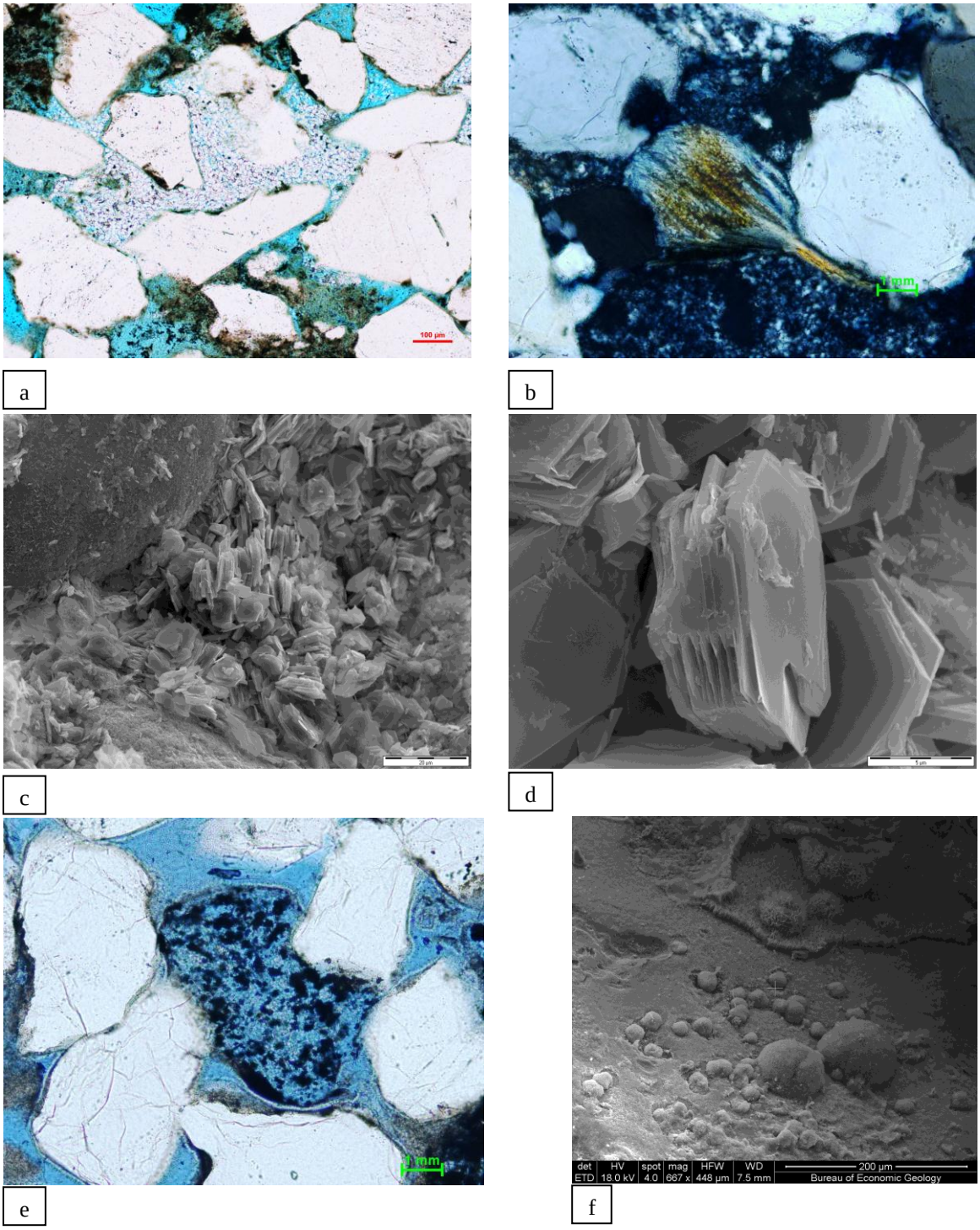

a b c d e f

Figure 3.33-Photomicrographs showing (a) pore filling kaolinite, (b) kaolinitized mica displaying accordion-like textures, expand into adjacent intergranular pores, and SEM images showing (c) pore-filling kaolinite with some booklet habit, (d) dickitized kaolinite, (e) photomicrograph of pyrite framboidal aggregates, (f) SEM image of pyrite framboids on the grains surface that are covered by chlorite.

3.10.3-Dissolution and porosity enhancement

During diagenesis of the Lower Tuscaloosa reservoir, various degrees of dissolution have produced secondary pores as both macropores (intragranular, moldic and oversized pores) and as micropores (with sizes less than 30 μm). Under the microscope, partial to complete dissolution of framework grains, authigenic minerals and matrix have been noted in the samples. Dissolution of volcanic and metamorphic rock fragments were the most important contributors to the formation of secondary porosity in the Lower Tuscaloosa sandstone reservoir (Figs. 3.5a and b). Dissolution occurred to a lesser degree in chert, mica, feldspar, rip-up clast, mud intraclast and matrix (Fig. 3.7c). In partial dissolution of framework grains, which resulted in formation of intragranular pores, some remnants of origin silicate component could be visible (Fig. 3.4c). Complete dissolution of detrital grains produced moldic porosity and dissolution of large mud intraclasts, matrix, or pseudomatrix generated oversize pores (Fig. 3.7a). In some instances, the detrital grains have been fully dissolved and only the chlorite coat that covered the grains has remained (Fig. 3.7b). The secondary fractured porosity also was rarely observed in the studied samples. As it discussed in the pore type and distribution, section 3.7, overall in the Lower Tuscaloosa sandstones, secondary macroporosity (sum of intragranular, moldic and two-thirds oversized pores) with average of 4.1% makes up to 21% of the total macroporosity, while the primary macroporosity (intergranular plus one third of oversized pores) with average of 15.2% constitutes up to 79% of the total macroporosity.

The secondary porosity also occurred as micropores, commonly generated by precipitation of the authigenic clays (chlorite and kaolinite) and oxides (Ti oxides and Fe oxides) and less commonly within partially dissolved rock fragments and cherts (Figs. 3.7d, e and f). In the studied samples, the total microporosity averages 5.5% of rock volume (for calculating microporosity, see pore type and distribution, section 3.7). However it is difficult to determine which portion of the microporosity is primary (e.g. related to matrix) and which portion is secondary (e.g. related to authigenic chlorite).

Although sizes of microporosities are very small (<30μm), the total amount in the studied samples is considerable, due to large volumes of the clay minerals and oxides in the reservoir sandstones.

In terms of reservoir quality, amount of secondary macroporosity (21% of the total macroporosity) compare to the primary macroporosity (79% of the total macroporosity) is considerable. Formations of secondary intergranular macropores, moldic and oversized pores resulted in porosity and permeability enhancement. However, the intragranular pores, which are poorly connected with the intergranular pore system, increased the total porosity but do not affect permeability. The relatively high amount of microporosity (5.5% of rock volume) results in high porosity but low permeability in the sandstones. This was proven by a cross-plot of core porosity versus permeability in the sandstones of Wells CFU#31F2 and CFU#31F3 (Figs. 3.34a and b). The core analysis data of the Lower Tuscaloosa reservoir sandstones provided good clues about distribution of porosity and permeability and their relationship. The measured porosity in all of the samples ranges from 1.29% to 31.44%, and permeability ranges from 0.009 md to 1890 md. Relatively poor correlation between porosity and permeability is typical for sandstones with high amounts of micropores in clay of all origins (depositional and/or diagenetic origins).

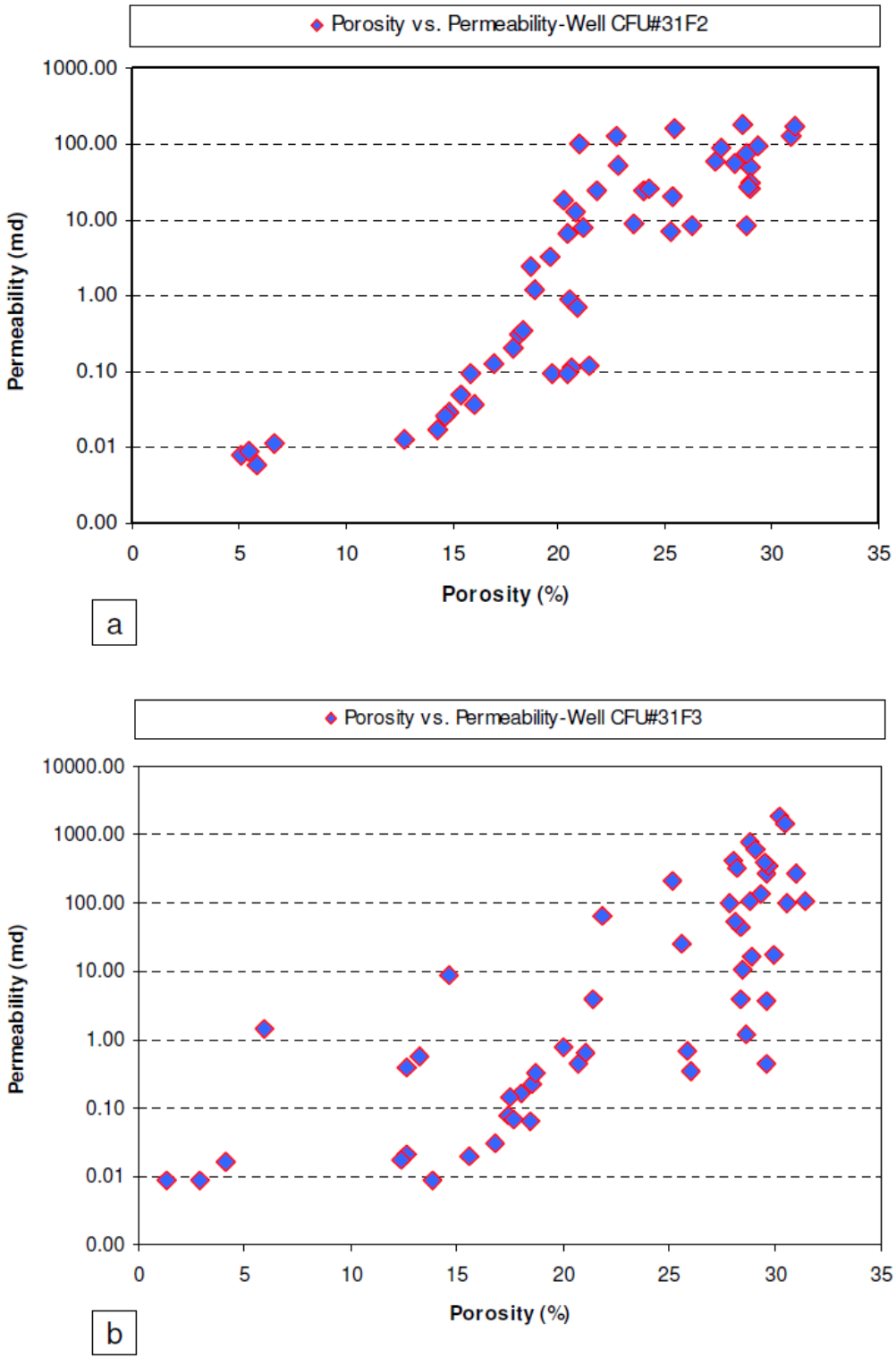

Figure 3.34-Cross-plots of core porosity versus permeability (a) in Well CFU#31F2, and (b) in Well CFU#31F3.

3.11-DISSCUSIONS

3.11.1-Diagenetic evolution and reservoir quality of the Lower Tuscaloosa Formation

The combination of positive and negative effects of diagenesis on porosity and permeability in the Lower Tuscaloosa sandstones results in complex reservoir quality. A combined burial and diagenetic history diagram of the Lower Tuscaloosa Formation is shown in Figure 3.35. Textural relationship and paragenetic sequences observed under optical microscope, SEM and BSE are used for determining relative timing and depth of different diagenetic phases. The terminology of diagenetic regimes (eodiagenesis, mesodiagenesis and telodiagenesis) defined by Morad et al., (2000) (Fig. 3.1; for definition of the diagenetic regimes see introduction section of this chapter) are used to facilitate the discussion.

The most important diagenetic events during eodiagenesis are mechanical compaction, kaolinite precipitation, pyrite and Fe oxide precipitation, early phase dissolution, early phase chlorite precipitation and early phase Ti oxide precipitation. The main diagenetic events during mesodiagenesis are chemical compaction, late phase dissolution, late phase Ti oxide precipitation, late phase chlorite precipitation, quartz cementation and carbonate precipitation. In this section evolution of the mentioned eogenetic and mesogenetic events will be described in more detail.

3.11.1.1-Eodiagenesis

In the Lower Tuscaloosa sandstones, mechanical compaction started soon after deposition by grain rearrangement and continued by ductile grain deformation. Due to presence of ductile grains (micas, argillaceous rock fragments, mud intraclasts and rip-up clasts) and dissolved/altered volcanic rock fragments in the sandstones, mechanical compaction is more penetrative and ductile deformation has more effect on reduction of pore volume than does brittle deformation. Mechanical compaction was more important

than chemical compaction and was slightly more important that cementation in reducing the original porosities during burial of the sandstones.

Another important diagenetic alteration in the Lower Tuscaloosa Formation that started after an initial phase of mechanical compaction or grain rearrangement is chlorite cementation and replacement. The chlorite precipitation started during eodiagenesis and continued during mesodiagenesis. Due to importance of authigenic chlorite in reservoir quality of the Lower Tuscaloosa Formation, I will discuss the chlorite formation time and process, as well as their interactions with quartz cementation that result in porosity-permeability preservation, in separate sections in discussions of this chapter.

Abundant Ti oxide coexisted with chlorite, showing that TiO_2 precipitated when Ti was liberated during alteration/dissolution of a Ti-bearing precursor (biotite, detrital mafic and ultramafic clasts and/or odinite) to chlorite or mixed layer serpentine-chlorite during late eodiagenesis to early mesodiagenesis (Eggleton and Banfield, 1985; Ryan and Reynolds, 1996, 1997). As revealed from modal analysis, most of the TiO_2 formed as replacive phase and not as porosity destructive cement. Presence of high microporosity associated with the TiO_2 increased total porosity, but not the permeability.

During eodiagenesis of the Lower Tuscaloosa Formation, kaolinite was derived from the dissolution of aluminosilicates and precipitation in intergranular spaces as pore-filling aggregates, or kaolinitization of the aluminosilicates by in-situ dissolution-precipitation processes. These diagenetic alterations were mostly caused by percolation of meteoric water containing CO_2 in shallow depths and low temperatures (Morad et al., 2000, 2010; Milliken, 2001; Ketzer et al., 2003a; El-Ghali et al., 2006a). At the Lower Tuscaloosa reservoir, precipitation of kaolinite occurred before significant compaction during the eogenetic regime, as indicated by: (1) the expanded texture of kaolinitized micas and the collapsed texture of kaolinitized feldspar grains, which imply formation prior to considerable compaction during burial (Ketzer et al., 2003a; Al-Ramadan et al., 2005; El-Ghali et al., 2006a); (2) the booklets and vermicular texture of kaolinite,

interpreted to have taken place by replacement of detrital grains shortly after deposition (Osborne et al., 1994; Wilkinson et al., 2004); (3) partial depth-dependent transformation of kaolinite to dickite, which results in a better-ordered, and hence a more stable crystal structure at elevated temperatures above 80º C (Ehrenberg et al., 1993; McAulay et al., 1994; Lanson et al., 2002); and (4) engulfment of kaolinite by quartz overgrowths and late ankerite cements, which are known to be mesogenetic in origin and to precipitate at high temperatures of about 70-120º C and burial depths of 2 km or greater in most sedimentary basins (McBride, 1989; Gluyas et al., 1993; Morad et al., 2000; Worden and Morad, 2003; Kordi et al., 2011).

In terms of reservoir quality at the Cranfield Field, formation of kaolinite increased the amount of microporosities, which are poorly connected with the intergranular pore system. The pore-filling kaolinite that fills pore throats may reduce the porosity and permeability. However, due to minor concentrations of kaolinite in the reservoir sandstone their effect on reservoir quality is not very important.

Presence of Fe oxide (hematite) at the shallow burial depth of the Lower Tuscaloosa Formation was reported by Ryan and Reynold (1996, 1997), indicating precipitation of Fe oxides during eodiagenesis. They also stated that the amount of Fe oxide decreases, whereas the pyrite content increases with burial depth. This indicates that pore water composition and chemical conditions were not constant during burial of the Tuscaloosa sandstones. The coexistence of hematite, Ti oxide and serpentine-chlorite shows that geochemical conditions were slightly oxidizing with nearly neutral to slightly reducing pH during shallow burial or early eodiagenesis (Garrels and Christ 1965; Annerston, 1968; Ryan and Reynolds, 1997; Anjos et al., 2003). However, it progressively transformed to reducing pore fluid conditions during more burial depth in late eodiagenesis (Garrels and Christ 1965; Ryan and Reynold, 1996, 1997), where the pyrites were precipitated. As observed in petrographic studies, covering of the pyrite framboids by chlorite coats indicates formation of pyrites before chlorite precipitation

during shallow to moderate burial depth. Due to low amounts of pyrite and Fe oxides (<1%), the effect of these minerals on the reservoir quality of the Lower Tuscaloosa Formation is negligible.

Dissolution of framework grains, authigenic minerals and matrix is another diagenetic event that usually starts during eodiagenesis and continues during mesodiagenesis. However, the rate of dissolution may be increased with increasing burial and temperature. The amount of secondary macroporosity (mostly by dissolution of volcanic rock fragments) in the Lower Tuscaloosa sandstones is considerable. Formations of secondary intergranular macropores, moldic and oversized pores resulted in porosity and permeability enhancement. However, the intragranular pores, which are poorly connected with the intergranular pore system, increased the total porosity but do not affect permeability.

3.11.1.2-Mesodiagenesis

As discussed above, chlorite precipitation, Ti oxide precipitation and dissolution are diagenetic events that started during eodiagenesis and continued during mesodiagenesis.

Chemical compaction is a mesodiagenetic event. Although the chemical compaction is not very abundant in the studied samples, it is more common in the fine to very fine grained sandstones at the top of the reservoir units (Fig. 3.2). The finer grained sandstones at top of reservoir interval contain thin or discontinuous chlorite coatings compared to the coarser grain sandstone at the base. This suggests the presence of a relationship between anti-compaction and chlorite coatings, most probably due to inhibition of pressure dissolution by thick well-formed chlorite coats in coarser-grained sandstones.

As observed in the petrographic studies, quartz overgrowths engulf, and thus postdate, chlorite crystals, but are engulfed by, and thus pre-date, ankerite cements.

Quartz overgrowth precipitation in sandstones generally occurs in deep burial (>2 km) at temperatures greater than 70°C (McBride, 1989; Bjørlykke and Egeberg, 1993; Walderhaug, 1994; Morad et al, 2000; Kordi et al., 2011). Weedman (1996) reported, based on the fluid-inclusion data that the quartz overgrowths in the Lower Tuscaloosa Formation precipitated at approximately 90° C.

In the reservoir interval of the Tuscaloosa sandstones, quartz overgrowths are more common in the top of the reservoir units, where it is composed of fine to very fine grained sandstone with thin and discontinuous chlorite coatings. In the lower parts of reservoir units with medium to very coarse grained sandstones, thick and continuous chlorite grain coatings prevented formation of quartz as overgrowths. Presence of thin and discontinuous chlorite coatings in the upper part of the reservoir could not inhibit formation of quartz overgrowths and thus in this part of the reservoir, quartz locally occurred as important porosity destructive cement.

Precipitation of ankerite cements after quartz overgrowths, which are commonly initiated at temperatures of 70-90 ºC (McBride, 1989; Walderhaug, 1994), implied that the ankerite occurred during the late mesogenetic regime. Smith and Ehrenberg (1989) reported that the ankerite cements in the sandstones originated from elimination of excess CO_2, generated by thermal maturation of organic matter, which occurs at 100-120º C.

As observed from cores of Cranfield Field, the ankerite cemented zones precipitated mostly in the basal conglomerate and very coarse to coarse grained sandstones of the reservoir interval. They occur as very low porosity-permeability tight–cemented zones that are approximately 10 to 25 cm thick. Minter, et al. (1992) reported that the ankerite cemented zones of the Lower Tuscaloosa Formation in Mississippi occur as streaks (approximately 1 cm thick) that coalesce to form thicker zones (10 cm and greater) and as sphericules (nodules) (average radius of 6 cm), however only parts of the nodular cemented zones can be seen within the conventional core. The carbonate streaks form in the area of anisotropic permeability along the bedding plane or oriented parallel

to the flow pathways of groundwater, while the concretionary growth occurs in the isotropic permeability area as a relatively spherical shape (McBride et al., 1994).

Regionally, the ankerite cemented zones were reported by Minter et al. (1992) within the Tuscaloosa Formation in east Mississippi, south and east of the Walthall County and in St. Helena Parish, Louisiana. These suggest possibility of presence of both streaks and nodules in the Lower Tuscaloosa Formation.

Overall, the ankerite cements have two effects on reservoir heterogeneity: (1) occurrence of ankerite cements is a potential problem for decreasing the reservoir quality even if the porosity was preserved by chlorite coats during deep burial, because formation of ankerite cements post-dated formation of the chlorite coats; (2) volumetrically the amount of carbonate cements in the Lower Tuscaloosa sandstones is not well-extended due to their localized patchy character, however they may affect fluid flow and accumulation by constructing permeability barrier and compartmentalizing in the sandstone reservoir.

Figure 3.35 shows the schematic paragenetic sequences of diagenetic processes and products in the Lower Tuscaloosa Formation through its burial history.

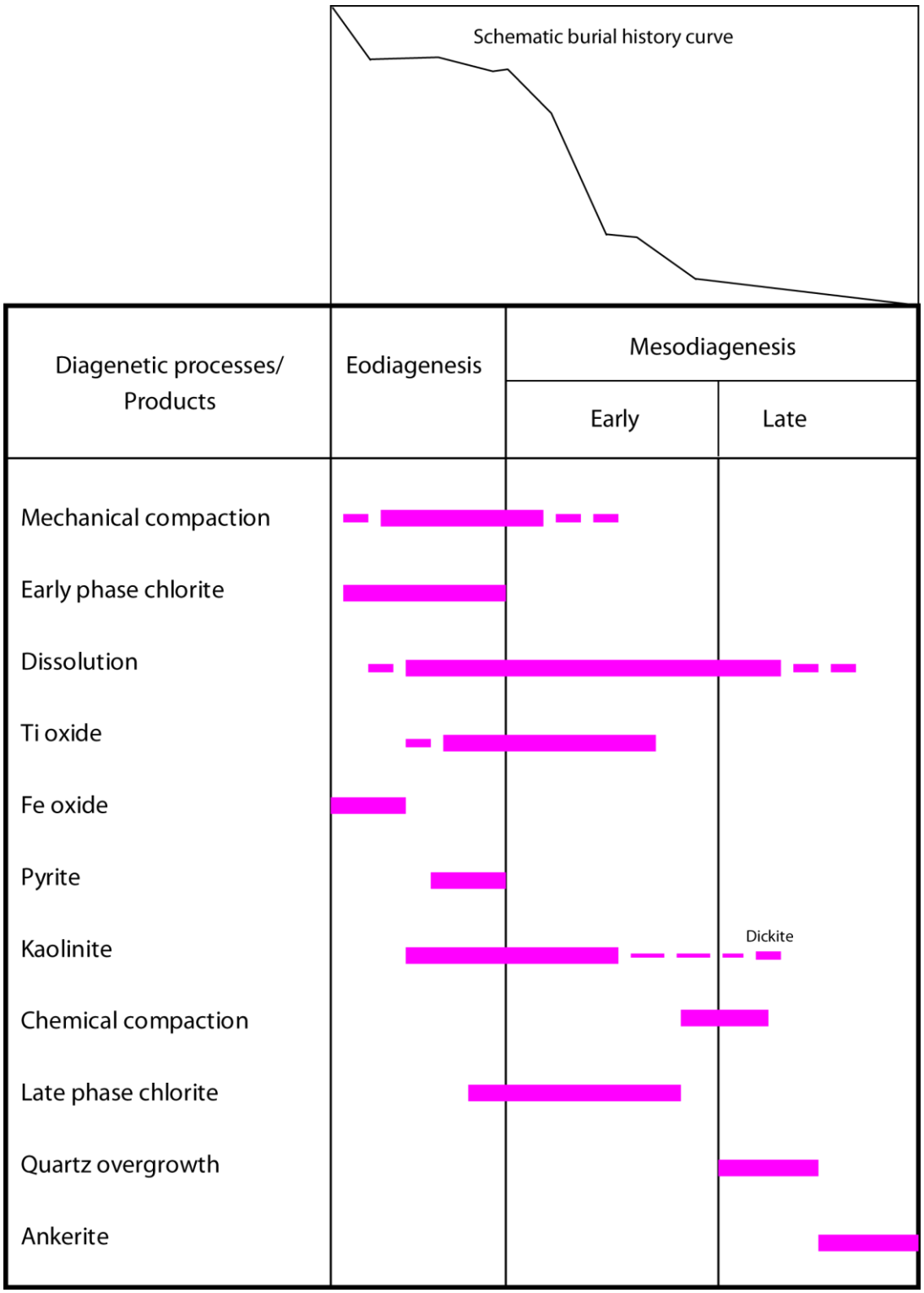

Figure 3.35-Combined burial and diagenetic history diagram showing diagenetic evolution of the Lower Tuscaloosa Formation.

3.11.2-Origin, time and process of chlorite coating

In this section, first I review different hypotheses for the origin, time and process of chlorite coating and then I will discuss the origin, time and process of chlorite coating in the Lower Tuscaloosa Formation.

3.11.2.1-General remarks-origin and controlling factors of chlorite coating

In the literature, there are several hypotheses for the origin of chlorite coating, suggesting variously that depositional environment and/or provenance and/or diagenesis play important roles, as below:

(1) Alteration of ferromagnesian grains like biotite, amphibole, metamorphic rock fragments and especially mafic and ultramafic volcanic rock fragments as an adequate source of Fe and Mg needed for formation of chlorite (e.g., Thomson 1979; Kaiser, 1984; Genuise and McBride 1990, Pittman et al., 1992, Remy, 1994; De Ros et al., 1994; Anjos et al., 2003; Worden and Morad, 2003). In this idea, chlorite coatings form by direct precipitation from pore waters in early to late mesogenetic regime at deep burial depths (Berger and Beaufort, 2003; Berger et al., 2009). The burial temperature for precipitation of this chlorite is 90 to 120°C (Zhu et al, 2008). This process generally occurs together with the chloritization of other mineral substrates (Anjos et al., 2003).

(2) Chloritization of mechanically infiltrated and autogenic clays like smectite and kaolinite (Thomson, 1979; Kaiser 1984; Ahn and Peacor, 1985; Hillier et al., 1996; Grigsby, 2001; Berger et al, 2009). This is a dissolution-reprecipitation process that initiates at a relatively shallow depth and a low diagenetic temperature in environments with high pH values and high Fe and Mg ion contents. The gradual transformation occurs via mixed-layer clays formation (e.g. kaolinite/chlorite or smectite/chlorite) with progressively higher ratio of chlorite forming as temperature increases during burial (Thomson, 1979; Bettison-Varga and Mackinnon, 1997).

(3) Transformation of Fe-rich green 7 Å clay precursors like berthierine or odinite of verdine facies (Odin and Sen gupta, 1988; Odin, 1990; Ehrenberg, 1993; Hiller, 1994; Ryan and Reynolds, 1996; Grigsby, 2001; Worden and Morad, 2003). This hypothesis suggests that the Fe-rich clays were initially formed as coatings composed of small (<5 μm), lath-shape crystals, as ooids, and as matrix below the sediment-water interface or in the upper few meters of deposits during deposition or soon after deposition (Odin et al., 1988; Ehrenberg, 1993). In later burial, with increasing formation pressure and temperature perhaps within a few meters or up to the first 2 km of the subsurface, the precursor clays were transformed to chlorite (Bailey, 1988a, b; Odin et al., 1988; Ehrenberg, 1993; Ryan and Reynolds, 1996; Grigsby, 2001; Worden and Morad, 2003; Moraes and De Ros, 1992). Transformation of metastable Fe-rich clays into chlorite coating has been considered through 7 Å-14 Å mixed-layer ferric clays via dissolution and reprecipitation processes (Bailey, 1988a, b; Odin, 1990; Ehrenberg, 1993; Ryan and Hillier, 2002).

The syndepositional Fe-rich clays form mostly in deltaic, estuarine, fluvial and inner-shelf settings particularly associated with areas of river discharge into marine environments in a tropical to subtropical climate (Odin and Sen gupta, 1988; Odin, 1990; Ehrenberg, 1993; Kronen and Glenn, 2000; jeans et al., 2000; Thamban and Purnachandra, 2000; Vaz, 2000; Den Hon et al., 2001; Ku and Walter, 2003; Gould et al., 2010; Tylor et al., 2010; Dowey et al., 2012). Baker's et al. (2000) study showed that the presence of the chlorite grain coatings indicates environments of onshore meteoric water influenced nearshore marine environments that are characterized by mixing of meteoric and marine waters. An increase in salinity in riverine waters, which transport Fe most likely as amorphous iron hydroxides, caused Fe flocculation and deposition mainly as amorphous colloid (Ehrenberg, 1993; Grigsby, 2001; Bloch et al., 2002). The role of rivers is decisive to the development of chlorite as these arteries can supply adequate dissolved ferric ions from the weathering of ferromagnesian minerals and volcanics in

upstream for Fe-rich clay film mineralization (Hearne and Lock, 1985; Odin et al., 1988; Ehrenberg, 1993; Bloch et al., 2002; Dowey et al., 2012). This mechanism allows introduction of Fe, due to low concentration of Fe in the seawater (Bloch et al., 2002). Chlorite literature review by Dowey et al., (2012) showed that latitudinal range of 60º N to 60º S and tropical and subtropical climates for process of chemical weathering at the time of deposition were the most favorable conditions for generating clay precursor minerals in sediments from the Devonian onward. The biologically mediated precipitation of berthierine films has been done by laboratory experiments (McIlroy et al., 2004; Needham et al., 2005). The transformation of amorphous, Fe-rich 7 Å clay films to 7 Å -14 Å Fe-rich chlorite through dissolution-precipitation process at about 90 °C has been also supported by laboratory synthesis by Aagaard et al., (2000) on the naturally-occurring sandstones from offshore Norway.

(4) Combination of these processes, especially in the studies that revealed two layers of pore-lining chlorite, indicating two different growth processes in different time and different physiochemichal conditions (e.g. Anjos, et al., 2003; Luo et al., 2009; Jun et al., 2009; Berger et al., 2009; Lynch, 1996; Zhang et al., 2012). For example, some studies have been reported that sandstones that were already covered by transformed coatings may also have been enclosed by coats formed by precipitation from pore waters (Remy, 1994; Anjos, et al., 2003; Luo et al., 2009). Some other researchers interpret that the inner layer formed by transformation of Fe-rich clay films at shallow burial depth, while the outer layer formed by dissolution-precipitation of the chloritic material of the first chlorite layer (Grigsby, 2001; Jun et al., 2009; Berger et al., 2009).

3.11.2.2-Origin, time and process of chlorite coating in the Lower Tuscaloosa Formation

As was discussed in the authigenic mineral section, detailed SEM observations revealed that the chlorite coats in the Lower Tuscaloosa reservoir sandstones are composed of two superimposed layers (Figs. 3.21a, b, c and d) including: (1) an inner

coating composed of fine (<1 μm), poorly crystallized chlorites, oriented oblique or tangential to the detrital grain surface; and (2) an outer coating containing coarse (5-10 μm) crystallized chlorites with subhedral to euhedral, pseudo-hexagonal crystal shape displaying face-to-edge crystal habits, oriented perpendicular to the grain surfaces. The underlying fine crystalline chlorites could only be seen at the interface between the two chlorite layers where the overlying coarse crystalline chlorites have broken away. EDS analysis showed that the two chlorite coating layers have variations in their compositions by having higher amount of Fe (av. 30%) and Mg (av. 6%) in the outer layer compared to contents of Fe (av. 14%) and Mg (av. 2%) in the inner layer (Figs 3.22 a and b; Tables 3.3 and 3.4).

The differences in crystal size and structure as well as chemical composition of these two layers indicate two different stages of precipitation, most probably related to two different origins of the chlorite layers. In this section a combination of depositional environment, provenance, and diagenesis was used to interpret the origin, time and process of the formation of the pore-lining chlorites in the Lower Tuscaloosa Formation.

Considering depositional environment, climate, latitude and host rock of the Lower Tuscaloosa sandstones, formation of Fe-rich clay precursors and their transformation to chlorite is a probable origin. Deposition of the Lower Tuscaloosa sandstones in incised valley and deltaic/estuarine environments (for depositional environment, see Chapter 2), influenced by marine water during the Cenomanian marine transgression, characterized by mixing of meteoric and marine waters, was a suitable environment for formation of Fe-rich clay precursor. The fluvial system could supply adequate constituents for formation of clay precursor by weathering of the volcanic and metamorphic rocks of the southern Arkansas and the Appalachians, from the hinterland to the Tuscaloosa depositional system. The paleogeographic setting in southwestern Mississippi was in 25º N (?), with warm, subtropical to semi-arid climate during deposition of the Lower Tuscaloosa Formation (Mancini et al., 1999). Presence of

lignite/coal interlaminations and paleosol in the cores of the Lower Tuscaloosa reservoir sandstones of the Cranfield Field confirmed these circumstances. This paleogeographic and depositional environment was favorable for formation of Fe-rich clay precursors (Odin and Sen gupta, 1988; Odin, 1990; Ehrenberg, 1993; Kronen and Glenn, 2000; Baker et al., 2000; jeans et al., 2000; Thamban and Purnachandra, 2000; Vaz, 2000; Den Hon et al., 2001; Ku and Walter, 2003; Gould et al., 2010; Tylor et al., 2010; Dowey et al., 2012).

Presence of mixed-layer serpentine-chlorite in the shallow buried Tuscaloosa Formation of the Gulf Coast region as an intermediate phase between Fe-rich clay precursor and chlorite was reported by Ryan and Reynolds (1996, 1997). They also suggested that based on similarities in depositional environment, texture and mineralogical structure, the mixed-layer serpentine-chlorite originated from odinite. Transformation of odinite to mixed-layer serpentine-chlorite started within upper few meters of the Lower Tuscaloosa sediment with an initial crystallization temperature of about 20ºC to 40ºC (Hornibrook and Longstaffe 1996; Ryan and Reynolds 1996). In later progressive burial, proportion of serpentine layers in the mixed-layer reduced from 21% to 1% over a 4300 m interval (Ryan and Reynolds 1996, 1997; Ryan et al., 1998). These imply development of chlorite in the Tuscaloosa Formation from precursor clay mineral via mixed-layer with increasing temperature and depth.

In the petrographic studies, presence of the matrix-like pore-filling chlorite-TiO_2 with floating grains (Fig. 3.26b) considered as an evidence for infiltration of Fe-rich clay precursors and their transformation to chlorite in the Tuscaloosa sandstones. The coexistence of chlorite and TiO_2 as meshwork or lace-like structure within altered infiltrated clays implies that infiltrated Fe-rich clays (odinite) were a source of ions for formation of chlorite and a source of Ti for precipitation of in situ TiO_2. Lack of chlorite coats between the grain contacts (Fig. 3.20b) indicates that the clay precursor precipitation occurred after an initial phase of mechanical compaction or grain

rearrangement. As stated by Odin et al., (1988) and Ehrenberg (1993), this could happen soon after deposition of the Lower Tuscaloosa Formation, within upper meters, below the sediment-water interface. Transformation of Fe-rich clay precursors to chlorite started in very early diagenesis in the early eogenetic regime.

Overall, the evidences show that transformation of the Fe-rich clay precursors (odinite) through mixed-layer clays (serpentine-chlorite) during early eodiagenesis was an important source of ions (Fe, Mg, Si, and Al) needed for precipitation of the chlorites. On the other hand, numerous studies reported the origin of chlorite in the Tuscaloosa Formation from dissolution and alteration of the volcanic rock fragments (e.g. Thomson, 1979; Hearne and Lock, 1985; Hamlin and Cameron, 1987; Klicman et al., 1988; Genuise and McBride 1990; Paxton et al., 1990; Pittman et al., 1992; Cameron et al., 1992; Ryan and Reynolds, 1996, 1997). Presence of abundant altered rock fragments and biotite remnants (now Ti oxide) (Figs. 3.5a, b; 3.20c; 3.26a) as well as partially to completely dissolved and chloritized versions of these components in the studied thin sections suggest that the dissolution of ferromagnesian grains was also one of the main sources of ions needed for formation of the chlorites. Modal analysis showed that the amount of original rock fragments was high (38.5% of framework grains) at the time of deposition and about 18.8% of original rock fragments content was lost during diagenesis. A cross-plot of chlorite coats versus intragranular plus moldic porosities (Fig. 3.36) shows a positive correlation, indicating that chlorites could be originated by dissolution of the rock fragments. The high amount of original rock fragments was related to the provenance of the Tuscaloosa Formations from volcanic and metamorphic rocks of the southern Appalachian and Ouachita Orogenic belts, the southern Arkansas volcanic belt and the continental interior (Fig. 1.7) (e.g. Salvador, 1991; Corcoran et al., 1993; Sayers and Uddin, 2010). The abnormally high content of TiO_2 (4.2% of rock volume), as remnant of altered grains show that the original composition of rock fragments were mafic and ultramafic, which can contain high amount of TiO_2 (up to

10%) in their composition (Whitney and McClelland 1983; Newman 1987; Brigatti et al. 1991; Deer et al. 1992).

The alteration of ferromagnesian fragments is interpreted to have occurred at the same time as chlorite growth to provide the ions for chlorite coat growth. This also resulted in precipitation of in situ TiO_2. Ryan and Reynolds (1996) reported that the cryptocrystalline TiO_2 precipitated due to incompatibility between the highly charged immobile Ti^{4+} by dissolved volcanic rock fragments and chlorite structure.

Alteration and dissolution of mafic and ultramafic fragments and precipitation of chlorite cements from pore water are favored at deeper burial depths during late eodiagenesis and mesodiagenesis (Zhang et al., 2012). Zhu et al, (2008) showed that temperature for precipitation of this type of chlorite is 90° to 120 °C. The preservation of chlorite coats outlining the dissolved original grain boundaries (moldic pores) (Fig. 3.7a) indicates that dissolution could also occur after the sandstone framework had become stabilized with respect to mechanical compaction; otherwise these chlorite coats would have collapsed. Paragenetic analysis showed that chlorites formed before precipitation of late mesogenetic cements (i.e. ankerite and quartz overgrowths; Figs. 3.25d, f ; Figs 3.32d, e, f). These evidences show that the dissolution and alteration of mafic and ultramafic grains was another source of ions needed for precipitation of the chlorites.

In general, considering the textural habits, crystal size and structure, chemical composition, relative timing and depth of chlorite formation, I interpret that chlorite coatings in the Lower Tuscaloosa Formation were precipitated in two stages. The inner fine crystalline chlorite coats formed by transformation of the Fe-rich clay precursors (odinite) through mixed-layer clays (serpentine-chlorite), during early eodiagenesis. Following development of the inner chlorite coats, detrital grains that were already covered by transformed coatings in shallow burial, additionally were coated by direct precipitation from pore waters during late eodiagenesis to early mesodiagenesis and formed the outer layer. By this interpretation, the origin of the poorly crystallized chlorite

coats are from Fe-rich clay precursors (odinite) and the coarser crystallized chlorite coats originate from dissolution and alteration of the mafic and ultramafic fragments. Figure 3.37 shows the schematic model for the two stages of the chlorite coats formation through progressive burial depth.

The origin of the inner chlorite coat layer in the Tuscaloosa sandstone reservoirs was also supported by presence of the preserved original Fe-rich clay morphology, which was explained by Grigsby (2001), as tangentially oriented of the inner chlorite coat layer. Moreover, higher Fe and Mg contents in chemical composition of outer chlorite coat layer compared to the inner chlorite coat layer confirm that the inner layer formed in shallower depth and lower temperature (early eogenetic regime) while the outer layer formed in deeper depth and higher temperature (late eogenetic to early mesogenetic regimes), before precipitation of quartz and ankerite cements. Jahren and Aagaard's studies (1992) showed that with rising temperature from 90 to 180 ºC, the iron content in chlorites increases from 2.4 to 4.1 atoms pfu. Inoue et al. (2009) also noted that with rising temperature, chlorite crystals tend to have a more ordered structure. This is the case for the well-formed coarser chlorite crystals of the outer coat layer that formed in higher diagenetic grade compared with the inner coat layer in the Tuscaloosa sandstones.

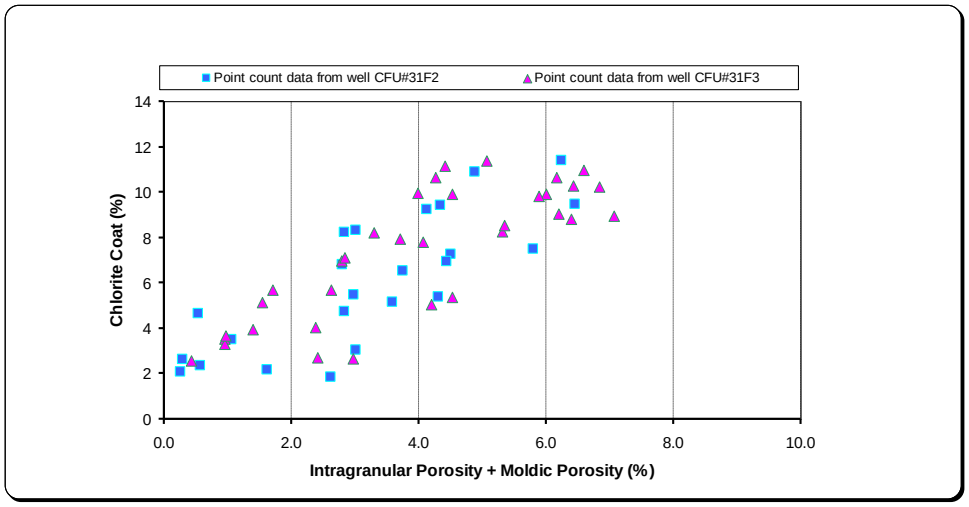

Figure 3.36-Cross-plot of chlorite coats versus intragranular plus moldic porosities indicating that chlorites could have originated by dissolution of the rock fragments.

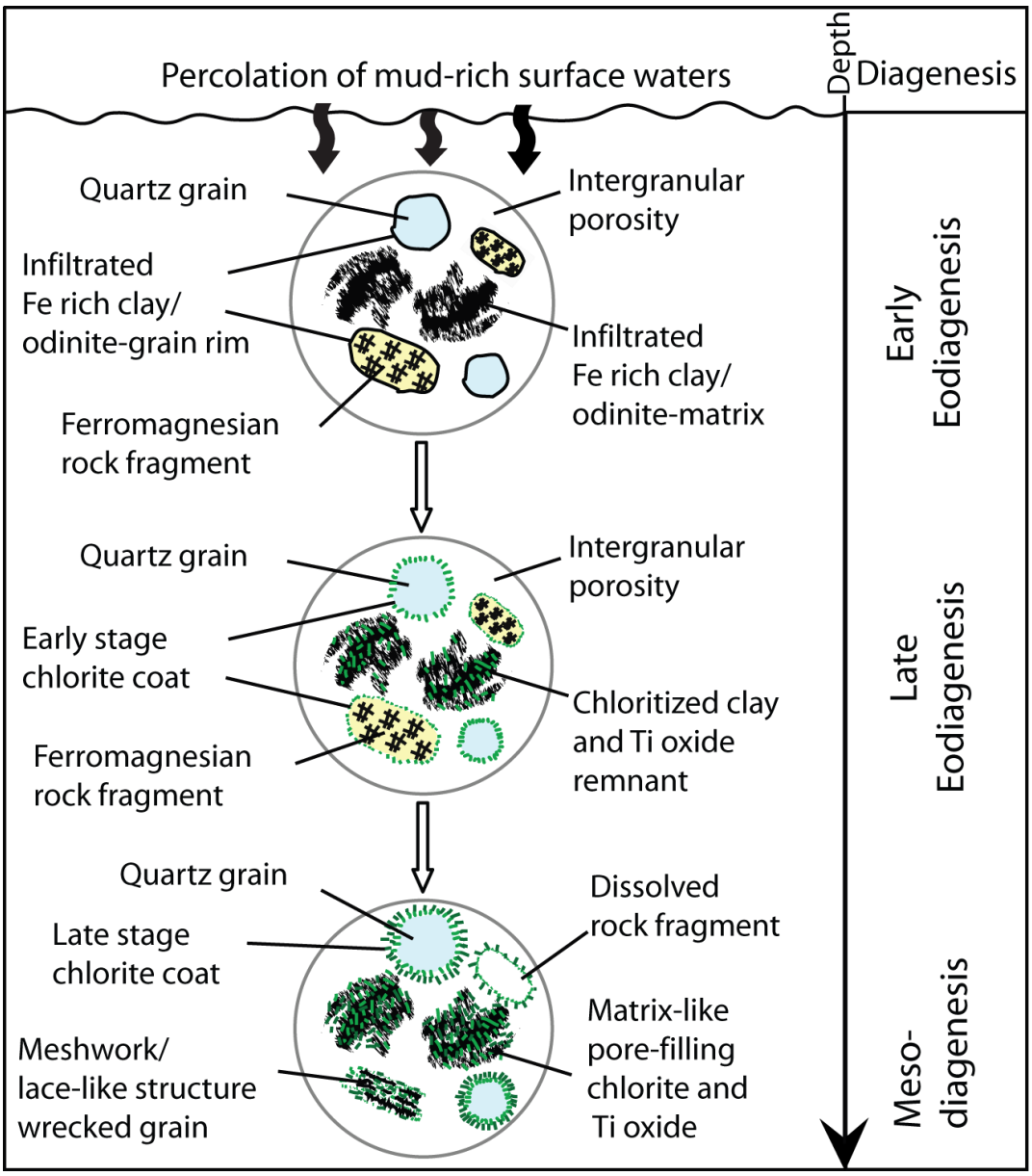

Figure 3.37-Schematic model for the two stages of the chlorite coats formation through progressive burial depth.

3.11.3-Interplay between chlorite coating and quartz cementation and their effects on reservoir quality

There are broad studies that show formation of chlorite as grain coating inhibit precipitation of quartz overgrowths, resulting in preservation of primary porosity and permeability in deep burial (e.g. McBride et al, 1987; Ehrenberg, 1993; Ryan and Reynolds, 1996; Bloch et al., 2002; Billault et al., 2003; Berger et al., 2009; Gould et al., 2010; Zhang et al., 2012). However the quantity correlation is highly complex and the extent of the inhibition process and its effect on reservoir quality are not well known. Precipitation of quartz cement, which has been considered as the most destructive porosity in deeply buried reservoir sandstones (McBride, 1987; Worden and Morad, 2000; Giles et al., 2000), could be prevented, if the chlorites are present as thick and complete coats on the grains.

Regardless of the silica source, two important factors that affect precipitation of quartz cements are surface area available for nucleation and rate of crystal growth per unit surface area (Lander and Walderhaug, 1999; Walderhaug, 2000; Lander et al., 2008). Walderhaug's studies (1994, 1996, and 2000) revealed that rate of quartz cementation would be dictated by the slowest step that is the rate of crystal growth and not the rate of silica production or transportation of dissolved silica. Therefore, the quartz cementation would be "rate-limited", even if it is thermodynamically favorable (Worden and Morad, 2000). The surface area is a function of the grain size, quartz grain abundance, and extent of grain coatings and also overall porosity (Dickinson and Milliken, 1995; Lander and Walderhaug, 1999; Walderhaug, 2000). Therefore, at the sandstones with well-coated chlorite, even if the conditions for precipitation of quartz cement be thermodynamically favorable and if the quartz crystallizing solutes were available, due to thick and continuous chlorite coats, quartz crystal growth cannot be formed. In this part where the nucleation sites are presented in the break points of chlorite coats, the quartz cement could precipitate as outgrowths.

Several reasons have been suggested for inhibition of quartz overgrowth on chlorite coated grains, including: (1) limitation in nucleation sites on the surface of the detrital grain for quartz overgrowths by isolating detrital quartz grain surfaces from pore waters (Ehrenberg, 1993; Bloch et al., 2002; Pe-Piper and Weir-Murphy, 2008; Berger et al., 2009; Taylor et al., 2010); (2) restriction of epitaxial growth of quartz crystals to the inter-particular space near the detrital quartz-chlorite coating interface due to geometrical selection (Billault et al., 2003); (3) limitation in grain-grain contact and pressure dissolution via compaction as a source of quartz cement (Pittman and Lumsden, 1968; Pittman et al., 1992); (4) maintaining pore waters and detrital quartz grain surfaces in an alkaline condition through precipitation of chlorite, which is not a suitable geochemical condition for precipitation of siliceous material; and (5) inhibition of quartz cement growth by forming barriers to early-overgrowth coalescence (Ajdukiewicz and Larese, 2012).

As observed in the thin sections of the Lower Tuscaloosa reservoir sandstones at the Cranfield Field, medium to very coarse grained sandstones, which are located at the lower portion of the fining-upwards units at the reservoir interval (Fig. 3.2), have chlorite with larger crystal size and thicker coats compared to fine to very fine grained sandstones at the top of the units. The well-formed, thick and continuous chlorite coatings in the coarser grain sandstones inhibited formation of quartz overgrowth, whereas the finer grain sandstones with the poorly-formed, thin and discontinuous chlorite coatings have been cemented by quartz overgrowths. This link has been supported in the modal analysis by a positive relationship in the cross-plot of grain size versus total chlorite (Fig. 3.23).

The reason for higher amount of chlorite in coarser-grained sandstones was examined by determining any possible link between grain size and original rock fragment abundance. As shown in Figure 3.38, there is no relationship between grain size and original rock fragment abundance. However, there is a relatively good link between amount of dissolved rock fragments (moldic + intragranular porosities) and chlorite coat

abundance (Fig. 3.36). These indicate that the amount of rock fragments was not varied by changing the grain size, but amount of dissolution of rock fragments was higher in the coarser grained sandstones. The higher dissolution of rock fragments in coarser grained sandstone, most probably to the higher permeability and better solution flow, is one of the reasons that could explain the relationship between grain size and amount of chlorite. The second plausible factor could be related to the lower surface area for nucleation of chlorite crystals with a particular amount of reactive elements in a given volume of sandstone, which result in higher amount of chlorite. The third season could be due to better formation of clay precursor in coarser gain sandstones. By higher percolation of mud-rich surface water in coarser grained sandstone that have higher permeability compared with finer grained sandstones, during diagenesis higher amount of chlorite could be form.

The modal analysis of the Lower Tuscaloosa Formation revealed that the optimum amount of chlorite to prevent formation of quartz overgrowth is 6% of rock volume. A cross-plot of quartz overgrowths abundance versus chlorite coat abundance (Fig. 3.39) showed that if the chlorite coat is less than 6%, it could not prevent formation of quartz overgrowth and quartz cement could form and reduce the porosity and permeability. This graph also shows that the quartz overgrowth volume correlates negatively with variation in chlorite coat volume.

The average amount of original rock fragments in the Tuscaloosa reservoir sandstones was 38.5% of the rock volume. This showed that the amount of rock fragments in the Tuscaloosa sandstones was enough to form the chlorites and thus with content of 6% chlorite coat or more, the quartz overgrowths could not precipitate, resulting in preservation of anomalously high porosity (average 25%) and permeability (average 50 md) in sandstones buried to depths as great as ~3 km (~10,000 ft).

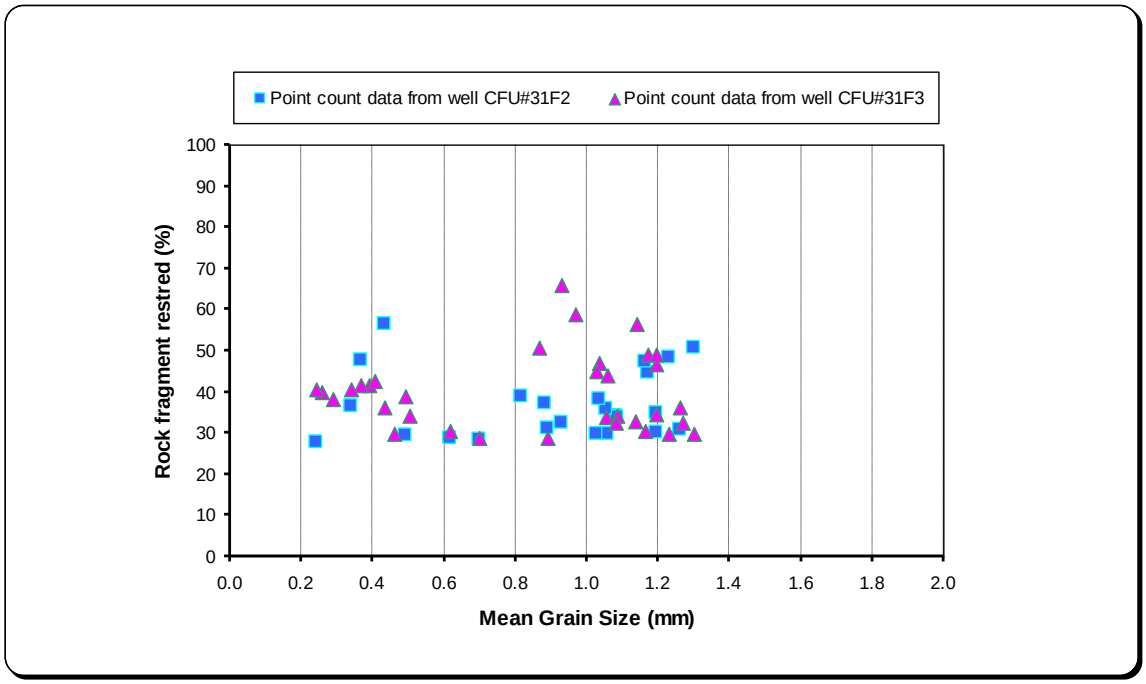

Figure 3.38-Cross-plot of grain size versus original rock fragment abundance does not show any relationship between them.

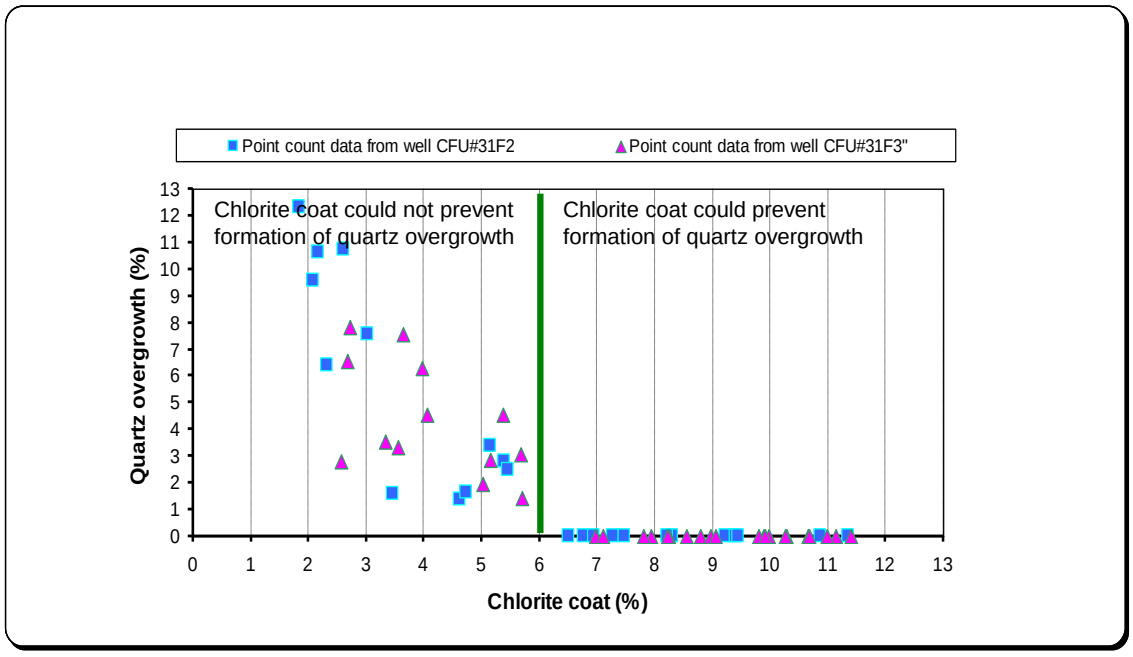

Figure 3.39-Cross-plot of quartz overgrowths abundance versus chlorite coat abundance showing that if the chlorite coat is less than 6%, it could not prevent formation of quartz overgrowths. This graph also shows that the quartz overgrowth volume correlates negatively with variation in chlorite coat volume.

3.12-CONCLUSIONS

The combination of positive and negative effects of diagenesis on porosity and permeability in the Lower Tuscaloosa sandstones results in complex reservoir quality. Mechanical compaction was an important process in reducing original porosity, more than chemical compaction and slightly more than cementation. Presence of chlorite coats played an important role in reservoir quality and developing the diagenetic heterogeneity. The two observed chlorite coats were precipitated in two stages. The inner fine crystalline chlorite coating formed by transformation of the Fe-rich clay precursors (odinite) through mixed-layer clays (serpentine-chlorite) during early eodiagenesis. Following development of the inner chlorite coats, detrital grains that are already covered by transformed coatings in shallow burial, additionally was coated by direct precipitation from pore waters during late eodiagenesis to early mesodiagenesis and formed the outer layer. The ions needed for precipitation of thick chlorite coats were from dissolution and alteration of the ferromagnesian fragments. By these processes, the well-formed, thick and continuous chlorite coatings in the coarser grain sandstones inhibited formation of quartz overgrowth, whereas the finer grain sandstones with the poorly-formed, thin and discontinuous chlorite coatings have been cemented by quartz overgrowths. The optimum amount of chlorite to prevent formation of quartz overgrowth is 6% of rock volume.

Dissolution and alteration of the high amount of original ferromagnesian fragments resulted in generation of secondary porosities, that compared to primary porosity are considerable. This also resulted in precipitation of abnormally high content of in situ TiO_2 that, along with authigenic kaolinite and chlorite, increased the amount of microporosity.

The chlorite coats were not effective on inhibition of late ankerite cement precipitation, because ankerite cementation postdating chlorite coat formation. The amount of ankerite, which formed as nodules and thin streaks, is not well-extended;

however it may affect fluid flow and accumulation by compartmentalizing in the sandstone reservoir.

Kaolinite, pyrite and Fe oxide are authigenic minerals that have low concentrations in the lower Tuscaloosa sandstones, and thus their effect on reservoir quality is negligible.

Overall, the best reservoir quality is in medium to coarse, moderately sorted sandstones that 1) have thick and continuous chlorite coat, 2) did not undergo cementation by quartz, 3) did not undergo late carbonate cementation, and 4) developed high amount of secondary porosity through the dissolution of rock fragments.

Chapter 4: Reservoir Quality Controls and Prediction in the Chlorite-coated Sandstones

4.1-CONTROLS ON RESERVOIR QUALITY OF CHLORITE-COATED SANDSTONES

Reservoir quality in sandstones is controlled both by depositional processes that result in lithologic variation during sedimentary deposition and by modification of sediments by diagenetic alterations during burial. In Chapters 2 and 3, I discussed these two factors affecting reservoir quality of the Lower Tuscaloosa Formation. In this chapter, as a conclusion, I will integrate depositional and diagenetic characteristics and will review the main controlling factors affecting reservoir quality variation and heterogeneity of the Lower Tuscaloosa Formation. This will help us in better understanding and even predicting the reservoir quality of chlorite-bearing sandstones in deep burial. In such a context, I will also link formation of chlorite to sequence stratigraphy and will discuss how reservoir-quality distribution of chlorite-bearing sandstones may be predictable within sequence stratigraphic framework.

4.1.1-Depositional environment control

Depositional environment controls stratigraphic architecture, vertical and lateral extent of facies, geometry of sandstone bodies, distribution of mudstone and other low-permeability baffles. These determine the depositional heterogeneities and distribution of original porosity-permeability. However, the original porosity-permeability may be substantially modified by diagenesis. In the sandstones containing chlorite grain coats, the original porosity and permeability can be preserved in deep burial by inhibiting the quartz cementation (e.g. McBride et al., 1987; Ehrenberg, 1993; Ryan and Reynolds, 1996; Bloch et al., 2002; Billault et al., 2003; Berger et al., 2009; Gould et al., 2010; Zhang et al., 2012).

Chlorite literature review by Dowey et al., (2012) showed that although chlorite-coats are found in sandstones deposited in a range of depositional environments, they

most commonly occur in delta-related environments (44%) and fluvial environments (19%).

The lower Tuscaloosa Formation was deposited in fluvial fill-incised valley system, associated with deltaic environment (see Chapter 2, section 2.9.2). This environment was favorable for formation of clay precursor chlorite precursor minerals (berthierine or odinite of verdine facies), which in turn became altered to chlorite coats by progressive burial (for more details see Chapter 3, section 3.11.2.2).

Therefore the depositional environment of the Lower Tuscaloosa Formation controls stratigraphic architecture and initial porosity and permeability and also provides favorable conditions for formation of chlorite precursor minerals, which could preserve the original porosity and permeability in deep burial.

4.1.2-Textural control

Reservoir quality variation in the sandstones is highly controlled by distribution of textural parameters, most importantly grain size and sorting, which are mainly linked to the energy of the transportation and depositional system. Coarser grained and better sorted sandstones have larger pore throats and better pore connectivity for fluid flow compared with finer grained sandstones.

The modal analysis of the Lower Tuscaloosa Formation revealed that sorting does not affect chlorite abundance; however, grain size shows a good relationship with chlorite abundance (Fig. 3.23). The medium to very coarse grained sandstones, which are located at the lower portion of the fining-upwards unit at the reservoir interval (Fig. 3.2), have chlorite with larger crystal sizes and thicker coats compared to fine to very fine grained sandstones at the top of the units. As a result, the well-formed, thick and continuous chlorite coatings in the coarser grain sandstones inhibited formation of quartz overgrowths, whereas the finer grain sandstones with the poorly-formed, thin and discontinuous chlorite coatings have been cemented by quartz overgrowths. The plausible

factors that could explain the higher amount of chlorite in the coarser grained size could be the lower surface area for nucleation of chlorite crystals with a particular amount of reactive elements in a given volume of sandstone, larger pore-throat size for better chlorite growth, higher permeability and better solution flow in the coarser-grained sandstones compared with the finer-grained sandstones.

4.1.3- Provenance control

Provenance has an important control on reservoir quality by influencing the composition of sediments, which in turn affect mechanical properties and chemical diagenetic processes (Kosanke et al., 2005, 2008). The petrographic studies of the Lower Tuscaloosa Formation showed that provenance played a major role in contributing chlorite into the system, which in turn affects on reservoir quality. Sediment provenances of the Tuscaloosa Formation, which were from the southern Appalachian and Ouachita Orogenic belts, the southern Arkansas volcanic belt and the continental interior (e.g. Salvador, 1991; Corcoran et al., 1993; Sayers and Uddin, 2010), supplied large amounts of ferromagnesian grains and specifically mafic and ultramafic rock fragments into the system. Dissolution and alteration of the ferromagnesian grains during diagenesis resulted in precipitation of authigenic chlorite, generation of secondary porosity and precipitation of in situ Ti oxide that highly affected the reservoir quality of the Lower Tuscaloosa Formation.

4.1.4- Diagenetic control

Diagenetic alterations have a substantial impact on modifying depositional porosity and permeability, and consequently, on reservoir quality of the Lower Tuscaloosa Formation. Petrographic studies of the sandstone showed that mechanical compaction was an important agent in reducing original porosity. Due to presence of ductile grains and dissolved/altered rock fragments, the mechanical compaction is more penetrative and the ductile deformation has more effect on reduction of pore volume than

brittle deformation. The mechanical compaction also is more important than chemical compaction and is slightly more important than cementation (Fig. 3.17). Modal analysis revealed that sandstones with more chlorite coat cements have undergone less mechanical compaction and thus display overall higher IGV, whereas sandstones with fewer chlorite coat cements were subjected to a considerable compaction and reduction of pore space during burial and thus lower IGV (Fig. 3.15). This could also be related to the relationship between thick well-formed chlorite coats in the coarser grain sandstones that act as anti-compaction by inhibition of pressure dissolution.

Formation of well-formed, thick and continuous chlorite coatings inhibited formation of quartz overgrowths, which is one of the most destructive cements in the deeply buried sandstones, resulting in preserving a high amount of original porosity. However, sandstones with the poorly-formed, thin and discontinuous chlorite coatings could not prevent formation of quartz overgrowths and thus the quartz cements destroyed the porosity. The modal analysis revealed that the optimum amount of chlorite to prevent formation of quartz overgrowths is 6% of rock volume. A cross-plot of quartz overgrowth abundance versus chlorite coat abundance (Fig. 3.39) showed that if the chlorite coat is less than 6%, it could not prevent formation of quartz overgrowth and quartz cement could form and reduce the porosity and permeability.

As a summary, Figure 4.1 shows the reservoir quality interpretation within the studied reservoir interval in Well CFU#31F3.

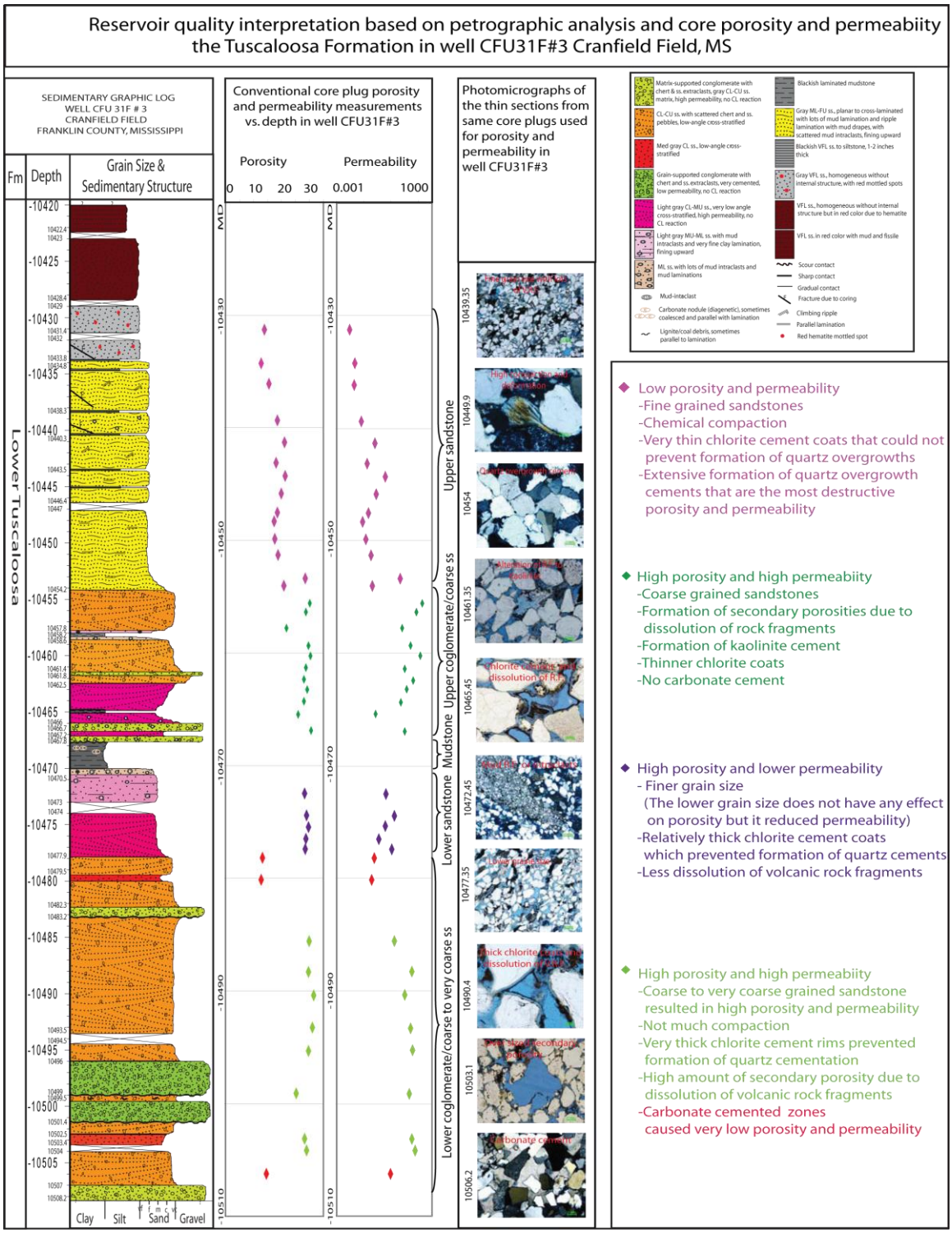

Figure 4.1-Reservoir quality interpretation within the studied reservoir interval in Well CFU#31F3 by a combination of core description, core porosity and permeability measurements and petrographic studies.

4.2-LINKING DIAGENESIS TO SEQUENCE STRATIGRAPHY FOR CHLORITE COATING PREDICTION

By integrating diagenesis and sequence stratigraphy, the basin-scale distribution of diagenetic alterations and their impact on reservoir quality can investigated within a sequence stratigraphic framework. In such a context, reservoir-quality distribution may be predictable through sequence stratigraphic analysis in the exploration plans (Morad et al., 2000; 2010; 2012; Ketzer et al., 2003a; Al-Ramadan et al., 2005; El-Ghali et al., 2006a; Kordi et al., 2011).

Linking diagenesis to sequence stratigraphy in siliciclastic sequences is feasible because changes in rate of sea level/base level and rate of sediment supply, which govern the sequence stratigraphic framework, also control the parameters that affect the types and extent of diagenetic alteration (Taylor et al., 1995, 2000; Morad et al., 2000, 2010; Ketzer et al., 2003a; Reed et al., 2005; Kordi et al., 2010, 2011). These parameters include: (1) changes in near-surface pore water chemistry that are controlled by the position and dynamics of the meteoric, mixed marine/meteoric and marine pore-water zones as a result of relative sea-level changes; (2) sedimentation rate and residence time of sediments under a certain set of geochemical conditions, which depend on the duration of cycles of relative sea-level change and which, in turn, affect the length of diagenetic reactions; (3) variations in the detrital composition and texture, particularly with regard to the type, amount and spatial distribution of intra- and extrabasinal grains; and (4) depositional environment and facies, which are controlled by regressive and transgressive events. These changes may be detected by the occurrence of specific eogenetic alterations, which can be predicted within a sequence stratigraphic framework. The near-surface diagenetic alterations related to sequence stratigraphy have an important impact on deep burial mesodiagenesis, and hence on the evolutionary pathways of the sandstones during progressive burial.

As discussed in Chapter 2, the Lower Tuscaloosa Formation (Massive Sand Member and Stringer Sand Member) deposited during the late Lowstand System Tract and Transgressive System Tract (Fig. 2.6) in a fluvial fill-incised valley within a deltaic/estuarine system. During this time, relative sea level rise and marine transgression resulted in retrogradation of the shoreline and thus mixing of meteoric and sea water, which was favorable for formation of chlorite precursor phases (berthierine or odinite of verdine facies). The fluvial system could supply adequate dissolved ferric ions for formation of clay precursor by weathering of the ferromagnesian volcanic and metamorphic rocks from the hinterland (Hearne and Lock, 1985; Odin et al., 1988; Ehrenberg, 1993; Bloch et al., 2002; Dowey et al., 2012). This mechanism allows introduction of Fe, due to low concentration of Fe in the seawater (Bloch et al., 2002). An increase in salinity in riverine waters, which transport Fe most likely as amorphous iron hydroxides, caused Fe flocculation and deposition mainly as amorphous colloid (Ehrenberg, 1993; Grigsby, 2001; Bloch et al., 2002). The marine transgression encountered low sedimentation rates, proceeded percolation of muddy water into sandstones, especially highly permeable fluvial channel successions, as infiltrated clays.

Therefore, the late Lowstand System Tract and early Transgressive System Tract are suitable for formation and deposition of chlorite precursor clays. Later, by progressive burial during late eodiagenesis and early mesodiagenesis, the clay precursors can be transformed to chlorite. Lack of extensive eogenetic cementation, especially carbonates, in the bioclast-poor fluvial sandstones, could lead to preservation of relatively good porosity during burial. Furthermore, the development of the thick and continuous chlorite coat could inhibit formation of quartz overgrowths. This results in relatively good porosity and permeability in deep burial.

Appendices

Appendix I: List of the 93 wells that have been used in this study including their API number, well label, well name, lease name and their coordinates.

API Numb	Well Label	Well Name	Lease Name	Surf X	Surf Y
23001001510000	GEO W ARMSTRONG #2	GEO W ARMSTRONG #2	G W ARMSTRONG	241507.5	393248.3
23001001530000	GEO W ARMSTRONG #4	GEO W ARMSTRONG #4	GEO W ARMSTRONG	240119	394961.4
23001001580000	CFU #1	CFU 48-3	CRANFIELD UNIT #1	242095.2	388183.6
23001001590000	CFU #2	CFU 29-9	CRANFIELD UNIT #1	240389.6	391641.6
23001001610000	CFU #3	CFU #3	CRANFIELD UNIT	239298	384119.7
23001001620000	CFU #4	CFU 47-1	CRANFIELD UNIT #4	243138.3	390209.3
23001001650000	CFU #8	CFU #8	CRANFIELD UNIT #8	241312.3	376552.3
23001001720000	CFU #13	CFU 24-3	CRANFIELD UNIT #13	235581.3	394141.4
23001001740000	CFU #15	CFU 44-2	CRANFIELD UNIT #15	235002.5	390595.4
23001001760000	CFU #17	CFU 29-1	CRANFIELD UNIT #17	237214.7	393928.7
23001001770000	CFU #20	CFU 44-4	CRANFIELD UNIT #20	233117.4	389311.4
23001001780000	CFU #21	CFU 29-2	CRANFIELD UNIT #21	238526.1	393958.6
23001001790000	CFU #22	CFU #22	CRANFIELD UNIT #22	235870.7	394906.7
23001001810000	CFU #25	CFU #25	CRANFIELD UNIT #25	235140.9	379546.2
23001001820000	CFU #26	CFU #26	CRANFIELD UNIT	231792.1	378029.9
23001001860000	HICKINGBOTHAM ETAL #1	HICKINGBOTHAM ETAL #1	M T HICKINGBOTHAM	231653.4	381796.2
23001001890000	VERNON JOHNSON #1	VERNON JOHNSON #1	VERNON JOHNSON	242422.3	392321
23001001900000	VERNON JOHNSON #2	CFU 28-2	VERNON JOHNSON	243336.1	392474.2
23001001910000	VERNON JOHNSON 3-4	CFU 27-4	VERNON JOHNSON	242274.8	391339.9
23001001940000	ELLA G LEES #3	CFU 29-11	GULF ELLA G LEES	237748.1	392014.7
23001001950000	ELLA G LEES #4	ELLA G LEES #4	ELLA G LEES	237481.3	392959
23001001960000	ELLA G LEES #5	CFU 29-10	GULF ELLA G LEES	236031.4	392337.2
23001001970000	ELLA G LEES #6	CFU 29-6	GULF ELLA G LEES	242138.8	377884.7
23001001990000	ELLA G LEES #7	ELLA G LEES #7	GULF ELLA G LEES	239485.8	392790.8
23001002000000	ELLA G LEES #8	CFU 29-4	ELLA G LEES	239924.6	393158.5
23001002010001	ELLA G LEES #9	ELLA G LEES #9	ELLA G LEES	238888.2	385523.4
23001002020000	ELLA G LEES #10	ELLA G LEES #10	ELLA G LEES	236440.2	393247.1
23001002030000	ELLA G LEES #11	ELLA G LEES #11	E G LEES	238546	393707.4
23001002090000	ELLA G LEES #17	CFU 29-7	GULF ELLA G LEES	240018.2	392357.5
23001002110000	ELLA G LEES #19	ELLA G LEES #19	ELLA G LEES	237246.3	393983
23001002120000	ELLA G LEES #20	CFU 29-8	ELLA G LEES	240918.3	391950.4
23001002130000	ELLA G LEES #22	ELLA G LEES #22	ELLA G LEES	238791.6	385924.3
23001002160000	ELLA G LEES #25	ELLA G LEES #25	ELLA G LEES	238393.2	384341.2
23001002260000	NATION GASOLINE LA #2	CFU 53-5	NATL GASOLINE CO OF LA	230922.9	383184.3
23001002280000	NATION GASOLINE LA #4	CFU 53-1	NATL GASOLINE CO OF LA	231187.5	385921.5
23001002290000	NATION GASOLINE LA #5	NATION GASOLINE LA #5	NATL GASO CO OF LA	232261.6	380289
23001002300000	NATIONL GASOLINE LA #6	CFU 53-4	NATL GASOLINE CO OF LA	231919	384668
23001002310000	NATIONL GASOLINE LA #7	NATIONL GASOLINE LA #7	NATL GASOLINE CO OF LA	233325.3	379258.4
23001002330000	NATIONL GASOLINE LA #9	NATIONL GASOLINE LA #9	NATL GASOLINE CO OF LA	233743.7	378171.1
23001002340000	NATIONL GASOLINE LA #10	NATIONL GASOLINE LA #10	NATL GASOLINE LA	234230.2	377028.6
23001002380000	NATIONL GASOLINE LA #15	NATIONL GASOLINE LA #15	NATL GASOLINE CO OF LA	235686.9	389687.9
23001002390000	NATL GAS LA #1	NATL GAS LA #1	NATL GAS LA	235797.5	383855.6
23001002450000	A M RATCLIFFE 2-1	A M RATCLIFFE 2-1	A M RATCLIFFE A C 2	238200.3	377882
23001002510000	A M RATCLIFFE 2-4	A M RATCLIFFE 2-4	A M RATCLIFFE A C 2	239321.5	376993

23001002570001	A M RATCLIFFE 2-6	A M RATCLIFFE 2-6	A M RATCLIFFE 2	240072.1	376136.1
23001002590000	A M RATCLIFFE ETL 2-8	A M RATCLIFFE ETL 2-8	A M RATCLIFFE A C 2	240899.5	375940.6
23001002600000	A M RATCLIFFE 2-9	A M RATCLIFFE 2-9	A M RATCLIFFE A C 2	240982.4	377013.1
23001002610000	A M RATCLIFFE 2-10	A M RATCLIFFE 2-10	A M RATCLIFFE A C 2	238892.3	382402.1
23001002660000	L G RATCLIFFE ETAL #3	L G RATCLIFFE ETAL #3	L G RATCLIFFE	234740.6	378949.1
23001002670000	L G RATCLIFFE ETAL #4	L G RATCLIFFE ETAL #4	L G RATCLIFFE	235218.2	377457.5
23001002680000	L G RATCLIFFE #5	L G RATCLIFFE #5	L G RATCLIFFE	236145.4	376879.2
23001002690000	L G RATCLIFFE ETAL #6	L G RATCLIFFE ETAL #6	L G RATCLIFFE ETAL	235162	376239.3
23001002700000	L G RATCLIFFE ETAL #7	L G RATCLIFFE ETAL #7	L G RATCLIFFE	236716.8	375816.2
23001002710000	L A WHITTINGTON #1	L A WHITTINGTON #1	L A WHITTINGTON	231854	387487.8
23001002720000	L A WHITTINGTON #2	CFU 44-7	L A WHITTINGTON	232484.2	388403.2
23001002730000	L A WHITTINGTON #3	L A WHITTINGTON #3	L A WHITTINGTON	233218.1	391042.2
23001017350000	ELLA G LEES #2	ELLA G LEES #2	GULF ELLA G LEES	242193	379281.2
23001017360000	ELLA G LEES #4	ELLA G LEES #4	GULF ELLA G LEES	242095.5	376688.2
23001017380000	ELLA G LEES #9	ELLA G LEES #9	GULF ELLA G LEES	243292	378756.4
23001017390000	ELLA G LEES #10	ELLA G LEES #10	GULF ELLA G LEES	243457.7	380075.6
23001017410000	ELLA G LEES #14	ELLA G LEES #14	GULF ELLA G LEES	243394.7	377500.5
23001017420000	ELLA G LEES #15	ELLA G LEES #15	ELLA G LEES	243285.1	376184.5
23001032440000	CRANFIELD UNIT 31	CRANFIELD UNIT 31	CRANFIELD UNIT #31	238376.9	389929
23001032510000	CRANFIELD UNIT 32	CRANFIELD UNIT 32	CRANFIELD UNIT	237733.3	380763
23001033940000	ARMSTRONG GEORGE W 1	CFU 27-3 (gx)	G W ARMSTRONG	241639.7	394251.3
23001214910000	RATCLIFF-LEES UNIT 1	RATCLIFF-LEES UNIT 1	RATCLIFF-LEES UNIT	241188.9	381642.5
23001216000000	RATCLIFFE UNIT A 1	RATCLIFFE UNIT A 1	RATCLIFFE UNIT A	241114.7	383774.8
23001216530000	RATCLIFFE /A 2	RATCLIFFE /A/ 2	RATCLIFFE /A/	239528	379552.5
23001216830000	RATCLIFFE 1	RATCLIFFE 1	RATCLIFFE	232786.3	376472.4
23001225630000	BLANCHARD-EDWARDS 2	CFU 29-13	BLANCHARD-EDWARDS	239758.4	390151.3
23001231620000	EDWARDS-RATCLIFFE 1	EDWARDS-RATCLIFFE 1	EDWARDS-RATCLIFFE	242626.8	387634
23001231830000	EDWARDS-RATCLIFFE 1	EDWARDS-RATCLIFFE 1	EDWARDS-RATCLIFFE	239001.3	385246
23001232910000	JOHNSON VERNON #1	JOHNSON VERNON #1	VERNON JOHNSON	241822.8	391299.7
23037000410000	CRANFIELD UNIT 18	CFU 32 F-3	CRANFIELD UNIT 18	245712.2	387017.8
23037000420002	CRANFIELD UNIT 19	CRANFIELD UNIT 19	CRANFIELD UNIT 19	245140.6	378884.4
23037000470000	HOMOCHITTO LBR 3-3	CFU 29 F-2	HOMOCHILTO LBR CO LSE #3	244687.4	387851.3
23037000480000	VERNON JOHNSON ETAL 3	CFU 28 F-2	VERNON JOHNSON ETAL	244817.7	390687.8
23037003300001	ELLA G LEES #1	ELLA G LEES #1	ELLA G LEES	245871.4	382047.4
23037003340000	ELLA G LEES #7	ELLA G LEES	ELLA G LEES	244563.2	385818.7
23037003350000	ELLA G LEES #11	ELLA G LEES #11	GULF ELLA G LEES	244433.4	381810.8
23037003360000	ELLA G LEES #13	ELLA G LEES #13	ELLA G LEES	244433.6	379751.8
23037003370000	ELLA G LEES #16	ELLA G LEES #16	ELLA G LEES	244386.1	380072.3
23037003390000	ELLA G LEES #17	ELLA G LEES #17	ELLA G LEES	244815	385755
23001233460000	CFU44-2	CFU 44-2	CRANFIELD FIELD UNIT 44-2	235699.8	390539
23001233620000	CRANFIELD 24-1	CRANFIELD 24-1	CRANFIELD 24-1	236137	396727.2
23001233650100	CFU 27-1 #1	CFU 27-1 #1	CFU	242565.7	393699.7
23001233670100	CFU # 28-1	CFU # 28-1	CFU	242557.9	393670.7
23001233800100	CFU27-5	Cranfield Field Unit 27-5 2	CRANFIELD FIELD UNIT 27-5	242234	395010.8
23037214850000	CFU31F-2	CFU 31F#2	CRANFIELD FIELD UNI	248516.9	387600.9
23037214860000	CFU31F-3	CFU 31F#3	CRANFIELD FIELD UNI	248616.9	387632.9
23001233420000	CFU29-12	CFU29-12	CFU	237304.8	391065
23037214880000	CFU31F-1	CFU 31F#1	CRANFIELD FIELD UNI	248555.2	387717
23001232210000	BLANCHARD EDWARDS E 3	CFU 48-2	BLANCHARD EDWARDS E	242727.3	388571.8

Appendix II: Sedimentary graphic logs of Well CFU#29-12 (left, Ambrose and Meckel, GCCC internal report, 2007) and Well CFU#28-1 (right, Kordi, GCCC internal report, 2010).

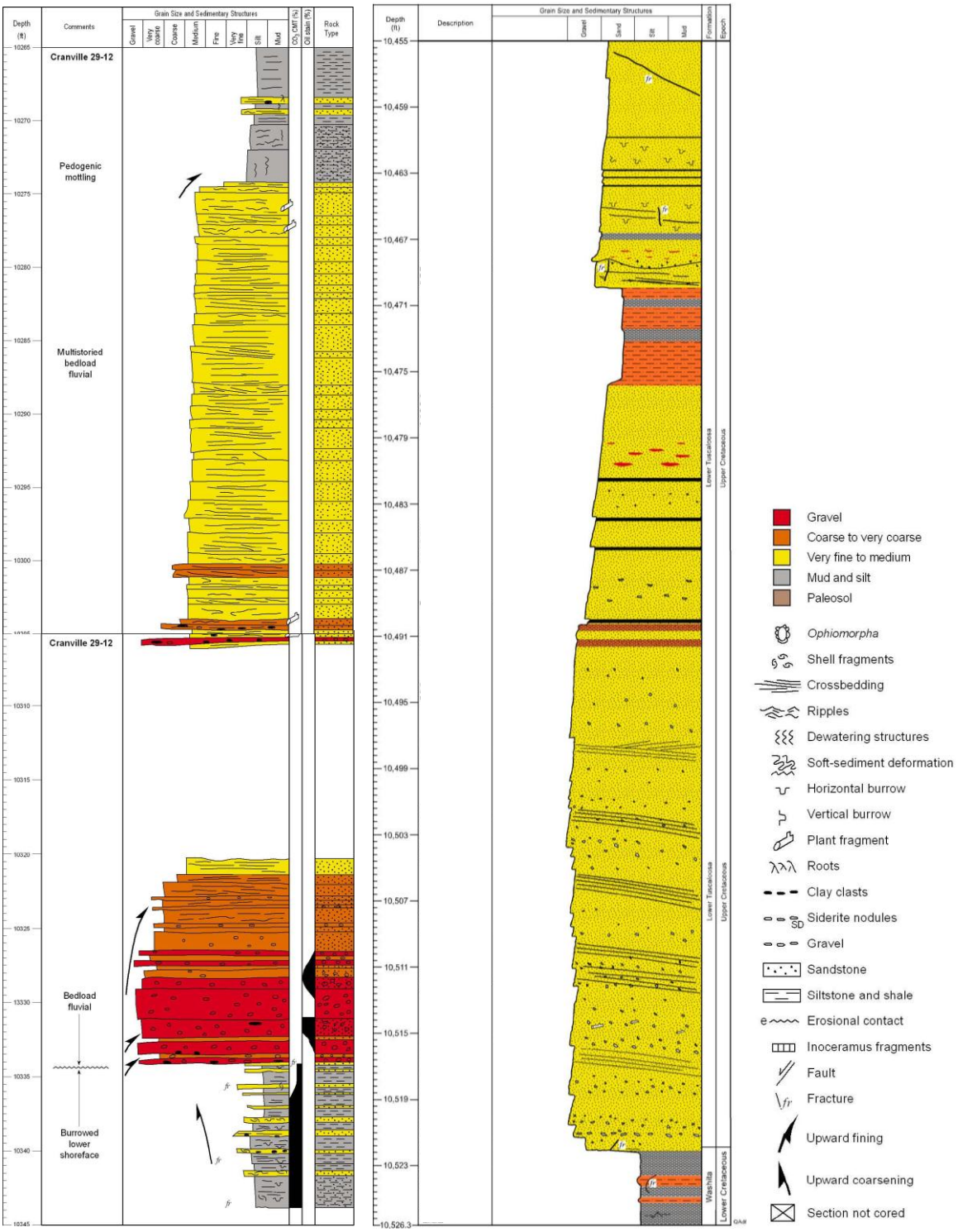

Appendix III: Point counting category and their related values in modal analysis for the 57 studied thin sections from Wells CFU 31F-2 and CFU 31F-3.

	Sample	%Qtz	%F	%L	%QFL	%Meta RF	%Sed RF	%Chert	%Silt/shl RF	%Rip up	%Qtz mono/Qtz	%Qtz<5 cryst/Qtz	%Qtz>5 cryst/Qt
CFU 31F-2 (Unit D)	10426.80	83.87	2.30	13.82	56.22	11.98	0.00	1.84	0.00	0.00	80.22	8.24	11.54
	10427.00	81.97	2.19	15.85	53.04	13.66	0.00	2.19	0.00	0.00	84.00	7.33	8.67
	10429.20	78.85	0.88	20.26	65.80	14.54	2.20	3.52	0.88	1.32	85.47	3.91	10.61
	10431.60	79.57	0.00	20.43	61.33	12.17	5.22	3.04	4.78	0.43	86.34	1.64	12.02
	10435.15	80.65	0.00	19.35	58.97	12.44	3.69	3.23	3.23	0.46	80.57	6.86	12.57
	10442.75	85.25	0.92	13.82	58.97	10.60	0.00	3.23	0.00	0.00	75.14	11.89	12.97
	10444.90	85.07	1.99	12.94	52.76	9.45	1.00	2.49	1.00	0.00	77.78	5.85	16.37
	10447.35	79.57	0.85	19.57	59.19	11.49	1.70	6.38	1.70	0.00	70.59	10.70	18.72
	10448.90	80.49	1.22	18.29	55.16	9.35	2.03	6.91	2.03	0.00	83.84	9.60	6.57
	10448.50	85.37	1.22	13.41	53.02	4.88	0.41	8.13	0.41	0.00	62.86	15.24	21.90
	10454.00	84.98	0.40	14.62	62.78	9.49	0.00	5.14	0.00	0.00	78.14	11.16	10.70
	10454.70	87.60	0.83	11.57	57.35	6.20	2.48	2.89	2.48	0.00	90.57	4.25	5.19
	10460.90	55.94	0.70	43.36	53.96	11.19	8.39	23.78	8.39	0.00	93.75	2.50	3.75
	10463.00	83.11	0.00	16.89	61.41	10.14	2.03	4.73	2.03	0.00	77.24	8.13	14.63
	10467.25	87.56	0.00	12.44	54.25	7.37	1.38	3.69	1.38	0.00	87.37	7.89	4.74
	10469.90	68.63	0.37	31.00	63.32	4.80	16.24	9.96	16.24	0.00	90.86	7.53	1.61
CFU 31F-2 (Unit E)	10475.60	69.83	0.00	30.17	50.71	4.47	0.00	25.70	0.00	0.00	92.00	3.20	4.80
	10477.60	60.42	0.00	39.58	58.25	4.17	0.00	35.42	0.00	0.00	80.69	6.21	13.10
	10482.50	67.70	0.00	32.30	61.41	3.54	0.00	28.76	0.00	0.00	84.31	5.88	9.80
	10484.15	76.07	0.00	23.93	56.39	2.99	0.00	20.94	0.00	0.00	83.71	7.30	8.99
	10486.40	84.03	0.00	15.97	54.84	7.14	0.00	8.82	0.00	0.00	92.50	4.00	3.50
	10493.80	76.92	0.00	23.08	55.40	1.03	3.08	18.97	3.08	0.00	83.33	6.67	10.00
	10495.50	65.63	0.00	34.38	56.14	4.02	1.34	29.02	1.34	0.00	89.80	5.44	4.76
	10498.80	89.11	0.00	10.89	56.11	1.49	0.50	8.91	0.50	0.00	87.22	7.78	5.00
CFU 31F-3 (Unit D)	10431.40	65.04	1.50	33.46	63.03	14.66	15.41	3.38	0.00	15.41	81.50	6.36	12.14
	10432.45	69.40	0.71	29.89	60.17	11.74	15.30	2.85	0.00	15.30	88.21	6.15	5.64
	10436.10	69.66	0.37	29.96	63.42	16.10	11.99	1.87	0.00	11.99	84.41	9.14	6.45
	10439.40	69.42	1.24	29.34	57.62	16.53	11.57	1.24	0.00	11.57	85.71	6.55	7.74
	10442.35	80.58	0.83	18.60	62.37	16.94	0.00	1.65	0.00	0.00	83.08	8.72	8.21
	10447.00	78.04	1.40	20.56	64.46	14.95	3.27	2.34	0.47	2.80	82.04	1.20	16.77
	10451.25	75.12	0.96	23.92	62.02	12.92	8.61	2.39	0.00	8.61	86.62	5.10	8.28
	10452.60	75.36	0.47	24.17	59.60	11.37	7.11	5.69	0.00	7.11	86.79	0.63	12.58
	10455.00	66.52	0.00	33.48	59.26	11.16	0.00	22.32	0.00	0.00	75.84	4.03	20.13
	10458.30	72.86	0.00	27.14	56.00	8.10	0.95	18.10	0.95	0.00	78.43	12.42	9.15
	10459.35	82.93	1.46	15.61	48.58	9.76	0.98	4.88	0.98	0.00	74.12	15.29	10.59
	10463.25	88.78	0.00	11.22	54.67	5.37	0.00	5.85	0.00	0.00	78.02	13.19	8.79
	10465.45	85.59	0.00	14.41	57.51	8.11	0.00	6.31	0.00	0.00	82.11	12.11	5.79
	10466.90	83.55	0.00	16.45	50.77	7.36	2.16	6.93	0.00	2.16	86.01	6.74	7.25
	10467.55	67.13	0.00	32.87	53.87	6.94	9.26	16.67	0.46	8.80	84.83	7.59	7.59
CFU 31 F-3 (Unit E)	10470.35	66.92	0.77	32.31	63.26	8.08	23.08	1.15	1.92	21.15	95.98	1.15	2.87
	10470.90	69.78	0.00	30.22	64.80	8.27	20.14	1.80	0.72	19.42	82.47	5.67	11.86
	10472.45	72.43	0.37	27.21	59.39	8.82	14.71	3.68	2.21	12.50	91.88	4.06	4.06
	10474.00	87.62	0.00	12.38	58.66	4.76	3.81	3.81	0.00	3.81	89.13	4.35	6.52
	10477.00	84.47	0.00	15.53	62.39	5.94	4.57	5.02	0.00	4.57	73.51	9.73	16.76
	10478.20	86.19	0.00	13.81	61.36	2.21	0.00	11.60	0.00	0.00	90.38	3.21	6.41
	10479.50	64.24	0.00	35.76	53.36	3.31	1.32	31.13	1.32	0.00	86.60	3.09	10.31
	10482.55	65.12	0.00	34.88	54.43	6.20	2.33	26.36	2.33	0.00	84.52	3.57	11.90
	10484.60	69.80	0.00	30.20	53.72	1.98	0.50	27.72	0.50	0.00	75.18	8.51	16.31
	10488.30	72.90	0.00	27.10	58.15	5.14	0.47	21.50	0.47	0.00	81.41	5.77	12.82
	10493.30	79.60	0.00	20.40	51.94	4.48	2.49	13.43	2.49	0.00	78.75	3.13	18.13
	10495.30	84.14	0.00	15.86	63.23	4.41	0.00	11.45	0.00	0.00	76.96	5.76	17.28
	10497.25	51.66	0.00	48.34	53.55	5.30	3.97	39.07	3.97	0.00	88.46	2.56	8.97
	10501.35	82.46	0.00	17.54	55.88	1.75	0.00	15.79	0.00	0.00	85.82	3.55	10.64
	10501.60	80.30	0.00	19.70	54.28	3.45	0.00	16.26	0.00	0.00	79.14	4.91	15.95
	10504.95	81.82	0.00	18.18	54.25	4.55	0.51	13.13	0.51	0.00	82.10	4.32	13.58
	10505.55	85.49	0.00	14.51	54.67	2.07	0.52	11.92	0.52	0.00	58.79	10.91	30.30
	10506.65	58.17	0.00	41.83	49.20	3.92	2.61	35.29	2.61	0.00	85.39	2.25	12.36
	10508.10	60.69	0.00	39.31	49.29	3.47	3.47	32.37	3.47	0.00	71.43	7.62	20.95

	Sample	%Grains	%Matrix	%Cem	%Intergr ph	%Over size ph	%Thin sec ph	%Prim macro ph	%Second micro ph	%Moldic ph	%Intragr ph	IGV
CFU 31F-2 (Unit D)	10426.80	56.22	0.00	17.10	10.88	0.00	11.14	10.88	0.26	0.09	0.17	27.98
	10427.00	53.91	2.03	17.97	11.01	0.00	11.30	11.01	0.29	0.10	0.19	31.01
	10429.20	65.80	3.19	9.28	11.01	0.00	11.59	11.01	0.58	0.19	0.39	23.48
	10431.60	62.40	8.80	5.87	11.20	0.00	12.27	11.20	1.07	0.36	0.71	25.87
	10435.15	60.87	10.60	5.98	9.24	0.00	9.78	9.24	0.54	0.18	0.36	25.82
	10442.75	58.97	0.54	13.04	11.41	0.54	13.59	11.59	1.99	0.54	1.09	25.00
	10444.90	52.76	2.62	14.17	11.02	1.05	14.70	11.37	3.32	0.87	1.75	26.51
	10447.35	59.70	2.27	10.58	7.56	2.02	12.59	8.23	4.37	1.01	2.02	20.40
	10448.90	55.38	5.38	8.74	9.42	2.47	15.47	10.24	5.23	1.20	2.39	20.85
	10448.50	53.02	0.00	8.19	19.40	2.16	25.86	20.11	5.75	1.44	2.87	27.59
	10454.00	63.03	4.22	7.94	10.67	0.99	14.64	11.00	3.64	0.99	1.99	21.59
	10454.70	57.58	0.00	6.87	18.48	0.95	22.27	18.80	3.48	0.95	1.90	25.36
	10460.90	54.34	0.00	8.30	24.91	0.75	28.68	25.16	3.52	1.01	2.01	33.21
	10463.00	61.41	0.00	7.47	13.69	0.00	19.50	13.69	5.81	1.94	3.87	21.16
	10467.25	56.50	0.00	6.75	23.50	0.00	27.25	23.50	3.75	1.25	2.50	30.25
	10469.90	63.32	1.17	6.78	13.55	0.00	16.36	13.55	2.80	0.93	1.87	20.33
CFU 31F-2 (Unit E)	10475.60	50.99	0.00	19.83	8.78	0.00	11.61	8.78	2.83	0.94	1.89	28.61
	10477.60	59.95	0.00	9.22	21.84	0.00	25.97	21.84	4.13	1.38	2.75	31.07
	10482.50	61.41	0.00	10.87	13.59	0.00	18.48	13.59	4.89	1.63	3.26	24.46
	10484.15	56.39	0.00	9.40	24.10	0.48	28.92	24.26	4.66	1.45	2.89	33.49
	10486.40	57.14	0.00	9.45	16.13	0.46	23.04	16.28	6.76	2.15	4.30	25.58
	10493.80	55.68	0.00	11.93	18.18	1.14	25.57	18.56	7.01	2.08	4.17	30.11
	10495.50	56.64	0.00	9.27	20.55	3.01	28.07	21.55	6.52	1.50	3.01	29.82
	10498.80	56.39	0.00	8.06	17.22	2.22	23.89	17.96	5.93	1.48	2.96	25.28
CFU 31F-3 (Unit D)	10431.40	64.45	13.27	8.06	6.64	0.00	7.58	6.64	0.95	0.32	0.63	27.96
	10432.45	60.17	10.28	10.28	10.71	0.00	11.13	10.71	0.43	0.14	0.29	31.26
	10436.10	63.90	7.13	7.84	12.83	0.00	13.78	12.83	0.95	0.32	0.63	27.79
	10439.40	57.86	2.86	9.05	12.86	6.19	21.43	14.92	6.51	0.79	1.59	24.76
	10442.35	62.89	5.67	11.34	9.79	0.00	11.34	9.79	1.55	0.52	1.03	26.80
	10447.00	64.46	0.00	10.54	10.24	0.00	12.65	10.24	2.41	0.80	1.61	20.78
	10451.25	62.02	0.00	9.20	12.46	0.00	15.43	12.46	2.97	0.99	1.98	21.66
	10452.60	59.60	1.13	9.89	10.73	0.56	15.82	10.92	4.90	1.51	3.01	20.90
	10455.00	59.26	0.79	7.94	20.63	0.00	24.34	20.63	3.70	1.23	2.47	28.57
	10458.30	56.27	0.80	8.80	16.53	0.00	22.93	16.53	6.40	2.13	4.27	25.33
	10459.35	48.58	0.71	10.66	18.96	4.27	29.38	20.38	9.00	2.05	4.11	29.62
	10463.25	54.67	3.20	11.20	14.40	1.60	20.27	14.93	5.33	1.42	2.84	25.60
	10465.45	58.29	0.00	13.99	13.47	1.81	19.69	14.08	5.61	1.47	2.94	27.46
	10466.90	50.77	0.00	12.31	22.42	0.00	29.01	22.42	6.59	2.20	4.40	34.73
	10467.55	54.11	0.00	19.20	8.23	0.00	12.22	8.23	3.99	1.33	2.66	27.43
CFU 31 F-3 (Unit E)	10470.35	64.96	0.00	19.46	4.87	0.00	5.84	4.87	0.97	0.32	0.65	24.33
	10470.90	65.50	4.66	13.29	7.69	0.00	9.09	7.69	1.40	0.47	0.93	23.08
	10472.45	59.61	0.00	9.17	23.14	0.00	25.76	23.14	2.62	0.87	1.75	32.31
	10474.00	59.22	3.35	7.26	15.64	0.00	19.83	15.64	4.19	1.40	2.79	22.91
	10477.00	63.53	0.00	7.12	16.52	0.00	18.23	16.52	1.71	0.57	1.14	23.65
	10478.20	61.36	6.44	11.53	6.78	0.00	10.85	6.78	4.07	1.36	2.71	20.68
	10479.50	53.36	0.00	20.49	9.54	0.00	15.55	9.54	6.01	2.00	4.00	30.04
	10482.55	54.43	0.00	17.72	14.35	0.00	19.41	14.35	5.06	1.69	3.38	32.07
	10484.60	53.99	0.00	8.24	23.94	1.60	30.85	24.47	6.38	1.77	3.55	32.18
	10488.30	58.15	0.00	9.24	16.30	1.63	25.00	16.85	8.15	2.36	4.71	25.54
	10493.30	52.71	0.00	9.30	24.29	0.00	30.49	24.29	6.20	2.07	4.13	33.59
	10495.30	63.51	0.00	7.80	15.04	0.56	18.38	15.23	3.16	0.93	1.86	22.84
	10497.25	53.55	0.00	15.25	13.48	0.00	16.31	13.48	2.84	0.95	1.89	28.72
	10501.35	55.88	0.00	9.80	17.65	0.00	23.53	17.65	5.88	1.96	3.92	27.45
	10501.60	54.28	0.00	9.89	22.99	0.00	28.34	22.99	5.35	1.78	3.57	32.89
	10504.95	54.25	0.00	10.41	22.74	0.00	26.03	22.74	3.29	1.10	2.19	33.15
	10505.55	54.67	0.00	11.33	18.13	0.00	22.66	18.13	4.53	1.51	3.02	29.46
	10506.65	49.20	0.00	15.11	20.26	0.00	26.69	20.26	6.43	2.14	4.29	35.37
	10508.10	49.57	0.00	15.10	19.37	0.00	26.21	19.37	6.84	2.28	4.56	34.47

	Sample	%Ductile gr	%Chl coat	%Chl rep	%TiO2 cem	%TiO2 rep	%Qtz cem	%Carb cem	%Carb rep	%Anker cem	%Anker rep	%Sider cem	%Kaolin cem
CFU 31F-2 (Unit D)	10426.80	0.00	2.07	9.84	0.00	3.37	9.59	5.44	0.00	0.00	0.00	5.44	0.00
	10427.00	0.00	2.61	10.72	0.00	2.03	10.72	4.06	0.00	0.00	0.00	4.06	0.29
	10429.20	1.45	2.32	7.25	0.00	2.32	6.38	0.00	0.00	0.00	0.00	0.00	0.58
	10431.60	3.20	3.47	6.93	0.00	3.73	1.60	0.00	0.00	0.00	0.00	0.00	0.80
	10435.15	2.99	4.62	8.15	0.00	3.80	1.36	0.00	0.00	0.00	0.00	0.00	0.00
	10442.75	0.00	2.17	7.34	0.00	4.62	10.60	0.00	0.00	0.00	0.00	0.00	0.27
	10444.90	0.52	1.84	8.66	0.00	3.15	12.34	0.00	0.00	0.00	0.00	0.00	0.00
	10447.35	1.26	3.02	7.81	0.00	5.79	7.56	0.00	0.00	0.00	0.00	0.00	0.00
	10448.90	1.35	5.16	8.30	0.00	4.48	3.36	0.00	0.00	0.00	0.00	0.00	0.00
	10448.50	0.22	5.39	6.90	0.00	3.66	2.80	0.00	0.00	0.00	0.00	0.00	0.00
	10454.00	0.00	5.46	4.22	0.00	4.47	2.48	0.00	0.00	0.00	0.00	0.00	0.00
	10454.70	1.42	4.74	4.27	0.00	7.35	1.66	0.00	0.00	0.00	0.00	0.00	0.00
	10460.90	4.53	8.30	4.91	0.00	3.02	0.00	0.00	0.00	0.00	0.00	0.00	0.00
	10463.00	1.24	7.47	3.32	0.00	8.30	0.00	0.00	0.00	0.00	0.00	0.00	0.00
	10467.25	0.75	6.50	3.75	0.00	5.75	0.00	0.00	0.00	0.00	0.00	0.00	0.00
	10469.90	10.28	6.78	5.37	0.00	4.21	0.00	0.00	0.00	0.00	0.00	0.00	0.00
CFU 31F-2 (Unit E)	10475.60	0.00	8.22	1.98	0.00	7.93	0.00	11.61	7.65	11.61	7.65	0.00	0.00
	10477.60	0.00	9.22	2.43	0.00	2.43	0.00	0.00	0.00	0.00	0.00	0.00	0.00
	10482.50	0.00	10.87	4.35	0.00	4.89	0.00	0.00	0.00	0.00	0.00	0.00	0.00
	10484.15	0.00	9.40	4.10	0.00	1.20	0.00	0.00	0.00	0.00	0.00	0.00	0.00
	10486.40	0.23	9.45	3.69	0.00	6.45	0.00	0.00	0.00	0.00	0.00	0.00	0.00
	10493.80	1.70	11.36	2.84	0.00	3.69	0.00	0.57	0.28	0.57	0.28	0.00	0.00
	10495.50	1.00	7.27	2.51	0.00	3.01	0.00	2.01	0.50	2.01	0.50	0.00	0.00
	10498.80	0.28	6.94	3.89	0.00	7.22	0.00	1.11	0.56	1.11	0.56	0.00	0.00
CFU 31F-3 (Unit D)	10431.40	10.43	3.55	4.74	1.18	0.47	3.32	0.00	0.00	0.00	0.00	0.00	0.00
	10432.45	9.21	2.57	5.35	2.36	2.36	2.78	1.71	0.00	0.00	0.00	1.71	0.21
	10436.10	7.84	3.33	5.23	0.24	1.43	3.56	0.00	0.00	0.00	0.00	0.00	0.48
	10439.40	6.67	4.05	4.76	0.24	2.14	4.52	0.00	0.00	0.00	0.00	0.00	0.24
	10442.35	0.52	5.15	5.93	2.84	1.80	2.84	0.00	0.00	0.00	0.00	0.00	0.52
	10447.00	2.11	2.71	6.02	0.00	3.01	7.83	0.00	0.00	0.00	0.00	0.00	0.00
	10451.25	5.34	2.67	6.82	0.00	3.86	6.53	0.00	0.00	0.00	0.00	0.00	0.00
	10452.60	4.24	5.37	5.65	0.00	5.37	4.52	0.00	0.00	0.00	0.00	0.00	0.00
	10455.00	0.00	7.94	5.56	0.00	2.12	0.00	0.00	0.00	0.00	0.00	0.00	0.00
	10458.30	0.53	8.80	5.33	0.00	5.87	0.00	0.00	0.00	0.00	0.00	0.00	0.00
	10459.35	0.47	10.66	4.27	0.00	6.40	0.00	0.00	0.00	0.00	0.00	0.00	0.00
	10463.25	0.00	10.67	4.80	0.53	5.87	0.00	0.00	0.00	0.00	0.00	0.00	0.00
	10465.45	0.26	11.14	4.92	2.85	3.11	0.00	0.00	0.00	0.00	0.00	0.00	0.00
	10466.90	1.10	10.99	3.96	0.00	2.86	0.00	0.00	0.00	0.00	0.00	0.00	0.00
	10467.55	5.24	9.98	5.49	0.00	2.74	0.00	9.23	5.74	9.23	5.74	0.00	0.00
CFU 31 F-3 (Unit E)	10470.35	14.60	3.65	3.65	0.00	3.16	7.54	8.27	0.97	8.27	0.97	0.00	0.00
	10470.90	13.05	3.96	3.73	0.00	3.03	6.29	3.03	0.70	3.03	0.70	0.00	0.00
	10472.45	8.73	5.68	2.84	0.00	2.62	3.06	0.00	0.00	0.00	0.00	0.00	0.00
	10474.00	2.51	5.03	6.42	0.00	3.63	1.96	0.00	0.00	0.00	0.00	0.00	0.00
	10477.00	2.85	5.70	4.84	0.00	6.27	1.42	0.00	0.00	0.00	0.00	0.00	0.00
	10478.20	0.00	7.80	3.73	1.02	6.10	0.00	2.37	0.00	2.37	0.00	0.00	0.00
	10479.50	0.71	9.89	2.12	0.00	3.18	0.00	10.60	5.30	10.60	5.30	0.00	0.00
	10482.55	1.27	11.39	5.91	0.00	0.42	0.00	6.33	2.11	6.33	2.11	0.00	0.00
	10484.60	0.27	8.24	3.99	0.00	2.93	0.00	0.00	0.00	0.00	0.00	0.00	0.00
	10488.30	0.27	8.97	3.80	0.27	3.80	0.00	0.00	0.00	0.00	0.00	0.00	0.00
	10493.30	1.29	9.04	3.10	0.00	4.39	0.00	0.26	0.00	0.26	0.00	0.00	0.00
	10495.30	0.00	6.96	4.46	0.00	5.01	0.00	0.84	0.84	0.84	0.84	0.00	0.00
	10497.25	2.13	7.09	6.03	0.00	5.32	0.00	8.16	3.55	8.16	3.55	0.00	0.00
	10501.35	0.00	9.80	5.88	0.00	4.90	0.00	0.00	0.00	0.00	0.00	0.00	0.00
	10501.60	0.00	8.56	3.48	0.00	3.74	0.00	1.34	0.27	1.34	0.27	0.00	0.00
	10504.95	0.27	8.22	3.84	0.00	5.48	0.00	2.19	0.00	2.19	0.00	0.00	0.00
	10505.55	0.28	9.92	4.82	0.00	6.52	0.00	1.42	0.00	1.42	0.00	0.00	0.00
	10506.65	1.29	10.29	5.14	0.00	3.22	0.00	4.82	0.64	4.82	0.64	0.00	0.00
	10508.10	1.71	10.26	3.99	0.00	3.99	0.00	4.84	0.85	4.84	0.85	0.00	0.00

	Sample	%Kaolin rep	%Pyrite cem	%Pyrite repl	%Acces min	%Rf restored	%Felds restored	%Qtz restored	COPL	CEPL	I comp
CFU 31F-2 (Unit D)	10426.80	1.81	0.00	0.52	0.00	30.15	6.26	63.59	16.69	14.24	0.54
	10427.00	2.03	0.29	0.00	0.87	30.89	5.71	63.39	13.03	15.63	0.45
	10429.20	0.58	0.00	0.00	0.00	32.41	2.96	64.63	21.59	7.27	0.75
	10431.60	0.00	0.00	0.00	1.07	34.17	1.50	64.33	19.06	4.75	0.80
	10435.15	0.00	0.00	0.82	1.90	33.85	1.50	64.65	19.12	4.84	0.80
	10442.75	1.63	0.00	0.27	0.00	29.59	4.23	66.17	20.00	10.43	0.66
	10444.90	3.94	0.00	0.00	0.00	29.72	7.78	62.50	18.36	11.57	0.61
	10447.35	1.26	0.00	0.00	0.50	38.87	4.28	56.85	24.62	7.97	0.76
	10448.90	1.79	0.22	0.45	0.22	37.13	5.07	57.81	24.19	6.63	0.78
	10448.50	2.37	0.00	0.00	0.00	31.00	5.81	63.19	17.14	6.79	0.72
	10454.00	1.49	0.00	0.00	0.25	28.62	3.71	67.67	23.48	6.08	0.79
	10454.70	1.66	0.47	0.00	0.24	28.34	4.30	67.36	19.62	5.52	0.78
	10460.90	0.75	0.00	0.00	0.38	56.55	3.21	40.24	10.17	7.46	0.58
	10463.00	0.00	0.00	0.00	0.00	36.32	1.50	62.18	23.89	5.68	0.81
	10467.25	0.00	0.25	0.00	2.25	27.69	1.50	70.81	13.98	5.81	0.71
	10469.90	2.80	0.00	0.00	0.00	44.46	3.98	51.56	24.69	5.10	0.83
CFU 31F-2 (Unit E)	10475.60	0.00	0.00	0.00	0.28	47.47	4.05	48.49	15.95	16.67	0.49
	10477.60	0.00	0.00	0.00	1.70	50.56	1.50	47.94	12.96	8.03	0.62
	10482.50	0.00	0.00	0.00	0.00	48.43	1.50	50.07	20.58	8.63	0.70
	10484.15	0.00	0.00	0.00	0.00	35.73	1.66	62.61	9.78	8.48	0.54
	10486.40	0.00	0.00	0.23	2.30	34.71	1.65	63.64	19.38	7.62	0.72
	10493.80	0.00	0.00	0.00	0.28	38.33	1.97	59.69	14.15	10.24	0.58
	10495.50	0.00	0.00	0.00	0.50	47.57	2.67	49.76	14.50	7.93	0.65
	10498.80	0.00	0.00	0.00	0.28	29.37	2.43	68.20	19.70	6.47	0.75
CFU 31F-3 (Unit D)	10431.40	0.00	0.00	1.42	1.42	41.62	3.00	55.38	16.71	6.71	0.71
	10432.45	0.21	0.64	0.21	0.00	40.03	2.43	57.54	12.71	8.97	0.59
	10436.10	0.48	0.24	0.24	0.48	38.18	1.31	60.51	16.91	6.51	0.72
	10439.40	1.67	0.00	0.24	0.24	42.69	6.47	50.84	20.25	7.22	0.74
	10442.35	0.77	0.00	0.26	0.52	29.87	3.10	67.03	18.03	9.30	0.66
	10447.00	3.31	0.00	0.00	0.00	34.01	6.22	59.78	24.26	7.98	0.75
	10451.25	2.67	0.00	0.00	0.00	38.68	4.46	56.86	23.41	7.05	0.77
	10452.60	2.54	0.00	0.00	0.00	41.54	4.44	54.03	24.14	7.50	0.76
	10455.00	0.00	0.00	0.00	0.00	46.86	1.50	51.64	16.00	6.67	0.71
	10458.30	0.00	0.00	0.00	0.27	46.74	1.50	51.76	19.64	7.07	0.74
	10459.35	0.00	0.00	0.00	0.00	33.92	2.93	63.14	14.75	9.09	0.62
	10463.25	0.00	0.00	0.00	0.00	29.70	2.79	67.51	19.35	9.03	0.68
	10465.45	0.00	0.00	0.00	0.78	29.57	2.19	68.24	17.29	11.57	0.60
	10466.90	0.00	1.32	1.10	0.00	30.36	0.38	69.26	8.08	11.31	0.42
	10467.55	0.00	0.00	0.50	0.25	49.00	3.41	47.59	17.32	15.88	0.52
CFU 31 F-3 (Unit E)	10470.35	1.95	0.00	0.00	1.70	40.45	3.07	56.48	20.71	15.43	0.57
	10470.90	0.00	0.00	0.00	0.70	40.61	1.73	57.66	22.00	10.36	0.68
	10472.45	0.00	0.44	0.00	0.22	36.15	1.02	62.83	11.35	8.13	0.58
	10474.00	0.00	0.28	0.28	0.56	28.63	1.50	69.87	22.17	5.65	0.80
	10477.00	0.00	0.00	0.00	1.14	30.35	1.50	68.15	21.42	5.60	0.79
	10478.20	0.00	0.34	0.00	0.00	28.69	0.74	70.57	24.36	8.72	0.74
	10479.50	0.00	0.00	0.00	0.00	50.84	3.27	45.90	14.24	17.58	0.45
	10482.55	0.00	0.00	0.00	0.00	48.98	2.20	48.82	11.68	15.65	0.43
	10484.60	0.00	0.00	0.00	0.27	44.96	2.03	53.00	11.53	7.29	0.61
	10488.30	0.00	0.00	0.00	0.00	43.88	1.71	54.41	19.42	7.45	0.72
	10493.30	0.00	0.00	0.00	0.78	34.27	0.13	65.59	9.65	8.40	0.53
	10495.30	0.00	0.00	0.00	0.28	32.30	3.26	64.44	22.24	6.06	0.79
	10497.25	0.00	0.00	0.00	0.00	65.71	2.68	31.61	15.82	12.84	0.55
	10501.35	0.00	0.00	0.00	0.00	36.21	1.50	62.29	17.30	8.11	0.68
	10501.60	0.00	0.00	0.00	0.00	34.36	1.59	64.05	10.60	8.84	0.55
	10504.95	0.00	0.00	0.00	0.00	32.78	1.50	65.72	10.25	9.34	0.52
	10505.55	0.00	0.00	0.00	0.00	32.37	1.50	66.13	14.94	9.64	0.61
	10506.65	0.00	0.00	0.00	0.00	58.84	1.71	39.45	7.16	14.03	0.34
	10508.10	0.00	0.00	0.28	0.28	56.41	1.78	41.81	8.43	13.83	0.38

Appendix IV: Textural parameters including mean grain size and sorting values for the 57 studied thin sections from Wells CFU 31F-2 and CFU 31F-3.

Sample	Mean grain size	Trask 25	Trask75	Sorting (Trask)
10508.10	559.47	365.69	615.16	1.68
10506.65	434.59	277.28	521.62	1.88
10505.55	449.13	325.37	548.57	1.69
10504.95	378.98	263.16	486.32	1.85
10501.35	357.43	261.53	435.32	1.66
10497.25	455.06	270.19	492.71	1.82
10495.30	389.53	319.79	450.35	1.41
10493.30	367.93	277.75	432.64	1.56
10488.30	350.34	251.60	431.74	1.72
10484.60	366.67	284.09	420.38	1.48
10482.55	477.71	295.70	574.06	1.94
10479.50	414.50	319.09	471.00	1.48
10478.20	342.03	214.15	422.51	1.97
10477.00	244.03	182.47	273.87	1.50
10474.00	244.52	182.12	284.99	1.56
10472.45	133.60	102.74	162.05	1.58
10470.35	139.91	108.49	166.69	1.54
10470.90	117.33	84.30	136.83	1.62
10467.55	329.30	247.28	391.01	1.58
10466.90	299.51	250.17	352.97	1.41
10465.45	212.81	155.91	247.12	1.59
10463.25	330.14	262.07	370.65	1.41
10459.35	323.75	215.30	408.53	1.90
10458.30	346.10	247.62	428.09	1.73
10455.00	382.66	296.20	456.84	1.54
10454.00	237.78	199.09	286.06	1.44
10451.25	165.18	107.90	215.90	2.00
10447.00	178.07	132.90	215.25	1.62
10442.35	141.38	112.08	168.51	1.50
10439.40	121.34	92.85	142.43	1.53
10436.10	99.06	78.58	116.91	1.49
10432.45	93.85	67.03	113.36	1.69
10431.40	97.56	74.44	113.21	1.52
10498.80	350.35	284.45	412.61	1.45
10495.50	262.88	199.21	328.73	1.65
10493.80	361.11	265.10	420.94	1.59
10486.40	235.55	192.89	268.09	1.39
10484.15	391.44	285.36	466.51	1.63
10482.50	305.47	206.40	344.56	1.67
10477.60	401.60	305.93	435.07	1.42
10475.60	360.36	239.31	455.69	1.90
10469.90	435.42	287.53	504.69	1.76
10467.25	287.09	227.28	341.70	1.50
10463.00	365.27	299.75	429.32	1.43
10460.90	264.11	197.75	315.82	1.60
10454.70	257.97	189.91	314.54	1.66
10454.00	287.75	196.51	352.56	1.79
10448.50	412.83	323.00	493.97	1.53
10448.90	310.46	234.37	372.55	1.59
10447.35	304.71	213.84	403.27	1.89
10444.90	216.48	172.46	259.71	1.51
10442.75	202.26	153.15	239.17	1.56
10435.15	107.50	74.13	131.08	1.77
10431.60	106.16	82.05	130.83	1.59
10429.20	134.48	103.38	164.04	1.59
10427.00	153.22	111.19	187.32	1.68
10426.80	140.88	107.43	175.43	1.63

References

Aagaard, P., Jahren, J., S., Harstad, A., O., Nilsen, O., and Ramm, M., 2000, Formation of grain-coating chlorite in sandstones. Laboratory synthesized vs. natural occurrences, Clay Minerals 35, p. 261–269.

Aguirre, O., Antelo, R., and Andina S., A. (Repsol YPF), 2001, Log Normalization, a Very Important Task in the Petrophysical Evaluation for La Peña and Tundy Fields, Society of Petroleum Engineers, SPE Latin American and Caribbean Petroleum Engineering Conference, 25-28 March, Buenos Aires, Argentina; ISBN: 978-1-55563-926-6.

Ahlbrandt, T., S., 1999, Conventional natural gas provinces of the world: American Association of Petroleum Geologists International Conference and Exhibition, p. 2–5.

Ahn, J., H., and Peacor, D., R., 1985, Transmission electron microscopic study of diagenetic chlorite in Gulf Coast argillaceous sediments, Clays and Clay Minerals, v. 33, p. 228–237.

Ajdukiewicz, J., M., and Lander, R., H., 2010, Sandstone reservoir quality prediction: The state of the art: American Association of Petroleum Geologists Bulletin, v. 94, no. 8, p. 1083–1091.

Ajdukiewicz J., M., and Larese, R., E., 2012, How clay grain coats inhibit quartz cement and preserve porosity in deeply buried sandstones: Observations and experiments, American Association of Petroleum Geologists Bulletin, v. 96, no. 11 (November), p. 2091–2119.

Ajdukiewicz, J., M., Paxton, S., T., and Szabo, J., O., 1991, Deep porosity preservation in the Norphlet Formation, Mobile Bay, Alabama (abs.): American Association of Petroleum Geologists Bulletin, v. 75, p. 533.

Allen, G., P., and Posamentier, H., W., 1993, Sequence stratigraphy and facies model of an incised valley fill: the Gironde Estuary, France: Journal of Sedimentary Petrology, v. 63, p. 378–391.

Al-Ramadan, K., Morad, S., Proust, J., N., and Al-Aasm, I., S., 2005, Distribution of diagenetic alterations in siliciclastic shoreface deposits within a sequence

stratigraphic framework: evidence from the upper Jurassic, Boulonnais, NW France. Journal of Sedimentary Research, v. 75, p. 943–959.

Anderson, J., B., Rodriguez, A., Abdulah, K., C., Fillon, R., H., Banfield, L., A., Mckeown, H., A., and Wellner, J., S., 2004, Late Quaternary stratigraphic evolution of the northern Gulf of Mexico margin: a synthesis, in Anderson, J.B., and Fillon, R.H., eds., Late Quaternary Stratigraphic Evolution of the Northern Gulf of Mexico Margin: SEPM, Special Publication 79, p. 1–23.

Anjos, S., M,. C., De Ros, L,. F. and Silva, C., M., A., 2003, Chlorite authigenesis and porosity preservation in the Upper Cretaceous marine sandstones of the Santos Basin, offshore eastern Brazil: International Association of Sedimentology Special Publication 34, p. 291–316.

Annerston H., 1968. A mineral chemical study of a metamorphosed iron formation in northern Sweden, Lithos 1:374-397.

Atkins, J., E. and McBride, E., F., 1992, Porosity and packing of Holocene river, dune and beach sands: American Association of Petroleum Geologists Bulletin, v. 76, p.339-355.

Bailey, S., W., 1988a, Odinite, a new dioctahedral-trioctahedral Fe^{3+}-rich 1:1 clay mineral. Clay Minerals, 23, 237–247.

Bailey, S., W., 1988b, Chlorites: structures and crystal chemistry. In S.W. Bailey, Ed., Hydrous Phyllosilicates (Exclusive of Micas), 19, 347–403, Reviews in Mineralogy, Mineralogical Society of America, Washington, D.C.

Baker, J., C., Havord, P., J., Martin, K., R., and Ghori, K., A., R., 2000, Diagenesis and petrophysics of the early Permian Moogooloo Sandstone, Southern Carnarvon basin,Western Australia. American Association of Petroleum Geologists Bulletin v. 84, p. 250–265.

Barrell, K., A., 1997, Sequence Stratigraphy and Structural Trap Styles of the Tuscaloosa Trend, Gulf Coast Association of Geological Societies Transactions, v. 47, p.27-34.

Beaufort, D., Cassagnabere A., Petit, S., Lanson, B., Berger, G., Lacharpagne, J., C., and Johansen, H., 1998, Kaolinite-to-dickite conversion series in sandstone reservoirs. Clay Minerals, 33, p. 297–316.

Berg, O., R., 1982, Seismic Detection and Evaluation Delta and Turbidite Sequences: Their Application to Exploration for the Subtle Trap: American Association of Petroleum Geologists Bulletin v. 66, no. 9, p. 1271–1288.

Berger, G. and Beaufort, D., 2003, Chlorites: occurrence, genesis and crystal chemistry _ introduction, Clay Minerals, 38, p. 279–280.

Berger, A., Gier, S., and Krois, P., 2009, Porosity-preserving chlorite cements in shallow-marine volcaniclastic sandstones: Evidence from Cretaceous sandstones of the Sawan gas field, Pakistan, American Association of Petroleum Geologists Bulletin, v. 93, p. 595–615, doi:10.1306/01300908096.

Bettison-Varga, L., and MacKinnon, I., D., R., 1997, The role of randomly mixed-layered chlorite/smectite in the transformation of smectite to chlorite: Clays and Clay Minerals, August, v. 45, p. 506–516.

Billault, V., Beaufort, D., Baronnet A., and Lacharpagne, J., C., 2003, A nanopetrographic and textural study of grain-coating chlorites in sandstone reservoirs, Clay Minerals, v. 38, p. 315–328.

Bjørlykke, K., O., and Egeberg, P., K., 1993, Quartz cementation in sedimentary basins: American Association of Petroleum Geologists Bulletin, v. 77, no. 9, p. 1538–1548.

Blache-Fraser, G., and Neep, J., 2004, Increasing seismic resolution using spectral blueing and colored inversion: Cannonball field, Trinidad: 74th Annual International Meeting, SEG, Expanded Abstracts, p. 1794–1797.

Blakey, R. C., 2011, North American paleogeographic map, late Cretaceous (85 Ma), <http://cpgeosystems.com/namK85.jpg> Accessed November 11, 2011.

Bloch, S., 1991, Empirical prediction of porosity and permeability in sandstones: American Association of Petroleum Geologists Bulletin, v. 75, p. 1145–1160.

Bloch, S., Lander, R. H., and Bonnell, L. M., 2002, Anomalously high porosity and permeability in deeply buried sandstone reservoirs: Origin and predictability: American Association of Petroleum Geologists Bulletin, v. 86, p. 301–328.

Blum, M., D., 1992, Climatic and eustatic controls on Gulf coastal plain sedimentation: An example from the late Quaternary of the Colorado River, in Armentrout, J. M., and Perkins, R.F., eds., Sequence Stratigraphy as an Exploration Tool: Concepts and Practices in the Gulf Coast, Eleventh Annual Research Conference: Houston, Gulf Coast Section, Society of Economic Paleontologists and Mineralogists Foundation, p. 71–84.

Bornhauser, M., 1966, Marine unconformities in the northwestern gulf coast: Gulf Coast Association of Geological Societies Transactions, v. 16, p. 45–51.

Brigatti, M., E., Poppi, L., Fabbri, A., 1991, Corrensites: genetic relationships assessed by multivariate statistical analysis: Bull Mineral 109, p. 543–553.

Brown, L., F., and Fisher, W., L., 1977, Seismic-stratigraphic interpretation of depositional systems: examples from Brazilian rift and pull-apart basins: American Association of Petroleum Geologists Memoir 26, p. 213–248.

Brown, L., F., and Fisher, W., L., 1980, Seismic-Stratigraphic Interpretation of Depositional Systems and its Role in Petroleum Exploration (Part 1 and 2), in Seismic Stratigraphic Interpretation and Petroleum Exploration, Course Notes, 125 p.

Buffler, R., T., 1991, Early evolution of the Gulf of Mexico basin, in D. Goldthwaite, ed. An Introduction to Central Gulf Coast Geology: New Orleans, New Orleans Geological Society, p. 1–15.

Bunge, R., J., 2011, Woodbine Formation Sandstone Reservoir Prediction and Variability, Polk and Tyler Counties, Texas, Search and Discovery Article #10331 (2011). Posted June 25, 2011, Minor adaptation from an article by the author, with the same title, in GCAGS Transactions, 2007, v. 57, p. 77–98.

Burley, S., D., Kantorowicz, J., D., and Waugh, B., 1985, Clastic diagenesis. In: Brenchley, P.J. and Williams, B.P.J., Sedimentology: Recent developments and applied aspects, Geological Society, London, Special Publication, 18, pp. 198–226.

Burruss, R., 2004, Geologic Sequestration of Carbon Dioxide in the Next 10 to 50 Years: An Energy Resource Perspective, Prepared for The 10-50 Solution: Technologies and Policies for a Low-Carbon Future, Pew Center on Global Climate Change and the National Commission on Energy Policy, March 25-26, Washington, DC.

Cameron, C., P., Patrick, D., M., and Keith, C., D., 1992, Authigenic Clay Mineral Distribution, Lower Tuscaloosa Formation, Southwest Mississippi: Impact on Sandstone Reservoir Quality in the North Hustler Field Area, Gulf Coast Association of Geological Societies Transactions, v. 42, p. 47–59.

Chasteen, H., R., 1983, Reevaluation of the Lower Tuscaloosa Dantzler Formations (Mid-Cretaceous) with emphasis on depositional environments and time-stratigraphic relationships: Gulf Coast Association of Geological Societies Transactions, v. 33, p. 31–39.

Childs, O., E., Steele, G., and Salvador, A., 1988, Correlation of stratigraphic units of North America (COSUNA) project, Gulf Coast region: American Association of Petroleum Geologists, oversize chart.

Corcoran, M., K., Cameron, C., P., and Meylan, M., A., 1993, The Lower Tuscaloosa Formation in the Greensburg Field and Joseph Branch Field areas, St. Helena Parish, Louisiana, Gulf Coast Association of Geological Societies Transactions, v. 43, p. 87–96.

Croize, D., Ehrenberg, S., N., Bjorlykke, K., Renard, F., and Jahren, J., 2009, Petrophysical properties of bioclastic platform carbonates: Implications for porosity controls during burial, Marine and Petroleum Geology, doi: 10.1016/j.marpetgeo.2009.11.008.

Curtis, C., D., 1977, Sedimentary geochemistry: Environments and processes dominated by involvement of an aqueous phase. Philosophical Transactions of the Royal Society 286, pp. 272–353.

Dalrymple, R,. W., Boyd, R., and Zaitlin, B., A., 1994, Incised-Valley Systems: Origin and Sedimentary Sequences: SEPM, Special Publication 51, 391 p.

Deer, W., A., Howie, R., A., and Zussrnan, J., 1992, An introduction to the rock-forming minerals, 2nd ed. New York: John Wiley. 696 p.

De Hon, R., A., Paul A., Washington, Lloyd N. Glawe, Leonard M. Young, Eric A. Morehead, 2001, Formation of Northern Louisiana Ironstones; Gulf Coast Association of Geological Societies Transactions, v. 51, p. 55–61.

Denbury Resources Inc., Annual report, 2009, Branching Out; 5100 Tennyson PkwySuite 1200 Plano, Texas 75024T: 972.673.2000, www.denbury.com, 162 p., http://www.denbury.com/index.php?id=13.

De Ros, L., F., Anjos, S., M., C., and Morad, S., 1994, Authigenesis of amphibole and its relationship to the diagenetic evolution of Lower Cretaceous sandstones of the Potiguar rift basin, northeastern Brazil: Sedimentary Geology, v. 88, p. 253–266, doi:10.1016/0037-0738(94) 90065-5.

Devery, D., M., 1980, The Lower Tuscaloosa of southern Mississippi: Mississippi Geology, v. 1, p. 6-7, 12.

Dickas, A., B., 1962, A regional stratigraphic study of the Tuscaloosa Group and associated Upper Cretaceous rocks of the central Mississippi Embayment [unpublished Ph. D. dissertation]: Michigan State University, 157 p.

Dickson, W., W., and Milliken, K., L., 1995, The Diagenetic Role of Brittle Deformation in Compaction and Pressure Solution, Etjo Sandstone, Namibia. Journal of Geology, v. 103, p. 339–347.

Dobson, L., M., 1990, Seismic stratigraphy and geologic history of Jurassic rocks, northeastern Gulf of Mexico: Unpublished Master's Thesis, The University of Texas, Austin, 165 p.

Dorn, G., 2013, Domain transform: A tool for imaging and interpreting geomorphology and stratigraphy in seismic volumes. The Leading Edge, 32(2), 146–153. doi: 10.1190/tle32020146.1

Dowey, P., J., Hodgson, D., M., Worden, R., H., 2012, Pre-requisites, processes, and prediction of chlorite grain coatings in petroleum reservoirs: A review of subsurface examples, Marine and Petroleum Geology, v. 32, p. 63-75.

Drennen, C., W., 1953, Reclassification of outcropping Tuscaloosa group in Alabama: American Association of Petroleum Geologists Bulletin, v. 37, p. 522-538.

Dubiel, R., F., 2002, Sequence stratigraphy of shelf to deep water depositional systems in the Tuscaloosa Woodbine down-dip trend, Louisiana and Texas; application to exploration for deep gas: Gulf Coast Association of Geological Societies Transactions, v. 52, p. 181-181.

Dubiel, R., F., and Pitman, J., K., 2004, Shelf Margin Complex in the Downdip Tuscaloosa-Woodbine Trend and Implications for the Assessment of Conventional Gas Resources, American Association of Petroleum Geologists Search and Discovery Article #90032.

Dubiel, R., F., Pitman, J., K., and Steinshouer, D., 2003, Seismic sequence stratigraphy and petroleum system modeling of the downdip Tuscaloosa-Woodbine, Louisiana and Texas, in G. Stone, J.Wrenn, and S. Bentley, eds., Gulf Coast Association of Geological Societies/Gulf Coast Section SEPM Transactions, 53rd Annual Convention, v. 53, p. 193–203.

Dunn, T., L., 1993, Early quartz grain fracturing and annealing: an important brittle deformation mechanism of early compaction in first cycle orogenic sandstones revealed by scanned cathodoluminescence microscopy (abstract): Geological Society of America, Abstracts with Programs, v. 25, p. 65.

Eggleton, R., A., and Banfield, J., E., 1985, The alteration of granitic biotite to chlorite. American Mineralogist, v. 70, p. 902–910.

Ehrenberg, S., N., 1993, Preservation of anomalously high porosity in deep buried sandstones by grain-coating: Example from the Norwegian Continental Shelf, American Association of Petroleum Geologists Bulletin, v. 77, p. 1260–1286.

Ehrenberg, S., N., 1995, Measuring sandstone compaction from modal analyses of thin-sections: how to do it and what the results mean: Journal of Sedimentary Research, v. A65, p. 369–379.

Ehrenberg, S., N., Aagaard, P., Wilson, M., J., Fraser, A., R., Duthie, D., M., L., 1993, Depth dependent transformation of kaolinite to dickite in sandstones of the Norwegian continental shelf, Clay Minerals 28, p. 325–352.

El-Ghali, M., A., K., Tajori, K., G., Mansurbeg, H., 2006a, The influence of transgression and regression on the spatial and temporal distribution of diagenetic kaolin in the Upper Ordovician glaciogenic sandstones within a sequence stratigraphic

framework, Murzuq Basin, SW Libya. Journal of Geochemical Exploration 89, p. 87–91.

Evans, R., 1987, Pathways of migration of oil and gas in the south Mississippi Salt Basin, Trans. Gulf Coast Assoc. Geol. Socs 37, 75-86.

Feldman, H., R., Franseen, E., K., Joeckel, R., M., and Heckel, P., H., 2005, Impact of longer-term modest climate shifts on architecture of high-frequency sequences (cyclothems), Pennsylvanian of mid-continent U.S.A: Journal of Sedimentary Research, v. 75, p. 1019–1043.

Fielding, C., R., and Gibling, M., R., 2005, Distinguishing between channel and valleyfills: definitions, diagnostic criteria and dimensional data [abstract]: 8th International Conference on Fluvial Sedimentology: Delft, Netherlands, Abstracts, 101 p.

Folk, R., L., 1980, The Petrology of Sedimentary Rocks. Austin, Texas, Hemphill Publishing Company. 182 pp. ISBN 0-914696-14-9.

Folk, R., L., 2005, Nannobacteria and the formation of Framboidal Pyrite, Journal of Earth System Science (Bangalore, India), 114:369–374

Fuchtbauer, H., 1967, Influence of different types of diagenesis on sandstone porosity: 7th World Petroleum Congress Proceedings, v. 2, p. 353–369.

Funkhouser, L., W., Bland, F., X., and Humphris, Jr., C., C., 1981, The deep Tuscaloosa gas trend of south Louisiana, *in* D. B. Steward, ed., Tuscaloosa trend of south Louisiana: New Orleans Geological Society, p. 5–25.

Galloway, W., E., 2008, Depositional evolution of the Gulf of Mexico sedimentary basin, in K.J. Hsu, ed., Sedimentary basins of the world, v. 5, The sedimentary basins of the United States and Canada, Miall, A.D., The Netherlands, Elsevier, p. 505–549

Garrels, R., M., and Christ, C., L., 1965, Solutions, minerals, and equilibria, Harper and Row, New York, 450 p.

Garrison, R., K., and Chancellor, R., 1991, Berwick field: the geologic half of the seismic stratigraphic story in the lower Tuscaloosa, Mississippi: Gulf Coast Association of Geological Societies Transactions, v. 41, p. 299–307.

Genuise, J.1., and McBride, E., F., 1990, SEM petrography and XRD analysis of authigenic chlorite in Oligocene and Cretaceous sandstones of the Texas/Louisiana Gulf Coast. Programs and Abstracts, 27th Annual Meeting of the Clay Minerals Society, Columbia, Missouri, p. 51.

Gibling, M., R., 2006, Width and thickness of fluvial channel bodies and valley fills in the geological record: A literature compilation and classification: Journal of Sedimentary Research, v. 76, p. 731–770.

Giles, M., R., 1997, Diagenesis: A quantitative perspective: Dordrecht, Kluwer Academic Publishers, 526 p.

Giles, M., R., and Marshall, J., D., 1986, Constrains on the development of secondary porosity in the subsurface: re-evolution of processes, Marine and Petroleum Geology 3, pp. 243–255.

Giles, M., R., Indrelid, S., L., Beynon, G., V., and Amthor, J., 2000, The origin of large-scale quartz cementation: Evidence for large data sets and coupled heat-fluid mass transport modeling, in R. H. Wordon and S. Morad, eds., Quartz cementation in sandstones: International Association of Sedimentologists Special Publication 29, p. 21–38.

Gluyas, J., G., Grant, S., M., Robinson, A., 1993, Geochemical evidence for a temporal link control on sandstone cementation, In: Horbury, A.D., Robinson, A.G. (Eds.), Diagenesis and Basin Development, vol. 36. Association of Petroleum Geologists Studies in Geology, pp. 23–33.

Gould, K., Pe-piper G., and Piper, D., J., W., 2010, Relationship of diagenetic chlorite rims to depositional facies in lower cretaceous reservoir sandstones of the Scotian basin, Sedimentology, v. 57, p. 587–610.

Grigsby, J., D., 2001, Origin and growth mechanism of authigenic chlorite in sandstones of the lower Vicksburg formation, south Texas, Journal of Sedimentary Research, v. 71, no. 1, p. 27–36.

Hamilton, W., S., and Cameron, C., P., 1987, Facies relationships and depositional environments of the Lower Tuscaloosa Formation reservoir sandstones in McComb and Little Creek Field areas, southwest Mississippi. Gulf Coast Association of Geological Societies and Gulf Coast Section of SEPM Meeting, Baton Rouge, LA. American Association of Petroleum Geologists Bulletin, v. 70, p. 1182.

Hamlin, K,. H., and Cameron, C., P., 1987, Sandstone petrology and diagenesis of Lower Tuscaloosa Formation reservoirs in the McComb and Little Creek field areas, southwest Mississippi, Transactions-Gulf Coast Association of Geological Societies, v. 37, p. 95–104.

Hansley, P., L., 1996, The Tuscaloosa Formation revisited: Gulf Coast Association of Geological Societies Transactions, v. 46, p. 167–177.

Harrison, F., W., Jr., 1980, Louisiana Tuscaloosa versus southeast Texas Woodbine: Gulf Coast Association of Geological Societies Transactions., v. 30, p. 105–111.

Harry, D., L., and Londono, J., 2004, Structure and evolution of the central Gulf of Mexico continental margin and coastal plain, southeast United States. Geol. Soc. America Bull., 116, p. 188–199.

Hearne, J., H., and Lock, B., E., 1985, Diagenesis of the Lower Tuscaloosa as Seen in the Dupont De Nemours #1 Lester Earnest, Harrison County, Mississippi: Gulf Coast Association of Geological Societies Transactions, v. 35, p. 387-393.

Hersch, J., B., 1987, Exploration methods-lower Tuscaloosa Trend, Southwest Mississippi, Transactions, Gulf Coast Association of Geological Societies Transactions, v. 37, p. 105–111.

Hillier, S., 1994, Pore-lining chlorites in siliciclastic reservoir sandstones: electron microprobe, SEM, and XRD data, and implications for their origin. Clay Minerals, v. 29, p. 665–679.

Hillier, S., Fallick, A., E., and Matter, A., 1996, Origin of porelining chlorite in the eolian Rotliegende of northern Germany: Clay Minerals, v. 31, p. 153–171.

Hines, L., 1950, Cranfield cycling pressure maintenance unit: World Oil, 130(Feb): p. 131–146.

Holloway, S., 2007, Carbon dioxide capture and geological storage, Philosophical Transactions of the Royal Society: Mathematical, Physical and Engineering Sciences, v. 365, no. 1853, p. 1095–1107.

Horn, B., W., 2011, Identifying new exploration fairways in the Gulf of Mexico: Deepwater Tuscaloosa/Woodbine play: Gulf Coast Association of Geological Societies Transactions, v. 61, p. 245–256.

Housekenecht, D., W., 1987, Assessing the relative importance of compaction processes and cementation to reduction of porosity in sandstones: American Association of Petroleum Geologists Bulletin, v. 71, p. 633–642.

Hovorka, S., D., Choi, J.- W. Meckel, T., A., Trevino, R., H., Zeng, H., Kordi, M., Wang, F., P., and Nicot, J.-P., 2009. Comparing Carbon Sequestration in an Oil Reservoir to Sequestration in a Brine Formation—Field Study, Energy Procedia 1, p. 2051–2056.

Hovorka, S., D., Meckel, T., A., and Trevino, R., H., 2013, Monitoring a large-volume injection at Cranfield Mississippi—Project design and recommendations, International Journal of Greenhouse Gas Control, 16 p., in press.

Hovorka, S., and Tinker, S., W., 2010, EOR as sequestration: Geoscience perspective: presented at the Symposium on the Role of Enhanced Oil Recovery in Accelerating the Deployment of Carbon Capture and Storage, Cambridge, MA, July 23, 2010, GCCC Digital Publication Series #10-12.

Inoue, A., Meunier, A., Patrier-mas, P., Rigault, C., Beaufort, D., and Vieillard, P., 2009, Application of chemical geothermometry to low-temperature trioctahedral chlorites, Clays and Clay Minerals, v. 57, no. 3, p. 371–382.

IPCC (Intergovernmental Panel on Climate Change) special report on Carbon Dioxide Capture and Storage, 2005, Prepared by working group III of the Intergovernmental Panel on Climate Change. Metz, B., O. Davidson, H. C. de Coninck, M. Loos, and L.A. Meyer (eds.). Cambridge University Press, 442 p.

IPCC (Intergovernmental Panel on Climate Change) special Report on Carbon Dioxide Capture and Storage, 2011, Technical Summary, Intergovernmental Panel on Climate Change, Chapter 5: Underground geological storage, Retrieved 2011-10-05, pp. 195-276, http://www.ipcc.ch/pdf/special-reports/srccs/srccs_chapter5.pdf

Jackson, M., L., W., and Laubach, S., E., 1991, Structural history and origin of the Sabine Arch, East Texas and northwest Louisiana: The University of Texas at Austin, Bureau of Economic Geology Geological Circular 91-3, 47 p.

Jeans, C., V., Wray, D., S., Merriman, R., J., and Fisher, M., J., 2000, Volcanogenic clays in Jurassic and Cretaceous strata of England and the North Sea basin. In: Mineral Diagenesis and Reservoir Quality, the Way Forward (Ed. by D.C. Bain, P.L. Hall, H.F. Shaw and D.A.Spears). Clay Mineral., 35, p. 25–55.

Johnson, R., C., and Nuccio, V., F., 1986, Structural and Thermal history of the Piceance Creek Basin, western Colorado, in relation to hydrocarbon occurrence in the Mesaverde Group: in Spencer, C. W., and Mast, R. F., eds., Geology of Tight Gas Reservoirs: American Association of Petroleum Geologists Studies in Geology No. 24, p. 165–205.

Jun, P., Jinku, L., Yan L., W., and Jianfeng, L., 2009, Origin and controlling factors of chlorite coatings—an example from the reservoir of T3x Group of the Baojie area, Sichuan Basin, China, Pet.Sci. 6: p. 376–382.

Kaiser, W., R., 1984, Predicting reservoir quality and diagenetic history in the Frio Formation (Oligocene) of Texas, *in* McDonald, D.A., and Surdam, R.C., eds., Clastic Diagenesis: American Association of Petroleum Geologists Memoir 37, p. 195–215.

Kazemeini, S., H., Yang, C., Juhlin, C., Fomel, S., and Cosma, C., 2010, Enhancing seismic data resolution using the prestack blueing technique: An example from the Ketzin C O2 injection site, Germany, Geophysics, 75(6), V101–V110. doi: 10.1190/1.3483900

Ketzer, J., M., Holz, M., Morad, S., and Al-Aasm, I., S., 2003a, Sequence stratigraphic distribution of diagenetic alterations in coal-bearing, paralic sandstones: evidence from the Rio Bonito Formation (early Permian), southern Brazil: Sedimentology, v. 50, pp. 855–877.

Kingston, D., R., Dishroon, C., P., and Williams, P., A., 1983, Global basin classification system: American Association of Petroleum Geologists Bulletin, v. 67, p. 2175–2193.

Klett, T., R., Ahlbrandt, T., S., Schmoker, J., W., and Dolton, G., L., 1997, Ranking of the world's oil and gas provinces by known petroleum volumes, Washington, D.C., U.S. Geological Survey.

Klicman, D., P., Cameron, C., P., and Meylan, M., A., 1988, Petrology and Depositional Environments of Lower Tuscaloosa Formation (Upper Cretaceous) sandstones in the North Hustler and Thompson field areas, southwest Mississippi, Transactions-Gulf Coast Association of Geological Societies Transactions, v. 38, p.47–58.

Kordi, M., Hovorka, S., D., Milliken, K., L., Treviño, R., H., and Lu, J., 2010, Diagenesis and reservoir heterogeneity in the Lower Tuscaloosa Formation at Cranfield Field, Mississippi, *in* 60th Annual Convention of the Gulf Coast Association of Geological Societies and the Gulf Coast Section of SEPM, San Antonio, Texas, October 10–12: GCCC Digital Publication Series #10-13.

Kordi, M., Turner, B., and Salem, A., M. K., 2011, Linking Diagenesis to Sequence Stratigraphy in Fluvial and Shallow Marine Sandstones: Evidence from the Cambrian-Ordovician Lower Sandstone Unit in Southwestern Sinai, Egypt. Marine and Petroleum Geology, v. 28, p. 1554–1571

Ku, T., C., W., and Walter, L., M., 2003, Syndepositional formation of Fe-rich clays in tropical shelf sediments, San Blas Archipelago, Panama, Chemical Geology, 197, p. 197– 213.

Kupecz, J., A., Gluyas, J., and Bloch, S., 1997, Reservoir quality prediction in sandstones and carbonates: An Overview American Association of Petroleum Geologists Memoir 69, pp. vii–xxiv.

Lake, L., W., 1989, Enhanced Oil Recovery, Englewood Cliffs, N.J. Prentice Hall, 550 p.

Lander, R., H., Larese, R., E., and Bonnell, L., M., 2008, Toward more accurate quartz cement models: The importance of euhedral versus noneuhedral growth rates: American Association of Petroleum Geologists Bulletin, v. 92, p. 1537–1563.

Lander, R., H., and Walderhaug, O., 1999, Predicting porosity through simulating sandstone compaction and quartz cementation: American Association of Petroleum Geologists Bulletin, v. 83, p. 433–449.

Lanson, B., Beaufort, D., Berger, G., Bauer, A., Cassagnabere, A., and Meunier, A., 2002, Authigenic kaolin and illitic minerals during burial diagenesis of sandstones: a review. Clay Minerals, 37, p. 1–22.

Leckie, D., A., and Singh, C., 1991, Estuarine deposits of the Albian Paddy Member (Peace River Formation), and lowermost Shaftsbury Formation, Alberta: Journal of Sedimentary Petrology, v. 61, p. 825–850.

Liu, K., 2005, Facies Changes of the Eutaw Formation (Coniacian-Santonian), Onshore to Offshore, Northeastern Gulf of Mexico Area, Gulf Coast Association of Geological Societies Transactions, v. 55, p. 431–441.

Lu, J., Kordi, M., Hovorka, S., D., Meckel, T., A., and Christopher, C., A., 2012, Reservoir characterization and complications for trapping mechanisms at Cranfield CO_2 injection site, International Journal of Greenhouse Gas Control, Available online 29 October 2012.

Lu, J., Milliken, K., Reed, R., M., and Hovorka, S., D., 2011, Diagenesis and sealing capacity of the middle Tuscaloosa mudstone at the Cranfield carbon dioxide injection site, Mississippi: Environmental Geosciences, 18(1), p. 1–19.

Lundegard, P., D., 1992, Sandstone porosity loss–A "big picture" view of the importance of compaction: Journal of Sedimentary Petrology, v. 62, p. 250–260.

Luo, J., L., Morad, S., Salem, A., Ketzer, J., M., Lei, X., L., Guo, D., Y., Hlal, O., 2009, Impact of diagenesis on reservoir-quality evolution in fluvial and lacustrine-deltaic sandstones: evidence from Jurassic and Triassic sandstones from the Ordos Basin, China. Journal of Petroleum Geology 32, p. 79–102.

Lynch, F., L., 1996, Mineral/water interaction, fluid flow, and Frio sandstone diagenesis: Evidence from the rocks: American Association of Petroleum Geologists Bulletin, v. 80, no. 4, p. 486–504.

Mackenzie, F., T., 2005, Sediments, Diagenesis, and Sedimentary Rocks (ed), Treatise on Geochemistry, vol. 7. Elsevier, 446 pp, ISBN 0-08-044849-6.

Makowitz, A., 2004, The genetic association between brittle deformation and quartz cementation: examples from burial compaction and cataclasis [Ph.D. dissertation]: University of Texas at Austin, Austin, Texas, 298 p.

Makowitz, A., and Milliken, K., L., 2003, Quantification of brittle deformation in burial compaction, Frio and Mount Simon Formation sandstones: Journal of Sedimentary Research, v. 73, no. 6, p. 1007–1021.

Mancini, E., A., 2003, Petroleum potential of aggrading sandstones of transgressive/regressive cycles in the Mississippi-Alabama area: Gulf Coast Association of Geological Societies Transactions, v. 53, p. 527–536.

Mancini, E., A., Mink, R., M., Payton, J., W., and Bearden, B., L., 1987, Environments of deposition and petroleum geology of Tuscaloosa Group (Upper Cretaceous), South Carlton and Pollard Fields, southwestern Alabama, American Association of Petroleum Geologists Bulletin, v. 71, p. 1128–1142.

Mancini, E., A., Obid, J., Badali, M., Liu, K., and Parcell, W., C., 2008; Sequence-stratigraphic analysis of Jurassic and Cretaceous strata and petroleum exploration in the central and eastern Gulf coastal plain, United States; American Association of Petroleum Geologists Bulletin, v. 92, no. 12, p. 1655 –1686.

Mancini, E., A., Parcell, W., C., Puckett, T., M., Llinas, J., C., 2001, Basin and petroleum migration modeling of the Mississippi interior salt basin, Project: Basin Analysis of the Mississippi Interior Salt Basin and Petroleum System Modeling of the Jurassic Smackover Formation, Eastern Gulf Coastal Plain, U.S. Department of Energy, DE-FG22-96BC14946, 46 p.

Mancini, E., A., and Puckett, T., M., 2005, Jurassic and Cretaceous transgressive-regressive (T-R) cycles, northern Gulf of Mexico, U.S.A., Stratigraphy, v. 2, no. 1, p. 31–48.

Mancini, E., A., Puckett, T., M., and Parcell, W., C., 1999, Modeling of the burial and thermal histories of strata in the Mississippi Interior Salt Basin: Gulf Coast Association of Geological Societies Transactions, v. 49, p. 332-341.

Mancini, E., A., Puckett, T., M., Parcell, W., C. and Panetta, B., J., 1999, Basin analysis of the Mississippi Interior Salt Basin and petroleum systems modeling of the Jurassic Smackover Formation, eastern Gulf Coastal Plain, Topical Reports 1 and 2, DOE contract no. DE-FG22-96BC14946, p. 425.

Mancini, E., A., Puckett, T., M., Tew, Berry H., and Smith, Charles C., 1995, Upper Cretaceous sequence stratigraphy of the Mississippi-Alabama area, Gulf Coast Assoc. Geol. Socs. Trans. v. 45, p. 377–384.

Marini, L., 2007, Geological Sequestration of Carbon Dioxide—Thermodynamics, Kinetics, and Reaction Path Modeling, Elsevier, The Netherlands, 453 p.

Martin, J., Cantelli, A., Paola, C., Blum, M., and Wolinsky, M., 2011, Quantitative modeling of the evolution and geometry of incised valleys, Journal of Sedimentary Research, 2011, v. 81, 64–79, DOI: 10.2110/jsr.2011.5

Maynard, J., R., Feldman, H., R., and Always, R., 2010, From bars to valleys: the sedimentology and seismic geomorphology of fluvial to estuarine incised-valley fills of the Grand Rapids Formation (Lower Cretaceous), Iron River Field, Alberta, Canada Journal of Sedimentary Research, v. 80, p. 611–638.

McAulay, G., E., Burley, S., D., Fallick, A., E., and Kusznir, N., J., 1994, Palaeohydrodynamic fluid flow regimes during diagenesis of the Brent Group in the Hutton-NW Hutton reservoirs: constraints from oxygen isotope studies of authigenic kaolin and reverse flexural modelling. Clay Minerals, 29, p. 606–626.

McBride, E., F., 1984, Rules of Sandstone Diagenesis Related to Reservoir Quality, Gulf Coast Association of Geological Societies Transactions, v. 34, p. 137–139.

McBride, E., F., 1989, Quartz cement in sandstones: a review: Earth Science Reviews, 26, p. 69–112.

McBride, E., F., 2012, Heterogeneous packing and quartz cementation of the Eureka Quartzarenite (Middle Ordovician), Utah and Nevada, U.S.A., Journal of Sedimentary Research, v. 82, p. 664–680. Doi: 10.2110/Jsr.2012.58.

McBride, E., F., Diggs, T., N., and Wilson, J., C., 1991, Compaction of Wilcox and Carrizo sandstones (Paleocene–Eocene) to 4420 m, Texas Gulf Coast: Journal of Sedimentary Petrology, v. 61, p. 73–85.

McBride, E., F., Land, L., S., and Mack, L., E., 1987, Diagenesis of eolian and fluvial feldspathic sandstones, Norphlet Formation (Upper Jurassic), Rankin County, Mississippi, and Mobile County, Alabama: American Association of Petroleum Geologists Bulletin, v. 71, p. 1019–1034.

McBride, E., F., Picard, M., D., and Folk, R., L., 1994, Oriented concretions, Ionian Coast, Italy–Evidence of groundwater flow direction: Journal of Sedimentary Research, v. A64, p. 535–540.

McIlroy, D., 2004, Some ichnological concepts, methodologies, applications and frontiers, in McIlroy, D., ed., The Application of Ichnology to Stratigraphic and Palaeonenvironmental Analysis: Geological Society of London, Special Publication 228, p. 3–27.

McMoRan Exploration Company, 2011, McMoRan Exploration Co. updates Gulf of Mexico exploration & development activities [Press release]

Meckel, T., A., Hovorka, S., D., and Kalyanaraman, N., 2008, Continuous pressure monitoring for large volume CO_2 injections, presented at the 9th International Conference on Greenhouse Gas Control Technologies (GHGT-9), Washington, D.C., November 16-20, GCCC Digital Publication Series #08-03a.

Meckel, T., A., Zeidouni, M., Hovorka, S., D., Hosseini, S., A., 2013, Assessing sensitivity to well leakage from three years of continuous reservoir pressure monitoring during CO_2 injection at Cranfield, MS, USA. International Journal of Greenhouse Gas Control, in press.

Meyer, D., 2007, From BAHA to Jack, evolution of the lower Tertiary Wilcox trend in the deepwater Gulf of Mexico: Sedimentary Record, v. 5, p. 4–9.

Meylan, M., A., 1997, Controls on the distribution of oil and gas, Mesozoic and Cenozoic of Mississippi: Gulf Coast Association of Geological Societies Transactions, v. 47, p. 367–375.

Miller, J., A., 1982, Structural control of Jurassic sedimentation in Alabama and Florida: American Association of Petroleum Geologists Bulletin, v. 66, p. 1289–1301.

Milliken, K., L., 2001, Diagenetic heterogeneity in sandstone at the outcrop scale, Breathitt Formation (Pennsylvanian), eastern Kentucky: American Association of Petroleum Geologists Bulletin, v. 85, no. 5, p. 795–815.

Minter, L., L., Cameron, C., P., Thomas, A., R., and Ward, W., C., 1992, Carbonate-Cemented Zones in the Lower Tuscaloosa Formation (Upper Cretaceous), Southwestern Mississippi, Gulf Coast Association of Geological Societies Transactions, v. 42, p. 279-304.

Mississippi Geological Society, 1957, Cranfield Field, in Mesozoic-Paleozoic producing area of Mississippi and Alabama.

Mississippi Oil and Gas Board, 1966, Mississippi Oil and Gas Board (MOGB), Cranfield Field, Cranfield unit, basal Tuscaloosa reservoir, Adams and Franklin Counties, p. 42–58.

Mitchum, R., M., Sangree, J., B. Vail, P., R., and Wornardt, W., W., 1991b, Sequence stratigraphy in Late Cenozoic expanded sections, Gulf of Mexico, *in* J. M. Armentrout and B. F. Perkins, eds., Sequence stratigraphy as an exploration tool: concepts and practices in the Gulf Coast: Gulf Coast Section of the Society of Economic Paleontologists and Mineralogists, Eleventh Annual Research Conference Proceedings, p. 237-256.

Mitchum, R., M., Sangree, J., B., Vail, P., R., and Wornardt, W., W., 1993, Recognizing sequences and systems tracts from well logs, seismic data, and biostratigraphy: examples from the Late Cenozoic of the Gulf of Mexico, *in* Paul Weimer and Henry Posamentier, eds., Siliciclastic sequence stratigraphy: recent developments and applications: American Association of Petroleum Geologists Memoir 58, p. 163-197.

Mitchum, R., M., and Van Wagoner, J., C., 1991a, High-frequency sequences and eustatic cycles in the Gulf of Mexico basin, *in* J. M. Armentrout and B. F. Perkins, eds., Sequence stratigraphy as an exploration tool: concepts and practices in the Gulf Coast: Gulf Coast Section of the Society of Economic Paleontologists and Mineralogists, Eleventh Annual Research Conference Proceedings, p. 257-267.

Morad, S., and AlDahan, A., A., 1986, Alteration of detrital Fe-Ti oxides in sedimentary rocks, Geological Society of America Bulletin, v. 97, p. 567–578.

Morad S., Al-Ramadan, K., Ketzer, J., M. and De Ros, L., F., 2010, The impact of diagenesis on the heterogeneity of sandstone reservoirs: A review of the role of depositional facies and sequence stratigraphy, American Association of Petroleum Geologists Bulletin, v. 94, no. 8 (August), p. 1267–1309.

Morad, S., Ben Ismail, H., De Ros, L., F., Al-Aasm, I., S., and Serrhini, N., E., 1994, Diagenesis and formation water chemistry of Triassic reservoir sandstones from southern Tunisia, Sedimentology, 41, p. 1253–1272.

Morad, S., Ketzer, J., M., and De Ros, F., 2000, Spatial and temporal distribution of diagenetic alterations in siliciclastic rocks: implications for mass transfer in sedimentary basins, Sedimentology v. 47 (Suppl. 1), pp. 95–120.

Morad, S., Ketzer, M., De Ros, L., F., 2012, Linking Diagenesis to Sequence Stratigraphy: an integrated tool for understanding and predicting reservoir quality distribution, International Association of Sedimentologists, Special Publication, 2012, 45, p. 1-36

Moraes, M., A., S., and De Ros, L., F., 1992, In: David, W.H., Edward, D.P. (Eds.), Depositional Infiltrated and Authigenic Clays in Fluvial Sandstones of the Jurassic Sergi Formation, Reconcavo Basin, northeastern Brazil. Origin, diagenesis, and petrophysics of clay minerals in sandstones, vol. 47. SEPM, Society for Sedimentary Geology, pp. 197–208.

Morton, R., A., Blum, M., D., and White, W., A., 1996, Valley fills of incised coastal plain rivers, southeastern Texas: Gulf Coast Association of Geological Sciences, Transactions, v. 46, p. 321–331.

Morton, R., A, and Suter, J., R., 1996, Sequence stratigraphy and composition of late Quaternary shelf-margin deltas, northern Gulf of Mexico, American Association of Petroleum Geologists Bulletin, v. 80, p. 505– 530.

Needham, S., J., Worden, R., H., McILroy, D., 2005, Experimental production of clay rims by macrobiotic sediment ingestion and excretion processes. Journal of Sedimentary Research 75, 1028–1037.

NETL (National Energy Technology Laboratory), 2010, Carbon Dioxide Enhanced Oil Recovery Untapped Domestic Energy Supply and Long Term Carbon Storage Solution, 32 p.

NETL (National Energy Technology Laboratory), 2012, The North American Carbon Storage Atlas – NACSA 2012. 51 p.

Newman, A., C., D., 1987, Chemistry of clays and clay minerals. New York: J Wiley. 480 p.

Nicot, J., P., Houseworth, J. E., Oldenburg, C., M., Choi, J., W., Lashgari, H., Coleman, S., Meckel, T., A., Jordan, P., Mazzoldi, A., 2010, Leakage Risk Assessment for the SECARB Phase III CO2 Storage Project at Cranfield, Mississippi; internal report, Bureau of Economic Geology, University of Texas.

Nicot, J., P., Oldenburg, C., M., Houseworth, J., E., and Choi, J., W., 2012, Analysis of potential leakage pathways at the Cranfield, MS, U.S.A. CO_2 sequestration site, International Journal of Greenhouse Gas Control (in press).

Odin, G., S., 1990, Clay mineral formation at the continent-ocean boundary: the verdine facies. Clay Minerals, v. 25(4): p. 477-483.

Odin, G., S., Bailey S., W., Amouric M., Frohlich F., and Waychunas G.A., 1988, Mineralogy of the facies verdine. In G.S. Odin, Ed., Green Marine Clays, Developments in Sedimentology, 45, p. 159–204. Elsevier, Amsterdam.

Odin, G., S. and Sen Gupta, B., K., 1988, Geological significance of the verdine facies. In G.S. Odin, Ed., Green Marine Clays, Developments in Sedimentology, 45, p. 205–219. Elsevier, Amsterdam.

Onasch, C., M., 1994, Assessing brittle volume-gain and pressure solution volume-loss processes in quartz arenite: Journal of Structural Geology, v. 16, p. 519–530.

Osborne, M., Haszeldine, R., S., and Fallick, A., E., 1994, Variation in kaolin morphology with growth temperature in isotopically mixed pore-fluids, Brent Group. UK North Sea. Clay Minerals 29, p. 591–608.

Paxton, S., T., Szabo, J., O., Ajdukiewicz, J., and Klimentidis, R., E., 2002, Construction of an intergranular volume compaction curve for evaluating and predicting compaction and porosity loss in rigid-grain sandstone reservoirs: American Association of Petroleum Geologists Bulletin, v. 86, p. 2047–2067.

Paxton, S., T., Szabo, J., O., Calvert, C., S., and Ajdukiewicz, J., M.,1990, Preservation of primary porosity in deeply buried aandstones: A new play concept from the Cretaceous Tuscaloosa Sandstone of Louisiana, American Association of Petroleum Geologists Search and Discovery Article #91003.

Payton, J., W., 1984, Paleoenvironmental determination of the Lower Tuscaloosa at South Carlton Field, Baldwin and Clarke counties, Alabama [unpublished M. S. thesis]: University of Alabama, 180 p.

Pe-Piper, G., and Weir-Murphy, S., 2008, Early diagenesis of inner-shelf phosphorite and iron-silicate minerals, Lower Cretaceous of the Orpheus graben, southeastern Canada: Implications for the origin of chlorite rims. American Association of Petroleum Geologists Bulletin, v. 92, no. 9, p. 1153–1168.

Pessango, E., A., Jr., 1990, Cretaceous microfossils of north central Texas, micropaleontology field trip, Geological Society of America 1990 Annual Meeting, Guidebook, 48 p.

Pettijohn, F., Potter, P., and Siever, R., 1987, Sand and sandstone, Springer-Verlag, New York, 533 pp.

Petty, A., J., 1997, Lower Tuscaloosa Clastic Facies Distribution (Upper Cretaceous), Federal and State Waters, Eastern Gulf of Mexico, Gulf Coast Association of Geological Societies Transactions, v. 47, p. 553–462.

Pilger, R., H., Jr., 1981, The opening of the Gulf of Mexico: implications for the tectonic evolution of the northern Gulf Coast: Gulf Coast Association of Geological Societies Transactions, v. 31, p. 377–381.

Pitman, J., K., 2007, Fact Sheet—U.S. Geological Survey Assessment of undiscovered gas resources in the Upper Cretaceous Tuscaloosa and Woodbine Formations, western Gulf Province of the Gulf Coast region, Louisiana and Texas, *in* R. F. Dubiel, P. H. Nelson, J. Kibler, R. R. Charpentier, T. A. Cook, T. R. Klett, R. M. Pollastro, and C. J. Schenk, eds., Fact Sheet, U.S. Geological Survey.

Pittman, E., D., and Larese, R., E., 1991, Compaction of lithic sands: Experimental results and applications: American Association of Petroleum Geologists Bulletin, v. 75, p. 1279–1299.

Pittman, E., D., Larese, R., E., and Heald, M. T., 1992, Clay coats: occurrence and relevance to preservation of porosity in sandstones, *in* D. W. Houseknecht and E. D. Pittman, eds., Origin, diagenesis, and petrophysics of clay minerals in sandstones: SEPM Special Publication 47, p. 241–255.

Pittman**,** E., D., and Lumsden**,** D. N., 1968*,* Relationship between chlorite coatings on quartz grains and porosity, Spiro Sand, Oklahoma, Journal of Sedimentary Petrology, v. 38, p. 668–670.

Posamentier, H., W., 2001, Lowstand alluvial bypass systems: Incised vs. unincised: American Association of Petroleum Geologists Bulletin, v. 85, p. 1771–1793.

Pryor, W., A., 1973, Permeability-porosity patterns and variations in some Holocene sand bodies: AAPG Bulletin, v. 57, p. 162–289.

Rains, D., B., 2007, The lower Tertiary Wilcox trend in the deepwater Gulf of Mexico: American Association of Petroleum Geologists Annual Meeting, v. 16, p. 114.

Reed, J., S., Eriksson, K., A., and Kowalewski, M., 2005, Climatic, depositional and burial controls on diagenesis of Appalachian Carboniferous sandstones: qualitative and quantitative methods: Sedimentary Geology, v. 176, pp. 225–246.

Remy, R., R., 1994, Porosity reduction and major controls on diagenesis of Cretaceous–Paleocene volcaniclastic and arkosic sandstone, Middle Park Basin, Colorado: Journal of Sedimentary Research, v. A64, no. 4, p. 797–806.

Rodriguez, A., B., Anderson, J., B., and Simms, A., R., 2005, Terrace inundation as an autocyclic mechanism for parasequence formation: Galveston Estuary, Texas, U.S.A.: Journal of Sedimentary Research, v. 75, p. 606–618.

Ryan P., C., Conrad M., E., Brown K., Chamberlain C., P., Reynolds, R., C. Jr. 1998, Oxygen isotopic compositions of serpentine/chlorite and illite/smectite in the Tuscaloosa Formation (US Gulf Coast): Implications for pore fluids and mineralogic reactions. Clays and Clay Minerals, v. 46, p. 357–368.

Ryan, P., C. and Hillier, S., 2002, Berthierine/chamosite, corrensite, and discrete chlorite from evolved verdine and evaporite-associated facies in the Jurassic Sundance Formation, Wyoming, American Mineralogist, v. 87, p. 1607–1615.

Ryan, P., C., and Reynolds, R., C., Jr., 1996, The origin and diagenesis of grain-coating serpentine-chlorite in Tuscaloosa Formation sandstone, U.S. Gulf Coast, American Mineralogist, v. 81, p. 213–225.

Ryan, P., C., and Reynolds, R., C., Jr., 1997, The chemical composition of serpentine/chlorite in the Tuscaloosa formation, united states gulf coast: edx vs. xrd determinations, implications for mineralogic reactions and the origin of anatase: Clays and Clay Minerals, v. 45, no. 3, p. 339–352.

Salvador, A. 1991, Origin and development of the Gulf of Mexico basin, In: Salvador, A., Ed., The Gulf of Mexico Basin. Decade of North American Geology. Boulder, Geological Society of America, v. J, p. 389–444.

Sassen, R., 1990, Lower Tertiary and Upper Cretaceous source rocks in Louisiana and Mississippi: implications to Gulf of Mexico crude oil: American Association of Petroleum Geologists Bulletin, v. 74, p. 857–878.

Sawyer, D., S., Buffler, R.,T., and R., H., Pilger, Jr., 1991, The crust under the Gulf of Mexico, in A. Salvador, ed., The Gulf of Mexico Basin: Decade of North American Geology, Boulder, p. 53–72.

Sayers, J. E., and Uddin, A., 2010, Provenance of the Cretaceous Tuscaloosa Formation in Eastern Alabama and Western Georgia, (abs.): Geological Society of America Abstracts with Programs, v. 42, no. 1, p. 72.

Schlager, W., and Camber, O., 1986, Submarine slope angles, drowning unconformities, and self-erosion of limestone escarpments: Geology, v. 14, p. 762–765.

Schumm, S., A., and Ethridge, F., G., 1994, Origin, evolution and morphology of fluvial valleys, in Dalrymple, R.W., Boyd, R., and Zaitlin, B.A., eds., Incised-Valley Systems: Origin and Sedimentary Sequences: SEPM, Special Publication 51, p. 10–27.

Schumm, S., A., Mosley, M., P., and Weaver, W., E., 1987, Experimental Fluvial Geomorphology: New York, John Wiley, 413 p.

SECARB (Southeast Regional Carbon Sequestration Partnership) Final report, Phase II, 2011, Final Report for Gulf Coast Stacked-Storage Project SECARB Phase II at Cranfield, Hovorka, S., D., Clift, S., J., Meckel, T., A., Treviño, R., Zeng, H., Nicot, J., P., Romanak, K., D., Smyth, R., C., Yang, C., Lu, J., Choi, J., W., Kordi, M., Gulf Coast Carbon Center, Bureau of Economic Geology, David Freeman – Sandia Technologies LLC, Robert Butsch – Schlumberger Carbon Services, Bureau of Economic Geology, John A. and Katherine G. Jackson School of Geosciences, The University of Texas at Austin, 83 p.

Sinha S., Routh P., S., Anno P., D. and Castagna J., P. 2005, Spectral decomposition of seismic data with continuous-wavelet transforms. Geophysics 70, p. 19–25.

Smith, J., T., and Ehrenberg, S., N., 1989, Correlation of carbon dioxide abundance with temperature in clastic hydrocarbon reservoirs: relationship to inorganic chemical equilibrium: Marine and Petroleum Geology, v. 6, p. 129–135.

Smith E., A., and Johnson, L., C., 1887, Tertiary and Cretaceous strata of the Tuscaloosa, Tombigbee, and Alabama Rivers: U.S. Geological Survey Bulletin 43, 189 p.

Smith, C., C., and Mancini, E., A., 1983, Calcareous nannofossil and planktonic foraminiferal biostratigraphy;. pp. 16–28 in E. E. Russell, D. M. Keady, E. A. Mancini, and C. C. Smith (eds.), Upper Cretaceous Lithostratigraphy and Biostratigraphy in Northeast Mississippi, Southwest Tennessee and Northwest Alabama, Shelf chalks and Coastal Clastics. Gulf Coast Section, Society of Economic Paleontologists and Mineralogists, Guidebook for Spring Field Trip.

Sneider, R., M., 1990, Introduction: reservoir description of sandstones, in J.H. Barwis, J.G. McPherson, and J.R.J. Studlick, eds., Sandstone petroleum reservoirs: New York, Springer-Verlag, p. 1–3.

Sohl, N., F., Martinez R, E., Salmeron-Urena, P. and Soto-Jaramillo, F., 1991, Upper Cretaceous: Geological Society of America, The Geology of North America, v. J, p. 205–244.

Spooner, Jr., H. V., 1964, Basal Tuscaloosa sediments, east-central Louisiana: American Association of Petroleum Geologists Bulletin, v. 48, p. 1–21.

Stancliffe, R., J., and Adams, E., R. 1986, Lower Tuscaloosa fluvial channel styles at Liberty field, Amite County, Mississippi: Gulf Coast Association of Geological Societies Transactions, v. 36, p. 305–313.

Szabo, J., O., and Paxton, S., T., 1991, Intergranular volume (IGV) decline curves for evaluating and predicting compaction and porosity loss in sandstones (abs.): American Association of Petroleum Geologists Bulletin, v. 75, p. 678.

Taylor, K., G., Gawthorpe, R., L., Curtis, C., D., Marshall, J., D., and Awwiller, D., N., 2000, Carbonate cementation in a sequence stratigraphic framework: Upper Cretaceous Sandstones, Book Cliffs, Utah-Colorado, Journal of Sedimentary Research, 70, pp. 360−372.

Taylor, K., G., Gawthorpe, R., L. and Van Wagoner, J., C., 1995, Stratigraphic control on laterally persistent cementation, Book Cliffs, Utah, Journal of Sedimentary Research, v. 69, p. 225–228.

Taylor, T., R., Giles, M. R. Hathon, L. A. Diggs, T. N. Braunsdorf, N. R. Birbiglia, G.V. Kittridge, M.G. Macaulay, C. I. and I. S. Espejo, 2010, Sandstone diagenesis and reservoir quality prediction:Models,myths, and reality: American Association of Petroleum Geologists Bulletin, v. 94, p. 1093–1132.

Taylor, T., R., Stancliffe, R., Macaulay, C., and Hathon, L., 2004, High temperature quartz cementation and the timing of hydrocarbon accumulation in the Jurassic Norphlet Sandstone, offshore Gulf of Mexico, U.S.A., in J. M. Cubitt, W. A. England, and S. R. Larter, eds., Understanding petroleum reservoirs; toward an integrated reservoir engineering and geochemical approach: Geological Society (London) Special Publication 237, p. 257–278.

Thamban, M., and Purnachandra, R., V., 2000, Distribution and composition of verdine and glaucony facies from the sediments of the western continental margin of India. In: *Marine Authigenesis; from Global to Microbial*, Society for Sedimentary Geology Special Publication 66 (Ed. by C.R. Glenn, L.L. Prevot and J. Lucas), Tulsa, OK, pp. 233–244.

Thomson, A., 1979, Preservation of porosity in the deep Woodbine/Tuscaloosa trend, Louisiana: Gulf Coast Association of Geological Societies Transactions, v. 30, p. 396–403.

Tobi, H., K., Braunsdorf, N., and Taylor, T., 2008, The Control of Provenance from Reservoir Quality and Rock Properties of Clastic Wilcox and Frio Sediments in the Gulf of Mexico, AAPG abs., American Association of Petroleum Geologists International Conference and Exhibition, Cape Town, South Africa.

Tobi, H., K., Taylor, T., R., Winker, C., D., Diggs, T., N., and Braunsdorf, N., R., 2005, The Control of Provenance on Reservoir Quality and Rock Properties in the Gulf of Mexico, American Association of Petroleum Geologists Search and Discovery Article #90039.

Trask, P., D., 1932, Origin and environment of source sediments of petroleum: Houston, TX, Gulf Publication Company, 323 p.

Tuttle, S., D., Milling, M., E., and Rusnak, R., S., 1966, Comparisons of Stream Sizes (Discharge) with Valley Sizes and Shapes: Geological Society of America, Special, Paper 101, 225 p.

Vail, P., R., and Wornardt, W., Jr., 1991, An integrated approach to exploration and development in the 90`s: well log-seismic sequence stratigraphy analysis: Gulf Coast Association of Geological Societies Transactions, v. 41, p. 630–650.

Van Wagoner, J., C., 1995a, Introduction, in Van Wagoner, J.C., and Bertram, G.T., eds., Sequence Stratigraphy of Foreland Basin Deposits—Outcrop to Subsurface Examples from the Cretaceous of North America: American Association of Petroleum Geologists Memoir 64, p. ix–xxi.

Van Wagoner, J., C., Mitchum, R., M., Campion, K., M., and Rahmanian, V., D., 1990, Siliciclastic sequence stratigraphy in well logs, cores, and outcrops: concepts for high-resolution correlation of time and facies: American Association of Petroleum Geologists Methods in Exploration Series No. 7, 55 p.

Vaz, G., G., 2000, Verdine and glaucony facies from continental margin off Chennai, bay of Bengal. J. Geol. Soc. India, 55, p. 297–306.

Walderhaug, O., 1994, Precipitation rates for quartz cement in sandstones determined by fluid-inclusion microthermometry and temperature-history modeling: Journal of Sedimentary Research, v. A64, p. 324–333.

Walderhaug, O., 1996, Kinetic modeling of quartz cementation and porosity loss in deeply buried sandstone reservoirs: American Association of Petroleum Geologists Bulletin, v. 80, p. 731–745.

Walderhaug, O., 2000, Modeling quartz cementation and porosity loss in Middle Jurassic Brent Group sandstones of the Kvitebjørn field, Northern North Sea: American Association of Petroleum Geologists Bulletin, v. 84, p. 1325–1339.

Waples, D., W., Pacheco, J. and Vera, A., 2004, A method for correcting log-derived temperatures in deep wells, calibrated in the Gulf of Mexico, Petroleum Geoscience, v. 10, p. 239–245.

Weedman, S., J., Brantley, S., L., Shiraki, R., and Poulson, S., R., 1996, Diagenesis, compaction, and fluid chemistry modeling of a sandstone near a pressure seal: Lower Tuscaloosa Formation, Gulf Coast: American Association of Petroleum Geologists Bulletin, v. 80, p. 1045–1064.

Whitney, P., R., and McClelland, J., M., 1983, Origin of biotite-hornblende-garnet coronas between oxides and plagioclase in olivine metagabbros, Adirondack Region, New York. Contrib Mineral Petrol., v. 82, p. 34–41.

Wilkinson, M., Haszeldine, R., S., and Fallick, A., E., 2004. Hydrocarbon filling history from diagenetic evidence: Brent Group, UK North Sea. Marine and Petroleum Geology 21, p. 443–455.

Wilson, M., D., 1992, Inherited grain rimming clays in sandstones from eolian and shelf environments: their origin and control on reservoir properties, In: Origin Diagenesis and Petrophysics of Clay Minerals in Sandstones SEPM Special Publication of the Society of Economic Paleontologists and Mineralogists, No 47, p. 209-225.

Winkler, C., D., and Buffler, R., T.,1988, Paleogeographic evolution of early deep-water Gulf of Mexico and margins, Jurassic to middle Cretaceous (Cenomanian): American Association of Petroleum Geologists Bulletin, v. 72, p. 318–346.

Wiygul, G., J., and Young, L., M., 1987, A subsurface study of the Lower Tuscaloosa Formation at Olive Field, Pike and Amity Counties, Mississippi, Gulf Coast Association of Geological Societies Transactions, v. 37, p. 295–302.

Woolf K., S. and Wood, L., J., 2011, Sequence stratigraphic and paleogeographic framework for the Lower Tuscaloosa Sandstone, eastern Gulf of Mexico Province, U.S.A.: Influences on sediment distribution and depositional environments, internal report, Bureau of Economic Geology, Jackson School of Geosciences, The University of Texas at Austin.

Worden, R., H., and Burley, S., D., 2003, Sandstone diagenesis: The evolution of sand to stone, in Burley, S.D., and Worden, R.H., eds., Sandstone Diagenesis: Recent and Ancient, Malden, Massachusetts, USA: Wiley-Blackwell Publishing, International Association of Sedimentologists Special Publications, vol. 4, p. 3–44.

Worden**,** R., H. and Morad**,** S., 2000, Quartz cementation in sandstones, International Association of Sedimentologists**,** Special Publication**,** v. 29, p. 342.

Worden, R. H., and Morad, S. 2003, Clay minerals in sandstones: controls on formation, distribution and evolution, in special publication of the International Association of Sedimentologists, no. 34, p. 1–41.

Wornardt, W. W., Jr., 2010, Well-log sequence stratigraphy of the ultra deepwater Shell #1, Alaminos Canyon block 557 in the Gulf of Mexico: Gulf Coast Association of Geological Societies Transactions, v. 60, p.851.

Wright, V., P., 1993, Sedimentology Review 1, Blackwell Publishing, 152 p.

Wu, S., 1990, Allochthonous salt, structure and stratigraphy of the north-eastern Gulf of Mexico; Part 1, Stratigraphy, *in* P. R. Vail, and C. Cramez, eds., Marine and Petroleum Geology: United Kingdom, Butterworth [in conjunction with the] Geological Society : Surrey, United Kingdom], p. 318–333.

Zaitlin, B., A., Dalrymple, R., W., and Boyd, R., 1994, The stratigraphic organization of incised valley systems associated with relative sea level changes, in Dalrymple, R.W.,Boyd, R., and Zaitlin, B.A., eds., Incised-Valley Systems: Origin and Sedimentary Sequences: SEPM, Special Publication, v. 51, p. 45–60.

Zarra, L., 2006, Emergence of the lower Tertiary Wilcox Trend in the deepwater Gulf of Mexico: Houston Geological Society Bulletin, v. 49, p. 21.

Zeng, H., 2009, Internal report, Gulf Coast Carbon Center, Bureau of Economic Geology, Jackson School of Geosciences, The University of Texas at Austin.

Zeng, H., Backus, M., M., Barrow, K., T., and Tyler, N., 1998a, Stratal slicing, part I: realistic 3-D seismic model: Geophysics, v. 63, no. 2, p. 502–513.

Zeng, H., Henry, S., C., and Riola, J., P., 1998b, Stratal slicing, part II: real seismic data: Geophysics, v. 63, no. 2, p. 514–522.

Zhang, X., Lin, C., M., Cai, Y., F., Qu, C., W., Chen, Z., Y., 2012, Pore Lining Chlorite Cements In Lacustrine-Deltaic Sandstones From The Upper Triassic Yanchang Formation, Ordos Basin, China, Journal of Petroleum Geology, v. 35, issue 3 (July), p. 273-290. ISSN: 0141-6421 DOI: 10.1111/j.1747-5457.2012.00530.x

Zhu, R., K., Zou C., N., Zhang, N., Wang, X., Cheng, R., Liu, L., Zhou, C., M, and Song, L., H., 2008, Diagenetic fluids evolution and genetic mechanism of tight sandstone gas reservoirs in the Upper Triassic Xujiahe Formation in Sichuan Basin, China, Sci China Ser D-Earth Sci. 2008. 50(1): p. 1340–1353.

Vita

Masoumeh Kordi earned a diploma in "Experimental Sciences" in Iran. She entered *Shahrood University*, Shahrood, Iran and received a Bachelor degree in Geology in 1997. She worked as a geologist in the Iranian Offshore Oil Company. In 2006, she pursued her education at *Uppsala University,* Uppsala, Sweden and awarded the degree of Master of Science in Geology specialized in Diagenesis and Sequence Stratigraphy. During her studies at Uppsala University, she worked as teaching assistant for a number of courses. She was admitted to the Jackson School of Geosciences at *The University of Texas at Austin* and started her Ph.D. as a research assistant in fall 2009. She did an internship with BP America Inc. in 2012.

Permanent email: Masoumeh.kordi@utexas.edu

This dissertation was typed by Masoumeh Kordi.